



HAL
open science

Conversion of mechanical energy into light : understanding the phenomenon in the case of phosphor-elastomer composite materials

Amira Saoudi

► To cite this version:

Amira Saoudi. Conversion of mechanical energy into light: understanding the phenomenon in the case of phosphor-elastomer composite materials. Fluid mechanics [physics.class-ph]. Université de Lyon, 2020. English. NNT : 2020LYSE1245 . tel-03290735

HAL Id: tel-03290735

<https://theses.hal.science/tel-03290735>

Submitted on 19 Jul 2021

HAL is a multi-disciplinary open access archive for the deposit and dissemination of scientific research documents, whether they are published or not. The documents may come from teaching and research institutions in France or abroad, or from public or private research centers.

L'archive ouverte pluridisciplinaire **HAL**, est destinée au dépôt et à la diffusion de documents scientifiques de niveau recherche, publiés ou non, émanant des établissements d'enseignement et de recherche français ou étrangers, des laboratoires publics ou privés.



Université Claude Bernard



Lyon 1

THÈSE de DOCTORAT DE L'UNIVERSITÉ DE LYON

Opérée au sein de :

l'Université Claude Bernard Lyon 1

Ecole Doctorale ED52 : PHAST
Physique et Astrophysique

Spécialité de doctorat : Physique

Soutenue publiquement le 23/11/2020 par:

Amira SAOUDI

Conversion of Mechanical Energy into Light

Understanding the phenomenon in the case of
phosphor-elastomer composite materials

Convertir l'Énergie Mécanique en Lumière

Compréhension du phénomène dans le cas des matériaux
composites phosphore-élastomère

Devant le jury composé de :

SMET Philippe

Professeur, Université de Ghent

VEDDA Anna

Professeure, Université Bicocca Milan

JOURNET-GAUTIER Catherine

Professeure, Laboratoire Multimatériaux et Interfaces Lyon 1

CHADEYRON Geneviève

Professeure, Institut Chimie Clermont Ferrand

GACOIN Thierry

Directeur de Recherches, École Polytechnique Palaiseau

DUJARDIN Christophe

Professeur, Institut Lumière Matière Lyon 1

MAHLER Benoît

Chargé de Recherches, Institut Lumière Matière Lyon 1

Rapporteur

Rapporteure

Examinatrice

Examinatrice

Examineur

Directeur de thèse

Co-Directeur de thèse

Université Claude Bernard – LYON 1

Administrateur provisoire de l'Université	M. Frédéric FLEURY
Président du Conseil Académique	M. Hamda BEN HADID
Vice-Président du Conseil d'Administration	M. Didier REVEL
Vice-Président du Conseil des Etudes et de la Vie Universitaire	M. Philippe CHEVALLIER
Vice-Président de la Commission de Recherche	M. Jean-François MORNEX
Directeur Général des Services	M. Pierre ROLLAND

COMPOSANTES SANTE

Département de Formation et Centre de Recherche en Biologie Humaine	Directrice : Mme Anne-Marie SCHOTT
Faculté d'Odontologie	Doyenne : Mme Dominique SEUX
Faculté de Médecine et Maïeutique Lyon Sud - Charles Mérieux	Doyenne : Mme Carole BURILLON
Faculté de Médecine Lyon-Est	Doyen : M. Gilles RODE
Institut des Sciences et Techniques de la Réadaptation (ISTR)	Directeur : M. Xavier PERROT
Institut des Sciences Pharmaceutiques et Biologiques (ISBP)	Directrice : Mme Christine VINCIGUERRA

COMPOSANTES & DEPARTEMENTS DE SCIENCES & TECHNOLOGIE

Département Génie Electrique et des Procédés (GEP)	Directrice : Mme Rosaria FERRIGNO
Département Informatique	Directeur : M. Behzad SHARIAT
Département Mécanique	Directeur M. Marc BUFFAT
Ecole Supérieure de Chimie, Physique, Electronique (CPE Lyon)	Directeur : Gérard PIGNAULT
Institut de Science Financière et d'Assurances (ISFA)	Directeur : M. Nicolas LEBOISNE
Institut National du Professorat et de l'Education	Administrateur Provisoire : M. Pierre CHAREYRON
Institut Universitaire de Technologie de Lyon 1	Directeur : M. Christophe VITON
Observatoire de Lyon	Directrice : Mme Isabelle DANIEL
Polytechnique Lyon	Directeur : Emmanuel PERRIN
UFR Biosciences	Administratrice provisoire : Mme Kathrin GIESELER
UFR des Sciences et Techniques des Activités Physiques et Sportives (STAPS)	Directeur : M. Yannick VANPOULLE
UFR Faculté des Sciences	Directeur : M. Bruno ANDRIOLETTI

*« Les savants des temps passés et des nations révolues n'ont cessé de composer des livres.
Ils l'ont fait pour léguer leur savoir à ceux qui les suivent.
Ainsi demeurera vive la quête de la vérité. »*

*« The scholars of times past and nations bygone have never ceased to compose books.
They did it to bequeath their knowledge to those who follow them.
So the quest for the truth will remain alive. »*

Al Khawarizmi

Acknowledgements

Ces trois années de doctorat auront été les plus marquantes de ma vie, riches en enseignements professionnels, scientifiques et personnels. Pour tout cela je tiens à remercier toutes les personnes ci-dessous pour m'avoir aidée à mener à bien ce beau projet:

Merci à mes directeurs de thèse Christophe Dujardin pour m'avoir fait confiance dans ce projet ainsi que pour son accompagnement et ses précieux conseils, et Benoît Mahler sans qui beaucoup de choses n'auraient pas pu se faire. Merci pour ta patience et ton amitié.

Merci aux partenaires du projet EFIGY qui ont permis à cette étude de voir le jour et de m'avoir fait confiance dans cette tâche. Je tiens tout particulièrement à remercier monsieur Patrice Vincent pour sa sympathie et son soutien.

Je remercie tout le laboratoire Institut Lumière Matière, tous ses services ainsi que tous ses membres, en commençant par la direction avec, à sa tête, monsieur Philippe Dugourd et les directeurs adjoints Loïc Vanel, Anne-Marie Jurdyc et Brigitte Prével. A cela je souhaiterais également citer Delphine Kervella, Dominique Farjot et Véronique Chavret pour leur aide et leur disponibilité.

Plusieurs aspects de mon travail ont nécessité de faire appel aux différents services du laboratoire notamment le service mécanique en les personnes de Jean-François Sevignon, Yann Guillin et Valentin Menu qui, au-delà de leur aide d'un point de vue technique, m'ont incluse dans leurs rires. Je remercie également le service électronique qui a supporté mes incessants va-et-vient lors de mes premiers mois de thèse et le service informatique pour son efficacité et sa réactivité.

L'équipe Luminescence m'a adoptée durant 3 années et s'est toujours montrée présente. Je tiens à chaleureusement remercier tous ses membres et à leur exprimer toute ma gratitude. Un grand merci à Gilles Ledoux et Julien Houel pour m'avoir accompagnée et aidée à avancer. Merci également à Amina Bensaleh pour nos discussions au cours desquelles on refaisait le monde!

Merci à tous mes compagnons de route: les stagiaires, doctorants et post-doctorants qui ont fait en sorte que cette aventure soit plus légère et m'ont permis de relâcher la pression. Merci à Justine Baronnier et Gaétan Laurens, à Arsène Chemin et Zhu Meng (mes compagnons de bureau), au trio d'exception Lionel Perrin, Ashkan Shahmanesh et Bhagyesh Purohit, à Austin Hubley, Max Gerin et Mariana Timm. Merci pour toutes les discussions que nous avons partagées, les tasses de cafés et de thé (et les gâteaux) qui ont été les témoins de nos échanges, merci pour tout ce que vous m'avez appris, pour votre bienveillance et votre amitié.

Pour finir, aucun mot n'est assez puissant pour remercier ma famille pour son amour sans limite, son soutien indéfectible et pour avoir toujours cru en moi. Merci à mes parents pour m'avoir toujours inspirée et été mes modèles. Merci à ma soeur pour m'avoir toujours protégée. Et merci à mon compagnon pour sa patience et sa compréhension.

Abstract

Elastico-MechanoLuminescence (EML), which is the phenomenon where luminescence is induced by elastic deformation of solids, has known an increasing interest these last few years. The study of composite materials ZnS:Cu/Mn-PDMS (polydimethylsiloxane) arose. Many devices are being developed from stretchable mechanoluminescent fibers, to wind-driven mechanoluminescent displays. However, the origin of this mechanism is not fully established. One of the models to explain EML invokes the self-recovery process of mechanoluminescence by the trap-depth reduction induced by piezoelectricity. Although this model is fairly well accepted, it is nevertheless contested by other authors who propose an alternative mechanism. In the case of a ZnS:Cu-PDMS composite material, it has been shown that triboelectricity is also suitable to explain this phenomenon of luminescence. This theory is supported by the fact that rigid matrix material, such as acryl resin, seem to extinguish the luminescence of ZnS:Cu upon loading.

The presented work discusses the different mechanisms of EML using two approaches. One is to evaluate a model material under stretch condition and analyse its optical response. The other is to synthesize different materials and test their efficiency against different structural and morphological parameters. Thus, various phosphors (piezoelectric or not) and heterostructures such as ZnS:Cu, ZnS:Mn, CaZnOS:Mn/Mn,Li are dispersed in PDMS-based matrixes and characterized upon various stretching conditions. The conclusions of these results lead to favour the triboelectricity model. This point highlights the importance of the surface of the microparticles. Thus, chemical surface treatments, such as coatings of silica SiO₂ or Teflon, make it possible to study the influence of the surface modification of the microparticles as well as to determine the interaction between the microparticles and the polymer. Indeed, the bond strength between these two elements plays a central role in the intensity of the light emitted during an elastic deformation. This approach helps to provide a better understanding of the phenomenon of elastic-mechanoluminescence and allowed us to propose a mechanism for activating EML and to establish a model applicable to the different materials we studied. We have been able to demonstrate that the weaker the interaction, the more intense the EML by highlighting elements observed under an optical microscope. These elements place triboelectricity as the sole mechanism responsible for EML. It helped make commercial microparticles effective, which makes it possible to consider expanding the range of phosphors for this application.

Context & Foreword

The textile industry seeks innovation and is always looking for new materials with efficient and inventive properties. In this context, smart textiles are booming and luminous clothing is gaining more and more interest.

The EFIGY (EFficient lumInous Glow Yarn) project, thanks to which the presented research was initiated, follows that path. It offers the possibility to explore optical properties that could be integrated directly into the textile itself. This research and development project carried by the innovation centre TECHTERA gathers different industrial collaborators and one laboratory:

Collaborator	Location	Role
Brochier Technologies (PME)	Villeurbanne (Rhône)	Project manager/ Weaving
SATAB (Group)	Saint-Just-Malmont (Haute-Loire)	Strap weaving
Blanchard (PME)	Saint Julien Boutières (Ardèche)	Grinding
JRC Reflex (PME)	Romans (Drôme)	Supplier of retroreflective additives
Massebeuf Textiles	Pont-de-Labeaume (Ardèche)	Grinding/Texturing
IFTH	Flaviac (Ardèche)	Coordinator/Spinning/ Compound
Institute of Light & Matter	Villeurbanne (Rhône)	Characterization/ Scientific monitoring

This goal's partnership is the following:

- Develop luminous additives for textiles,
- Develop phosphorescent multi-filament for security in transportation and buildings, sport & leisure activities (e.g. cyclist equipment) and for personal protective equipment (e.g. firefighter equipment) purposes as well,
- Develop retroreflective multi-filament for sport & leisure activities (high visibility),
- Develop mechanoluminescent multi-filament for smart textiles,
- Combine phosphorescent and retroreflective properties in a cloth with and without optical fibres.

ILM's role in this project was, on one hand, to establish the technical and functional specifications by monitoring the luminous additives for retro reflection and persistent luminescence; study the existing phosphors and verify their quality and understand the impact of different light sources on the efficiency of selected phosphors. On the other hand, it was important to implement an experimental protocol for the characterization of phosphorescent and retroreflective materials (glass beads), evaluate and test retroreflective yarns through luminance measurements. The first year of my PhD was mainly dedicated to the EFIGY project. I built an optical setup which excites different persistent phosphors with different wavelengths and measures their afterglow according to applicable standards. Retroreflective materials were studied as well with another setup and compared

to commercially available products that meet the norms. Moreover, each measured material (persistent luminescent and retroreflective) was also characterized using SEM and EDX. However, this study is not presented in this manuscript.

This project was mainly focused on providing scientific help on products which could be directly integrated to industry. Thanks to this, it was also possible to explore and investigate another topic more in depth: mechanoluminescence or ML. This type of luminescence is triggered when you apply a mechanical action like crushing, pressing, breaking or rubbing on a solid. Outside the spectrum of the EFIGY project of designing efficient systems and characterizing materials, studying ML has a great advantage from the scientific point of view and addresses a real physical problem: How exactly does it work?

The present manuscript focuses only on the research and work done on mechanoluminescence.

Contents

Acknowledgements	i
Abstract	iii
Context & Foreword	v
Contents	vii
List of Figures	xi
List of Tables	xix
Introduction	1
1 Conversion of mechanical energy into light	3
1.1 Luminescence	3
1.1.1 What is luminescence?	3
1.1.2 Types of luminescence	4
1.2 Mechanoluminescence	5
1.2.1 Introduction to mechanoluminescence	5
1.2.2 How ML understanding originates from EL	7
1.2.3 Mechanoluminescent materials	10
1.2.4 Elastico-mechanoluminescence EML	14
1.2.4.1 Definition and first approach	14
1.3 Mechanisms of Elastico-mechanoluminescence	14
1.3.1 Mechanism 1: Piezoelectrically induced trap-depth reduction	15
1.3.2 Mechanism 2: Detrapping of charge carriers by movement of dislocation	17
1.3.3 Mechanism 3: Triboelectricity-induced luminescence	17
1.3.4 Point of debate	18
1.3.5 EML applications	19
1.4 Objectives and challenges	21
2 A model study	23
2.1 The right materials	23
2.1.1 Doped ZnS phosphor	23
2.1.1.1 From paste to powder	24
2.1.1.2 Material characterization	25
2.1.1.3 Conclusion	27
2.1.2 Using different PDMSs	27
2.1.2.1 Polydimethylsiloxane	27
2.1.2.2 Experimenting with different brands of PDMS	31
2.1.2.3 Sample manufacture	34

2.1.2.4	Characterization of the composite material	35
2.1.3	Conclusion	36
2.2	EML experimental methods	37
2.2.1	Camera based setup	37
2.2.1.1	Setup description	37
2.2.1.2	EML results	38
2.2.1.3	Conclusion	40
2.2.2	Local measurement: optical fibre + PMT	40
2.2.2.1	Setup description	41
2.2.2.2	EML results: first observations	45
2.2.3	Conclusion	46
2.3	Conclusion & Discussion	48
3	Material Synthesis and Particle Coatings	49
3.1	Material Synthesis	50
3.1.1	Synthesis of $ZnS : Mn$	50
3.1.1.1	Microwave assisted method	50
3.1.1.2	Influence of synthesis parameters	52
3.1.1.3	Conclusion	58
3.1.2	Synthesis of doped $CaZnOS$	60
3.1.2.1	Calcium zinc sulphide $CaZnOS$	60
3.1.2.2	Solid state reaction method	64
3.1.2.3	Material Characterization	65
3.1.2.4	Influence of synthesis parameters	68
3.1.2.5	Conclusion	71
3.2	Other doped-ZnS phosphors	74
3.2.1	Material Selection	74
3.2.2	Phosphor characterization	75
3.2.2.1	502B: ZnS:Cu phosphor	75
3.2.2.2	512C: Al_2O_3 -coated ZnS:Cu phosphor	76
3.2.2.3	611C: Al_2O_3 -coated ZnS:Mn phosphor	76
3.2.3	Conclusion	78
3.3	Particle coatings	79
3.3.1	Aluminum oxide coating Al_2O_3	79
3.3.2	Silicon dioxide (SiO_2) coating	81
3.3.3	Tetrafluoroethylene TFE coating	83
3.3.4	Conclusion	83
3.4	Conclusion	85
4	Mechanism of elasto-mechanoluminescence	87
4.1	Elastico-mechanoluminescence of Gwent ZnS:Cu	88
4.2	When the EML models are put to the test	90
4.2.1	Piezoelectrically-induced trap-depth reduction	91
4.2.2	Triboelectricity-induced luminescence	92
4.2.3	Proposed mechanism	94
4.2.4	Alternative explication	95
4.2.5	Conclusion	95
4.3	Computer simulation of EML	95
4.3.1	Threshold force	95
4.3.2	Working principle of the computer simulation	96
4.4	Evolution of the EML signal	99
4.4.1	Evolution of the EML intensity	99

4.4.2	Impact of polymer ageing	100
4.4.2.1	Evolution of the S and R emissions	100
4.4.2.2	Mullins Effect	101
4.4.3	Conclusion	102
4.5	Influence of surface modifications	103
4.5.1	Silicon Dioxide coating SiO_2	103
4.5.2	Teflon coating	104
4.5.3	Conclusion	106
4.6	Influence of the Matrix on EML	107
4.6.1	RTV slow catalyst	108
4.6.1.1	Camera-based setup	108
4.6.1.2	Photomultiplier setup	110
4.6.1.3	Conclusion	111
4.6.2	Wacker Elastosil RT A/B	112
4.6.3	Conclusion	112
4.7	Conclusion & Discussion	114
5	Beyond Gwent Group material	115
5.1	Cu-doped materials	115
5.1.1	502B: uncoated ZnS:Cu phosphor	115
5.1.1.1	EML behaviour of 502B	116
5.1.1.2	EML behaviour of SiO_2 -coated 502B-ZnS:Cu	116
5.1.1.3	EML behaviour of teflon-coated 502B	118
5.1.1.4	Conclusion	118
5.1.2	512C ZnS:Cu coated with Al_2O_3 phosphor	119
5.1.2.1	EML behaviour of 512C-ZnS:Cu coated with Al_2O_3	119
5.1.2.2	EML behaviour of SiO_2 -coated 512C-ZnS:Cu coated with Al_2O_3	120
5.1.2.3	EML behaviour of teflon-coated 512C-ZnS:Cu coated with Al_2O_3	121
5.1.2.4	Conclusion	122
5.1.3	Conclusion on Cu-doped materials	122
5.2	Mn-doped materials	123
5.2.1	611C ZnS:Mn@ Al_2O_3 phosphor	123
5.2.2	ZnS:Mn microwave synthesis	124
5.2.3	CaZnOS:Mn,Li	126
5.2.4	Conclusion on Mn-doped materials	127
5.3	Conclusion & Discussion	128
	General Conclusion	129
	French Summary	133
	Résumé	133
	Contexte & Avant propos	134
	Introduction	136
	Chapitre 1: Convertir l'énergie mécanique en lumière	138
	Chapitre 2: Un système modèle	139
	Chapitre 3: Synthèses de Matériaux et Traitements de surface	140
	Chapitre 4: Mécanisme de l'élastico - mécanoluminescence	141
	Chapitre 5: Influence des traitements de surface	142
	Conclusion & Perspectives	143

CONTENTS

Bibliography

147

List of Figures

1.1	<i>Schematic diagram of the luminescence mechanism.</i>	3
1.2	<i>Classification of mechanoluminescence types. Adapted from[1]</i>	6
1.3	<i>Mechano-electro-optical triangle interactions and related effects. Adapted from[2]</i> .	7
1.4	<i>Structure of an AC-driven electroluminescent device.</i>	8
1.5	<i>(a) ML and EL spectra from the sample with $x=0.70$ excited by stress and AC electric field, (b) The ML and EL intensity dependencies on the Ca composition of $Ba_{1-x}Ca_xTiO_3:Pr$. Adapted from[3]. (c) Comparison of normalized ML and EL (1 kHz) spectra. Adapted from [4]</i>	9
1.6	<i>(a-b) EL spectra of ACEL sample under the lowest (50 Hz) and highest (1 kHz) frequency conditions, insets are photos of the EL for ACEL samples. (c) Photograph of a partially sliced ML composite enclosed by a ring holder. (d) ML spectra from the ML composites during gas flow at flow rates between $30 L min^{-1}$ and $80 L min^{-1}$. Adapted from [5]</i>	10
1.7	<i>(a) Structure of an electroluminescent panel, light is visible after AC input. (b) Electroluminescent samples (dimension 20 mm x 20 mm), without (left) and with current input (right).</i>	10
1.8	<i>Photographs of the Stretching-Releasing system. From [4]</i>	11
1.9	<i>Diffraction patterns of ZnS with crystal representations. Left, sphalerite (or cubic). Right: Wurtzite (or hexagonal)</i>	12
1.10	<i>Schematic energy level band diagram of Cu-doped and Mn-doped ZnS crystal. V_S Sulphur vacancy.</i>	13
1.11	<i>(a) Dependence of the EML intensity of $SrAl_2O_4:Eu,Dy$ phosphors on the number of repetitive pressings and effect of UV light irradiation (365 nm). From [6]. (c) Response of ZnS:Mn material to compression stress of 500 N. From [7]. (b-d) Stress and strain rate dependences of the EML intensity (Theoretical). From [8]</i> .	15
1.12	<i>Schematic diagram for the EML mechanism in ZnS:Mn nanoparticles when stress is applied. 1. Electron detrapping and moving to the CB - 2. Electron-hole recombination - 3. Energy transfer to Mn^{2+} ions and excitation of Mn^{2+} - 4. Light emission. Adapted from [9]</i>	17
1.13	<i>(a) Photographs of ZnS:Cu-PDMS and ZnS:Cu-Acryl resin composites under unloading and loading at 1 Hz. A thin band-type specimen was elongated up to 5 N in a tensile mode for ZnS:Cu-PDMS and a disc type specimen was compressed up to 500 N for ZnS:Cu-Acryl resin. (b) Plots of ML signal with an applied cyclic load for ZnS:Cu-PDMS composite. From[10]</i>	18
1.14	<i>Triboelectricity scale of oxide dielectric materials. Adapted from[11]</i>	19
1.15	<i>(a-c) Photographs obtained from the wind-driven ML. The inset of a partially sliced ML composite enclosed by a ring holder. (d) Schematic illustration of the set-up. (e) Photograph of the ML image showing the distribution of the ML emission in the vibrating rods. (f,g) Photographs of the patterned wind-driven ML. Adapted from [5]</i>	20

LIST OF FIGURES

1.16	(a) Schematic showing the ML fiber fabrication process adopting two approaches. (b) Schematic illustration of cross-sectioned ML fiber. SEM images of (c) +fiber and (d,e) ML fiber. (f) Photograph of manually stretched ML-emitting fiber.(g) ML-emitting fabric undergoing hand-stretching. From [12].(h-j) photographs of the mechanoluminescent fabrics based on mechanoluminescent fibers (h), ribbons (i) and dots (j); (k) photographs of the mechanoluminescent fabrics shown in (h-j) during the stretch and release process. Adapted from [13]	21
1.17	Various colors from ML response to lips corner (a), canthus (b), and cheek (c) muscle movements. From [14]	21
1.18	Visualization of dynamic pressure distributions.(a) Schematic illustration of the acquisition and processing system.(b) Visualization of pressure distributions generated by a stamp.(c) Visualization of dynamic pressure distributions generated from a handwriting.(d) 2D distribution of relative ML intensity.(e) The line profile of relative ML intensity.(f,g) Consecutive frames of the signing process.(h) Demonstrations of recording the signing habits with different forces. From [15]	22
2.1	Gwent Group electroluminescent kit. From left to right: green phosphor paste, dielectric paste, silver paste	24
2.2	Gwent phosphor from paste (left) to powder (right) after the washing process.	25
2.3	Characterization of the washed Gwent ZnS particles. (a,c) SEM images. (b) EDX analysis, presence of Zn, S, Al and O elements. (d) EDX mapping analysis. Detection of Zn, S, Al and O.	25
2.4	Images of Gwent ZnS:Cu particles under an optical microscope. (a) bright-field mode, (b) polarization mode.	26
2.5	(a) Photoluminescence spectrum, large emission band centered at 509 nm. (b) XRD diffractogram showing peaks corresponding to a hexagonal structure and few others belonging to the cubic phase.	26
2.6	Chemical structure of polydimethylsiloxane or PDMS, where n is the number of repeating $[\text{SiO}(\text{CH}_3)_2]$ units. From [16]	27
2.7	Hydrogen and vinyl terms crosslink in the presence of a platinum catalyst. From [17]	28
2.8	Peroxide curing process of PDMS. From [18]	29
2.9	Condensation curing process of PDMS. From [18]	29
2.10	Addition curing process of silicon rubber. From [18]	30
2.11	Formation of a Sn-O-Si complex with TEOS. From [19].	30
2.12	Transfer of hydrolyzed TEOS to hydroxy end group of PDMS chain and regeneration of the activated catalyst. From [19].	30
2.13	Polymerization of TEOS and regeneration of the activated catalyst. From [19].	31
2.14	Addition curing process. From [20]	33
2.15	Dip coating with PDMS of the samples. process.	34
2.16	Steps of sample making. From left to right: mixing the ZnS:Cu particles and the PDMS, degasing the sample, shaping the samples by pouring the mixture into a mould, and curing at room temperature.	35
2.17	Photographs of an EML sample under a 365 nm UV-light (left) and natural light (right). Sample dimensions: 70 mm x 10 mm x 0.7 mm	35
2.18	Characterization of an EML sample. (a) SEM image. (b) Photoluminescence spectrum for an excitation wavelength of 350 nm. Large emission band at 504 nm.	36
2.19	Photographs of an EML sample made of Gwent ZnS:Cu phosphor powder and Wacker Elastosil RT601 PDMS under elastic deformation performed by hand.	36
2.20	Schematic diagram and photographs of the camera-based stretching-releasing setup, front (left) and top (right) view.	37

2.21	Photographs of an EML sample made of ZnS:Cu Gwent phosphor powder and RTV67 PDMS under one cycle of elastic deformation (stretching and releasing).	38
2.22	Experimental curves of the EML response of the Gwent ZnS:Cu-PDMS composite material. Left, curve of the average brightness over time; inset: zoom of the curve. Right, curve of the recorded applied force on the sample over time; inset: zoom of the curve.	39
2.23	Experimental curves of the EML response of the Gwent ZnS:Cu-PDMS composite material.	39
2.24	Experimental EML results at constant applied force of 10 N on the Gwent ZnS:Cu-PDMS composite material. Left, EML response curve. Right, applied force curve.	40
2.25	Schematic diagram of the photomultiplier-based stretching-releasing setup.	41
2.26	Amplitude response of the detector depending on the movement of the actuator.	43
2.27	Curve of the EML response of the Gwent ZnS:Cu-PDMS composite material. Number of emitted photons per second as a function of time.	45
2.28	Zoom in the curve of the EML response. Number of emitted photons per second for two periods (left: beginning, right: after 2h of cycling).	46
3.1	Synthesis steps of Mn-doped ZnS nanoparticles using a microwave reactor.	51
3.2	Steps of the synthesis of Mn-doped ZnS microparticles.	52
3.3	Emission spectra centered at 584 nm of μ waved ZnS nanoparticles synthesized at different reaction times (5 min, 10 min and 5 hours) at an excitation wavelength of $\lambda_{ex} = 340$ nm. Right, normalized spectra. np: nanoparticles.	52
3.4	TEM images showing ZnS nanoparticles for different reaction times. Bottom, zoom of the particles.	53
3.5	Superposition of XRD diffractograms of ZnS nanoparticles synthesized at different reaction times (5 min, 10 min and 5 hours) showing cubic crystal structure. np: nanoparticles.	53
3.6	Images of ZnS:Mn pellets synthesized at different doping percentages before (left) and after (right) sintering 3h at 900° C.	54
3.7	Emission spectra of ZnS:Mn synthesized at different doping percentages at an excitation wavelength of $\lambda_{ex} = 340$ nm before sintering. Right, normalized spectra centered at 585 nm.	55
3.8	Emission spectra of ZnS:Mn synthesized at different doping percentages at an excitation wavelength of $\lambda_{ex} = 340$ nm after sintering 3h at 900° C. Right, normalized spectra centered at 579 nm.	56
3.9	SEM images of ZnS:Mn powders synthesized at different doping percentages after sintering 3h at 900° C.	56
3.10	SEM images of ZnS:Mn particles at 1% doping sintered 3h at different temperatures (900° C, 1000° C and 1100° C).	57
3.11	Emission spectra of ZnS:Mn particles at 1% doping sintered 3h at different temperatures (900° C, 1000° C and 1100° C) at $\lambda_{ex} = 340$ nm. Right: normalized spectra.	57
3.12	XRD diffractograms of ZnS:Mn powder at 1% doping sintered 3h at different temperatures. (a) 900° C, (b) 1000° C and (c) 1100° C.	58
3.13	Crystal structure of CaZnOS. From [21]	60
3.14	(a) and (b) SEM images of $CaZn_{0.99}Mn_{0.01}OS$ and of $Ca_{0.97}Li_{0.06}Zn_{0.99}Mn_{0.01}OS$, respectively. (c) Photo-excitation and emission spectra of $CaZn_{0.99}Mn_{0.01}OS$ and $Ca_{0.97}Li_{0.06}Zn_{0.99}Mn_{0.01}OS$. From [22].	62
3.15	Photographs of $CaZn_{1-x}Mn_xOS$ ($x = 0, 0.001, 0.002, 0.003, 0.004, 0.005, 0.01, 0.02, 0.03, 0.04, 0.06, 0.08, \text{ and } 0.1$): (a) in daylight and (b) under 254 nm UV lamp. (c-d) Normalized PL spectra of $CaZn_{1-x}Mn_xOS$ under 282 nm excitation source. (e) Enlarged PL spectra, showing the red shift. From [23]	62

LIST OF FIGURES

3.16	<i>ML spectra of CaZnOS doped with: a) Pr³⁺, b) Ho³⁺, c) Er³⁺, d) Dy³⁺, e) Sm³⁺, f) Eu³⁺, g) Tm³⁺, h) Nd³⁺, and i) Yb³⁺. Inset: photographs of the corresponding samples under single-point dynamic pressure of a ballpoint pen. From [24]</i>	63
3.17	<i>Schematic diagram of the elasto-mechanoluminescence (EML) mechanism of CaZnOS:Mn²⁺, Nd³⁺. CB: conduction band, VB: valence band. The electronic energy level of Mn²⁺ ions is deep under the VB, but is drawn beside the band diagram. From [25]</i>	64
3.18	<i>Synthesis of CaZnOS:Mn by solid state reaction.</i>	65
3.19	<i>SEM images of CaZn_{0.99}Mn_{0.01}OS in (a) and Ca_{0.97}Li_{0.06}Zn_{0.99}Mn_{0.01}OS in (b) synthesized by solid state reaction and sintered 3 hours at 1100° C in argon atmosphere.</i>	65
3.20	<i>Optical microscope images of Ca_{0.97}Li_{0.06}Zn_{0.99}Mn_{0.01}OS in bright-field mode (a) and crossed polarization (b).</i>	66
3.21	<i>Excitation and photoluminescence spectra of CaZnOS:Mn and CaZnOS:Mn,Li. Sintering conditions: 1100° C for 3h, argon atmosphere.</i>	67
3.22	<i>Top: XRD diffractograms of CaZnOS:Mn ((a)) and CaZnOS:Mn,Li ((b)). Sintering conditions: 1100° C for 3h in argon atmosphere. Bottom: XRD references corresponding to the CaZnOS phosphors.</i>	67
3.23	<i>Photographs of CaZnOS:Mn powders at different doping percentages (0.1%, 0.2%, 0.6%, 2%, 6% and 10%) sintered 3h at 1100° C under a 256 nm UV light.</i>	69
3.24	<i>Emission spectra of CaZnOS:Mn at different doping concentrations (0.1%, 0.2%, 0.6%, 2%, 6% and 10%) sintered 3h at 1100° C upon an excitation of λ_{ex} = 280 nm.</i>	69
3.25	<i>Emission spectra of CaZnOS:Mn 0.6% (right), 2% (left) sintered 3h at 1100° C (argon atmosphere) upon an excitation λ_{ex} spanning from 250 nm to 350 nm.</i>	70
3.26	<i>XRD diffractograms of CaZnOS:Mn powders at different doping percentages (1%, 2%, 6% and 10%) sintered 3h at 1100° C, argon atmosphere.</i>	70
3.27	<i>SEM images of CaZnOS:Mn powders at 1% doping synthesized via solid state reaction at different sintering temperatures, 1100° C, 1200° C and 1300° C for 3 hours in an argon atmosphere.</i>	72
3.28	<i>(a-c) XRD diffractograms and (d) Emission spectra at an excitation wavelength λ_{ex} = 280 nm of CaZnOS:Mn powders at 1% doping synthesized via solid state reaction at different sintering temperatures, 1100° C, 1200° C and 1300° C.</i>	73
3.29	<i>Characterization of 502B commercial ZnS:Cu particles. (a) SEM image. (b) EDX analysis. (c) Emission spectrum, band peaking at 484 nm, under excitation wavelength λ_{ex} = 360 nm. (d) XRD diffractogram.</i>	75
3.30	<i>Optical microscope images of ZnS:Cu 502B particles using bright-field mode (a) and crossed polarization (b).</i>	76
3.31	<i>Characterization of commercial 512C particles: Al₂O₃-coated ZnS:Cu. (a) SEM image. (b) EDX analysis. (c) Emission spectrum, band peaking at 500 nm, under excitation wavelength λ_{ex} = 360 nm. (d) XRD diffractogram.</i>	77
3.32	<i>Optical microscope images of ZnS:Cu 512C particles using bright-field mode (a) and crossed polarization (b).</i>	77
3.33	<i>Characterization of commercial 611C Al₂O₃-coated ZnS:Mn. (a) SEM image. (b) EDX analysis. (c) Emission spectrum, band at 585 nm, excitation wavelength λ_{ex} = 360 nm. (d) XRD diffractogram.</i>	78
3.34	<i>EDX mapping analysis of ZnS:Cu particles coated with aluminium oxide Al₂O₃. Detection of Zn, S, O and Al.</i>	80
3.35	<i>XRD diffractograms of Al₂O₃-coated ZnS:Cu 502B (a) and Al₂O₃ (b).</i>	81
3.36	<i>XRD diffractograms of boehmite. From the American Mineralogist Crystal structure Database.</i>	81

3.37	SEM image and EDX analysis of ZnS:Cu particles (512C) coated with silicon dioxide SiO ₂ . Detection of Zn, S, O, Al and Si.	82
3.38	EDX mapping analysis of ZnS:Cu particles (512C) coated with silicon dioxide SiO ₂ . Detection of Zn, S, O, Al and Si.	82
3.39	Chemical structure of the 1H, 1H, 2H, 2H – Perfluorooctyltriethoxysilane purchased from Sigma Aldrich [26].	83
3.40	Diffractiongram of the ZnS:Cu 502B coated with tetrafluorosilane.	84
4.1	Elastico-mechanoluminescent response of Gwent ZnS:Cu material. (a) Whole response. (b-c) Close-ups taken from the beginning (b), around 200 s, and the end (c), around 5000 s, of the signal. (d-e) EML intensity of one S-R cycle (in black) accompanied by the displacement curve (in red) at around 200 s (d) and 5000 s (e) of the experiment.	89
4.2	Elastico-mechanoluminescence of Gwent ZnS:Cu as a function of the displacement drawn from data taken at 200 s (a) and 5000 s (b).	90
4.3	Elastico-mechanoluminescence of Gwent ZnS:Cu over one S-R cycle. 1, 2, 3: emission phases.	90
4.4	Images of the composite material under an optical microscope. (a) Sample at rest, (b) 65% stretching, (c) Close up on a single particle during a 65% deformation, (d) Schematic diagram of a single particle (in green) in a polymer matrix (in grey) at 65% stretching.	92
4.5	Elastico-mechanoluminescent response of the Gwent ZnS:Cu material at variable applied deformation.	93
4.6	Band diagrams of the Gwent ZnS:Cu@Al ₂ O ₃ - PDMS sample for the stretching (left) and releasing phases (right). VB: Valence Band. CB: Conduction Band.	94
4.7	EML intensity of Gwent ZnS:Cu of one S-R cycle (in black) accompanied by the displacement curve (in red) at around 200 s of the experiment.	96
4.8	Schematic of a creation of a vacuum pocket after a threshold force (or deformation).	96
4.9	Stretching emission for different values of D _{th} . Simulated data.	97
4.10	(a) Histogram of the distribution of the deformation threshold D _{th} for 10.000 particles. (b) EML signal during the unsticking. Simulated data.	98
4.11	Comparison of the elastico-mechanoluminescent response of Gwent ZnS:Cu material through one stretching-releasing cycle taken from the beginning (in black) and the end (in blue) of the experiment.	98
4.12	Decay curves of the Gwent ZnS:Cu@PDMS sample. Excitation at 470 nm (in red) and 517 nm (in black).	98
4.13	EML intensity as a function of the displacement for Gwent ZnS:Cu: experimental results in black dots, computer simulation results in red.	99
4.14	Top: Elastico-mechanoluminescent response of the Gwent ZnS:Cu material. Bottom: (a-c) optical microscope images of the composite material taken at different times of the experiment: beginning (0s), middle (1500s) and end (4500s), respectively.	100
4.15	Elastico-mechanoluminescence of Gwent ZnS:Cu at 200 s and 5000 s of the stretching-releasing experiment, (a) and (b) respectively. EML intensity as a function of the displacement at 200 s (c) and 5000 s (d) of the experiment.	101
4.16	Comparison of the elastico-mechanoluminescent response of the Gwent ZnS:Cu material through one stretching-releasing cycle taken from the beginning (in black) and the end (in blue) of the same experiment.	102
4.17	The idealised behaviour of stress-softening in rubber. From [27]	102
4.18	Elastico-mechanoluminescence response of the Gwent@SiO ₂ sample using the PMT-based setup. (a) whole response as a function of time. Close ups at the beginning (b) and at the end (c) of the signal, respectively.	104

LIST OF FIGURES

4.19	<i>Elastico-mechanoluminescence response of the Gwent@SiO₂ sample using the PMT-based setup as a function of the displacement. Plots of the beginning (a) and the end (b) of the signal.</i>	104
4.20	<i>Light intensity as a function of the displacement of Gwent@SiO₂: experimental result in black dots, computer simulation result in red.</i>	105
4.21	<i>Elastico-mechanoluminescence response of the Gwent@teflon sample using the PMT-based setup. (a) whole response as a function of time. Close ups from the beginning (b) and the end (c) of the signal.</i>	105
4.22	<i>Elastico-mechanoluminescence response of the Gwent ZnS:Cu@teflon (TF) sample using the PMT-based setup as a function of the displacement. Plots from the beginning (a) and the end (b) of the experiment.</i>	106
4.23	<i>Light intensity as a function of the displacement of Gwent@teflon: experimental result in black dots, computer simulation result in red.</i>	107
4.24	<i>Elastico-mechanoluminescence response of the Gwent/RTV-SC sample using the camera-based setup. (a) whole response. (b-c) close ups at the beginning (b) and at the end (c) of the signal.</i>	109
4.25	<i>Successive images of Gwent ZnS:Cu/PDMS-SC extracted from a film during an EML experiment (top). Average brightness as a function of time, one S-R cycle (bottom).</i>	109
4.26	<i>Elastico-mechanoluminescence response of the Gwent/RTV-SC sample using the PMT-based setup. (a) whole response. Close ups at the beginning (b) and at the end (c) of the signal.</i>	110
4.27	<i>Elastico-mechanoluminescence response of the Gwent/RTV-SC sample using the PMT-based setup. (a) Superimposition of two S-R responses (black and blue). (b) and (c) S-R response with a displacement curve (in red) taken from the beginning and the end of the signal, respectively.</i>	111
4.28	<i>EML response as a function of the displacement of Gwent/RTV-SC. Drawn from data in figure 4.26 (b-c).</i>	112
4.29	<i>Elastico-mechanoluminescence response of the Gwent/Elastosil sample using the PMT-based setup. (a) whole response. Close ups at the beginning (b) and at the end (c) of the signal.</i>	113
4.30	<i>(a) and (b) Elastico-mechanoluminescence response of the Gwent/Wacker-Elastosil sample using the PMT-based setup with the displacement curve in red, at 54 s and 392 s of the experiment, respectively.</i>	113
5.1	<i>Elastico-luminescent response of 502B ZnS:Cu. (a) whole response. (b) and (c) close-ups taken from the beginning and the end of the experiment, respectively. (d) one S-R cycle (in black) and the displacement curve (in red) taken from (b).</i>	116
5.2	<i>Elastico-luminescent response of SiO₂-coated 502B ZnS:Cu. (a) whole response (in black) compared to un-coated 502B (in blue). (b) close-up. (c) one S-R cycle of 502B@Si₂ (in black), un-coated 502B (in blue) and the displacement curve (in red). (d) EML intensity as a function of the displacement, experimental (black dots) and computer simulation results (red). (b), (c) and (d) data taken at 6500 s of the experiment.</i>	117
5.3	<i>Elastico-luminescent response of teflon-coated 502B ZnS:Cu. (a) whole response (in black) compared to un-coated 502B (in blue). (b) close-up. (c) one S-R cycle of 502B@TF (in black), un-coated 502B (in blue) and the displacement curve (in red). (d) EML intensity as a function of the displacement, experimental (black dots) and computer simulation results (red). (b), (c) and (d) data taken at 6500 s of the experiment.</i>	118

5.4	<i>Elastico-luminescent response of 512C (ZnS:Cu@Al₂O₃) (a-c), compared to Gwent (ZnS:Cu@Al₂O₃) (d-f). (a),(d) whole response. (b),(e) close-ups taken from the end of each the experiment. (c),(f) EML intensity as a function of the displacement, experimental (black dots) and computer simulation results (red).</i>	120
5.5	<i>Elastico-luminescent response of SiO₂-coated 512C (ZnS:Cu@Al₂O₃). (a) whole response (in black) compared to un-coated 512C (in blue). (b) close-up.(c) EML intensity as a function of the displacement, experimental (black dots) and computer simulation results (red). (b) and (c) data taken from the end of the experiment.</i>	121
5.6	<i>Elastico-luminescent response of teflon-coated 512C (ZnS:Cu@Al₂O₃). (a) whole response (in black) compared to 512C@SiO₂ (in blue). (b) close-up. (c) EML intensity as a function of the displacement, experimental (black dots) and computer simulation results (red). (b) and (c) data taken from the end of the experiment.</i>	122
5.7	<i>Elastico-luminescent response of 611C (ZnS:Mn@Al₂O₃). (a) whole response. (b) close-up taken from the end of the experiment. (c) EML intensity as a function of the displacement, experimental (black dots) and computer simulation results (red).</i>	124
5.8	<i>Elastico-luminescent response of synthesized ZnS:Mn.</i>	125
5.9	<i>Elastico-luminescent response of synthesized ZnS:Mn. (a) whole response. (b) close-up taken from the beginning of the experiment. (c) one S-R cycle (in black) and the displacement curve (in red).</i>	125
5.10	<i>Elastico-luminescent response of CaZnOS:Mn,Li@TF. (a) whole response. (b) close-up taken from the beginning of the experiment. (c) one S-R cycle (in black) with the displacement curve (in red).</i>	127

List of Tables

1.1	<i>Table of luminescence types. Adapted from [1]</i>	5
1.2	<i>Mechanoluminescent compounds and their properties. Piezo: - non piezoelectric, + piezoelectric. Adapted from [28]</i>	11
2.1	<i>Sylgard 184 PDMS curing time as a function of temperature. From [29]</i>	32
2.2	<i>Properties of Sylgard 184 PDMS cured 4 hours at 65° C. From [29]</i>	32
2.3	<i>Wacker Elastosil RT601 A/B PDMS curing time as a function of temperature. From [30]</i>	33
2.4	<i>Properties of Wacker Elastosil RT601 PMDS cured 30 min at 150 °C in a circulating air oven, 23° C. From [30]</i>	33
2.5	<i>Properties of Esprit Composite RTV67 PMDS cured at room temperature. From [31]</i>	34
2.6	<i>Preliminary EML results over PDMS efficiency. The percentages are compared to the length of the sample at rest. *hand stretching. **from hand stretching, eye perception. ***from finger pressure, eye perception</i>	35
2.7	<i>Experimental parameters of the camera-based S-R setup.</i>	38
2.8	<i>Conversion table from SMAC actuator values to SI values.</i>	44
3.1	<i>ML and PL properties in RE³⁺ doped CaZnOS. From [32]</i>	63
3.2	<i>Table of the phosphors purchased from Shanghai Keyan Phosphor Technology Co.,Ltd. (KPT) and their given properties.</i>	74
3.3	<i>Table of the quantities of the materials used in a Stöber process.</i>	81
3.4	<i>Table of the studied phosphor materials and the implemented coatings.</i>	84
4.1	<i>Values of MeanD_{th} obtained from computer simulations for Gwent ZnS:Cu, Gwent@SiO₂ and Gwent@TF. S: stretching, R: releasing.</i>	107
5.1	<i>Summary table of Values of MeanD_{th} and EML intensities of the Cu-doped materials. *: photons/10ms</i>	123

Introduction

Man has always sought to escape the darkness. He discovers fire and venerates a star which lavishes light and heat on him. This notion is so important that it is found in the book of Genesis 1:3 "*And God said, "Let there be light," and there was light"*". From flint to switch, we seek that glow, and although understanding it today seems commonplace, there are still certain phenomena of light that elude us.

For example, a simple piece of sugar is capable of emitting light upon fracture. How can it be? In 1605, Francis Bacon first reported this phenomenon in his book "The Advancement of Learning"; he wrote: "*It is not the property of fire alone to give light ... loaf-sugar in scraping or breaking*" [33]. This new discovery paved the way to what is called today **mechanoluminescence**. This word is composed of *mechano-*, which means mechanical and *-luminescence* which originates from the latin word *lumen* meaning "light". In other words, mechanoluminescence describes a phenomenon in which a solid emits light when a mechanical action is applied on it. Afterward, this phenomenon was observed in a large number of materials which led to a wider classification of these compounds. Because each ML material can be triggered differently and depends on different parameters, this classification was necessary. It was first introduced by *Chandra et al.* in 1995 [34]. That is how two main types emerged: the first one is Deformation-ML (DML), which can also be subcategorised to fracto-ML, plastico-ML and elastico-ML. The second one is Tribo-ML (TML) in which we find ML triggered by chemical reaction, electrification or thermal effect. In the first type (DML), the luminescence depends on the material itself whereas in the second (TML), the luminescence depends on the nature of the material under deformation as well as on the material used to produce it. Although all these phenomena require a deeper understanding, there is one that stood out: **elastico-mechanoluminescence (EML)**. Unlike the other categories of ML, EML exhibits self-recovery properties. An elastic deformation can be applied on such material, and light is emitted. This light can be restored and released again upon a second deformation, a third, and so on. Moreover, the non-destructive nature of EML materials allowed researchers to design new devices and technologies that are less energy consuming than traditional electrically-powered devices.

Generally, EML devices comprise an emitting phosphor, typically a doped zinc sulphide (ZnS), embedded in a soft matrix, such as polydimethylsiloxane (PDMS). An elastic deformation can be performed through different ways. The EML can be generated by pressure [15], air flow [5], human motion [12], facial expressions [14], and stretching and releasing [4]. The luminescence is recorded by a spectroradiometer which is able to measure both the wavelength and amplitude of the emitted light. These flexible devices can be used as pressure, fracture and impact sensors.

The literature abound on EML devices, however, the origin of this mechanism is not fully established. Alongside the ML classification, *Chandra et al.* proposed an EML model invoking the self-recovery process of mechanoluminescence by the trap-depth reduction induced by piezoelectricity. It is based on the idea that piezoelectricity is triggered by the deformation of crystalline structures and generates an internal electric field,

which helps the release of trapped charge carriers (electrons and holes). This explanation is offered in the case of $\text{SrAl}_2\text{O}_4:\text{Eu,Dy}$ [35] and $\text{ZnS}:\text{Mn}$ [36] phosphors. These two materials are largely used for EML applications, but they display very different behaviours. $\text{SrAl}_2\text{O}_4:\text{Eu,Dy}$ is a persistent luminescent phosphor which requires UV-irradiation to restore its luminescence. $\text{ZnS}:\text{Mn}$, on the other hand, does not. Despite this divergence, Chandra's model seem to be applied for both. That is one of the elements that led other scientists to question this model, and an alternative mechanism was proposed. In the case of a $\text{ZnS}:\text{Cu}$ -PDMS composite material, it has been shown that triboelectricity [10] is also suitable to explain this phenomenon. Triboelectricity results from the friction or the separation of two surfaces from two dissimilar materials, thus, creating electric charges on both materials. But which of the two models really explains EML?

This research work was achieved with those elements in mind with a central question being: What is the most inclusive mechanism we can propose to explain EML? For this study, the chosen candidate is copper-doped zinc sulfide ($\text{ZnS}:\text{Cu}$) powder incorporated in a PDMS polymer. This material is well documented and is reported to exhibit the brightest light upon elastic deformation. The first objective is to understand the behaviour of that composite material. It is done through sample fabrication, characterization, implementation of a measurement setup and computer simulations. The second one is to optimize the phosphor to increase the light intensity by chemical modifications of the particles themselves, and control their efficiency. As third objective, we want to synthesize and develop other phosphors.

1. The first chapter is dedicated to the state of the art and theoretical aspects of mechanoluminescence. Elastico-mechanoluminescence is detailed with the different applications and devices designed until now, accompanied by the proposed EML models. Our main material, namely doped zinc sulphide, is also presented.
2. The second one discusses the experimental study of $\text{ZnS}:\text{Cu}$, characterizing it and then producing the first samples and testing them with a stretching and releasing device in order to study the optical behaviour. Our system being made of two main materials (phosphor and polymer), more fundamental aspects of the PDMS are presented.
3. The third chapter is dedicated to the chemical tools at our disposal for the synthesis and optimization of phosphor materials. Chemical protocols of the synthesis of $\text{ZnS}:\text{Mn}$, $\text{CaZnOS}:\text{Mn}/\text{Mn,Li}$ and three particle coatings are presented: silicon oxide SiO_2 , aluminium oxide Al_2O_3 and teflon. Moreover, other purchased zinc sulphide materials ($\text{ZnS}:\text{Mn}$ and $\text{ZnS}:\text{Cu}$) are introduced alongside their chemical, spectral, morphological and optical characterizations.
4. The fourth chapter offers an interpretation of the elastico-mechanoluminescent behaviour of $\text{ZnS}:\text{Cu}$ during deformation (stretching-releasing). The impacts of the polymer matrix and the surface conditions of the phosphor microparticles are also studied. Computer simulations and optical microscope observations shaped our understanding of the phenomenon and thankfully, these elements allowed us to modify the luminescence, either increase it or decrease it.
5. Finally, in the fifth chapter, the experimental results of other phosphors are displayed, namely, $\text{ZnS}:\text{Mn}$ and $\text{CaZnOS}:\text{Mn,Li}$.

Chapter 1

Conversion of mechanical energy into light

In this chapter, I will present the relevant elements to comprehend what is behind the topic of mechanoluminescence (ML). From basic concepts of luminescence to existing theoretical models of elastically-mechanoluminescence (EML), I will introduce the most common ML compounds and present some possible applications. These various aspects help us mould our understanding of the current state of this study and question it.

1.1 Luminescence

We will review here the concept of luminescence, its basic principles and types depending on the excitation tool. Moreover, we present the different recombination mechanisms involved in this phenomenon.

1.1.1 What is luminescence?

Luminescence is the phenomenon in which electronic states of solids are excited by some energy from an external source and the excitation energy is released as light. It is referred to as "cold emission of light". The relaxation of electrons from a high energy state (excited state) to a lower energy state results often in the release of energy as electromagnetic radiation or light [1].

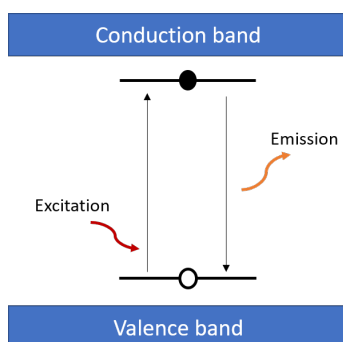


Figure 1.1: *Schematic diagram of the luminescence mechanism.*

Luminescence comprises two main steps:

1. Excitation energy absorption,

2. Light emission.

An electron-hole pair is created after a crystalline structure absorbs energy from ionizing radiation. If this energy is sufficient, an electron can move from the Valence Band (VB), across the band gap and jump to the Conduction Band (CB). There, it can move freely in the crystal. In the same way, a hole in the VB can also move freely. The electron may either fall back to the VB because it lost its excitation energy and recombine with a hole, or get trapped in defects present in the crystal. We also find some of the holes getting trapped in other defects. When energy is given to the system, electrons may recombine with the holes which results in an emission of light. When the emission occurs during stimulation we say it is an "optically stimulated luminescence"[36].

The luminescent materials are called phosphors. They mostly are inorganic solids consisting of a host lattice doped with low concentration impurities. Energy absorption can take place by either the host or the doped impurity. The impurity ions are responsible for the emission and are also called activator ions when the desired emission is generated. A second kind of impurity can be added, called sensitizer, which absorbs the energy and transfers it to the activator. The energy transported by the lattice can also take place through: migration of electric charges (electrons, holes), migration of excitons (an electron-hole pair), resonance between atoms, or re-absorption of photons emitted by another activator ion or sensitizer [37]. Usually, the emission wavelength can be tuned by doping the appropriate impurity ions without changing the host lattice.

Luminescence can be divided into *intrinsic* and *extrinsic* luminescence (localized and unlocalized, respectively). Intrinsic luminescence can be also divided into [1]:

- Band-to-band luminescence: the recombination of an electron in the conduction band with a hole in the valence band,
- Exciton luminescence: the recombination of bond e^-h^+ pair,
- Cross-luminescence: recombination of an electron in the valence band with a hole created in the outermost core band.

Extrinsic luminescence occurs in doped phosphors. In the unlocalized type, the electrons and holes of the host, that is, free electrons in the conduction band and free holes in the valence band, participate in the luminescence process. In the case of the localized type, the luminescence excitation and emission processes are confined in a localized luminescent centre. Intrinsic luminescence of localized type are: donor-acceptor pair luminescence and luminescence owing to isoelectronic traps. Extrinsic luminescence of localized type are: luminescence of allowed transition-type (the $s \leftrightarrow p$, $s^2 \leftrightarrow sp$ and the $f \leftrightarrow d$ transitions) and luminescence of forbidden transition type ions ($d \leftrightarrow d$ and $f \leftrightarrow f$ transitions) [1].

1.1.2 Types of luminescence

Luminescence can originate from different kinds of energy sources. When electrons are excited by electromagnetic radiations it gives rise to what is called photoluminescence in which we find fluorescence and persistent luminescence (also known as phosphorescence) which is found in cathode ray applications. After UV-irradiation, the electrons present in the ground state will go up to an excited state. Light emission occurs when the electrons, by de-excitation, return to the ground state (cf. figure 1.1). The population of the excited state will decrease exponentially with time. A rapid time response corresponds to fluorescence, its lifetime is about few nanoseconds. Whereas, in the case of persistent luminescence, the decrease is long and its lifetime can last few milliseconds up to several hours. This long light emission is due to the presence of intermediate states in

which electrons, or holes, are trapped. The photo-excited charge carriers are trapped as the optical excitation energy is stored in the lattice. $\text{SrAl}_2\text{O}_4:\text{Eu}$, Dy is one of the most known long afterglow phosphor. Dy acts as an intermediate reservoir which delays the emission of light. The Eu^{2+} ions are oxidized to Eu^{3+} and Dy^{3+} reduced to Dy^{2+} after optical excitation of Eu^{2+} . The delayed Eu^{2+} emission results from the thermal release of an e^- by Dy^{2+} to Dy^{3+} , followed by its capture by Eu^{3+} leading to Eu^{3+*} . This material can still emit visible light in the dark up to 24h. This type of phosphor is used in watches and safety applications like exit signs.

Even though this phenomenon is known since ancient history, it remained misunderstood for centuries. Before *Wiedemann* introduced the word luminescence, it was named phosphorescence regardless of its origin. It is only in the middle of the XIXth century that light emission (or photon emission) was comprehended, which led scientists to distinguish between the different forms of luminescence. Table 1.1 lists the other types of excitation that can trigger luminescence[1]:

Luminescence type	Mean of excitation
Photoluminescence	Short wavelengths
Cathodoluminescence	High energy electrons (cathode rays)
Ionoluminescence	Ion irradiation
Electroluminescence	Electric current
Thermoluminescence	Heating following absorption of energy (radiation)
Lyoluminescence	Dissolution in a liquid following irradiation
Sonoluminescence	Sound field
Bioluminescence	Biochemical process
Chemiluminescence	Chemical process
Mechanoluminescence	Mechanical action

Table 1.1: *Table of luminescence types. Adapted from[1]*

Except mechanoluminescence, the other kinds of luminescence were not further studied in this thesis.

1.2 Mechanoluminescence

Mechanoluminescence, or ML, is a type of luminescence triggered after a mechanical action. This section details this phenomenon from its discovery to nowadays. There are two kinds of ML, each one divided into three others. Our work was mainly focused on one of them: **elastico-mechanoluminescence or EML**. Many materials and compounds exhibit a mechanoluminescent behaviour and few exhibit EML. Some of these materials are presented in here and one of them is doped zinc sulphide which constitutes our main subject of study. EML has interested scientists for its remarkable property of converting mechanical action into light. They have designed several devices for applications in security, transportation, textile, etc. Being an intriguing phenomenon, they have also proposed theories to explain it.

1.2.1 Introduction to mechanoluminescence

Originally called Triboluminescence, mechanoluminescence describes the non-thermal light emission by a solid under a mechanical action like pressing, scratching, rubbing, cutting, compressing, grinding, cleaving, ultrasound, laser-generated shock wave,

crystallization, dissolution of crystals, wind, or shaking [1]. In 1605, Francis Bacon first reported this phenomenon in his book "**The Advancement of Learning**"; he wrote: "*It is not the property of fire alone to give light ... loaf-sugar in scraping or breaking*" [33]. He has discovered that sugar could emit light when crushed in the dark. This first statement paved the way to a new field of research that is still nowadays active. ML materials allow a large number of applications to emerge such as stress, crack or impact sensors which are used to test structures and materials like bridges, airplane wings or reinforced concrete, and monitor the crack propagation and stress distribution. Other fields like military and security benefit from this technology by detecting the passage of vehicles or soldiers, and producing counterfeiting inks. Also, other ML-based products can be found like t-shirts, balls and wrapping papers.

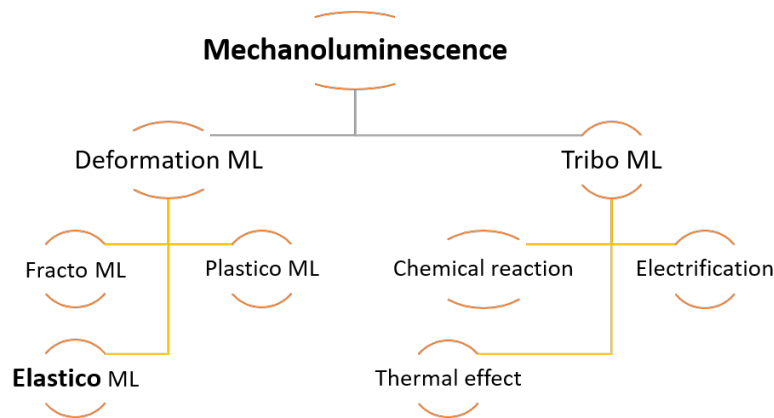


Figure 1.2: *Classification of mechanoluminescence types. Adapted from[1]*

Mechanoluminescence can be divided into two families depending on the involved physical process:

1. Deformation-ML (DML): depends only on the material under deformation and is independent of both the material used to produce the deformation and the contact phenomenon. For example: rubbing sugar or ZnS crystal with a rod; the luminescence is independent of the rod's nature. It is sometimes referred to as intrinsic luminescence as ML comes from the sample only.
2. Tribo-ML (TML): depends on the nature of the material under deformation as well as on the material used to produce it, and arises solely owing to contact phenomena. For example: separation of a tape from a substrate; it depends on the nature of the tape but also the substrate's.

As shown in figure 1.2, TML can also be sub-classified into three types: electrically-induced, chemically-induced and thermally-induced TML. We can sub-categorise DML into three types:

- Fracto-ML (FML): luminescence is produced during the fracture of solids (piezoelectric materials) due to the creation of new surfaces. Processes like Piezoelectrification, defective-phase piezoelectrification, charged dislocation movements, and

charged-defect barodiffusion produce charged surface during fractures. The charge carrier and ions produced neutralize the surface charge. As a result, light is emitted resembling a gas discharge or luminescence of a solid or even a combination of both. e.g. sucrose, tartaric acid and Rochelle salt exhibit FML resembling a gas discharge; coumarin and resorcinol exhibit FML like their photoluminescence (PL); while uranyl nitrate hexahydrate and saccharin (impure) exhibit FML resembling both a gas discharge and PL emission [1].

- **Plastico-ML (PML):** luminescence is produced under plastic deformation or an irreversible deformation where fracture is not needed. It results from mechanical or electrostatic interactions between crystal dislocations and defect centres or by electrification of crystal surfaces, e.g. crystals of colored alkali halides, certain non-colored alkali halides, II-VI compounds, alkaline-earth oxides, metals, and certain varieties of rubber.
- **Elastico-ML (EML):** luminescence is produced under elastic deformation or a reversible deformation where neither plastic deformation nor fracture are needed, e.g. single crystals x- or γ -irradiated alkali halides, lanthanide-doped inorganic salts like aluminates silicates, gallates or titanates[38]. Many of these materials are piezoelectric.

Despite this classification, some materials can exhibit several types of mechanoluminescence. For example, $\text{SrAl}_2\text{O}_4:\text{Eu}$, Dy can be FML, PML or EML depending on the strength of the imposed mechanical strain[37].

1.2.2 How ML understanding originates from EL

Some observations categorised as triboluminescence (TL), like splitting materials or rubbing crystals, arise from electroluminescence (EL) instead. Electroluminescence is used in lighting devices (e.g. light-emitting diodes) and electronic displays. In the case of piezoelectric materials, a difference in electric potential results from compression and causes a piezoelectric discharge. The ML mechanism can be electric in nature [38].

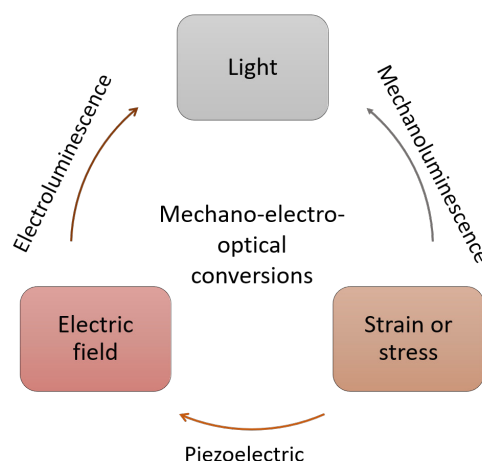


Figure 1.3: *Mechano-electro-optical triangle interactions and related effects. Adapted from[2]*

It is no surprise that scientists started associating ML to EL. ZnS powder is the most used material for alternating current electroluminescence (AC-EL) and its discovery dates back to 1936 by *George Destriau* while working on the conductivity of certain metal alloys. The AC-driven electroluminescent devices are made of electrodes, an emissive layer

(phosphor) and a single or multi layer of insulating dielectric, cf. figure 1.4. These devices can be divided into [39]:

- AC-driven thin film electroluminescence (AC-TFEL): the light emission is generated by the hot electron impact excitation mechanism. A hot electron (or hole) is an electron (or hole) which has gained a very high kinetic energy after being accelerated by a strong electric field in areas of high field intensities within a semiconductor. First, the injection of electrons at the interface into the phosphor layer under the AC electric field takes place. Second, the injected electrons are accelerated. Third, the luminescent centers are excited by the high-energy electrons impact. Finally, the optical transition of the excited energy levels in the luminescent centers takes place [39].
- AC-driven light-emitting (AC-LEDs),
- AC-driven light-emitting field effect diodes (AC-LEFETs), AC-LEDs and AC-LEFETs rely on the same mechanism. The light emission results from the radiative recombination of electrons in the emitting layer.

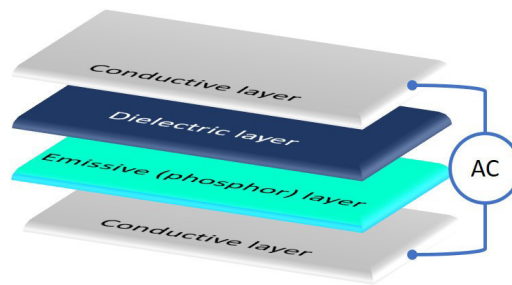


Figure 1.4: Structure of an AC-driven electroluminescent device.

Other types of EL exist, namely DC-power luminescence, AC-EL with evaporated or sputtered thin ZnS films (TFACEL), and DC-EL with injection luminescence[40]. But ACEL is the one that conquered the market because of its advantages over the others as explained below. The frequency used for thick film AC-EL is between 50 and 1000 Hz and the devices operate at voltages above 50 V. ZnS microparticles (ZnS:Cu,Cl, ZnS:Cu,Al, ZnS:Cu,Mn,Al and ZnS:Cu) can be subject to deterioration due to electrical driving conditions, like high applied frequency, and to environmental phenomena like humidity. That is why hermetic encapsulation ensures the durability of the phosphors like dense coatings of Al_2O_3 or SiO_2 on the microparticles achieved by Chemical Vapour Deposition (CVD). This element is particularly important as its role in the ML mechanism will further be discussed. We can note that some projects that study ML also implement EL measurements and samples. For example, the same ZnS phosphors can be used to fabricate EML and EL devices [5].

Based on the triangle figure 1.3 we find that some ML materials, like ZnS:Mn; ZnS:Cu/Cu,Mn; ZnS:Al,Cu/Al,Cu,Mn; SrAl_2O_4 :Eu; $(\text{Ba,Ca})\text{TiO}_3$:Pr; $\text{SrMg}_2(\text{PO}_4)_2$:Eu, display all three properties: piezoelectric, ML and EL.

To understand the triangular relationship between these elements, let us consider $(\text{Ba,Ca})\text{TiO}_3$:Pr. Zhang *et al.*[3] studied the diphasic $\text{Ba}_{1-x}\text{Ca}_x\text{TiO}_3$:Pr³⁺ over the range of $0.25 < x < 0.90$. This material has a Ba-rich piezoelectric phase and a Ca-rich phosphor phase. Their results show that the EL and ML intensity have similar dependencies on the Ca composition (cf. figure 1.5(b)). The EML intensity of the sample with $x = 0.70$ is the strongest and it is 153% of that of the sample near the solubility limit ($x = 0.30$).

Moreover, the ML and EL spectra are coincident with a similar emission peak (cf. figure 1.5(a)). To them, these two observations indicate that the EL and ML properties of this material might have the same origin and that the piezoelectric field causes the ML of $\text{Ba}_{1-x}\text{Ca}_x\text{TiO}_3:\text{Pr}^{3+}$. To ensure their conclusions, they calculated the piezoelectric field, strength and constants and found out that the applied stress on the material generates a piezoelectric field that is sufficiently large to induce EL.

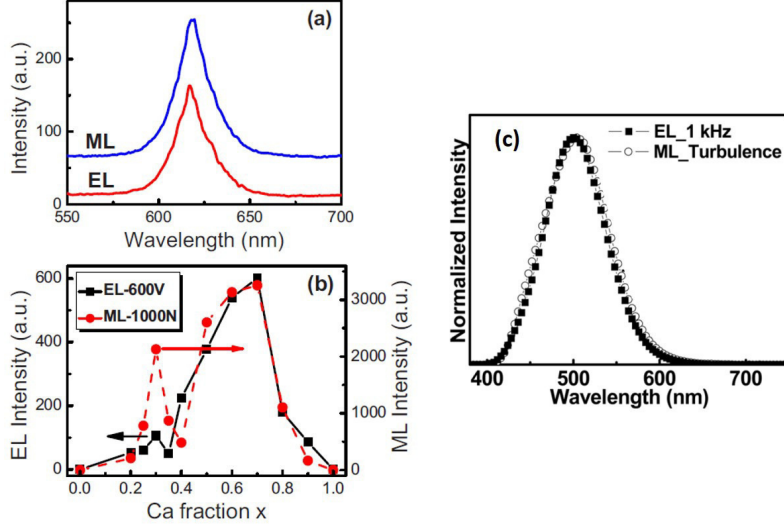


Figure 1.5: (a) ML and EL spectra from the sample with $x=0.70$ excited by stress and AC electric field, (b) The ML and EL intensity dependencies on the Ca composition of $\text{Ba}_{1-x}\text{Ca}_x\text{TiO}_3:\text{Pr}$. Adapted from [3]. (c) Comparison of normalized ML and EL (1 kHz) spectra. Adapted from [4]

Many other studies suggest that the ML originates from a piezoelectric field-induced EL and several other materials show similar behaviours to the ones laid out above. In the case of $(\text{Ca},\text{Sr})\text{Al}_2\text{Si}_2\text{O}_8:\text{Eu}^{2+}$, we see a similar dependence of luminescent intensity on Sr composition [41], and for $\text{ZnS}:\text{Mn}^{2+}$ EL and ML spectra coincide perfectly [4] (cf. figure 1.5(c)) and exhibit similar color shift [42]. In this last study, they compare the ML spectra to electroluminescent (EL) spectra driven by low frequency condition. They generally use a stretching technique to induce mechanoluminescence, but because this approach cannot produce high vibrations, they built an ACEL device with the same materials used for ML composite (i.e. $\text{ZnS}:\text{Cu}$ microparticles + PDMS). EL and ML spectra are superimposed on each other using EL at 10 Hz, it implies that ML and EL were emitted from the same emission centre. Moreover, blue colour shift is observed for the ACEL sample and is associated with increasing frequency (from 50 Hz to 1 kHz) due to the activation of the blue emission, cf. figure 1.6(a-b). The ACEL devices changed colour with increasing frequency which can be reproduced on $\text{ZnS}+\text{PDMS}$ composites if a stress activator can provide sufficiently fast vibrations. To do so, they built a wind-driven system based on wind using nitrogen gas flow over a partially sliced ML film. High vibrations can be achieved by increasing the gas flow from which results bright ML. For ZnS , a blue peak was observed using a low gas flow rate of (30 L min^{-1}) . The same peak was found for EL between 200 and 500 Hz. As the gas flow rate increases (until 80 L min^{-1}), the green component starts decreasing and the blue becomes the only one caused by the fast vibrations applied on the sample, cf. figure 1.6(d).

An electroluminescent kit was purchased for the purpose of this study. This kit comprises a silver based paste, a dielectric paste, a phosphor paste and an indium tin oxide (ITO) coated polymer film. We have experimented these materials on the ITO film and on

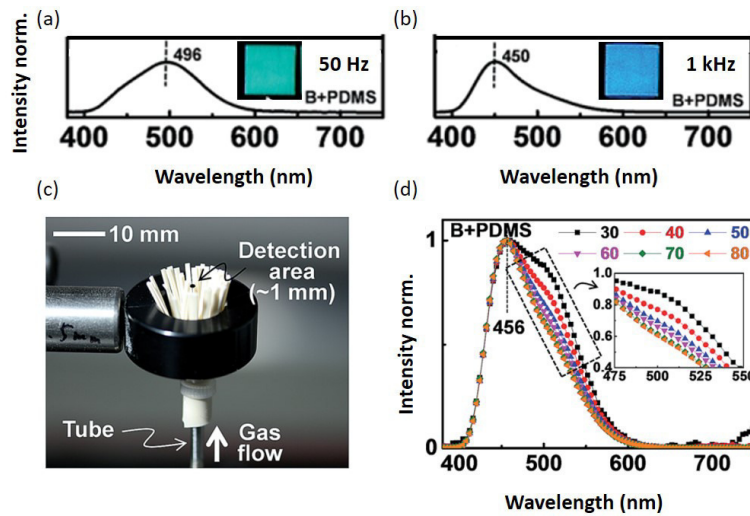


Figure 1.6: (a-b) EL spectra of ACEL sample under the lowest (50 Hz) and highest (1 kHz) frequency conditions, insets are photos of the EL for ACEL samples. (c) Photograph of a partially sliced ML composite enclosed by a ring holder. (d) ML spectra from the ML composites during gas flow at flow rates between 30 L min^{-1} and 80 L min^{-1} . Adapted from [5]

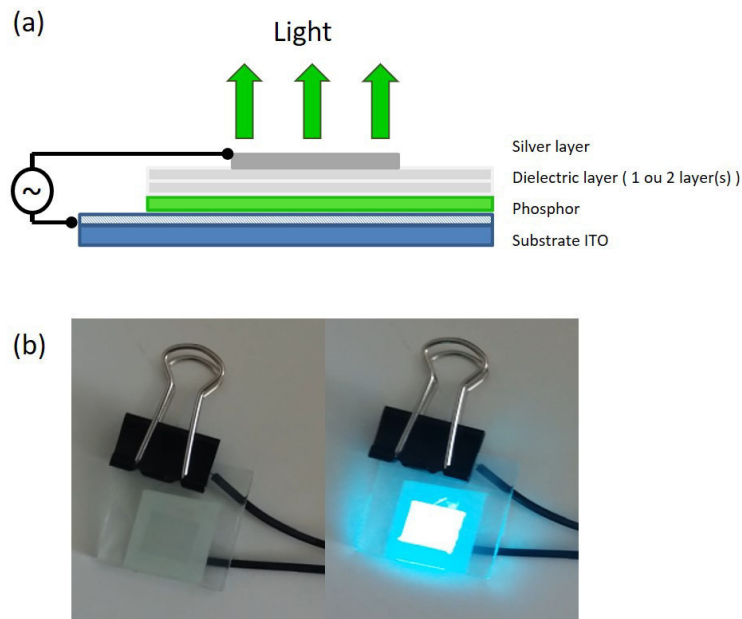


Figure 1.7: (a) Structure of an electroluminescent panel, light is visible after AC input. (b) Electroluminescent samples (dimension $20 \text{ mm} \times 20 \text{ mm}$), without (left) and with current input (right).

a ITO coated glass substrate, cf. figure 1.7. By applying an AC current, the panel lights up and exhibits a bluish color.

1.2.3 Mechanoluminescent materials

It exists hundreds of inorganic materials that exhibit ML property. For a long time, the most studied crystal was zinc sulfide (ZnS) doped with copper or manganese. After that, scientists started looking for other materials and that is when strontium alumi-

nates doped with rare-earth elements emerged, such as $\text{SrAl}_2\text{O}_4:\text{Eu}$ and $\text{SrAl}_4\text{O}_6:\text{Eu,Dy}$, as they exhibit very intense and bright ML. A classification of EML phosphors was proposed by *Zhang et al*[43]. They report several phosphors like KCl, KBr or LiF (alkali halide crystals); CdS:Ag, ZnS:Cu,Mn, ZnS:Al,Cu, and ZnS:Mn,Al,Cu (doped II-VI semi-conductor phosphors); Eu-doped SrAl_xO_y phosphors (doped aluminate phosphors); $\text{Sr}_2\text{MgSi}_2\text{O}_7:\text{Eu}$, $\text{SrCaMgSi}_2\text{O}_7:\text{Eu}$, and $\text{Ca}_2\text{MgSi}_2\text{O}_7:\text{Eu}$ (doped silicate phosphors); but also $\text{SrMg}_2(\text{PO}_4)_2:\text{Eu}$, $\text{CaZnOS}:\text{Mn}$, $\text{BaTiO}_3\text{-CaTiO}_3:\text{Pr}$ and $\text{ZnO}_2:\text{Ti}$. The emission of all these materials covers a large spectrum from UV to infrared light.

A. Feng & P. F. Smet[28] listed the ML materials according to their properties and to their crystal structures (cf. table 1.2 below).

Structure	Host	Piezo	Dopant	$\lambda_{ML}(nm)$
Rock Salt	KCl	-	.	430, 520
	KBr	-	.	465
	NaCl	-	.	282, 318, 362, 610
	LiF	-	.	290, 560, 650
Tridynamite	SrAl_2O_4	+	$\text{Eu}^{2+}/\text{Dy}^{3+}$	520
	CaAl_2O_4	-	Eu^{2+}	440
	$\text{Zn}_2\text{Ge}_{0.9}\text{Si}_{0.1}\text{O}_4$	+	Mn^{2+}	535
Spinel	MgGa_2O_4	-	Mn^{2+}	506
	ZnGa_2O_4	-	Mn^{2+}	505
	ZnAl_2O_4	-	Mn^{2+}	560
Wurtzite	ZnS	+	Mn^{2+}	585
	ZnS	+	Cu^+	520
	ZnS	+	$\text{Cu}^+/\text{Al}^{3+}$	(475), 525
	CaZnOS	+	Mn^{2+}	580
	CaZnOS	+	Cu^+	450, 530
	CaZnOS	+	Er^{3+}	525, 540, 560
	CaZnOS	+	Sm^{3+}	566, 618, 655
	BaZnOS	-	Mn^{2+}	634
Melilite	$\text{Ca}_2\text{MgSi}_2\text{O}_7$	+	Eu^{2+}	530
	$\text{Sr}_2\text{MgSi}_2\text{O}_7$	+	Eu^{2+}	499
	$\text{SrCaMgSi}_2\text{O}_7$	+	Eu^{2+}	496
Perovskite	$\text{Ba}_{1-x}\text{Ca}_x\text{TiO}_3$ ($0.25 < x < 0.8$)	+	Eu^{2+}	612
	Sr_2SnO_4	-	Sm^{3+}	575, 625, 660
	CaNb_2O_7	+	Pr^{3+}	613

Table 1.2: *Mechanoluminescent compounds and their properties. Piezo: - non piezoelectric, + piezoelectric. Adapted from [28]*

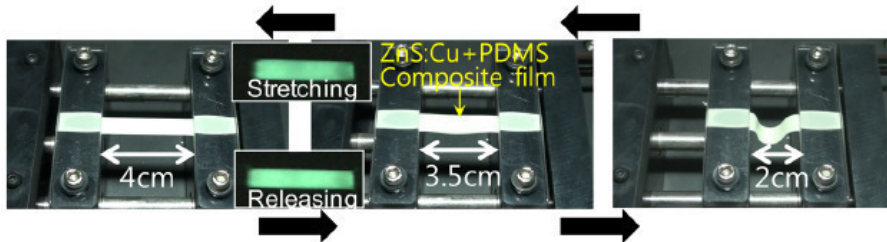


Figure 1.8: *Photographs of the Stretching-Releasing system. From [4]*

Even though copper doped zinc sulphide ($\text{ZnS}:\text{Cu}$) is an old and well studied

material, it is still full of surprises. In 2013, *Jeong et al.*[4], embedded microscopic ZnS particles in a polydimethylsiloxane (PDMS) elastomer. By designing such a system, they demonstrated that it is possible to obtain bright (120 cd/m^2) and durable mechanoluminescence (over 100 000 repeated mechanical stresses, cf. figure 1.8). This first article initiated many others where composite materials ZnS:Mn/Cu+PDMS were used to create new applications and new systems (see section 1.2.4).

Zinc Sulfide

Zinc sulfide is an inorganic compound, it is an undoped II-IV wide band gap semiconductor which exists in two crystalline forms (cf. figure 1.9):

- Cubic (fcc-faces centered cubic) also known as zinc blende or sphalerite is more stable for temperatures below 1020°C . This form is found in nature and the band gap is 3.54 eV at 300K [44] but was also found at 3.66 eV at 300K [45].
- Hexagonal (hcp-hexagonal closed packed), known as the mineral wurtzite. The band gap is 3.91 eV at 300K [44] .

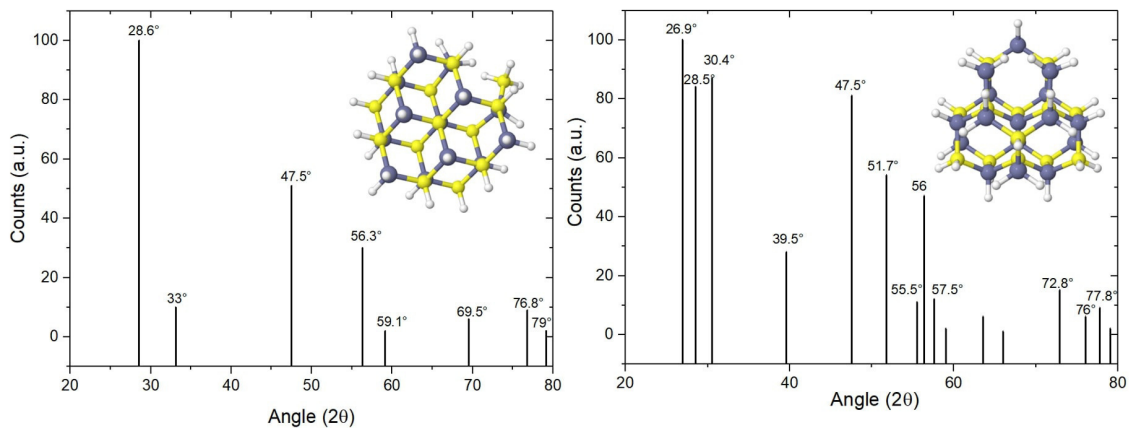


Figure 1.9: *Diffraction patterns of ZnS with crystal representations. Left, sphalerite (or cubic). Right: Wurtzite (or hexagonal)*

The band gap represents the energy between the lowest energy level in the conduction band (CB) and the highest energy level in the valence band (VB). Therefore, to excite an electron from the VB to the CB an energy 3.54 eV (and 3.91 eV for the hexagonal structure) is required. The Planck-Einstein relation is given by:

$$E = h\nu \quad (1.1)$$

Where E is the energy of a photon with frequency $\nu = c/\lambda$ and h is the Planck's constant equal to $h = 6.63 \times 10^{-34} \text{ Js}$. A 3.54 eV energy photon would have a wavelength of 351 nm and a 3.91 eV energy photon would have a wavelength of 318 nm.

Under a 350 nm light excitation, photons are absorbed and free electrons are generated. The generated hole in the VB also moves freely in the VB. The electrons present in the CB tend to relax to the VB due to their instability. They do so by releasing photons. However, these electrons can also fall to lower intermediate energy levels first by non-radiative relaxation. Then they relax to the valence band accompanied by photon emission, cf. figure 1.10. The emission spectrum will display a maximum at a higher wavelength than the one displayed for the excitation spectrum.

We find a certain number of activators for sulfide phosphors which are transition metal ions of valence similar to Zn^{2+} . The most important ones are copper (Cu^{2+}), silver (Ag^+), aluminium (Al^{3+}), then manganese (Mn^{2+}). Zn^{2+} is substituted by the dopant ion in the crystal lattice. The luminescent properties depend on their nature and concentration. The ion's energy level would be added as energy level to the host crystal band structure, in the forbidden band gap. This new energy level could be closer to the conduction band as a donor level, or closer to the valence band as an acceptor level. Cu^{2+} , Ag^+ and Mn^{2+} are more likely to accept electrons from higher energy levels which means that they create new acceptor levels close to the VB. On the contrary, Al^{3+} creates donor levels close to the CB. Donor levels are referred to electron traps whereas acceptor levels are referred to hole traps.

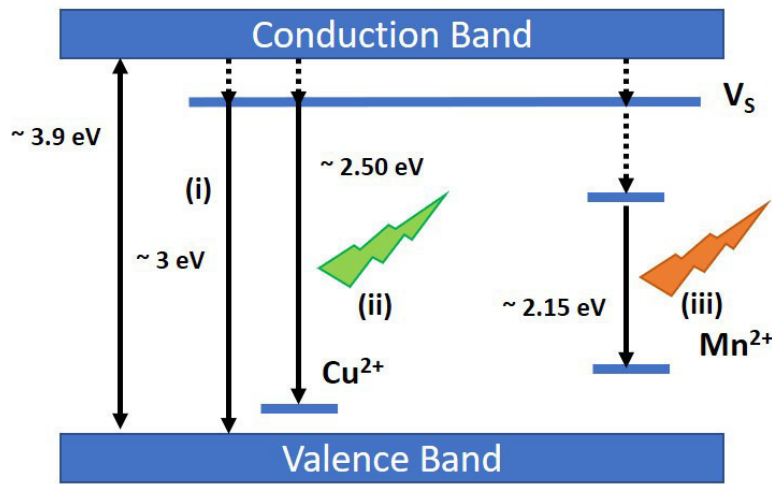


Figure 1.10: Schematic energy level band diagram of Cu-doped and Mn-doped ZnS crystal. V_S Sulphur vacancy.

An electron trap is a small localized region of higher energy than the ground state. Excited electrons in the crystal can be captured there being trapped by the activator. In such a case, an additional energy input is required to release the e^- from the trap and excite the activator. This process is called detrapping of electron trap. The electron traps act as shallow donor levels below the conduction band [46]. They are created by the S^{2-} vacancies present in the crystal. Also, hole traps act as shallow acceptor levels above the valence band created by the Zn^{2+} vacancies.

In the case of a ZnS:Cu, a 350 nm light causes electron excitation from the VB to the CB, followed by non-radiative relaxation to intermediate energy levels. From there, the electrons drop to the acceptor level of the dopant ion, cf. figure 1.10 (ii). The emitted photons have a low energy and the wavelength is characteristic of Cu^{2+} with a peak at 460 nm. A second emission band was also determined at 525 nm. The first one is attributed to associates between Cu^+ ions occupying Zn^{2+} positions and interstitially incorporated Cu^+ ions. The monovalent copper ions present in the host lattice substitute the zinc positions, with halide ions acting as co-activators, are responsible for the green band [47]. ZnS:Mn has an emission band around 580 nm corresponding to the yellow-orange region, cf. figure 1.10 (iii), [48] due to the inner transitions of Mn^{2+} ions incorporated into the Zn positions. This emission is linked to the ${}^4T_1 - {}^6A_1$ transition of Mn^{2+} ions.

1.2.4 Elastico-mechanoluminescence EML

The doped zinc sulphide material is often used for mechanoluminescence (ML) studies and particularly for elastico-mechanoluminescence (EML). EML distinguishes itself from the other types of ML thanks to its self-recovery property which led scientists to imagine and design EML devices for several applications. Some of these applications are presented in this section.

1.2.4.1 Definition and first approach

Elastico-mechanoluminescence (EML) corresponds to luminescence induced under elastic deformation. This deformation is reversible which makes this type of mechanoluminescence open to a large panel of applications. The EML emission takes place when the applied pressure reaches a given threshold and its intensity usually increases linearly with the applied pressure in the elastic region. If the deformation force is constant, the intensity decreases with time. The EML is obtained from a reversible deformation. Most non-centrosymmetric crystals and many centrosymmetric crystals exhibit EML. The local piezoelectric field near the defects in crystals is responsible for the EML emission in the crystals. The bulk piezoelectricity is not solely responsible for the EML excitation. In this case all piezoelectric crystals should exhibit EML and non-piezoelectric crystals should not. Experimental results support this fact as they show that intense elastico-mechanoluminescence can be achieved by using appropriate dopants both in non-centrosymmetric and centrosymmetric crystals. Rare-earth doped alkaline aluminates and silicates, ZnS:Mn, ZnS:Cu and ZnS:Mn,Cu phosphors are the most promising EML materials[6].

The most popular elastico-mechanoluminescent samples are composed of a phosphor, usually ZnS:Cu, encapsulated in a hard matrix (such as acryl resin) or a soft polymer (like polydimethylsiloxane PDMS). A stress can be applied by elastic actuation or pressing.

Electron trapping can play an important role in EML. When we consider the persistent luminescent phosphor $\text{SrAl}_2\text{O}_4:\text{Eu,Dy}$ (figure 1.11, (a)) we see that the diminished EML intensity caused by a number of pressings can be recovered completely by the irradiation to UV light. The mechanical action acts on the detrapping. This fact proves the trapping of charge carriers during the exposure to irradiation. But figure 1.11 (c) displays the EML intensity when a load is applied on ZnS:Mn nanoparticles coated on a quartz substrate. The EML appears after a threshold pressure of 1 MPa. The first peak I shows that the intensity increases with time and then decreases after a maximum value. The second peak I' corresponds to when the pressure is released from the sample. New peaks II and II' correspond exactly to I and I' , respectively, but during a second pressure cycle. For ZnS:Cu and ZnS:Mn phosphors the ML intensity will continue to increase linearly even for comparatively high values of the applied pressure and strain rate as shown figure 1.11, (b-d) [8]. The ML spectra of ZnS:Mn are similar to their photoluminescence and electro-luminescence spectra[49]. A phenomenon of self-recovery of the detrapped charge carriers takes place.

1.3 Mechanisms of Elastico-mechanoluminescence

Are presented in this section the three main mechanisms found in the literature which explain EML: piezoelectrically induced trap-depth reduction, detrapping of charge carriers by movement of dislocation, and triboelectricity-induced luminescence.

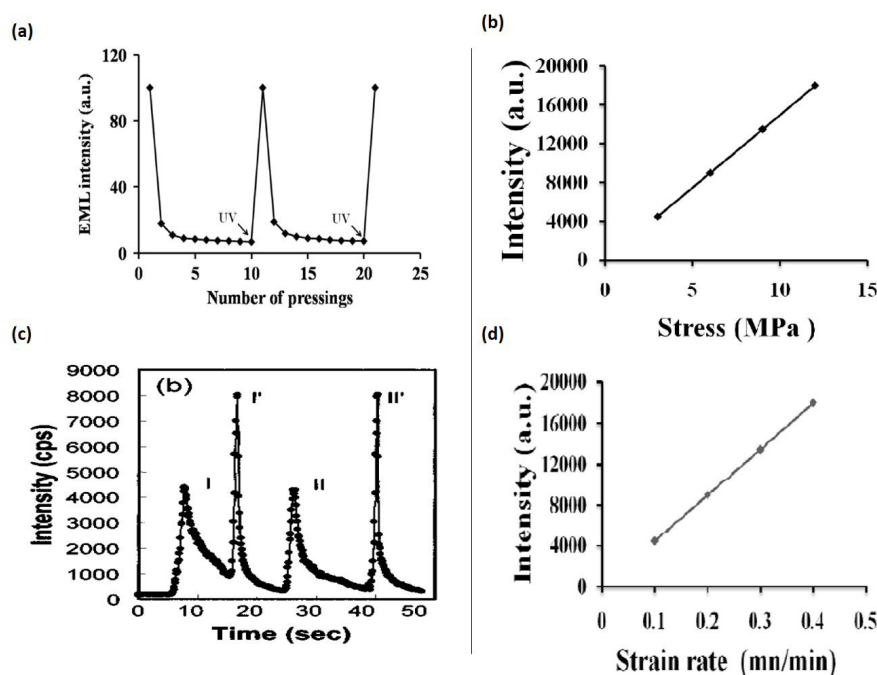


Figure 1.11: (a) Dependence of the EML intensity of $\text{SrAl}_2\text{O}_4:\text{Eu,Dy}$ phosphors on the number of repetitive pressings and effect of UV light irradiation (365 nm). From [6]. (c) Response of ZnS:Mn material to compression stress of 500 N. From [7]. (b-d) Stress and strain rate dependences of the EML intensity (Theoretical). From [8]

1.3.1 Mechanism 1: Piezoelectrically induced trap-depth reduction

This first proposed mechanism seems to apply for most persistent phosphors. It is based on the idea that piezoelectricity is triggered by the deformation of crystalline structures and generates an internal electric field, which helps the release of trapped charge carriers (electrons and holes). It can be applied to microcrystalline, nanocrystalline and single crystal phosphors. The trap-depth of charge carriers decreases with increasing piezoelectric field and after a threshold electric field, the trapped electrons become unstable and they get released. The recombination of these electrons with the hole centres results in the excitation of the luminescent centres. This model can be applied to EML induced by application of static pressure and EML induced by impact pressure[36]. Piezoelectricity usually appears in non-centrosymmetric compounds[28]. It is to note that centrosymmetric compounds are crystals with an inversion center and cannot exhibit certain properties like the piezoelectric effect.

The EML of persistent phosphors with Eu^{2+} as dopant was explained by *B.P.Chandra et al*[35] as such:

1. UV-irradiation of persistent luminescent materials creates Eu^{3+} ions (ionization of the electrons of Eu^{2+} ions from 4f level to 5d band lying very close to the bottom of the conduction band),
2. When a pressure is applied, it produces a piezoelectric field in the crystal because it is non-centrosymmetric,
3. The piezoelectric field reduces the trap-depth of hole-traps,
4. Electron detrapping (to the conduction band CB) takes place,

5. Some recombine with the photo-generated Eu^{3+} ions and generate excited Eu^{2+} ions,
6. The radiative recombination of excited Eu^{2+} ions results in the emission of light.

The mechanoluminescence discovered in the piezoelectric semiconductors is generally restricted to transitional metal activators such as Mn^{2+} and Cu^{2+} ions. ZnS:Mn exhibits elastico-ML only in the presence of Mn; the undoped ZnS single crystal does not, but exhibits photoluminescence. Because of the non-centrosymmetric structure, the piezoelectric constant is high near the Mn^{2+} ions, and low in regions away from them. It should result in a gradient of the electric field. For low values of stress, filled electron traps near the Mn ions may be detrapped by tunneling process or thermal ionization, those need higher values of stress[8].

The piezoelectric constant d of ZnS:Mn crystals is $3.2 \times 10^{-12} \text{CN}^{-1}$ [50], and the threshold pressure P_{th} to cause ML in ZnS:Mn crystals is 10^6Nm^{-2} . So, the piezoelectric charge density for the threshold pressure is:

$$\rho = dP_{th} = 3.2 \times 10^{-12} \times 1 \times 10^6 \text{Cm}^{-2}.$$

The piezoelectric field is:

$$E = \rho/\epsilon_0,$$

where ϵ_0 is the permittivity of free space equal to $8.85 \times 10^{-12} \text{C}^2 \text{N}^{-1} \text{m}^{-2}$.

Thus, the external electric field E developed near the surface of crystals is:

$$E = 1.08 \times 10^6 \text{Vm}^{-1} = 3.6 \times 10^3 \text{Vcm}^{-1}$$

As the detrapping of charge carriers needs an external electric field of the order of 10^5Vcm^{-1} [9, 51] and the impact ionization needs an internal electric field of the order of 10^6Vcm^{-1} , the external bulk piezoelectric field of the order of $3.6 \times 10^3 \text{Vcm}^{-1}$ produced by P_{th} may not cause the detrapping and impact ionization. The appearance of EML by P_{th} of $1 \times 10^6 \text{Cm}^{-2}$ in crystals indicates that the local piezoelectric field near Mn^{2+} ions in ZnS:Mn crystals should be nearly 10 times higher, where the piezoelectric constant should be high.

According to the same author[36], the EML of the ZnS:Mn crystals is described below:

1. As a result of the presence of impurities in the ZnS:Mn crystal, and when a pressure is applied, one surface of a local piezoelectric region produced gets positively charged and the other surface gets negatively charged,
2. Electron detrapping follows the trap depth reduction caused by the local piezoelectric field. The released electrons move to the CB,
3. These detrapped electrons may recombine with the holes. The energy released during the electron-hole recombination is transferred to the Mn^{2+} ions,
4. The radiative recombination of the Mn^{2+} ions gives light characteristic of the Mn^{2+} ions.

For a better understanding of the piezoelectric effect in EML, *Chandra et al.* proposed a mathematical theory in which we find expressions presenting the detrapping and recombination rate of charge carriers, the pressure temporal, thermal, spectral and other characteristics of EML materials[36].

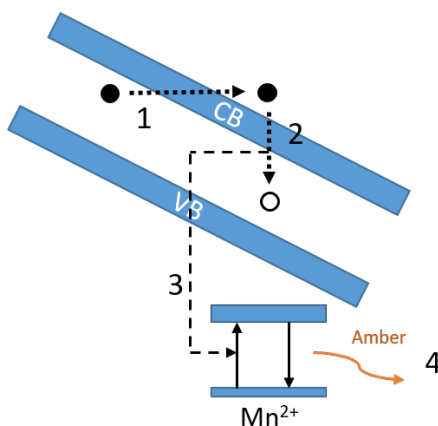


Figure 1.12: Schematic diagram for the EML mechanism in ZnS:Mn nanoparticles when stress is applied. 1. Electron detrapping and moving to the CB - 2. Electron-hole recombination - 3. Energy transfer to Mn^{2+} ions and excitation of Mn^{2+} - 4. Light emission. Adapted from [9]

1.3.2 Mechanism 2: Detrapping of charge carriers by movement of dislocation

Chandra et al.[52, 34] introduced another mechanism which seems to be better suited for plastico-mechano-luminescence (PML). For II-VI semiconductors, the continuous plastic deformation causes movement of dislocations. This deformation causes movement of charges dislocations to opposing surfaces causing buildup of surface charge and electric field within the crystal. The electric field generated induces bending of the valence band (VB), conduction band (CB) and dislocation bands. The electrons from filled electron traps tunnel to the CB and recombine with the holes to give rise to light emission characteristic of the activator centres[37]. In the case of EML, the elastic deformation was shown to be sufficient to cause bending of the dislocation lines whereby the interaction between dislocation line and colour centres transfer the electrons to the dislocation bands. The electrons can either recombine with holes or are captured by other deep traps present in the crystal. If the moving dislocation containing electrons encounters the defect centres containing holes, the dislocation electrons may be captured by these centres and luminescence may arise due to the radiative electron-hole recombinations[34].

1.3.3 Mechanism 3: Triboelectricity-induced luminescence

No to be confused with triboluminescence, which is generated through the breakage of chemical bonds, triboelectricity-induced luminescence is non-destructive and results from the soft friction on the interface between two different materials namely between PDMS and phosphor microparticles such as ZnS:Cu .

This new theory was proposed by *Sohn et al*[10] and they support their claim with the following elements:

- They realised that embedding ZnS:Cu particle in rigid matrix like acryl resin extinguishes the luminescence upon loading and this even when a high level of stress is applied to the sample (figure 1.13(a)),
- By using Piezoresponse Force Microscopy (PFM) measurements, they showed that there is no piezoelectric influence on the mechanically driven luminescence for ZnS:Cu -PDMS composites,

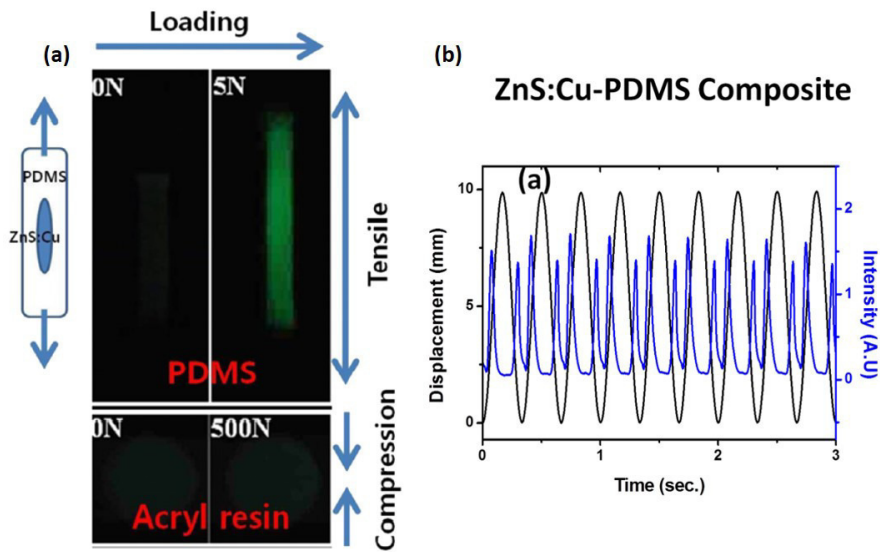


Figure 1.13: (a) Photographs of ZnS:Cu-PDMS and ZnS:Cu-Acryl resin composites under unloading and loading at 1 Hz. A thin band-type specimen was elongated up to 5 N in a tensile mode for ZnS:Cu-PDMS and a disc type specimen was compressed up to 500 N for ZnS:Cu-Acryl resin. (b) Plots of ML signal with an applied cyclic load for ZnS:Cu-PDMS composite. From[10]

- Upon cyclic loading on the ZnS:Cu-PDMS sample, the luminescent response was not decaying like most ML materials even though no UV-irradiation was used to re-pump the system (figure 1.13(b)),
- Appearance of a double-peak-shaped luminescence response upon cyclic loading. This double peak is explained as being the separation and retreat of the interface. Also, the ML intensity strongly depends on the frequency of the loading; the number of emitted photons increases with the increase of the frequency,
- Conventional ML is triggered at high loading values[53], but in this case, a 9 N load was sufficient.

Moreover, the triboelectricity-induced luminescence is the only theory, so far, that explains the enhancement of EML with the presence of aluminium oxide coating on ZnS particles. We notice that Al_2O_3 is very high on the triboelectricity scale (positive charge) while PDMS is very low (negative charge), cf. figure 1.14. This favours the creation of charges when these two materials are rubbed together.

Earlier in 2004, ML was observed in $\text{ZnAl}_2\text{O}_4:\text{Mn}^{2+}$ material upon friction with a rod [54]. The ML was linked to the generated voltage in the vicinity of the frictional area. These observations pointed out toward the effect of triboelectrification since the trapped charge carrier in the spinel (and centrosymmetric) crystallographic structure of ZAO:Mn can be excited by the local electric field. This field being generated after friction between two different materials, the excited carrier can move toward the Mn^{2+} ions and subsequently, generate light. The article concludes on a new mechanism, i.e. triboelectricity-induced EL.

1.3.4 Point of debate

It was previously stated in subsection 1.2.2 that commercially available ZnS particles are coated with Al_2O_3 . Many studies report that bare ZnS exhibits very weak ML or, in some cases, does not exhibit ML at all[55]. This suggests that the coating plays

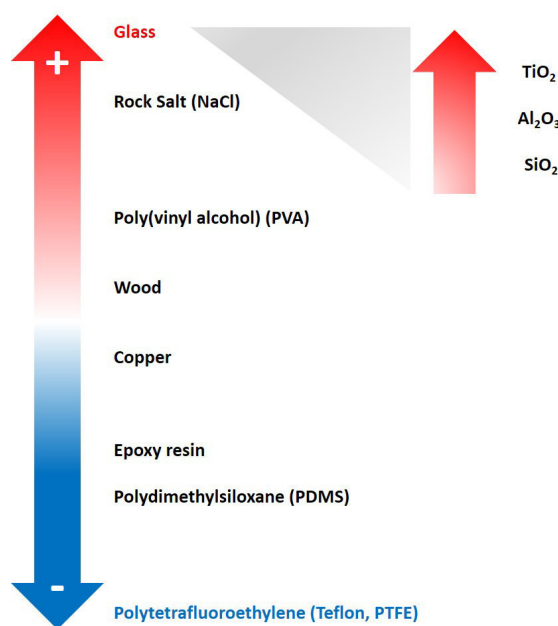


Figure 1.14: *Triboelectricity scale of oxide dielectric materials. Adapted from [11]*

a major role in the ML mechanism in the case of embedded particles in a soft polymer matrix. In this article [56], they demonstrated that the Cu-doped ZnS particles were coated with 500 nm of metallic Al. They suggest that this layer acts as an electron source for ML emission. The electron current forms a positive surface charge layer in the metal, inducing an electric field and allowing electrons to flow from the metal into the semiconductor. This electrical behavior leads to the electric potential and downward bending of the bands in the semiconductor.

Although stimulating, the descriptions and explanations offered for the phenomenon are not based on strong proofs. In this article, the TEM measurements (BF-TEM or bright field mode and SAED or Selected Area Diffraction) cannot be trusted and Al does not exist in its metallic state but as aluminium oxide Al_2O_3 . *Krishnan et al.*[55] believe that the coating plays a role mechanically, and not electronically, by increasing stress transfer to the particles. In agreement with this article, the layer forms an adhesive bond with the PDMS in which the particles are encapsulated and its absence would prevent stress transfer and, therefore, EML emission.

The mechanism proposed by *Chandra* (piezoelectrically induced trap-depth reduction) is restricted to ZnS:Mn material and does not take into account the presence of a coating and, therefore, its role in EML. On the other hand, triboelectricity is based on the ability of two dissimilar materials to create electric charges. On the triboelectricity scale figure 1.14 Al_2O_3 and PDMS are on both ends of the scale indicating that these two materials are more likely to create positive and negative charges, respectively.

1.3.5 EML applications

There is a large variety of possible EML applications. Some of them are detailed in this section:

Figure 1.15 shows devices made of ZnS microparticles embedded in a PDMS (polydimethylsiloxane) elastomer. In the upper part of the figure we see the wind-driven ML coming from a partially sliced sample made of a blue, green and orange phosphor+PDMS.

There is a linear relationship between the gas flow rate and the brightness: the latter increases with increasing the gas flow. This means that the stronger the vibrations are, the higher ML brightness we obtain. On the lower part of the figure there is a different system with the same previous idea. To mimic the air flow, a N_2 gun is used to generate ML in small, vibrating rods. Such devices can be used as displays and light sources.

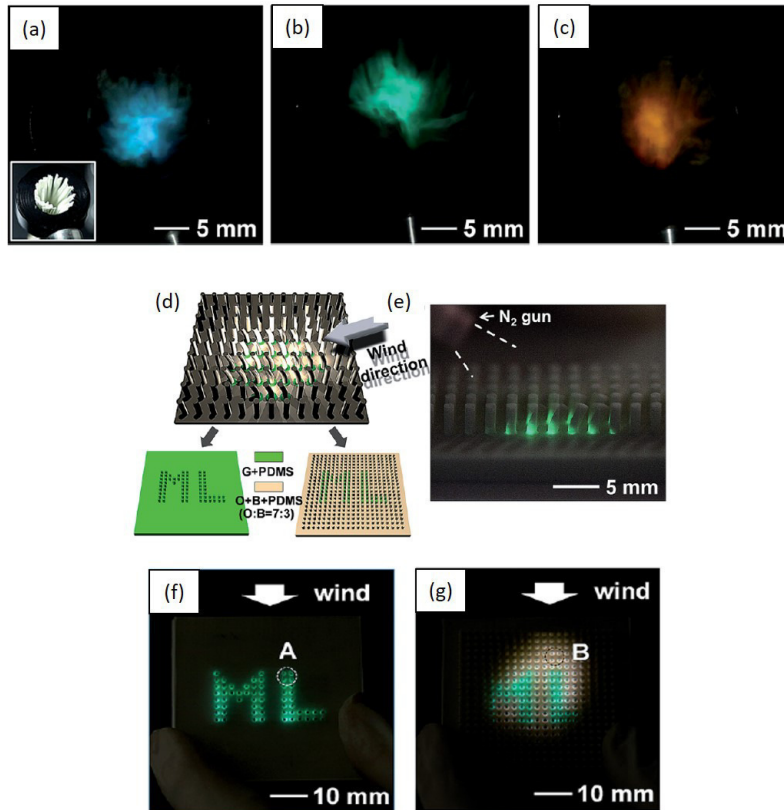


Figure 1.15: (a-c) Photographs obtained from the wind-driven ML. The inset of a partially sliced ML composite enclosed by a ring holder. (d) Schematic illustration of the set-up. (e) Photograph of the ML image showing the distribution of the ML emission in the vibrating rods. (f,g) Photographs of the patterned wind-driven ML. Adapted from [5]

Wearable devices are a rising topic. Smart textiles attract a particular attention and specially light-emitting textiles for their high visibility and are adopted for safety purposes. Today, we find fiber-shaped electroluminescent devices powered by an electric current [57]. Jeong *et al.* [12] propose an alternative. They created light-emitting fabrics powered by body movement only. Once again, ZnS microparticles are used in PDMS and shaped to form fibers (cf. figure 1.16 (a-g)). Zhang *et al.*[13] fabricated structures of mechanoluminescent fibers that could display green, orange and blue lights with maintaining the ML intensity over repeated deformation (cf. figure 1.16 (h-m)).

Others focused on facial expressions to trigger luminescence[14]. Because facial deformations cannot normally trigger ML, they enhanced the sensitivity of their device by adding SiO_2 nanoparticles in ZnS-PDMS composite material. This method seems efficient, Qian *et al.* showed some remarkable results (cf. figure 1.17).

We can also find ML-based flexible pressure sensors to secure signature collections by recording handwriting and signing habits of a person [15] (cf. figure 1.18). This technique could achieve high-security level thanks to its reliability.

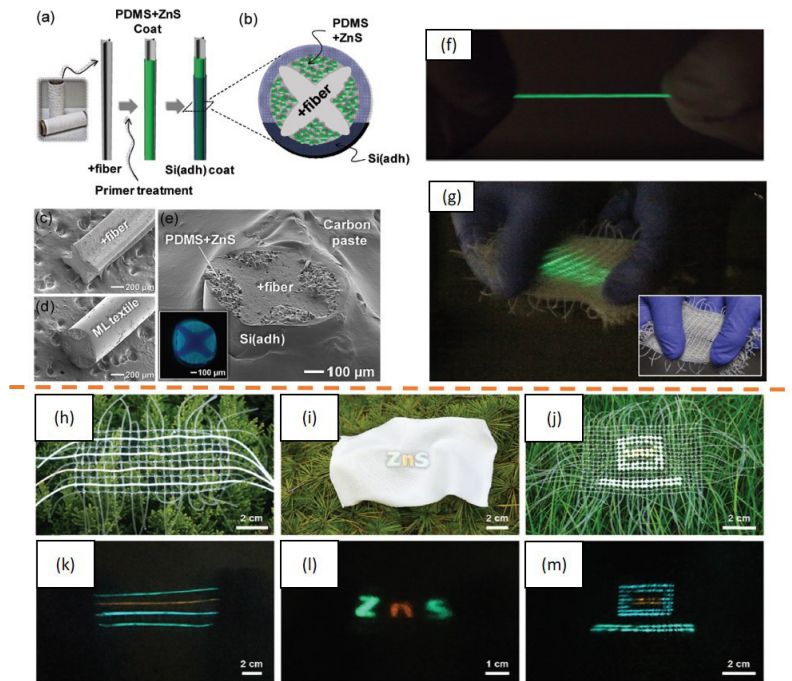


Figure 1.16: (a) Schematic showing the ML fiber fabrication process adopting two approaches. (b) Schematic illustration of cross-sectioned ML fiber. SEM images of (c) +fiber and (d,e) ML fiber. (f) Photograph of manually stretched ML-emitting fiber. (g) ML-emitting fabric undergoing hand-stretching. From [12]. (h-j) photographs of the mechanoluminescent fabrics based on mechanoluminescent fibers (h), ribbons (i) and dots (j); (k-m) photographs of the mechanoluminescent fabrics shown in (h-j) during the stretch and release process. Adapted from [13]

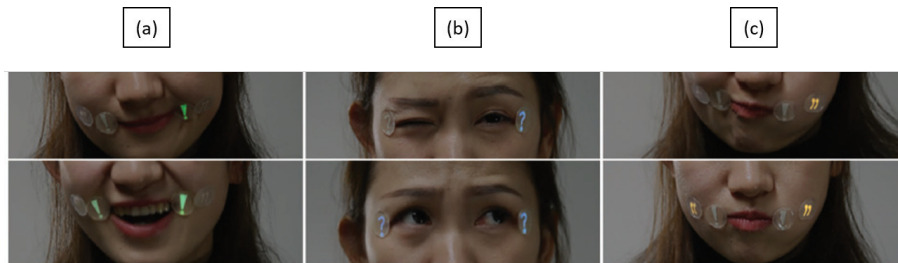


Figure 1.17: Various colors from ML response to lips corner (a), canthus (b), and cheek (c) muscle movements. From [14]

1.4 Objectives and challenges

Over the past decade, a significant number of articles were published. In the frame of environmentally friendly devices, elasto-mechanoluminescence became a trendy subject because it corresponds to a direct converter of mechanical energy to light. It allows researchers to imagine and design new devices and tailor materials in order to enhance the intensity of luminescence, its duration and its emitted wavelength. They are thought for applications in stress sensing[58], dynamic pressure mapping[15], displays and light sources[5] and the detection of electric and magnetic fields[59].

Because it is a promising alternative to known energy intensive means, the main goal is to be able to enhance the emitted light and to develop other phosphors, but a big obstacle stands on the way. The ML mechanisms are not completely understood and a full

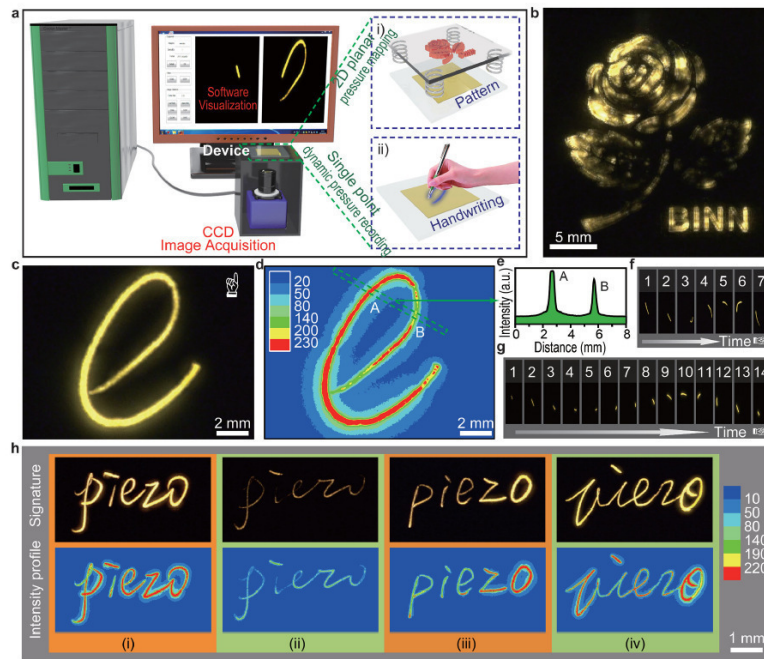


Figure 1.18: Visualization of dynamic pressure distributions. (a) Schematic illustration of the acquisition and processing system. (b) Visualization of pressure distributions generated by a stamp. (c) Visualization of dynamic pressure distributions generated from a handwriting. (d) 2D distribution of relative ML intensity. (e) The line profile of relative ML intensity. (f, g) Consecutive frames of the signing process. (h) Demonstrations of recording the signing habits with different forces. From [15]

explanation is needed. So far, the piezoelectricity model, on which most scientists agree, answers to some questions concerning two main materials ZnS:Mn and $\text{SrAl}_2\text{O}_4:\text{Eu,Dy}$. By applying this model to ZnS:Cu particles in a soft matrix, we notice that it fails to explain the luminescence of that system as the required piezoelectric field to induce luminescence is not created due to insufficient loading on the particles. This led to the emergence of a new theory "triboelectricity-induced luminescence" [10]. This model does not take into account the creation of a piezoelectric field but rather holds for responsible the friction between the particles and the matrix as the source of the generation of charge carriers in the crystal [10].

Also, even though ZnS and SrAl_2O_4 belong to the EML category, their luminescence behaves differently. In the case of the strontium aluminate, luminescence appears upon loading of typically 1000 N on an epoxy resin containing the phosphor particles and vanishes after repeated solicitation. This EML can only be fully recovered after UV-irradiation of the sample [60]. Yet, for a sample made of ZnS:Cu particles embedded in matrix like PDMS, it does not need irradiation in order to recover its EML [4]. This shows that maybe a new classification of EML materials is needed and that this process is still in need of a comprehensive mechanism which can be applied to any EML material. Thanks to this understanding, we could modify or develop emitting particles and reach the scientists' objectives of a more intense luminescence and, thus, shape efficient systems for practical applications.

Chapter 2

A model study

This chapter will focus on a model elasto-mechanoluminescent (EML) system. This system comprises the sample, and therefore the materials used for its manufacture, and the experimental EML testing device and setup. The main ZnS compound is presented and detailed here: its origin, its chemico-physical characterization as well as its EML results after testing it with two different setups.

2.1 The right materials

The system we want to design consists of two main elements: the phosphor (doped-zinc sulphide ZnS particles), and the polymer (polydimethylsiloxane or PDMS). As stated previously, Cu-doped ZnS is the one material that exhibits very bright elasto-mechanoluminescence (EML) when incorporated in a soft matrix. Most published experiments were conducted using ZnS:Cu particles purchased from Osram Sylvania Inc. and Wacker ELASTOSIL RT601 as PDMS [4, 5, 56]. Because Osram Sylvania Inc. no longer produces these phosphors, other articles name Global Tungsten & Powders Corp. as a phosphor provider [12, 61, 62], LONCO Company Limited [10] or even Shanghai Keyan Phosphor Technology Company Limited [63]. This was hinting toward the difficulty of finding easily the phosphor material, fact which was confirmed at the beginning of the study. Moreover, another PDMS is named as being a good candidate for the EML: the Sylgard 184 [10]. Although different brands are used, the experimental protocol of sample making is the same. It first appeared in an article by *Jeong et al.* [4] and several other articles followed the lead: the PDMS is first prepared as advised by the manufacturer, it is then mixed with the phosphor at a weight ratio of 7:3 (70wt% of phosphor and 30wt% of polymer) and, finally, left for curing. PDMS is a very viscous liquid polymer and curing is the process during which the polymer solidifies, and confers elastic properties. The samples are usually shaped like strips of few centimeters in length. This shape is suitable for the testing setup which consists of a device capable of extending and relaxing the sample at a certain rate, and an optical measurement device to record the emitted light by the sample; it is referred to as a stretching-releasing device or S-R device.

To be able to observe the elasto-mechanoluminescence phenomenon, we decided to recreate the system mentioned above as model material, following the same steps and using the same materials.

2.1.1 Doped ZnS phosphor

The first and most important stage was to get hold of the doped zinc sulphide material and this task took longer than expected since most phosphor providers do not,

or no longer, supply the required material. Only one matched our criteria which are ZnS:Cu microparticles coated with aluminium oxide Al_2O_3 like Osram Sylvania Inc. used to provide. This supplier is *GWENT GROUP*.

Gwent Electronic Materials Ltd. is a supplier of paste and ink to industry. It offers conductor pastes, dielectric pastes, polymer based pastes, pastes for sensors, industrial, automotive and biosensors, pastes for all forms of passive components and synthetic metallo-organic materials for the electronic industries. Additionally, materials for the electroluminescent market are proposed: silver-based paste to contact onto ITO coated polymer film, conductive carbon paste to act as the other electrode, dielectric and phosphor pastes for high brightness and long life panels [64]. The phosphor present in the paste is suited for our EML application.



Figure 2.1: *Gwent Group electro luminescent kit. From left to right: green phosphor paste, dielectric paste, silver paste*

That electroluminescent kit (figure 2.1) was purchased and tested (cf. subsection 1.2.2, chapter 1). For the EML study only the phosphor paste was used for it is the one composed of the Cu-doped ZnS particles. Nevertheless, this paste cannot directly be employed because of all the undesirable chemical constituents.

2.1.1.1 From paste to powder

The composition of the pastes is not given by the manufacturer but a phosphor paste, for plasma display panels for example, usually comprises phosphor particles dispersed in an organic paste made of a solvent, a binder (polyvinyl butyral) and at least one dispersant comprising stearic acid, and a plasticizer (phthalate). These components ensure stability and desirable screen-printing properties and do not prevent the phosphor contained in the paste from having high brightness [65]. These elements will not further be detailed here as they will not influence our study but will be removed through a washing process after which only the phosphor powder will remain.

To do so, toluene was first added to the paste. It is a good solvent because it can dissolve many organic compounds. Shaking the mixture separates the phosphor particles from the organic paste and the former starts sedimenting. After a few minutes in the centrifuge, we remove the solvent and, then, the operation is repeated a second time. Toluene is then replaced with another solvent: Ethanol which can dissolve both polar (hydrophilic) and non-polar (hydrophobic) elements. It is also easy to remove from any solution thanks to its low boiling point (79°C). The same steps are repeated twice more. A wet powder is obtained, it is dried in a 60°C oven. After 12 hours, the powder is ready to be used and ready for characterization (cf. figure 2.2).

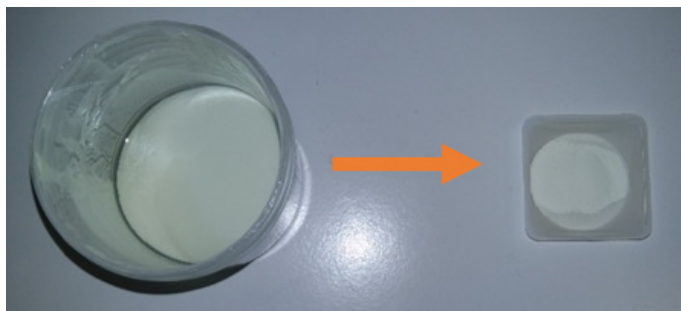


Figure 2.2: *Gwent phosphor from paste (left) to powder (right) after the washing process.*

2.1.1.2 Material characterization

The morphological and chemical characterization was conducted using a SEM-EDX G2 Pro from Phenom, which is a Scanning Electron Microscope equipped with Energy Dispersive X-ray spectroscopy; a spectrofluorometer FS5 from Edinburgh Instruments and a Malvern Panalytical X-Ray diffractometer.

The SEM image presented figure 2.3 (a) shows heterogeneity in the size and the shape of the Gwent particles. The particles' size is on average $40\ \mu\text{m}$ but we find particles of $20\ \mu\text{m}$ in diameter as well as of $60\ \mu\text{m}$. The elemental composition of the sample was assessed using EDX analysis.

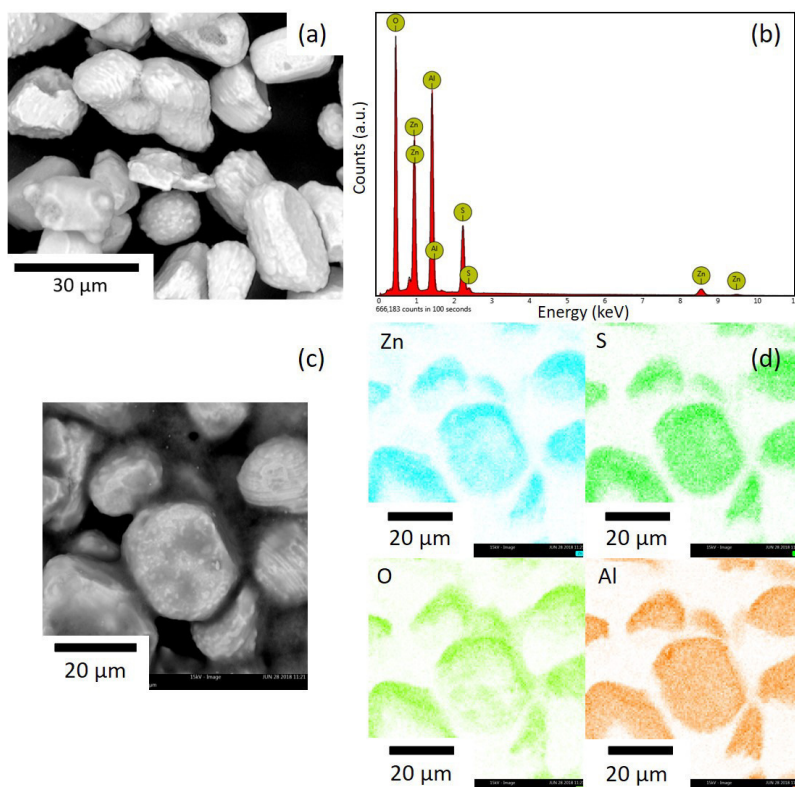


Figure 2.3: *Characterization of the washed Gwent ZnS particles. (a,c) SEM images. (b) EDX analysis, presence of Zn, S, Al and O elements. (d) EDX mapping analysis. Detection of Zn, S, Al and O.*

The spectrum figure 2.3 (b) displays peaks corresponding to the following elements: Zinc (Zn), Sulfur (S), Oxygen (O) and Aluminium (Al). This technique cannot

detect the presence of any dopant but confirms that the material is zinc sulphide (ZnS). The detection of Al and O suggests the existence of aluminium oxide as it is the case for particles from Osram Sylvania Inc. Moreover, previously acquired ZnS powders, which were not meant for electroluminescent applications, were analysed and their EDX spectra did not show these two peaks, namely Al and O. Figure 2.3 (d) is a mapping analysis of the particles in (c) and shows that the particles are covered with Al and O. This supports the fact that Al_2O_3 is acting as coating on the Gwent particles as suspected. However, its thickness was not determined.

These particles were also observed under an optical microscope as shown figure 2.4. The samples are lit from below using the bright-field mode (a) and using crossed polarization (b). Polarized light is a contrast-enhancing technique that improves the quality of the image obtained with birefringent materials. In (a), we see white to translucent particles, whereas in (b) the polarization unravels various colours yellow, red, orange, green). This proves that the Gwent particles are single crystals.

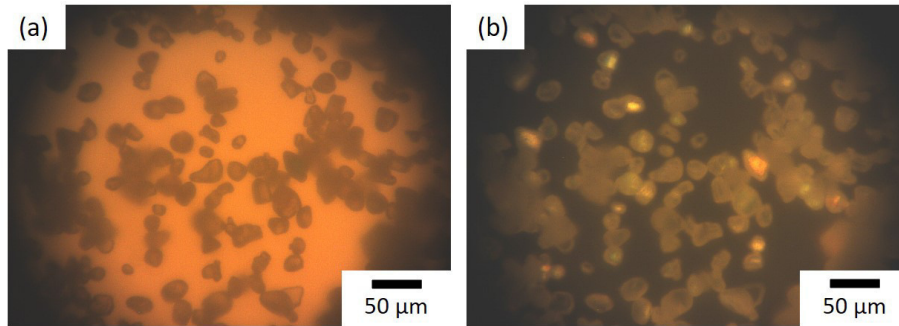


Figure 2.4: Images of Gwent ZnS:Cu particles under an optical microscope. (a) bright-field mode, (b) polarization mode.

The photoluminescence (PL) spectrum (cf. figure 2.5) shows an asymmetrical large band at 509 nm for an excitation wavelength of 350 nm. Franz *et al.* [47] suggest that this band is probably the combination of two bands, one at 460 nm and the other at 525 nm, concluding that Cu^+ is the active center leading to this emission.

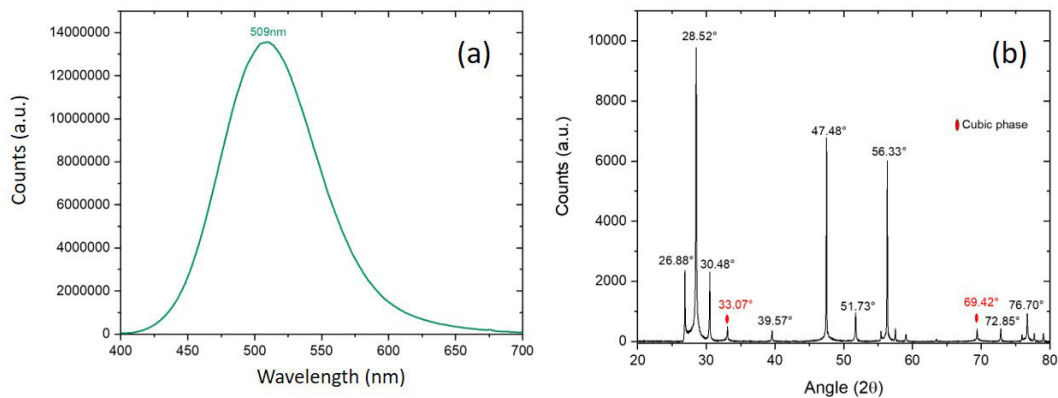


Figure 2.5: (a) Photoluminescence spectrum, large emission band centered at 509 nm. (b) XRD diffractogram showing peaks corresponding to a hexagonal structure and few others belonging to the cubic phase.

As mentioned previously in section 1.2.3, ZnS exists in two crystal structures:

cubic (fcc) and hexagonal (hcp). To determine the crystal structure of our material, we performed X-ray diffraction (XRD). This measurement shows a wurtzite (hcp) pattern due to the distinctive peaks at 26.88° , 28.5° , 30.5° , 39.5° , 47.5° , 51.7° and 56.3° corresponding to the planes $[2\bar{1}10]$, $[\bar{2}4\bar{2}0]$, $[\bar{1}2\bar{1}1]$, $[2\bar{1}\bar{1}2]$, $[11\bar{2}0]$, $[2\bar{1}\bar{1}3]$ and $[11\bar{2}2]$ respectively. However, the Gwent material is not purely hexagonal as peaks at 33° and 69.4° correspond to the zinc blende crystal structure ($[0002]$ and $([8\bar{4}\bar{4}0])$). Thus, the Gwent material exhibits both hexagonal and cubic crystal structures.

2.1.1.3 Conclusion

The copper-doped zinc sulphide (ZnS:Cu) purchased as phosphor paste from Gwent Group was firstly washed to obtain a powder free from any chemical constituent present in the paste. This powder is made of microparticles of $40 \mu\text{m}$ in diameter and exhibits a hexagonal (hcp) crystal structure put to light thanks to an XRD analysis. In addition to the zinc (Zn) and sulphur (S) elements, the SEM-EDX analysis showed the presence of oxygen (O) and aluminium (Al) on the particles. These two new elements reveal the presence of an aluminium oxide (Al_2O_3) coating. As for the photoluminescence properties, the Gwent ZnS:Cu exhibits a green-blue color with an emission band centered at 509 nm.

2.1.2 Using different PDMSs

Understanding the polymer matrix is a very important step toward the comprehension of elasto-mechanoluminescence. In this section, the properties of polydimethylsiloxane (PDMS) and the curing processes are presented. Moreover, a detailed protocol is given for the fabrication of the composite materials. Also, in order to determine the most efficient system, different types of PDMSs are described and their effect on the elasto-mechanoluminescence was also investigated.

2.1.2.1 Polydimethylsiloxane

Definition

PDMSs are polymeric organosilicon substances or “silicones”. They are used in industrial, pharmaceutical, food and medicinal applications and are not risky for human life or the environment. The linear polymer is generally composed of dimethylsiloxy units and trimethylsiloxy end groups (cf. figure 2.6). PDMS can be found under different names: siloxanes, silicon fluids or oils, dimethicone (found in shampoos) or E900 depending on the field (pharmaceutical, food as antifoaming agent, cosmetics)[66]. It is also highly hydrophobic since water, or other polar solvents, can hardly wet the PDMS.

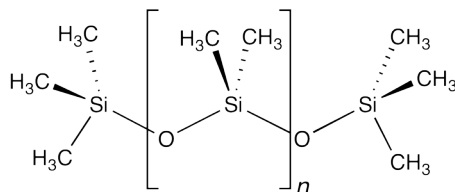


Figure 2.6: Chemical structure of polydimethylsiloxane or PDMS, where n is the number of repeating $[\text{SiO}(\text{CH}_3)_2]$ units. From [16]

PDMS empirical formula is $(\text{C}_2\text{H}_6\text{OSi})_n$ and its fragmented formula is $\text{CH}_3[\text{Si}(\text{CH}_3)_2\text{O}]_n \text{Si}(\text{CH}_3)_3$, n being the number of monomers repetitions. For the fabrication

of EML samples, PDMS (liquid) is mixed with a cross-linking agent and poured into a mold to obtain an elastomeric replica of the mold (PDMS cross-linked). Cross-linking, or curing, makes the material more rigid through the formation of bonds to link one polymer chain to another. It can be triggered by different parameters like heat, pressure, or irradiation. This process is irreversible, if the material is heated after, it will burn or degrade but not melt. This property affects thermosetting materials like epoxy resin or polyester. In the case of rubbers, vulcanization is another type of cross-linking. It can be found under the name of sulfur curing as sulfur is the atom that initiates the reaction; the polymeric rubber chains are bridged with polysulfur bonds.

The glass transition temperature of linear PDMS is very low (-125°C) and a shear elastic modulus of 250 kPa, which changes at a very small rate of 1.1 kPa per 1°C change in temperature [67]. The dielectric constant ranges from 2.72 to 2.75, which implies a low refractive index as well [68].

Curing processes

The structure of the PDMS shows a siloxane backbone, with alternating silicon and oxygen atoms. Methyl groups $-\text{CH}_3$ are connected to the silicon atoms. These groups are replaced by a hydrogen atom, or vinyl groups $-\text{CH}=\text{CH}_2$ to facilitate curing. There are different possible curing processes depending on the functional groups bore by the polymeric chain. When a platinum catalyst is present (cf. figure 2.7), the hydrogen and the vinyl terminated groups react with each other and form crosslinks, and heat is released.

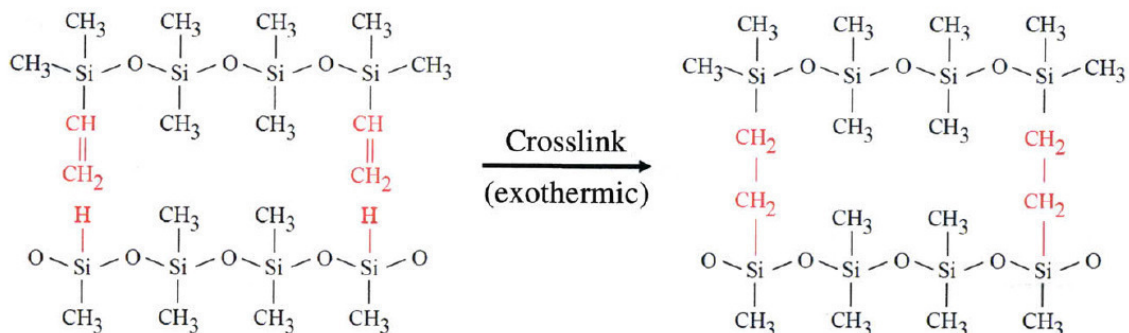


Figure 2.7: *Hydrogen and vinyl terms crosslink in the presence of a platinum catalyst. From [17]*

At the beginning, the polymer is viscous and composed of many short strands. During crosslinking, strands combine, and the viscosity increases as more crosslinks are formed over time. The molecular weight of each strand increases as it is linked to viscosity. Finally, the gelation happens, and the material becomes an elastic solid. Each original strand is connected at two points. The functionality of a strand is defined as the number of hydrogen or vinyl groups that are connected to the strand[17].

Silicone elastomers are crosslinked according to the following reactions[18]:

1. **Peroxide curing:** Peroxide curing involves the use of organic peroxides. When vinyl groups are present on the polymer chain, organic peroxides decompose, at high temperature, to form highly reactive radicals which chemically crosslink the polymer chains. The result is a highly elastic, three-dimensional network.
2. **Condensation:** Condensation takes place at room temperature and two types of systems belong to this category: one part system and two parts system. Crosslinking occurs for the first one when it comes in contact with air, i.e. humidity, and occurs

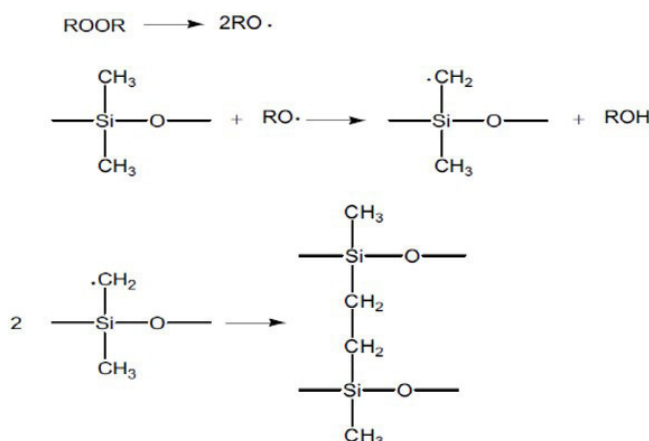


Figure 2.8: Peroxide curing process of PDMS. From [18]

for the second one when the catalyst and the cross-linking agent are mixed together. As by-product, alcohol is released and this leads to shrinkage (0.5 to 1% linear shrinkage).

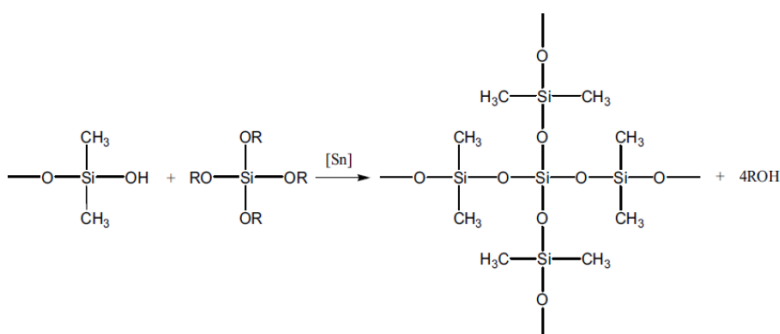


Figure 2.9: Condensation curing process of PDMS. From [18]

This is the case for the RTV or Room Temperature Vulcanisation cure which occurs after condensation of hydroxy terminated PDMS and silicon-alkoxide in the presence of a tin catalyst. We can find RTV-2 as a two-parts system, and RTV-1 as a one-part system. RTV-1 is used as construction sealant and as adhesive; while RTV-2 is used in molding, mould making, and encapsulation. They are also used to produce microfluidic devices by soft lithography[19].

3. **Addition:** This curing method calls for platinum, palladium or rhodium salts as catalysts and the presence of vinyl groups in the chains. There are no by-products with this reaction and shrinkage is eliminated. Crosslinked silicone is produced via Si-H group attachment to double bonds.
4. **Irradiation:** High energy electron beam or gamma rays have been used for a long time as a cross-linking method for silicone rubbers.

An example of an alkoxy condensation cure was given by *Brook Devlin*[19]. It shows the reaction of hydroxy terminated PDMS with TEOS (tertaethylorthosilicate) in

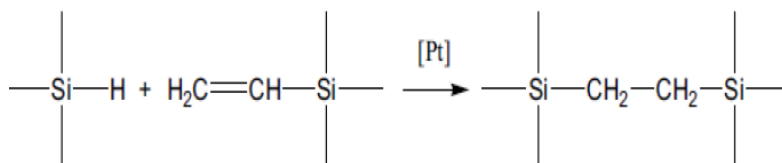


Figure 2.10: Addition curing process of silicon rubber. From [18]

the presence of DBTDA (dibutyltin diacetate) as catalyst. The catalyst, in low concentration (0.05-0.5wt%), needs to be activated with water. The hydrolysis turns tin to acetate bond, forming tin hydroxide, and liberating acetic acid.

The catalyst, now activated, forms Sn-O-Sn complex with TEOS by hydrolyzing a silicon-alkoxy bond and eliminating a volatile ethanol (cf. figure 2.11). Then, hydrolyzed TEOS is transferred to the hydroxy end group of a PDMS chain. A proton is extracted from the group in order to regenerate the activated catalyst (cf. figure 2.12).

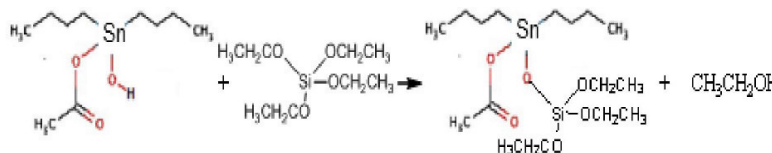


Figure 2.11: Formation of a Sn-O-Si complex with TEOS. From [19].

It may complex with either unhydrolyzed TEOS or with the remaining silica-ethoxy groups of the TEOS now bound to PDMS. The complex will react with the hydroxy end groups, in both cases, until they have all been consumed. Flexible PDMS molecules are bound to each other by rigid O-Si-O linkages.

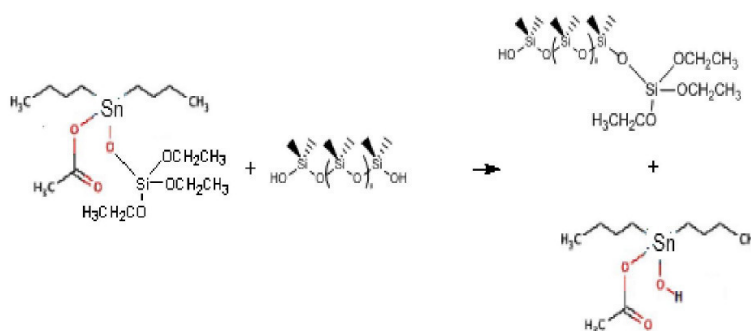


Figure 2.12: Transfer of hydrolyzed TEOS to hydroxy end group of PDMS chain and regeneration of the activated catalyst. From [19].

The hydroxy end groups of a PDMS chain are most likely to encounter two different catalyst/TEOS complexes because TEOS is in a much higher quantity than the catalyst. This excess and the increase resistance to hydrolysis ensures that each of the encountered complexes by a given hydroxy terminated PDMS molecule is most likely to contain a TEOS that has only been hydrolyzed once. That is why the PDMS chains contain mainly triethoxy end groups.

The regenerated activated catalyst can complex with the unhydrolyzed TEOS, still in high concentration in the mixture. However, it is no longer possible for any hydroxy group to react with the DBTDA/TEOS complex because all the hydroxy/PDMS has been end capped, and thus, the reaction stops.

One part RTV sealants consist of just this type of liquid reaction mixture. Because they are sealed in a waterproof container, when opened, the reaction initiates due to atmospheric moisture. The moisture plays the same role as previously mentioned for the tin catalyst: the water forms alkoxy-silicon-hydroxides by hydrolyzing the silicon-alkoxy bonds of TEOS. The resulting hydroxide may then react with the catalyst/TEOS to polymerize TEOS and regenerate the activated catalyst (cf. figure 2.13), which is the fastest reaction, or it may polymerize TEOS by condensing with each other.

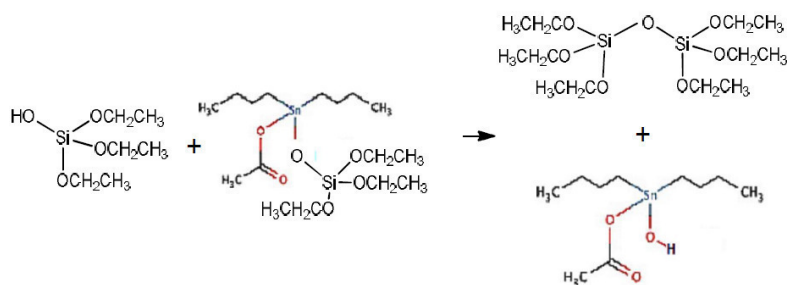


Figure 2.13: *Polymerization of TEOS and regeneration of the activated catalyst. From [19].*

The concentration of unhydrolyzed TEOS decreases as the reaction continues. Ethoxy group can be found on the triethoxy structures. The activated catalyst or water may either complex with or hydroxylate such a group. Diethoxy groups can form large silicon-oxygen linked structures that arise from condensation. Because the concentration of the triethoxy containing compounds decreases, the catalyst and water can complex or hydroxylate an ethoxy group on the available diethoxy structures. At the end, many nano-domains of amorphous silica are formed following the full hydrolyzation and condensation of TEOS. These domains are distributed throughout the elastomer network. Under moderately acidic to basic conditions the catalyzed condensation reaction is favored and the silica forms dense nano-domains by nucleation.

Polydimethylsiloxane or PDMS is a polymer which becomes rigid after a cross-linking or curing process. The silicone elastomers are crosslinked through: peroxide curing (use of organic peroxides), condensation (Room Temperature Vulcanisation RTV curing), addition (use for catalysts like platinum) or irradiation.

2.1.2.2 Experimenting with different brands of PDMS

In order to evaluate the influence of the polymer, three PDMSs were tested. They all are two-parts polymers but their curing processes are different as one of them is an RTV.

Sylgard 184 Silicone Elastomer

The Sylgard 184, Dow Corning Corporation product, is a silicone elastomer kit. The kit contains two chemicals: base (part A) and curing agent (part B) which need to be mixed together with respect 10:1 mass ratio. They are both transparent but viscous in nature and each part is nonreactive on its own. Sylgard 184 is a flexible rubber which protects against mechanical shock and thermal cycling stress and against moisture. Vacuum de-airing is

recommended for 30 minutes. The curing process can be achieved at room temperature as well as at a higher temperature[29]. Table 2.1 lists the recommended schedules:

Temperature	Curing time
23°C	24 h
65°C	4 h
100°C	1 h
150°C	15 min

Table 2.1: *Sylgard 184 PDMS curing time as a function of temperature. From [29]*

Here is the chemical composition of this PDMS:

- The base (part A) contains:
 - Dimethyl siloxane, dimethyl terminated,
 - Dimethyl and trimethyl silica,
 - Terta (trimethoxysiloxy) silane,
 - Ethyl benzene.
- The curing agent (part B) contains:
 - Dimethyl, methylhydrogen siloxane,
 - Dimethyl siloxane, dimethylvinyl terminated,
 - Dimethylvinylated and trimethylated silica,
 - Tetramethyl tetravinyl cyclotetra siloxane,
 - Ethyl benzene.

Property	Value
Color	Clear
Density	$1.02g/cm^3$
Hardness, Shore A	50
Tensile strength	$7.1MPa$
Elongation at break	140%
Tear strength	2.6 kN/m
Permittivity	2.75
Dielectric strength	21 kV/mm

Table 2.2: *Properties of Sylgard 184 PDMS cured 4 hours at 65° C. From [29]*

WACKER Elastosil RT601 A/B

Along with the Sylgard 184, Wacker Elastosil is the most used PDMS for EML studies. This PDMS is also a two-parts polymer with 9:1 mixing ratio. The component A contains the platinum catalyst and B the crosslinker. The two parts need to be mixed at a 9:1 weight ratio and a vacuum encapsulation is recommended in order to eliminate the air introduced during the mixing. The curing time depends on the temperature and size of the prepared sample.

During platinum-catalyzed addition curing, the crosslinker's Si-H groups react with the vinyl groups of the polymer to form a three-dimensional network. Unlike peroxide-curing, platinum-catalyzed addition reactions do not produce odor- or flavor- impairing by-products. Curing is fast and the speed can be controlled via temperature.

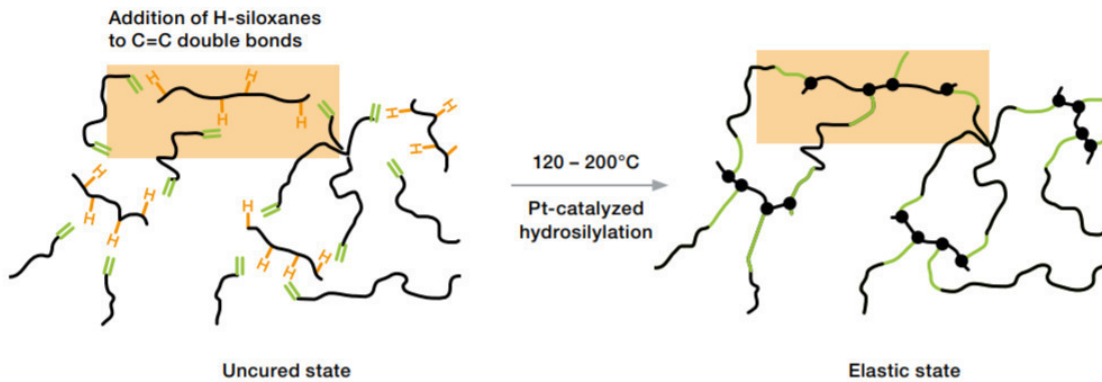


Figure 2.14: Addition curing process. From [20]

Temperature	Curing time
23°C	24 h
70°C	20 min
100°C	10 min

Table 2.3: Wacker Elastosil RT601 A/B PDMS curing time as a function of temperature. From [30]

Property	Value
Color	Colorless, transparent
Density	1.02 g/cm ³
Hardness, Shore A	45
Tensile strength	6 MPa
Elongation at break	100%
Volume resistivity	10 ¹⁵ Ohm.cm
Permittivity	2.8

Table 2.4: Properties of Wacker Elastosil RT601 PDMS cured 30 min at 150 °C in a circulating air oven, 23°C. From [30]

Esprit Composite: RTV 67

It is a bi-component silicon which requires a curing of at least 24 hours at room temperature. This product is designed for the manufacture of molds to produce waxes used in artistic foundries, for polyurethane polyester casting and epoxy resins, and of molds for rosettes and decorative stucco[31]. It is used with a 5% curing agent and a vacuum encapsulation is recommended to ensure optimal tensile strength.

RTV stands for Room Temperature Vulcanisation and is a type of silicone rubber which cures at room temperature. RTV silicones can be cured with a catalyst consisting of either a platinum or a tin compound. Compared to the other PDMSs, the RTV67 is not transparent but translucent. This color can be attributed to the presence of SiO₂ even though this was not clearly stated in the data sheet. Adding fumed silica to PDMS provides better mechanical reinforcement to silicon rubbers and was reported in the literature as early as 1948 (Warrick). When fumed silica is incorporated to the PDMS, hydrogen bonds will form between these groups and oxygen atoms of the PDMS backbone.

An additional step was added after noticing the easy fracture of the samples. Using a technique similar to dip-coating, the samples are coated with PDMS to reinforce

Property	Value
Color	Translucent
Density	1.08 g/cm^3
Hardness, Shore A	12 ± 2
Elongation at break	$900 \pm 100\%$
Tear resistance	$26 \pm 3 \text{ kg/cm}^2$

Table 2.5: *Properties of Esprit Composite RTV67 PMDS cured at room temperature. From [31]*

them, cf. figure 2.15.

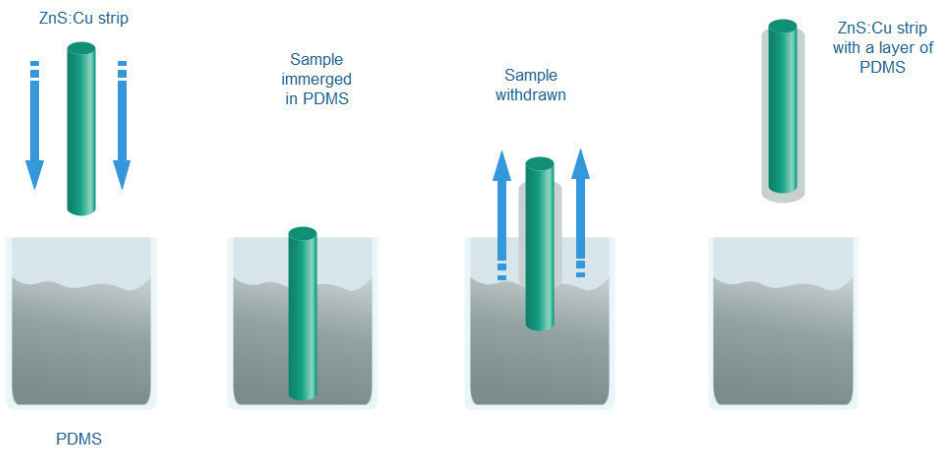


Figure 2.15: *Dip coating with PDMS of the samples. process.*

The Wacker Elastosil RT601 A/B and Sylgard 184 PDMSs are similar as they show close mechanical properties obtained through a vinyl platinum condensation (density, hardness, tensile strength). However, the RTV 67 PDMS is obtained through tin catalized condensation and presents different mechanical properties. In particular, the elongation at break is much higher than the other two ($900 \pm 100\%$).

2.1.2.3 Sample manufacture

The fabrication of the composite material was done according to the detailed procedure of *Jeong et al.*[4]. The ZnS:Cu particles were mixed with polydimethylsiloxane (PDMS) at a weight ratio of 7:3 (respectively). The PDMS is previously prepared using a curing agent at a ratio depending on the PDMS used for the experiment. The general process used for making EML samples is the following (cf. figure 2.16):

1. Prepare the PDMS by mixing the two components: the base and the curing agent respecting the weight ratio precised in the data sheet,
2. Add the ZnS:Cu particles to the PDMS at a 7:3 weight ratio,
3. De-air (or degase) the mixture for a few minutes to remove any trapped air,
4. Pour gently to avoid the introduction of air onto an aluminium mould. This mould shapes samples of 70 mm in length, 10 mm in width and around $700 \mu\text{m}$ in height,
5. Wait for the PDMS to be cured using either a heat treatment (oven) or leaving it at room temperature for a few hours. This step depends on the PDMS used (cf. tables 2.3, 2.1 and subsection 2.1.2.2).



Figure 2.16: *Steps of sample making. From left to right: mixing the ZnS:Cu particles and the PDMS, degasing the sample, shaping the samples by pouring the mixture into a mould, and curing at room temperature.*

2.1.2.4 Characterization of the composite material

Figure 2.17 is a photograph of an EML sample under UV-light (365 nm), left image, and natural light, right image. The SEM image (figure 2.18(a)) is a transverse plane of an EML strip. The particles are well dispersed in the PDMS but some clusters can be found. The photoluminescence spectrum in figure 2.18(b) shows a broad emission band centered around 504 nm. We notice a shift of 5 nm from the Gwent powder PL spectrum figure 2.5(a).



Figure 2.17: *Photographs of an EML sample under a 365 nm UV-light (left) and natural light (right). Sample dimensions: 70 mm x 10 mm x 0.7 mm*

Before using an experimental setup to test the samples, preliminary assessments are achieved. One can test the elasticity and the EML intensity by manually stretching a strip in the dark. Different results were obtained with the 3 PDMSs, they are summarized in the table below:

PDMS	Elasticity*	EML**	ML***
SYLGARD 184	Low	No	Yes
WACKER Elastosil	~ 50%	Yes - Weak	Yes
RTV67	~ 150%	Yes - Intense	Yes

Table 2.6: *Preliminary EML results over PDMS efficiency. The percentages are compared to the length of the sample at rest. *hand stretching. **from hand stretching, eye perception. ***from finger pressure, eye perception*

The Sylgard 184 PDMS showed very poor properties for our study, the sample stays very rigid under elastic deformation and, therefore, does not exhibit EML. However,

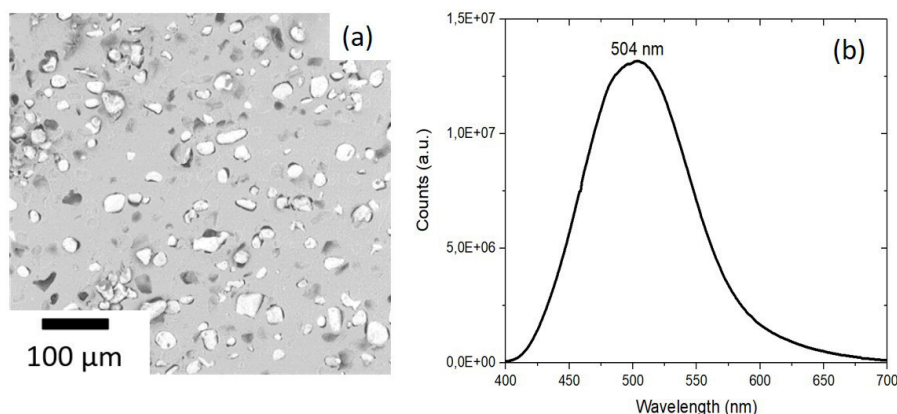


Figure 2.18: *Characterization of an EML sample. (a) SEM image. (b) Photoluminescence spectrum for an excitation wavelength of 350 nm. Large emission band at 504 nm.*

ML is visible in the dark by the naked eye when the sample is strongly pressed between two fingers. Compared to the previous one, the Wacker Elastosil PDMS has a better elasticity. The composite strip can be stretched up to 50% of its original length and does demonstrate EML as shown in figure 2.19. Also, as for the Sylgard, ML is visible under finger pressure.



Figure 2.19: *Photographs of an EML sample made of Gwent ZnS:Cu phosphor powder and Wacker Elastosil RT601 PDMS under elastic deformation performed by hand.*

Amongst the three tested PDMSs, the RTV67 is the one showing the most satisfying results. An intense and bright EML is visible even in a dimly lighted room thanks to the high elasticity offered by the PDMS (up to 150%).

Even though Wacker Elastosil and Sylgard are the ones generally used for these studies, only the RTV67 exhibited the EML portrayed in the scientific literature.

2.1.3 Conclusion

Crystal ZnS:Cu was used for our EML experiments. The phosphor powder was incorporated in a polymer matrix polydimethylsiloxane (PDMS). Three different PDMSs were presented in this section: Sylgard 184, Wacker Elastosil RT601 A/B and Esprit Composite RTV 67. Although they share a common curing process condensation through the use of a catalyst, they have different mechanical properties. In particular, the RTV 67 stands out with its high elongation at break compared with the other two. The EML samples were manufactured using 70wt% of phosphor and 30wt% of PDMS. They exhibit a broad emission band centered at 504 nm. The emission of the EML sample shifted slightly from the powder itself characterized at 509 nm. The elasticity of the sample and the EML intensity depend greatly on the type of PDMS. The RTV 67 is the one showing the best EML properties with a high elasticity, and a bright and intense luminescence upon stretching.

2.2 EML experimental methods

The elasto-mechanoluminescence was investigated using the stretching and releasing (S-R) method. The sample is under elastic deformation through constant S-R cycling (one cycle corresponds to one stretching and one releasing). The frequency and the percentage of deformation are the two main parameters used to control the experiment. In this section, two different experimental setups are presented.

2.2.1 Camera based setup

This first setup is 2 meters long and was originally designed to perform fatigue tests on polymers (collaboration with Loïc Vanel). It was particularly suitable for our study as it offers the possibility to change different parameters like velocity and displacement, and monitor the experiment with a camera.

2.2.1.1 Setup description

In this setup, the sample is stretched symmetrically on both ends. From a 0 initial position, two mechanical arms move to $+x$ and $-x$ positions. Using the appropriate software, the displacement, the displacement rate (or velocity) and the acceleration can be set by the user. The displacement can reach up to 2 meters in total at velocities from 0.002 to $1 \text{ m}\cdot\text{s}^{-1}$. In addition, a force sensor is attached to one extremity of the setup. The sensor has a 0 to 220 N force range. It is connected to a National Instruments data acquisition card and is controlled via a MATLAB program which displays the evolution of the force over time.

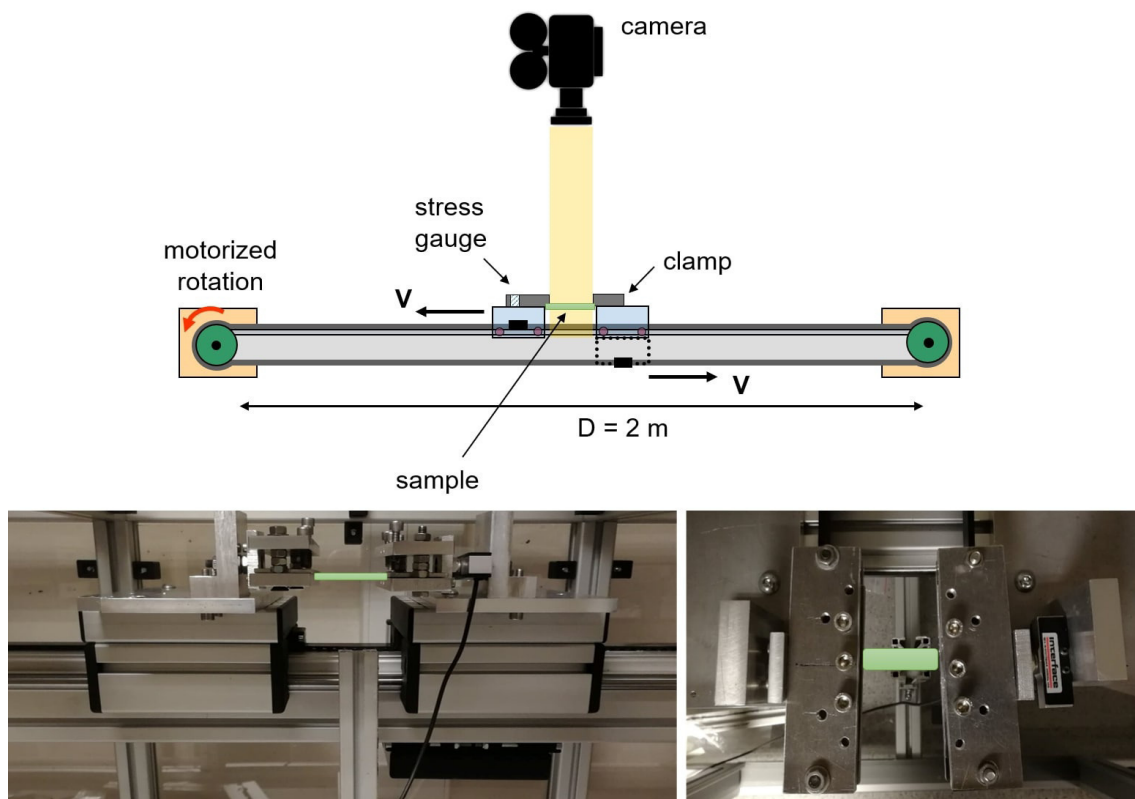


Figure 2.20: Schematic diagram and photographs of the camera-based stretching-releasing setup, front (left) and top (right) view.

A JAI GO camera is placed on top of the sample to record and monitor the emitted light during the experiment. From Matlab toolbox, we can choose the camera parameters and settings: frames per second (fps), observation window, brightness & contrast and gain. It generates a video which is later processed with a Matlab program or Image J software to extract the average light intensity of the whole sample as a function of time.

1 motor step leads to $27.5 \mu\text{m}$ displacement for each arm. For example, knowing that the sample is 7 cm in length and attached at both extremities, the active part of the sample is reduced on average to 5 cm. If we want an 80% elastic deformation at 1 Hz (this means that one S-R cycle will be performed at 2 Hz) , then the parameters will be the following:

Displacement			Displacement speed	
%	cm	counts	cm.s^{-1}	counts.s^{-1}
80	4	727	4	1454

Table 2.7: *Experimental parameters of the camera-based S-R setup.*

Here are the parameters for a routine experiment:

- Speed 4 cm.s^{-1} ,
- Number of cycles: the user enters manually all the instructions (deformation, speed, etc). Each instruction corresponds to a movement performed by the mechanical arms and 1 cycle corresponds to two instruction lines.
- Deformation percentage 64%: this percentage appeared to be the most appropriate after numerous preliminary tests. A higher deformation would cause a premature degradation of the sample and early fracture, a lower one would not induce sufficient luminescence to be detected by our camera.

2.2.1.2 EML results

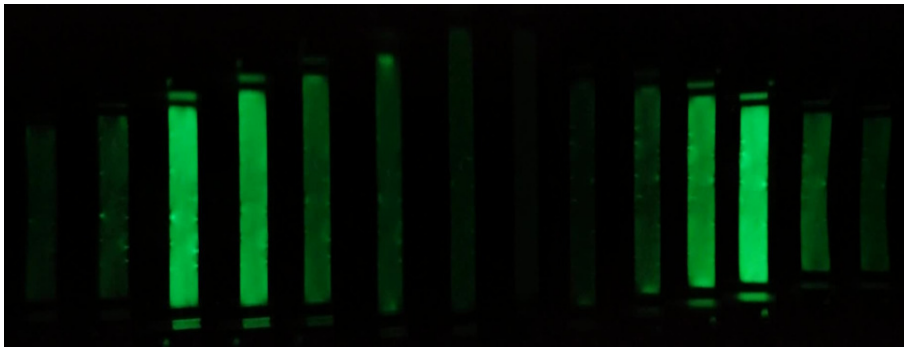


Figure 2.21: *Photographs of an EML sample made of ZnS:Cu Gwent phosphor powder and RTV67 PDMS under one cycle of elastic deformation (stretching and releasing).*

Figure 2.22 shows the results obtained from the composite sample Gwent ZnS:Cu-PDMS under a 64% deformation. The average brightness of the sample during S-R deformation presented on the left of the figure decreases rapidly over time. After 2 minutes, the brightness is almost 20 times lower than at the beginning of the experiment. The inset shows a close up of the start of the curve. We can distinguish the presence of two emission peaks. Each peak corresponds to an applied deformation, i.e. one peak is attributed to the stretching phase and the other one to the releasing phase. The first peak visible on

the inset matches the first extension of the sample and we notice that this peak is very weak. The releasing peak is sharp and symmetrical whereas the stretching one increases rapidly and takes twice as long to decrease; it is asymmetrical. We observe also that the luminescence seems to extinguish completely before a new S-R cycle begins. As for the applied recorded force, it starts at 11 N, decreases and then stabilizes around 7 N.

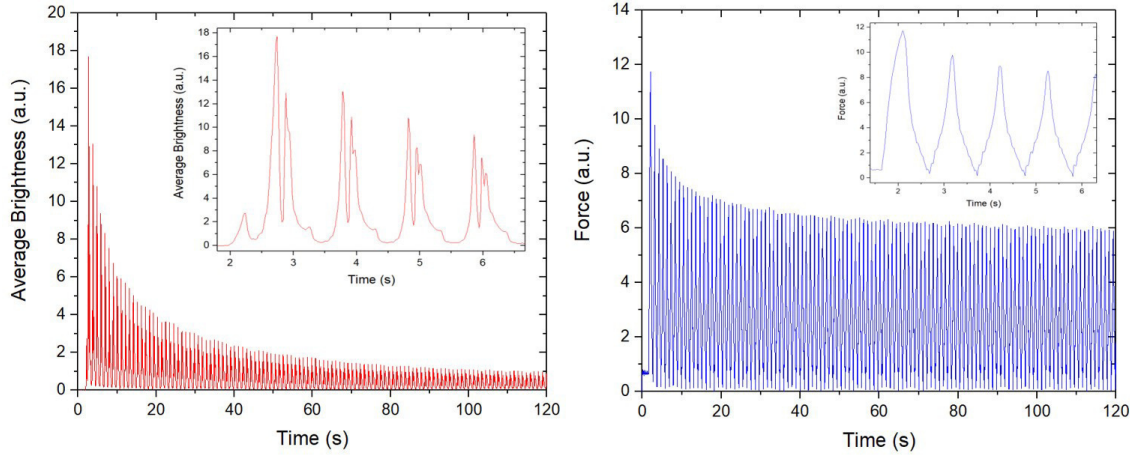


Figure 2.22: *Experimental curves of the EML response of the Gwent ZnS:Cu-PDMS composite material. Left, curve of the average brightness over time; inset: zoom of the curve. Right, curve of the recorded applied force on the sample over time; inset: zoom of the curve.*

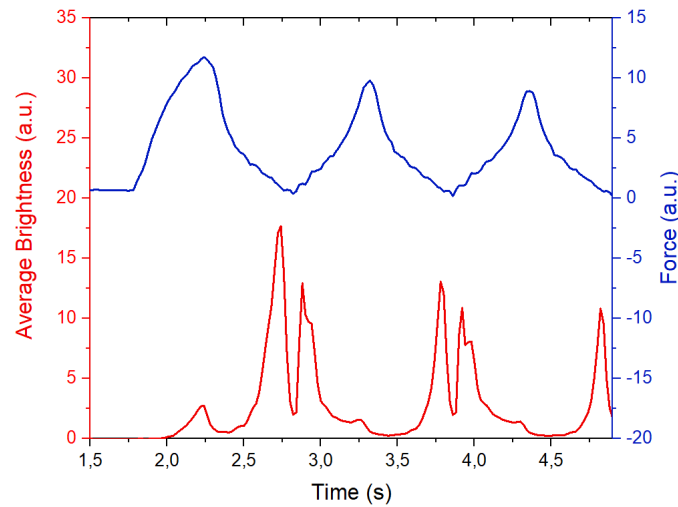


Figure 2.23: *Experimental curves of the EML response of the Gwent ZnS:Cu-PDMS composite material.*

This experiment provides important information on the behaviour of the Gwent ZnS:Cu-PDMS composite material under elastic deformation. However, this setup has a certain number of limitations which prevent a complete and correct interpretation of the results. Before studying the self-recovery phenomenon, each experiment required a new and untouched sample; considering the time needed to manufacture a sample, this system is consuming.

The force is given directly by Matlab and it is not possible to set a force value for the experiment which explains the decrease in the average brightness emitted by the sample. This causes a fast loss of light intensity and prevents the possibility to conduct long measurements (longer than a few minutes). In order to have a constant force (cf. figure 2.24),

the displacement is increased gradually but only a few cycles can be performed as each instruction line is entered by the user one by one.

One of the biggest problems encountered with this setup is the impossibility to have accurate and precise synchronisation between the force curve and the brightness curve due to the use of two different software. The software controlling the motor is lunched after the force and the time gap between the two actions is determined.

The camera recorded large files which makes the processing very long even for short videos of 2 minutes long. Moreover, this detection method can blind us from seeing details that can be present locally on the sample because we observe but the sample as a whole. Also, not all samples can be studied using this method. For composite materials made of less than 70wt% of ZnS:Cu phosphor, the detection is almost impossible even by changing the camera parameters; only bright samples could be recorded because the sensitivity of the camera is not sufficient.

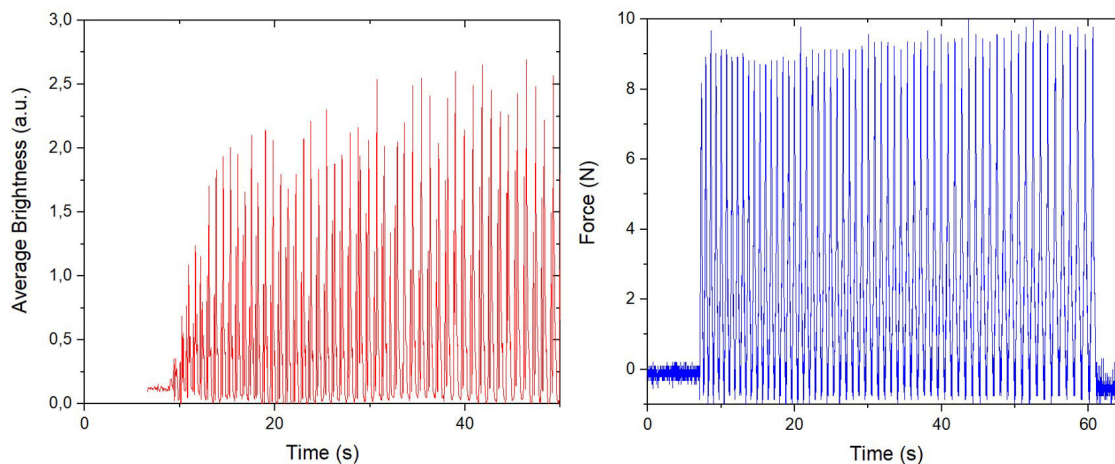


Figure 2.24: *Experimental EML results at constant applied force of 10 N on the Gwent ZnS:Cu-PDMS composite material. Left, EML response curve. Right, applied force curve.*

2.2.1.3 Conclusion

The elasto-mechanoluminescence is very bright and intense at the beginning of an experiment but it decreases greatly in a short period of time. However, by recording the applied force, we notice that it is not constant over time and could explain the intensity decrease. When a constant force is applied, the EML intensity is also constant. We have also observed that the emitted light is composed of two emission peaks: one during the stretching phase of the sample and the second during the releasing. Even though this method allows to gather useful information on the behaviour of EML samples, it is impossible to detect weaker light intensities. We thus move to a local detection setup using a photomultiplier (PMT).

2.2.2 Local measurement: optical fibre + PMT

The aforementioned encountered issues with the camera-based setup, such as the sensitivity of the detection method, led us to develop a new experimental system to study the elasto-mechanoluminescence response of the ZnS:Cu-PDMS composite material. This setup is entirely dedicated and designed to our study. The primary goal was to control as

many parameters as possible: displacement, velocity, acceleration, force, synchronisation. Of course, finding the right device has required dedicated development.

2.2.2.1 Setup description

Setup components

This setup comprises a high speed linear actuator from SMAC which can be controlled through position, speed and acceleration parameters. The piston can move up to 30 mm and the high speed can go up to 2500 cpm at 10 mm and 1500 cpm at 25 mm. Because only one actuator is used, the deformation is asymmetrical as it is applied on one side of the strip, the other end is fixed in the sample holder. The piston (carries coil, rod and DC motor) is mounted to a linear bearing carriage, which slides in a linear motion. A copper coil rides inside a magnet assembly. When current flows in the coil, a reaction force is produced causing the piston to slide along the guide rail. Adjustable end stop, or bumpers, are set at each end of the travel to cushion any impact force that may occur. Flags carried by the piston activate limit switches (end of stroke sensors) before the end of travel is reached. Either the glass scale of the optical encoder (which measures the distance travelled by the piston) or the reader head is carried by the piston. As the piston moves, the detector head reads the distance travelled. An index line (locates a fixed position on the scale) on the glass scale (optical encoder scale) is used as a home location. The actuator rod exits the body through the bearing to maintain alignment. A thermistor is also present in the actuator to signal an overheating condition [69].

The actuator is connected to a controller which is a one axis stand-alone controller and driver, with input/output (I/O) capabilities, designed for the control of the actuator. It implements a mnemonic type command instruction set via a standard RS-232 serial communications interface. These commands can be executed directly or used to create command macros using the SMAC software [70].

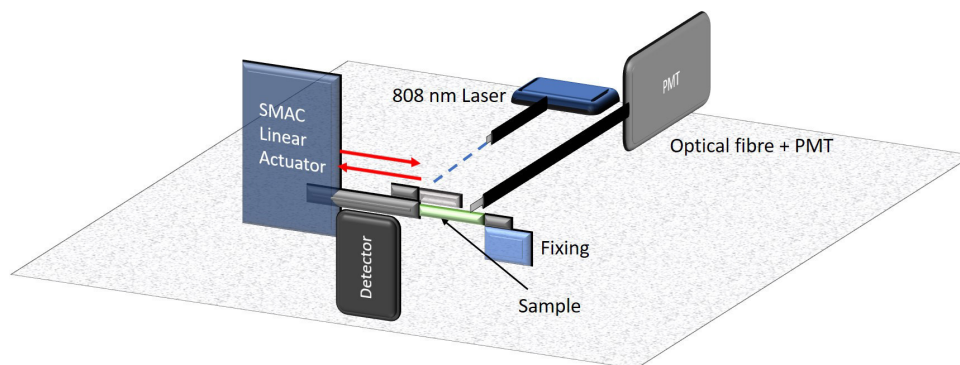


Figure 2.25: Schematic diagram of the photomultiplier-based stretching-releasing setup.

The SMAC linear actuator has the following characteristics:

- Dimensions: L x W x H : 120 mm x 85 mm x 120 mm
- Force range : from -115 N to 115 N
- Stroke : 30 mm

There are three methods with which the actuator can be commanded to move: force mode, velocity mode and position mode:

- Force mode: it is an open loop, using no feedback from the encoder. Actual position is still monitored but has no effect on the output.

- Velocity Mode: the rod can be moved with a given velocity, acceleration, force and direction.
- Position Mode: the actuator can be moved to various positions along the stroke. It is possible to set acceleration, velocity and force during the move. It is possible to make absolute or relative moves or to store learned positions, which can be recalled later in the program.

Our interest is to be able to set different deformations to the sample and the appropriate mode for that is the position mode. Below are the standard parameters used for the experiments. They are repeated in an endless loop until the user stops the motion.

- Speed: 4 cm.s^{-1}
- Acceleration: 4000 cm.s^{-1}
- Deformation percentage: 63%

The force can be extracted only twice per cycle: when the sample is completely stretched and when it comes back to its initial position. So far, it is not possible to display values continuously. At rest, the sample length is 20 mm.

To detect the luminescence signal, an optical fibre connected to a photomultiplier (PMT) is placed very close to the sample so as the detected area is about 1 mm^2 . For a high sensitivity, the photomultiplier is operated in photon-counting mode. In this mode, a single electron is ejected from the photocathode after the interaction with a single photon. After multiplication, an output electric pulse is produced. A discriminator and a photon counter give the number of counts/s. Typically, the output current pulse is converted to a voltage and amplified by the preamplifier. The use of a discriminator is essential for photon-counting. If an input pulse falls within a determined range of amplitudes then the pulse will be output. This range is determined by a lower- and upper-level discriminator (LLD and ULD). Pulses of low amplitude and those larger than the photon pulses are removed. Afterward, the pulse is shaped to be TTL and is finally counted.

So that the signal can be seen on a computer, this TTL signal goes through a National Instruments data acquisition (DAQ) device operated for counting which in turn is connected to the computer. The DAQ NI USB 6001 is a full-speed USB device that provides eight single-ended analog input (AI) channels, which may also be configured as four differential channels. It also includes two analog output (AO) channels, 13 digital input/output (DIO) channels, and a 32-bit counter and a max input frequency of 5 MHz. The PFI 0 or PFI 1 pins can be configured as a source for counting digital edges. In this mode, either rising- or falling-edges are counted using a 32-bit counter [71].

Moreover, an optical density coupled to an 808 nm laser was implemented to simultaneously track the movement of the sample. The density is placed on top of the sample, on the mechanical arm of the actuator, and a detector is placed behind it, cf. figure 2.25. As the arm moves, the sample is stretched and the optical density follows the same movement. The laser is aimed at the optical density and the detector returns an amplitude value which corresponds to the displacement performed by the linear actuator, cf. figure 2.26.

Operating software and Data acquisition

The signal is read by the computer through a LabVIEW program. LabVIEW (Laboratory Virtual Instrument Engineering Workbench) is a systems development software for applications which require test, measurement, and control with rapid access to hardware and data insights from National Instruments. It offers a graphical programming approach, called "G". It is commonly used for data acquisition, instrument control, and industrial automation. This program displays the number of photons detected over time in real time

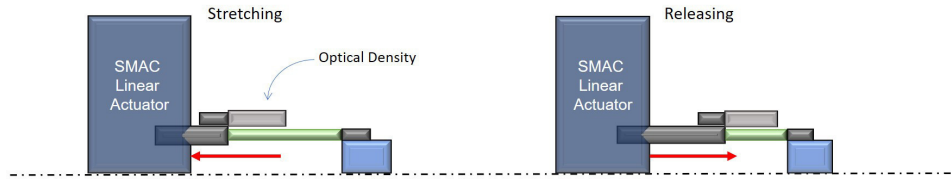
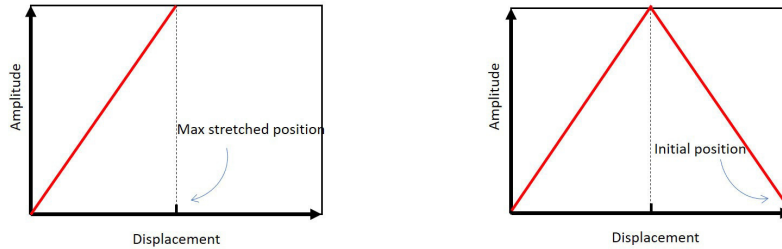
Movement of the actuatorResponse of the detector

Figure 2.26: *Amplitude response of the detector depending on the movement of the actuator.*

and records a data file. Using this tool, it is possible to adjust the integration time between two points (or two values of the detected photons) up to a lower limit of 10 ms.

The experiment operates thanks to two software: LabVIEW, to display and record the light intensity over time, and SMAC software, with which the motor can be controlled and trigger the movement of the piston that stretches the sample. At first, the goal was to have only one program combining all the actions above, and operating on LabVIEW only. However, conflicts between the data control and acquisition arose and the actuator did not respond to the commands. Moreover, the RS-323 serial communication interface made it difficult for LabVIEW to perform properly. That is why, we separated the two.

How to program on the SMAC software The SMAC commands are unique and not user friendly. Below is an example on how to run the motor from a start position to another x position.

$PM, MN, SG100, SI100, SD1200, IL5000, SA20000, SV104840,$
 $MA - 3000, GO, WP - 3000, MA - 500, GO, WP - 500, RP$ (2.1)

- PM - enter position mode
- MN - Motor On
- SG, SI, SD, IL - set the proportional, integral and derivative gains, and the integration limit
- SA - set acceleration
- SV - set velocity
- MA - move target absolute
- GO - start motion
- WP - wait for absolute position
- RP - repeats the command line

When operating using the position mode (PM), the position (MA), the acceleration (SA) and the velocity (SV) can be chosen by defining an "n" value. This value is not given using the International System of Units (SI) but necessitates unit conversion depending on the type of controller used. In addition, the PID parameters are essential (SG, SI, SD). PID is a control loop mechanism employing feedback that is widely used in industrial control systems and a variety of other applications requiring continuously modulated control. A PID controller continuously calculates an error value $e(t)$ as the difference between a desired setpoint (SP) and a measured process variable (PV) and applies a correction based on proportional, integral, and derivative terms (denoted P, I, and D respectively), hence the name. In practical terms it automatically applies accurate and responsive correction to a control function. The "n" value lies between 0 and 32,767.

The IL command clamps the level of influence that the PID digital filter integral term can use to reduce the static position error, thereby reducing integral "wind up". When properly adjusted, this can enhance loop stability and operation. The Integral Limit (IL) and Set Integral Gain (SI) must both be set to a non-zero value in order for the integral term to have any effect.

The move target absolute (MA_n) sets the target position of the servo to absolute position $-p \leq n \leq p$ with $p = 2,147,483,647$ (32 bits). The absolute position is relative to the point of initialization (home or 0). As the Move Absolute (MA) command will not initiate a motion, a Go (GO) command must be used. The servo's target position will be adjusted whether the servo is on or off.

SA_n and SV_n set the acceleration rate and the desired velocity for the servo. The 32 bit argument to this command is scaled by 65536 (16 bits) and $0 \leq n \leq 1,073,741,823$.

When wanting to retrieve the force, the returned n value ranges from 0 to 32,767.

To translate the "n" value to SI, we use the following expressions:

For the position:

$$x = n \cdot \frac{5}{1000} \text{ mm} \quad (2.2)$$

For the velocity:

$$v = \frac{n}{2621} \text{ mm} \cdot \text{s}^{-1} \quad (2.3)$$

For the acceleration:

$$a = n \cdot \frac{10}{5} \text{ mm} \cdot \text{s}^{-2} \quad (2.4)$$

For the force:

$$F = n \cdot \frac{115}{32767} \text{ N} \quad (2.5)$$

Considering expression (2.1), we obtain the following values for the acceleration, velocity and position (table 2.8):

	n SMAC value	SI value
Acceleration	20,000	40,000 $\text{mm} \cdot \text{s}^{-2}$
Velocity	104,840	40 $\text{mm} \cdot \text{s}^{-1}$
Position (= end - start)	2,700	13.5 mm

Table 2.8: *Conversion table from SMAC actuator values to SI values.*

Many other commands exist for configuration, reporting, sequencing as well as motion, register and input/output commands. They were not used.

Encountered problems

Some problems still need to be addressed. For the programming aspect, and as mentioned earlier, the use of two dissociate programs prevents the synchronisation between the brightness curve and the force values returned by the SMAC software. Also, it was noticed that the actuator reinitiates the position value almost after each use. If not attended to, this leads to errors as the value of the start position will change and so will the deformation previously set; these values need to be adjusted at the beginning of each experiment. Moreover, the motor itself will stop because of this error and get stuck. A whole reboot is necessary to restart the device afterwards. Regarding LabVIEW, long experiments showed a flaw in the program. The integration time varied and increased over time. Initially set at 1 ms, it could reach up to 50 ms after one hour and keep going up. To solve this problem, the program has been redesigned. Instead of showing in real time the curve, only few points are displayed and the data file is recorded as the experiment goes on. Furthermore, the integration time has been set to 10 ms to avoid any saturation risk from the DAQ. The previous architecture displayed data on the screen continuously. This caused the program to store all the data in its memory and impacted its speed performance. The integration time was impacted as it was considerably slowed down. As for the setup itself, the monitoring area is not the same between the stretching and the releasing phase. The piston moves, and so does the sample, while the optical fibre is immobile.

2.2.2.2 EML results: first observations

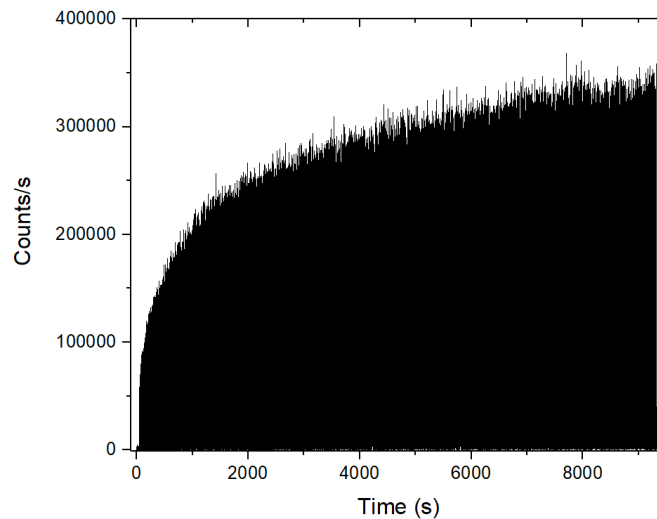


Figure 2.27: *Curve of the EML response of the Gwent ZnS:Cu-PDMS composite material. Number of emitted photons per second as a function of time.*

The setup presented previously allows us to conduct EML measurements and present data as to have the luminescence intensity as a function of time. Figure 2.27 shows the results in the case of the ZnS:Cu Gwent sample. Thanks to the use of a photomultiplier enabling individual photons to be detected, the y-scale is given in number of emitted photons per seconds and x-scale in seconds. The experiments are usually several hours long in order to study the evolution of the light intensity for long periods of time. Unlike figure 2.22, the light emitted by the sample increases with time. This increase is rapid at the beginning and then stabilizes and almost reaches a plateau of 350,000 photons per

seconds after 2.5 hours. This change in the behaviour in contrast with the results obtained with the first setup indicates that the applied force is constant.

By looking closely at the light intensity curve, we see the presence of two distinctive peaks: one rather large and the other thin and intense. Over time, the intensity ratio between the two peaks changes, i.e. if peak 2 is 5 times more intense than peak 1 when the experiment starts, it is reduced to approximately 1.5 times at the end. Furthermore, the first large peak is symmetrical, but this feature is not shared by the other one. Similarly to former results (cf. figures 2.22 and 2.23), this pattern repeats itself and was found to match the movement of the S-R cycling: the first one corresponds to the stretching phase and the second one to the releasing phase. However, we notice some differences between the two results. The shapes do not match one another and, where peaks were closely tight together in figure 2.23, they are, on the contrary, separated and clearly defined in figure 2.28. But, these differences are caused by a number of elements primarily due to the use of two different measurement systems: the sample is not deformed in the same way; the light detection is, in the first case, extracted from a video of the whole sample, whereas, in the second case, individual photons are detected from a localized portion of the sample. Also, a different PDMS catalyst was used for the PMT-setup which might change the behaviour and mechanical properties of the sample under deformation.

From these observations, we can conclude on the fact that the stretching peak is always wider and less intense than the releasing peak in the case of this ZnS:Cu Gwent-PDMS composite material.

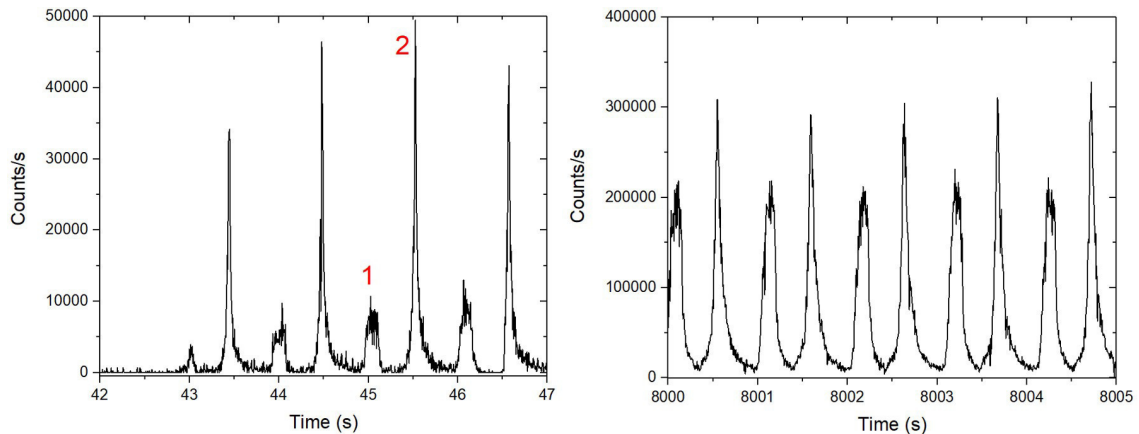


Figure 2.28: Zoom in the curve of the EML response. Number of emitted photons per second for two periods (left: beginning, right: after 2h of cycling) .

Thanks to this new setup it is possible to conduct experiments spreading over hours. Contrary to what was observed on the camera-based setup, the EML intensity increases greatly over time. Two distinctive emission peaks are visible and their maxima constitute the EML envelop.

2.2.3 Conclusion

Two different experimental setups were implemented for the study of elasto-mechanoluminescence. The first one was based on a camera and where the sample was stretched symmetrically on both ends. The EML intensity could be recorded on the whole sample after setting the experimental parameters (velocity, deformation percentage and

number of elongations). The applied force on the sample during the stretching and the releasing (S-R) experiment could also be recorded. The sample exhibits very strong luminescence upon the first cycles of S-R made of two emission peaks. Unfortunately, the EML decreases rapidly and so does the applied force. However, when the force is constant, the EML intensity is constant as well.

The second setup consists of an optical fibre connected to a photomultiplier (PMT). This device makes possible the counting of the emitted photons by the sample. Moreover, the light is only recorded locally determined by the diameter of the optical fibre. Instead of a force sensor, the displacement of the sample could be tracked thanks to a laser, an optical density and a detector. In this new setup, the sample is stretched on one side only and the following parameters could be adjusted: velocity, acceleration, deformation percentage, time of experiment, integration time of the PMT. The sample shows intense EML during the experiment. The light intensity increases over time and is composed of two peaks: one appearing during the stretching and the other during the releasing.

2.3 Conclusion & Discussion

Many scientific articles about elasto-mechanoluminescence (EML) describe an efficient system. However, EML samples are not easy to design and require specific materials in order to observe bright and intense luminescence upon stretching. The two starting materials being the Cu-doped ZnS and the PDMS polymer need to be well chosen. First, the phosphor powder must display specific size particle between 20 and 40 μm , and be coated with aluminium oxide Al_2O_3 . Second, the polymer must display high elasticity. Moreover, the sample itself needs to be robust enough to endure repeated elastic deformation.

The EML response showed interesting results. The experiments consist of repeated deformation of a strip-shaped sample. The sample goes from an initial position, where it is at rest, to a maximum stretch position, defined by the user. This cycle is then repeated n times. Thanks to the use of two different experimental setups, we can gather many useful information. We observed the presence of two emission peaks: the first one corresponds to the stretching phase, and the second one to the releasing phase. We note that these peaks are different from one another and change depending on the setup that is used. These differences and many more will further be discussed in chapter 4.

After being able to observe this phenomenon, many questions rise: what are the driven parameters for the efficiency of the EML? How do we explain the EML behaviour during deformation? Why does the light intensity rise in one case, decrease in the other? Can we design a more efficient system? Is zinc sulphide the only suitable material for EML? These are the questions we will attempt to answer to in the next chapters.

Chapter 3

Material Synthesis and Particle Coatings

The study on the copper doped zinc sulphide (ZnS:Cu) Gwent phosphor has provided information about the main characteristics of elasto-mechanoluminescence (EML). However, it also raised several questions on what makes an EML system, such as ZnS:Cu-PDMS (polydimethylsiloxane), efficient. We have experienced great difficulty into finding the ZnS:Cu material which was only available in small quantities (300 g). It requires a perfect knowledge of the compound and control its different parameters: size of the particles, crystal structure, surface coating and method of synthesis. This can only be achieved by synthesizing our own material.

We have synthesized ZnS:Mn using a hydrothermal method. We have investigated the influence of the temperature, the doping concentration and the duration of the synthesis. Moreover, commercial doped-ZnS phosphors are usually coated with aluminium oxide (Al_2O_3), which, at this stage, its exact role in the EML process was not yet determined. Consequently, we propose chemical routes for this coating and two others (SiO_2 and teflon). The addition of a coating changes the interaction between the polymer (PDMS) and the particles which, we believe, has an impact on the elasto-mechanoluminescence.

In addition to Gwent ZnS:Cu, we have also purchased other ZnS powders (ZnS:Cu and ZnS:Mn). They are Al_2O_3 -coated and non-coated. The morphological and optical characterizations are presented in this chapter.

We also have synthesized another phosphor showing *a priori* good properties for EML: CaZnOS. Like ZnS, it is a piezoelectric material with a hexagonal crystal structure and it has demonstrated mechanoluminescent properties. These characteristics make CaZnOS a good candidate for EML. Solid state reaction method was used and it was doped with manganese (Mn), and with lithium (Li) for codoping.

All the chemical protocols can be found in this chapter. Here are the chemicals used:

Calcium oxide (CaO 99.99% from Strem), zinc sulfide (ZnS 99.99% from Aldrich), manganese carbonate (MnCO_3 99.90% from Alfa Aesar), lithium carbonate (LiCO_3), 1H, 1H, 2H, 2H – Perfluorooctyltriethoxysilane from Sigma Aldrich, ammonium hydroxide in water (NH_4OH in 28% H_2O), sodium sulfide (Na_2S nonahydrate 98% from Acros), zinc sulfate (ZnSO_4 heptahydrate 99% from Aldrich), tetraethyl orthosilicate (TEOS 99.999% from Aldrich), aluminium isopropoxide ($\text{Al}(\text{O}-i\text{-Pr})_3$), octadecene (ODE 90% from Alfa-Aesar). These chemicals were used without further purification.

Washing step in the protocols: this step consists of adding a solvent, usually ethanol, to the solution in a centrifuge tube. The tube is placed in a centrifuge for 2 to 5 minutes. The solvent is then thrown out.

3.1 Material Synthesis

Is ZnS:Cu the only material which can exhibit elastico-mechanoluminescence? We have seen, in the previous chapter, that ZnS:Cu is an efficient material for EML when incorporated into a polymer matrix like PDMS (polydimethylsiloxane). The phosphor exhibits a cubic and a hexagonal crystal structure, is piezoelectric, is coated with aluminium oxide (Al_2O_3) and has controlled particle size (20 - 40 μm). This material is directly purchased, but many elements remain obscure such as the exact method used for the aluminium oxide coating, its thickness and its role in the EML. Synthesizing our own materials provides the possibility to control such aspects and more like the crystal structure and the particles' size. We have designed a chemical protocol using a microwave reactor followed by a sintering step to obtain ZnS:Mn microparticles. This was only possible after investigating the influence of the change in the reaction time, the doping concentration and the sintering temperature on the morphological and optical properties of the material.

In addition to zinc sulphide, another piezoelectric mechanoluminescent phosphor was synthesized: CaZnOS. Like ZnS:Cu, CaZnOS is piezoelectric, exhibits a hexagonal crystal structure and is used as a mechanoluminescent material. We propose two materials synthesized by solid state reaction: one doped with Mn, and the other co-doped with Li. We present in this section a study of the influence of the synthesis parameters (doping concentration and sintering temperature) on the properties of doped-CaZnOS.

3.1.1 Synthesis of $\text{ZnS} : \text{Mn}$

The scientific literature abounded on ZnS:Mn for EML. Although, ZnS:Cu is the most present as an efficient and bright EML material, *Chandra et al*, shaped their piezoelectricity-based model on ZnS:Mn and not ZnS:Cu. Therefore, we wanted to test this model directly by synthesizing it, specially when this material is hard to find for purchasing.

We have found several chemical protocols for the synthesis of ZnS particles using a hydrothermal method [72]. *Qian et al* proposed a way in which they started by synthesizing ZnS:Cu nanoparticles which they, then, coated with aluminium oxide. These information can be found in their supporting documents [14]. We wanted to use the same strategy and design a synthesis to obtain microparticles without organic contamination. The microwave reaction is a good method to copy hydrothermal conditions and to perform the reaction in a short amount of time. Mn-doped ZnS nanoparticles were synthesized using a microwave synthesis reactor, they were then sintered to obtain microparticles.

We carried out a full investigation on our own in order to find the right parameters for the synthesis of ZnS:Mn. The microwave reaction time, the doping concentration and the sintering temperature were all varied. The morphological and optical characterizations are presented for each parameter.

3.1.1.1 Microwave assisted method

Discover SP: the Microwave Synthesis Reactor from CEM

The Discover® SP is a microwave synthesizer for performing a wide range of organic and inorganic synthetic chemistry. It features an accurate infrared (IR) sensor for temperature control, temperatures up to 300°C can safely be reached in few minutes. It has a vigorous electromagnetic stirring, and rapid compressed air cooling [73]. The pressure and power limits are respectively 21 bar and 300 W.

It is possible to run the microwave with different methods or modes:

- Standard: rapid with temperature monitoring only,
- Dynamic: with temperature and pressure monitoring only,

- Power Cycling: temperature increase and decrease, several times,
- SPS: for peptide synthesis, reaches a temperature, stops with no cooling down.

The dynamic mode was used for the synthesis of ZnS:Mn. In this mode, the following parameters can be set:

- The pre-stirring time,
- The temperature,
- The pressure,
- The total reaction time,
- The power.

It is a rapid and efficient method for synthesising materials like ZnS.

Chemical protocol for ZnS:Mn synthesis

First, Mn-doped ZnS nanoparticles are synthesized using a microwave reactor. This method was inspired by a hydrothermal method as referenced in an article by *Hoa et al.*[72]. Second, ZnS:Mn microparticles are synthesized as mentioned in the article by *Qian et al.*[74] in their supporting information.

In a scintillation vial, 4.8 g of Na₂S are dissolved in 10 mL of water (2 mmol/mL). To disperse efficiently, the solution is heated for a few minutes using a hot air gun. In another vial, 5.75 g of ZnSO₄ and 0.023 g of MnCO₃ are dissolved in 10 mL of water (2 mmol/mL). The solution is then transferred to a 35 mL pressure vial.

The Na₂S solution is incorporated into the second one using a syringe pump at 60 mL/h inducing the precipitation of ZnS. The vial is placed in the microwave at 210°C for 10 min as shown figure 3.1. Finally, the resulting milky solution is washed with water four times and left to dry for 24 hours in a 60°C oven.

The reactions that take place are the following:

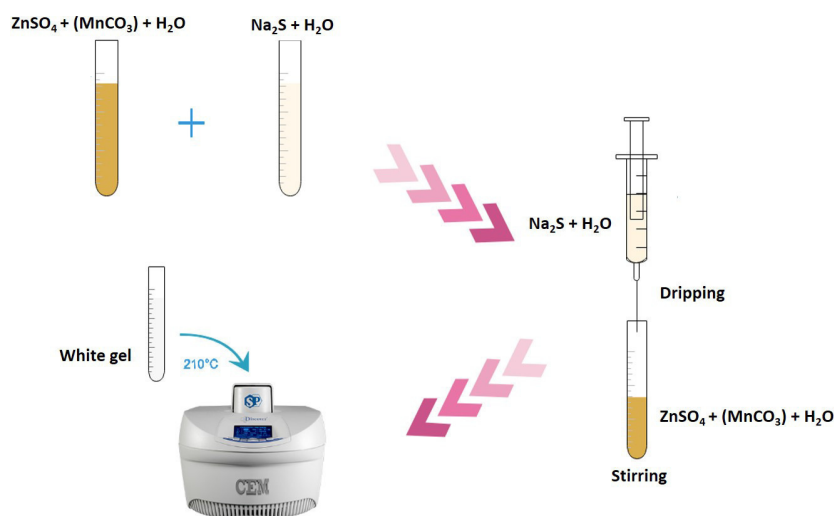
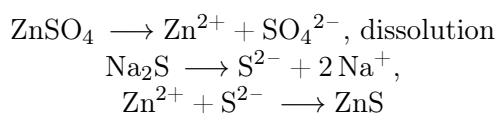


Figure 3.1: Synthesis steps of Mn-doped ZnS nanoparticles using a microwave reactor.

The powder is ground in a mortar and pelletized to form pellets of 20 mm in diameter. The pellets are sintered at 1100°C for 3 h under argon atmosphere in a horizontal tube furnace. Sintering or frittage is the process of compacting and forming a solid mass of material, here by heat, without reaching the melting point of the material. In the case of zinc sulphide, this point is at 1850°C. They are later ground again and sieved to obtain particles between 20 and 60 μm in diameter.

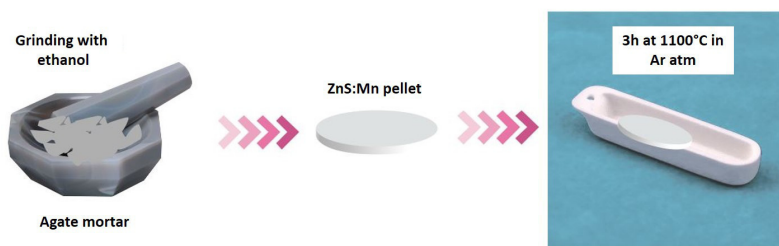


Figure 3.2: Steps of the synthesis of Mn-doped ZnS microparticles.

3.1.1.2 Influence of synthesis parameters

Several experiments were conducted in order to see the influence of changing the synthesis parameters:

- reaction time: 5 min, 10 min and 5 hours,
- doping ratio: 1%, 2%, 3%, 5% and 10%, and
- sintering temperature: 900°C, 1000°C and 1100°C.

SEM, TEM, XRD and spectral analysis were used to characterize our materials.

Microwave reaction time

Freshly acquired, the microwave reactor offered many features and it was important to find the right parameters for our reaction to take place. The synthesis of ZnS:Mn starts by precipitating ZnS which is mainly amorphous. The sample becomes crystallized after annealing in the microwave. The time for crystallization is the time needed for the reaction to be complete. Several times were tested: 5 min, 10 min and 5 hours.

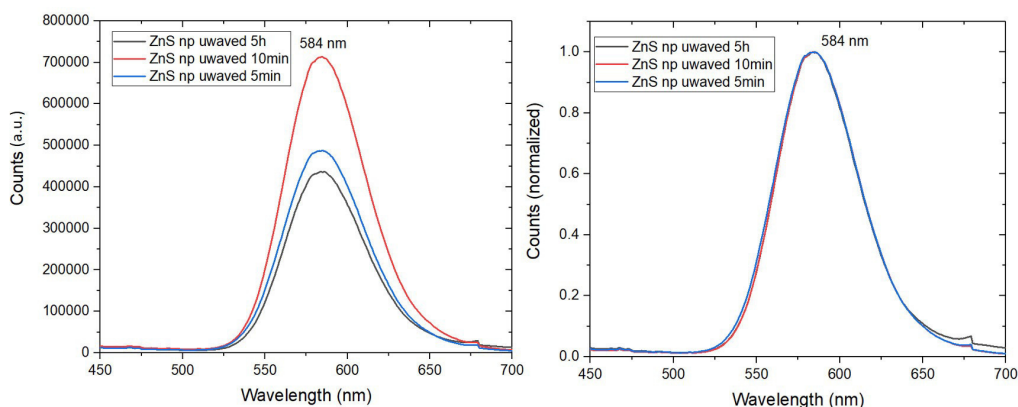


Figure 3.3: Emission spectra centered at 584 nm of μ waved ZnS nanoparticles synthesized at different reaction times (5 min, 10 min and 5 hours) at an excitation wavelength of $\lambda_{ex} = 340$ nm. Right, normalized spectra. np: nanoparticles.

Figure 3.3 shows photoluminescence spectra of ZnS:Mn nanoparticles at an excitation wavelength of $\lambda_{ex} = 340$ nm. The particles were synthesized at a 1% Mn doping

at different reaction times. On the left, we observe that ZnS:Mn nanoparticles synthesized during 10 minutes show the most intense luminescence of the three samples, followed by the 5-minute synthesis, whereas the 5-hour synthesis shows the weakest photoluminescence. However, they all share a large emission band at 584 nm, confirmed by the normalized spectra, on the right. This emission originates from the 4T_1 - 6A_1 transition of the Mn^{2+} ions.

Figure 3.4 shows TEM (Transmission Electron Microscope) images of synthesized ZnS nanoparticles for different reaction times, namely 5 min, 10 min and 5 hours. They display nanoparticles of 20 to 50 nm in diameter. By zooming on the particles, we see a crystalline structure.

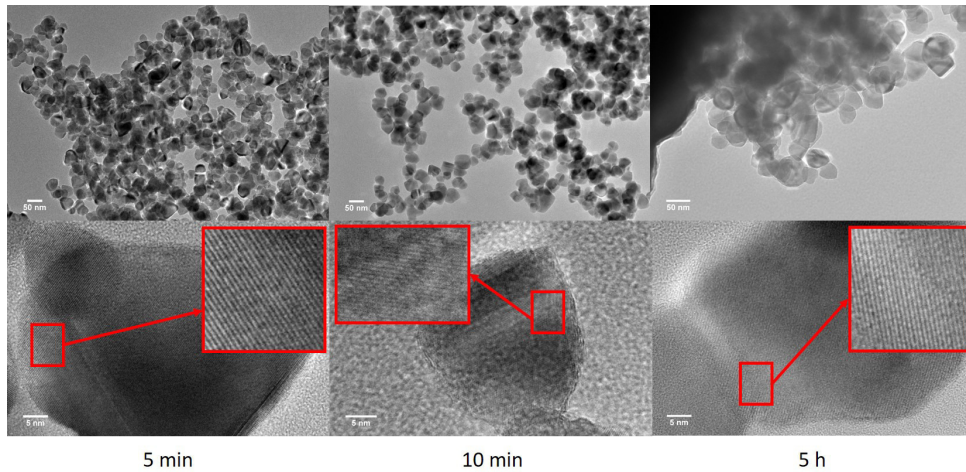


Figure 3.4: TEM images showing ZnS nanoparticles for different reaction times. Bottom, zoom of the particles.

The XRD pattern presented figure 3.5 shows zinc blende (cubic) crystal structure shared by the three different samples. All of their diffractograms are overlaid on each other. The presence of peaks at 28.5° , 33° , 47.5° and 56.3° corresponding to the planes $[11\bar{2}1]$, $[4\bar{2}20]$, $[2\bar{2}40]$ and $[5\bar{1}41]$ are characteristic of this phase. There are also peaks at 59° , 69.3° , 76.7° and 79° also belonging to the cubic phase.

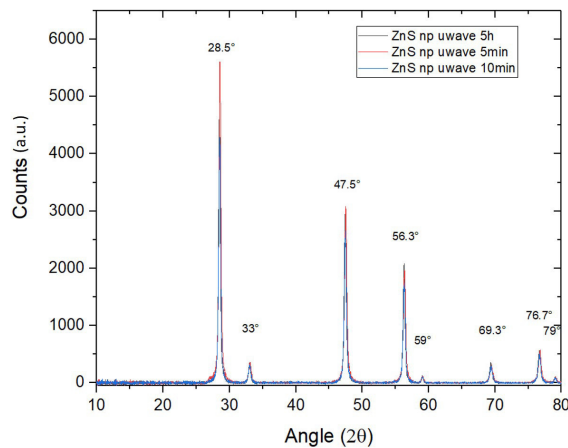


Figure 3.5: Superposition of XRD diffractograms of ZnS nanoparticles synthesized at different reaction times (5 min, 10 min and 5 hours) showing cubic crystal structure. np: nanoparticles.

The samples annealed at 5, 10 and 300 min with the microwave reactor exhibit the same photoluminescence property (emission band centered at 585 nm), particle size (35 nm in average) and crystal structure (zinc blende, cubic). These results demonstrate that the reaction can take place in a short amount of time and does not require hours to be complete as it is the case when using the hydrothermal method. However, in the same condition analysis, the band emission shows a stronger intensity for the 10 min sample. That is why it was chosen as the appropriate time for our synthesis.

Doping concentration

In their article, *Qian et al*, [74] suggest the preparation of 1 at% MnCO_3 and 99 at% ZnS which corresponds to a 1% doping. We have previously introduced 1% of Mn for the synthesis of ZnS:Mn. This material exhibited bright luminescence under UV-light. Here, we investigate the influence of the Mn doping on said luminescence **before** and **after sintering** the particles 3 hours at 900°C under the protection of argon), cf. figure 3.6. The following doping concentrations were considered: 1%, 2%, 3%, 5% and 10%. The actual doping concentrations were not measured.



Figure 3.6: Images of ZnS:Mn pellets synthesized at different doping percentages before (left) and after (right) sintering 3h at 900°C .

Figure 3.7 shows the photoluminescence spectra of ZnS:Mn 1%, 2%, 3%, 5% and 10% for an excitation wavelength of $\lambda_{ex} = 340$ nm **before** the sintering takes place. We notice that the ZnS:Mn 10% is almost 4 times brighter than ZnS:Mn 1%. The second brightest is ZnS:Mn 2%, followed by the 1%. The normalized spectra on the right show that the curves share a common large band at 585 nm as seen previously in figure 3.3. This emission is related to the 4T_1 - 6A_1 transition of the Mn^{2+} ions.

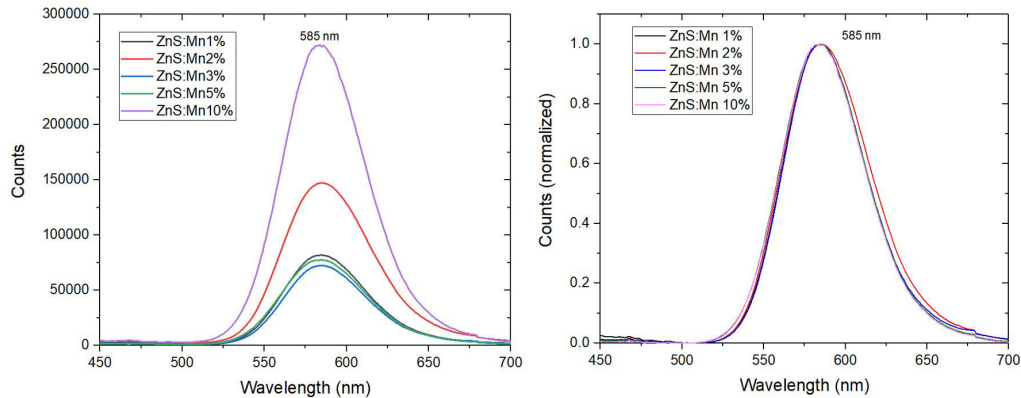


Figure 3.7: *Emission spectra of ZnS:Mn synthesized at different doping percentages at an excitation wavelength of $\lambda_{ex} = 340$ nm **before** sintering. Right, normalized spectra centered at 585 nm.*

The pellets figure 3.6 are sintered 3 hours at 900°C in an argon atmosphere and then ground for characterization. We first see that the doping concentration had an impact on the colours of the pellets themselves. The more manganese in the material, the more the pellet exhibits an orange shade. At 10%, the pellet is completely orange. The high concentration of manganese in ZnS resembles the creation of an alloy. By doing so we add absorption levels that can be responsible for the orange colour. However, in that case, the pellets would first turn yellow before turning orange, and this is not what we see.

The corresponding photoluminescence spectra can be found figure 3.8. At an excitation wavelength of $\lambda_{ex} = 340$ nm, the ZnS:Mn 5% is the brightest and the 1% exhibits the least luminescence of the 5 samples. Nonetheless, their spectra are overlaid on each other and a large emission band at 579 nm is visible. We notice a spectral shift of 6 nm between the emission before (cf. figure 3.7) and after the sintering. This could be due to the impact of sintering on the grain growth.

The SEM images figure 3.9,a) of ZnS:Mn 1% shows a porous particle. The ZnS:Mn 2% in (b) exhibits less porosity, whereas smaller particles seem glued to one another in the ZnS:Mn 3%. This is the sign of sintering. The particle on image (d) is completely sintered. However, the porosity seems to be back for ZnS:Mn 10%, in (e). Despite that, the porosity is less and less present and the particles more compact as the doping percentage increases. This is also supported by the fact that the grinding process is more difficult for pellets with higher Mn concentration.

The luminescence properties of phosphors depend on their morphology, their size and their crystal structure. As sintering acts on the grain growth the luminescence changes and shifts (from 585 nm to 579 nm) because of it. The Mn doping concentration has a visible impact during the sintering stage. The more Mn in the crystal, the more compact the material would be.

Sintering temperature

Controlling the temperature is very important to the sintering process. The size and

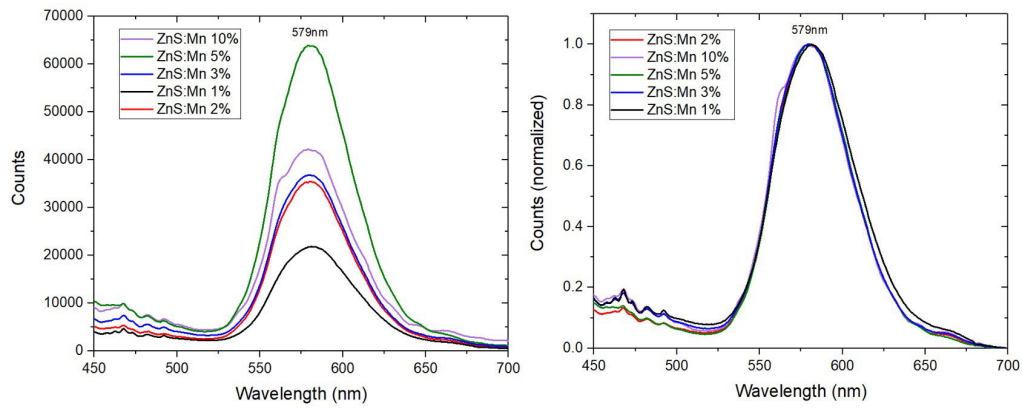


Figure 3.8: *Emission spectra of ZnS:Mn synthesized at different doping percentages at an excitation wavelength of $\lambda_{ex} = 340$ nm after sintering 3h at 900°C . Right, normalized spectra centered at 579 nm.*

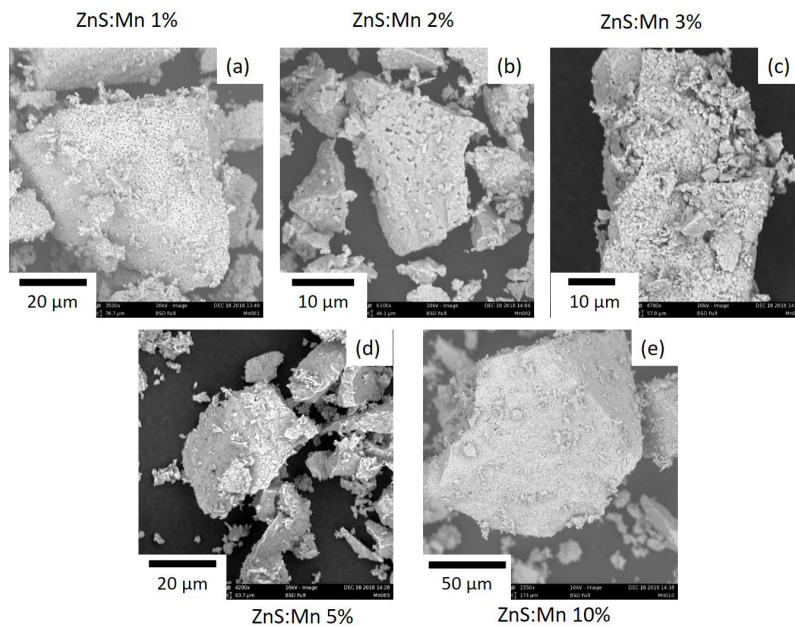


Figure 3.9: *SEM images of ZnS:Mn powders synthesized at different doping percentages after sintering 3h at 900°C .*

distribution of the particles and the material composition depend on the sintering environment which needs to be controlled.

The following samples are from the same starting preparation. They were then divided into 3 to be sintered at different temperatures.

Figure 3.10 shows the morphology of ZnS:Mn 1% particles under different sintering conditions 900°C , 1000°C and 1100°C in an argon atmosphere during 3 hours. To obtain these particles, the pellets (like observed in figure 3.6) were ground by hand. Image (a) shows a porous particle and crumbles easily. However, at 1100°C , the particle has no longer this porosity but shows a compact material, which is harder to grind. As for image (b), we see an intermediate state between (a) and (c). As the temperature increases, the ZnS:Mn particles are less porous and the densification increases.

The emission spectra of the three samples are given figure 3.11. Excited at 340 nm, a large band appears at 583 nm for the three samples (900°C , 1000°C and 1100°C).

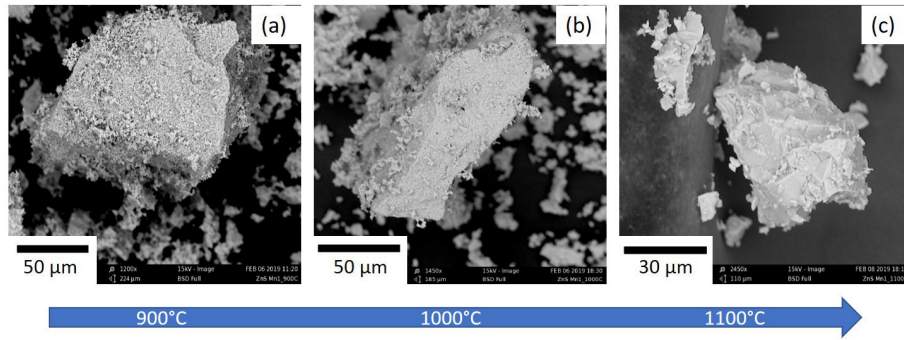


Figure 3.10: SEM images of ZnS:Mn particles at 1% doping sintered 3h at different temperatures (900°C, 1000°C and 1100°C).

The ZnS:Mn sintered at 1100°C exhibits the highest fluorescence intensity, followed by the ZnS:Mn sintered at 1000°C, then finally ZnS:Mn 900°C. This emission corresponds to the one found figures 3.3 and 3.7 before sintering. However, a 4 nm shift is noticed with the spectra figure 3.8 corresponding to the emission after sintering. One can consider a different incorporation of Mn in ZnS between the two synthesis which would cause a shift in luminescence.

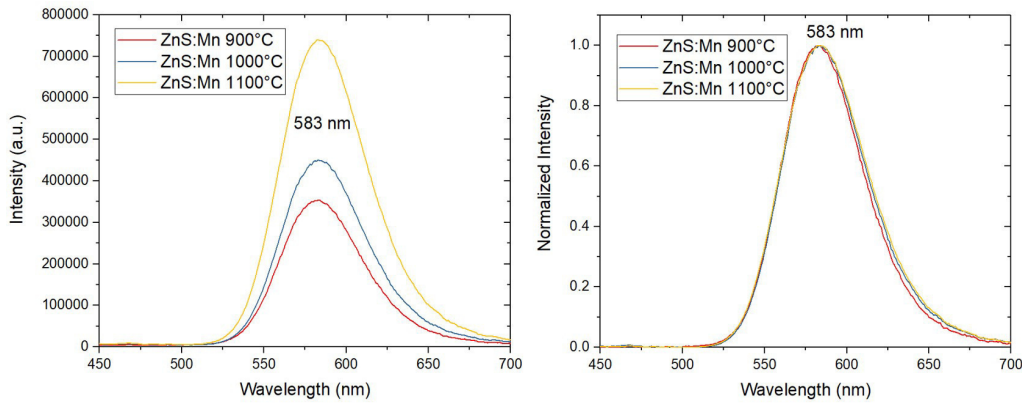


Figure 3.11: Emission spectra of ZnS:Mn particles at 1% doping sintered 3h at different temperatures (900°C, 1000°C and 1100°C) at $\lambda_{ex} = 340$ nm. Right: normalized spectra.

The diffractograms obtained via X-ray diffraction (XRD) figure 3.12 display mainly a hexagonal (hcp), or wurtzite, crystal phase with the presence of peaks at 26.88°, 28.5°, 30.5°, 39.5°, 47.5°, 51.7° and 56.3° corresponding to the planes $[2\bar{1}\bar{1}0]$, $[\bar{2}4\bar{2}0]$, $[\bar{1}2\bar{1}1]$, $[2\bar{1}\bar{1}2]$, $[11\bar{2}0]$, $[2\bar{1}\bar{1}3]$ and $[11\bar{2}2]$, respectively. We also find in (a) one peak at 33° (or the plane $[0002]$) corresponding to the cubic (fcc), or zinc blende, crystal structure. This peak is not present in (b) and (c). Peaks belonging to ZnO phase appear also on the diffractograms (showed in green dots) but are less intense as the temperature increases. The ZnS:Mn nanoparticles were cubic but the heat treatment induced a phase transition toward the hexagonal structure. This structure is shared by the Gwent ZnS:Cu.

The densification of the microparticles is influenced by the sintering temperature with 1100°C showing no porosity. The variation of temperature (900°C, 1000°C and 1100°C) does not impact the 583 nm emission band of ZnS:Mn but rather its intensity (under and excitation wavelength of 340 nm) with ZnS:Mn@1100°C showing the most intense luminescence. The hexagonal crystal structure was determined after XRD analysis with decreasing amount of impurities as the sintering temperature increases. The ZnO phase

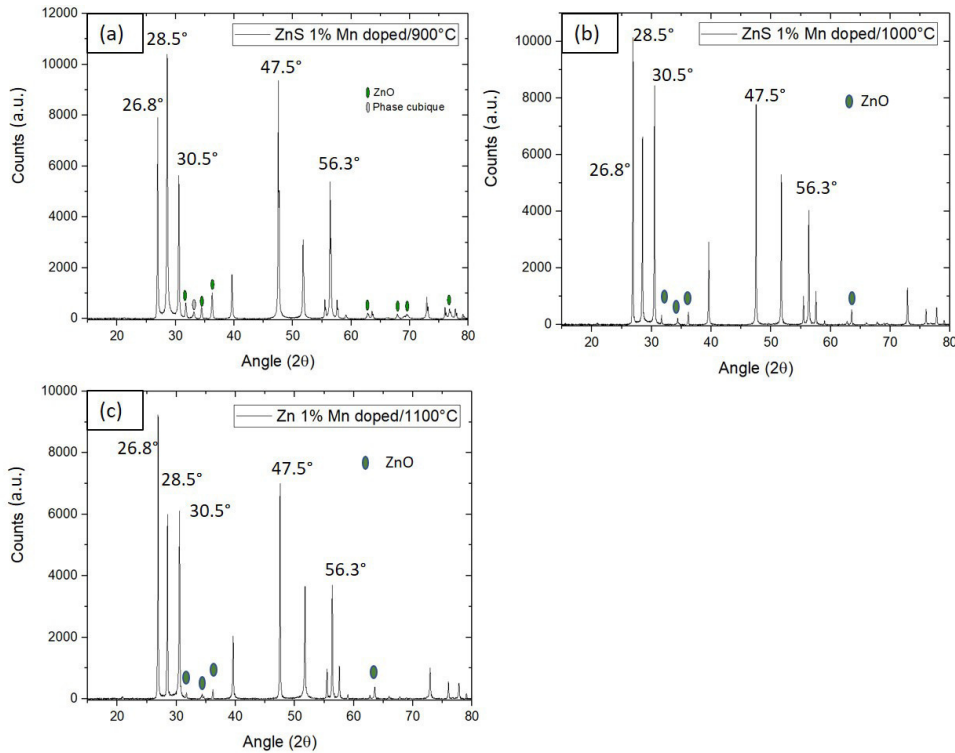


Figure 3.12: XRD diffractograms of ZnS:Mn powder at 1% doping sintered 3h at different temperatures. (a) 900°C, (b) 1000°C and (c) 1100°C.

visible on the ZnS:Mn@900°C is less detectable on the ZnS:Mn@1100°C. 1100°C was then chosen as the sintering temperature for the synthesis of ZnS:Mn microparticles.

3.1.1.3 Conclusion

ZnS:Mn nanoparticles were synthesized using a microwave assisted method where ZnSO_4 , Na_2S and MnCO_3 were used as precursors. The nanocrystals exhibited a cubic zinc blende structure and a particle size ranging from 20 nm to 50 nm. The emission spectrum highlighted an emission band at 585 nm (orange). The investigation to determine the appropriate reaction time revealed that 10 min were sufficient to crystallize our material completely.

To obtain ZnS particles of the micro-scale, it is necessary to sinter them at high temperature. 900°C, 1000°C and 1100°C were each tested and the morphological, optical and crystal properties were determined for each. These characterizations revealed a higher particle densification at 1100°C alongside an intense luminescence and the purest hexagonal crystal of the three. After sintering, particles between 20 and 60 μm were obtained. It is noteworthy to add that sintering leads to a phase transition from cubic to hexagonal with impurities appearing depending on the sintering temperature.

Furthermore, the doping concentration impacts the photoluminescence and the microparticle's morphology. We have doped ZnS at 1%, 2%, 3%, 5% and 10%. For high Mn concentration, the powders are less porous but the photoluminescence spectra show a more intense luminescence in the case of ZnS:Mn@2%.

For our study, we have used the particles prepared with the following parameters:

- Microwave reaction time: 10 min,
- Doping concentration: 2%,
- Sintering temperature: 1100°C for 3h in an argon atmosphere. Nitrogen was also used

during the sintering stage and the same results were obtained.

3.1.2 Synthesis of doped CaZnOS

To study in more depth elastically-mechanoluminescence, we were looking for another mechanoluminescent material like doped-ZnS. The oxysulfide CaZnOS is identified as a piezoelectric and mechanoluminescent phosphor (cf. Chapter 1, table 1.2), and shows great potential in light sources, displays, and stress imaging.

In this section we propose a presentation of this material, its optical and morphological properties, its applications and a proposed mechanism, all of which can be found in the literature. Then, a detailed protocol is offered of the synthesis of Mn-doped and Li-codoped CaZnOS which were achieved by solid state reaction. These materials were characterized using SEM, XRD and a spectrofluorometer. Furthermore, the doping concentration and the sintering temperature were varied as to assess of their impact in the properties of the CaZnOS:Mn material.

3.1.2.1 Calcium zinc sulphide CaZnOS

The study of elastically-mechanoluminescence (EML) has witnessed the discovery of several materials. Most of these materials are aluminates, silicates, stannates, titanates and phosphates systems and other oxynitrides. They cover a large spectral range from ultraviolet to infrared light. They are appealing to several applications in detection and monitoring stress stimulus (mapping, hand writing) thanks to the different loads or stresses applied to them which result in different light intensities. Because of that, EML materials need to demonstrate some properties such as a prompt response, intense EML, multi-stress sensitivity, and a wide measurement range for the dynamic load [75].

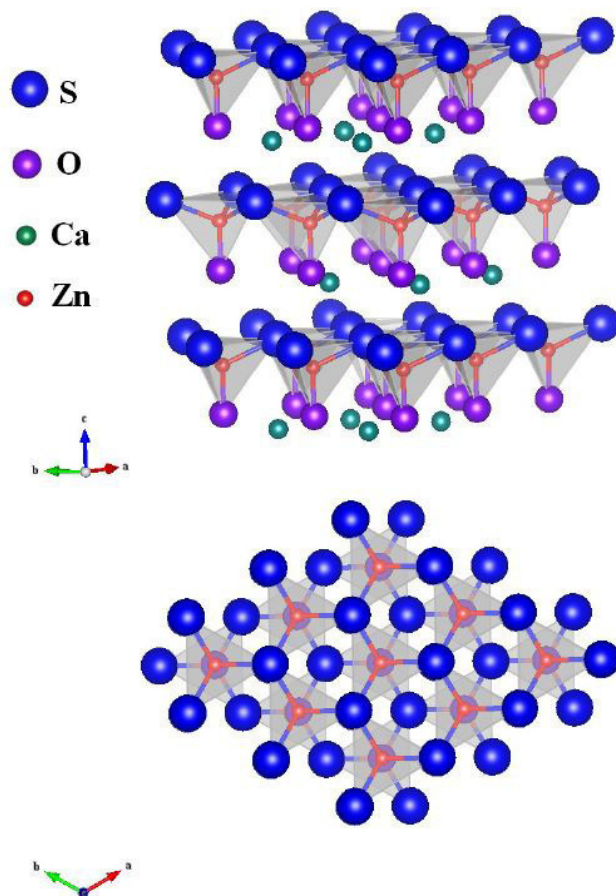


Figure 3.13: *Crystal structure of CaZnOS . From [21]*

Usually, efficient mechanoluminescent (ML) materials are chosen according to their piezoelectric property like ZnS, LiNbO₃ and CaZnOS thanks to their ability to form lattice-defect complexes by stress-induced piezoelectric potential due to strong electron-lattice coupling [76, 77, 22]. In ML mechanisms, these complexes act as active energy carriers and migration centers [78, 9]. Furthermore, the stress-to-photon conversion requires substitutional dopant ions which can seize strain-induced energies linked to lattice defects. This results in photon emission at high efficiencies. Also, the emission can be tuned thanks to these dopants having their own spectral characteristics [79, 28].

For CaZnOS, Mn²⁺ ions are the most commonly used to substitute for Zn²⁺ in the host material. It can be incorporated in CaZnOS at high concentrations without deleterious effects [23]. The transition metal activator (Mn²⁺) can enter into the interior host lattice by replacing Ca²⁺ ions [80].

Calcium zinc sulfide is composed of ZnS and CaO layers, and was first discovered in 2003 by *Petrova et al.*[81] as an intermediate product of zinc from its sulfide by carbothermal reduction in the presence of lime. In 2007, *Sambrook et al.*[82] investigated its structure and physical properties. They showed that CaZnOS is a large band gap semiconductor with a direct band gap of 3.71 eV. This material is piezoelectric and crystallizes in the hexagonal phase which makes it non-centrosymmetric. It is an excellent host lattice for several luminescent centers. In 2009, *Duan et al.*[80] studied this material as a novel phosphor doped with Mn²⁺ ions, with a red emission color around 614 nm [23, 21] upon a 280 nm excitation wavelength, and then proposed other activators such as: Pb²⁺, Eu²⁺, Ce³⁺, Tb³⁺ [83].

In 2010, CaZnOS:Eu²⁺ was reported as a high color rendering red-emitting phosphor applied for white LEDs [84]. The synthesis of a single-phase CaZnOS phosphor is challenging because of the great difficulty in controlling the phase purity. CaZnOS crystal is formed between 1370 K and 1520 K. At higher temperatures, a weight loss is observed [85], as a result, CaS is formed [86] :



Zhang et al., focused their attention on CaZnOS:Mn²⁺ as they found in 2013 that it is a very effective multi-stress sensor of intense mechanoluminescence [87]. Later on, they studied its ML and EML properties. Mn²⁺-doped CaZnOS can sense many kinds of mechanical stresses like friction, compression and ultrasonic vibration. They attribute this property to the large piezoelectric coefficient of this material [75] of $d_{33} = 38$ pm/V. CaZnOS became a new interest for scientists. Some managed to enhance the ML intensity [22] by co-doping the material with transition metal and alkali ions, and especially by co-doping Mn²⁺ with Li⁺ (cf. figure 3.14).

The emission color of CaZnOS:Mn²⁺ can be tuned from yellow to red (cf. figure 3.15) by varying the Mn²⁺ concentration in the host material [23]. *Wang et al.*[88] showed a linear intensity response to the applied dynamic pressure in the case of CaZnOS:Sm³⁺.

In 2018, *Li* and his team [32] noticed that ML and EML were not considered suitable for bio-imaging because the usual ML materials cannot emit NIR (near infrared) photons. They wanted to design "transparent" materials for biological samples. Thus, they combined the piezoelectric semiconductor CaZnOS with the rare earth species: Ho³⁺, Pr³⁺, Dy³⁺ and Nd³⁺. The introduction of rare earth ions improves the EML as a result of a modification in the symmetry of the crystal by chemical substitution which causes changes in the piezoelectric field or reshapes the traps [89, 90, 91, 41]. Their results are shown table 3.1. We see that NIR ML is observed in CaZnOS: Nd³⁺. Also, they demonstrated that this material displays an efficient EML, a high cycling stability and a high ML efficiency as it is 5 times greater than that of the known SrAl₂O₄: Eu²⁺, Dy³⁺ under 3000 N.

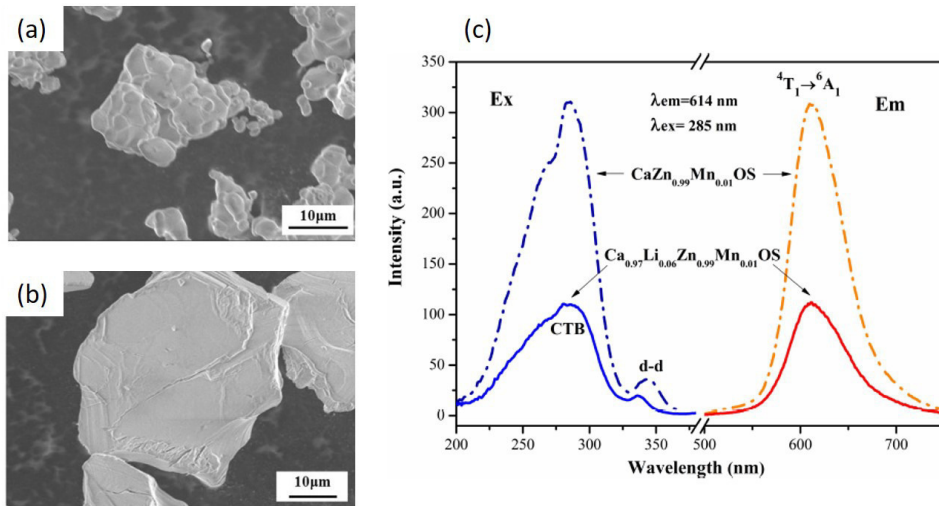


Figure 3.14: (a) and (b) SEM images of $\text{CaZn}_{0.99}\text{Mn}_{0.01}\text{OS}$ and of $\text{Ca}_{0.97}\text{Li}_{0.06}\text{Zn}_{0.99}\text{Mn}_{0.01}\text{OS}$, respectively. (c) Photo-excitation and emission spectra of $\text{CaZn}_{0.99}\text{Mn}_{0.01}\text{OS}$ and $\text{Ca}_{0.97}\text{Li}_{0.06}\text{Zn}_{0.99}\text{Mn}_{0.01}\text{OS}$. From [22].

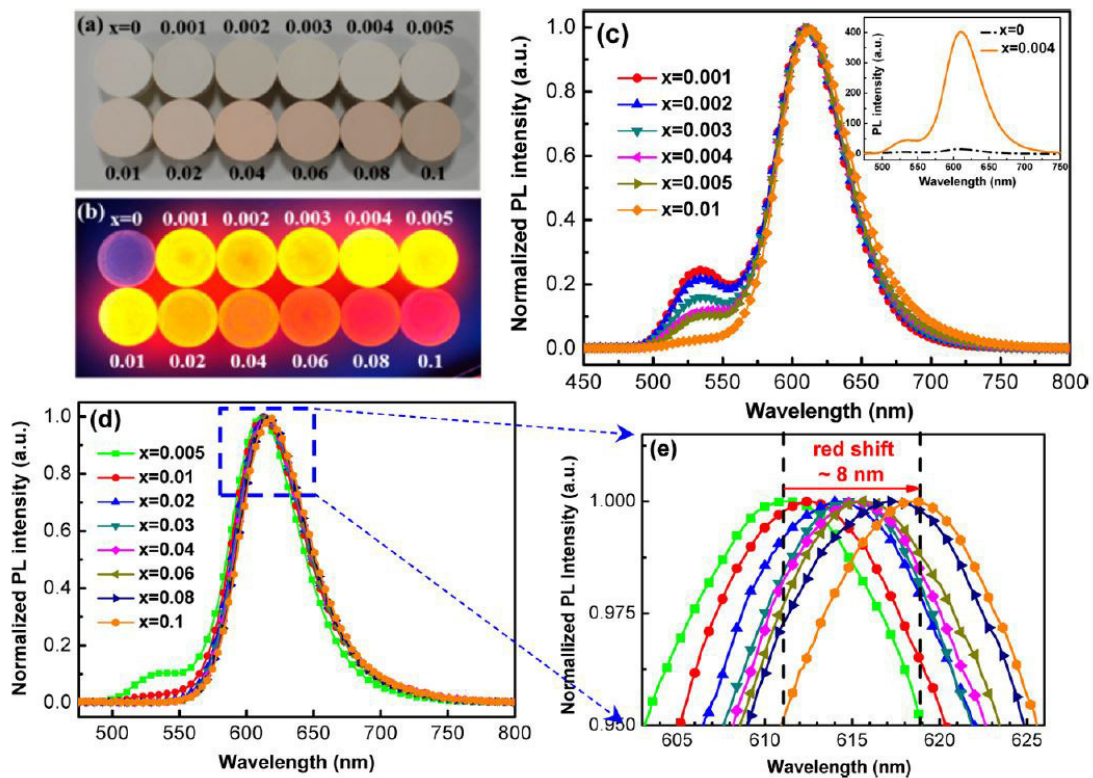


Figure 3.15: Photographs of $\text{CaZn}_{1-x}\text{Mn}_x\text{OS}$ ($x = 0, 0.001, 0.002, 0.003, 0.004, 0.005, 0.01, 0.02, 0.03, 0.04, 0.06, 0.08, \text{ and } 0.1$): (a) in daylight and (b) under 254 nm UV lamp. (c-d) Normalized PL spectra of $\text{CaZn}_{1-x}\text{Mn}_x\text{OS}$ under 282 nm excitation source. (e) Enlarged PL spectra, showing the red shift. From [23]

Multi-color mechanoluminescent emission, from violet to infrared, can also be achieved by mechanical excitation through lanthanide doping Tb^{3+} , Eu^{3+} , Pr^{3+} , Sm^{3+} , Er^{3+} , Dy^{3+} , Ho^{3+} , Nd^{3+} , Tm^{3+} and Yb^{3+} [24] (cf. figure 3.16). Moreover, by mixing

Dopant	Visible peaks (nm) PL / ML	NIR peaks (nm) PL / ML
Nd^{3+}		908 / 908 1094 / 1094 1390 / 1390
Pr^{3+}	519 / 519 671 / 671	1024 / No 1080 /
Ho^{3+}	559 / 559 757 / 757	1051 / No 1200 /
Dy^{3+}	488 / 484 574 / 574 669 / 669 754 / 754 852 / 852	1029 / No

Table 3.1: *ML and PL properties in RE^{3+} doped CaZnOS . From [32]*

Mn^{2+} and Tb^{3+} dopants at different mass ratios, it is possible to tune the ML colours from green to red with high brightness.

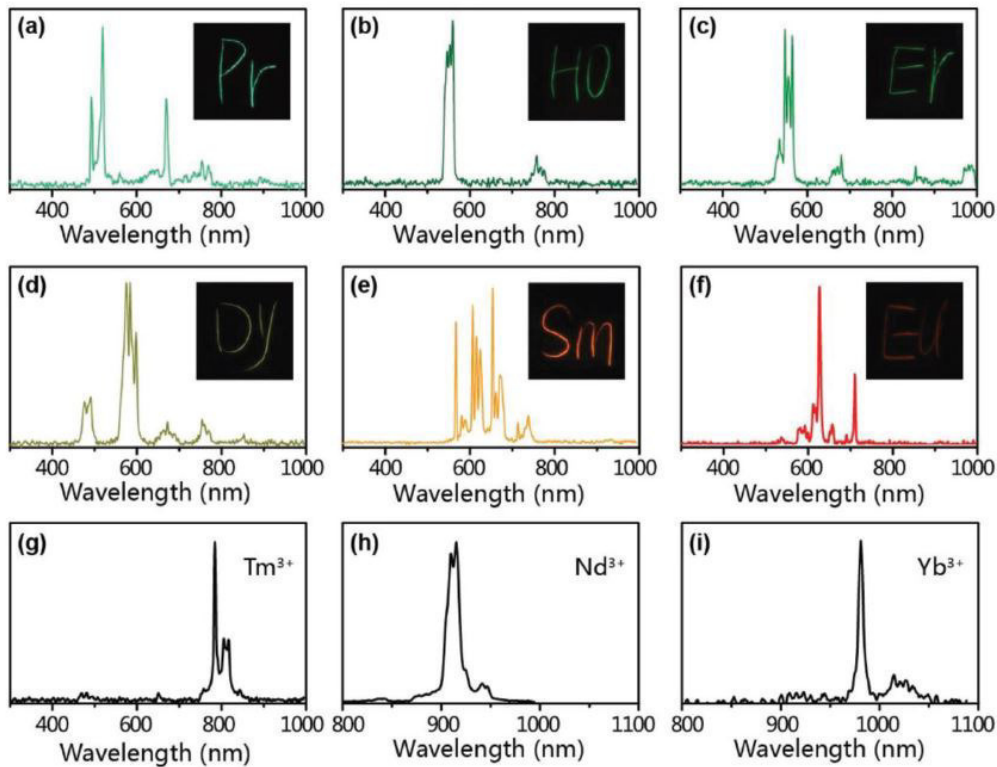


Figure 3.16: *ML spectra of CaZnOS doped with: a) Pr^{3+} , b) Ho^{3+} , c) Er^{3+} , d) Dy^{3+} , e) Sm^{3+} , f) Eu^{3+} , g) Tm^{3+} , h) Nd^{3+} , and i) Yb^{3+} . Inset: photographs of the corresponding samples under single-point dynamic pressure of a ballpoint pen. From [24]*

Su et al.[25] propose a mechanism of elasto-mechanoluminescence for CaZnOS : Mn^{2+} , Nd^{3+} (cf. figure 3.17). This description requires a preliminary UV excitation: Upon irradiation, electrons are excited and move to the CB. The created charges can be trapped by defects. Under stress, the crystal is deformed and a local electric field

is created in the piezoelectric region. The electrons move to the CB, and non-radiative recombination with the trapped holes takes place. This recombination releases energy which can be transferred to Mn^{2+} ions and results in a red light emission.

A large number of deep traps are produced thanks to the Nd^{3+} , this facilitates the capture of electrons and generates a stronger EML emission.

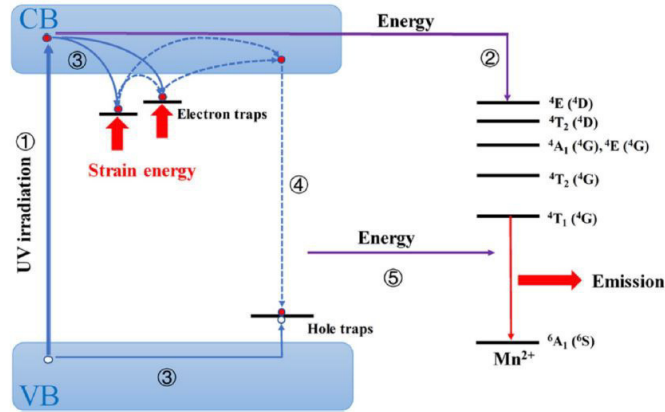


Figure 3.17: Schematic diagram of the elasto-mechanoluminescence (EML) mechanism of $CaZnOS:Mn^{2+}, Nd^{3+}$. CB: conduction band, VB: valence band. The electronic energy level of Mn^{2+} ions is deep under the VB, but is drawn beside the band diagram. From [25]

3.1.2.2 Solid state reaction method

$CaZnOS$ is synthesized via solid state reaction at high temperature which is the standard procedure for this material. The following two materials were synthesized: $CaZnOS:Mn$ and $CaZnOS:Mn, Li$. Thanks to its chemical and thermal stability, $CaZnOS$ is a good host for Mn^{2+} ions. Below are presented detailed protocols for the synthesis. These materials were characterized using XRD, SEM, an optical microscope and a spectrofluorometer. Also, the influence of the Mn concentration and the impact of the sintering temperature on the optical and morphological properties of $CaZnOS:Mn$ were studied.

Chemical protocols for doped $CaZnOS$ synthesis

Here are the chemical protocols for the synthesis of $CaZnOS:Mn$ and $CaZnOS:Mn, Li$.

- $CaZnOS :Mn$

$CaZnOS :Mn$ is synthesized using solid-state reaction to obtain a 2% Mn doping ($CaZn_{0.98}Mn_{0.02}OS$). Stoichiometric amounts of starting materials CaO , ZnS and $MnCO_3$ are weighed and mixed in a mortar with ethanol.

To obtain 5 g of $CaZnOS:Mn$, 1.8 g of ZnS (32.6 mmol) and 3.2 g of CaO (32.6 mmol) are first mixed together with a spatula. Then, 0.075 g of $MnCO_3$ are dispersed in ethanol, and blended with the rest of the mixture with the spatula. Afterward, ethanol is added until the powder is completely wet. The mixture is ground with the pestle for several minutes. When the mixture becomes thick and hard to blend, ethanol is added again. These steps are performed three times in total. Finally, when the powder has a sticky aspect, it is compacted in an alumina crucible and sintered for 3h at $1100^\circ C$ in a horizontal tube furnace under a flowing Ar atmosphere.

- $CaZnOS :Mn, Li$

$\text{Ca}_{0.97}\text{Li}_{0.06}\text{Zn}_{0.99}\text{Mn}_{0.01}\text{OS}$ material (CaZnOS:Mn,Li) is synthesized using solid-state reaction. Stoichiometric amounts of starting materials CaO , ZnS , MnCO_3 and LiCO_3 are weighed and mixed in a mortar with ethanol.

To obtain 5 g of CaZnOS:Mn,Li , 1.8 g of ZnS (32.6 mmol) and 3.2 g of CaO (32.6 mmol) are first mixed together with a spatula. Then, 0.037 g of MnCO_3 are dispersed in ethanol, and blended with the rest of the mixture with the spatula. The same is done with 0.0144 g of LiCO_3 . Afterward, ethanol is added until the powder is completely wet. The mixture is ground with the pestle for several minutes. When the mixture becomes thick and hard to blend, ethanol is added again. These steps are performed three times in total. Finally, when the powder has a sticky aspect, it is compacted in an alumina crucible and sintered for 3h at 1100°C in a horizontal tube furnace under a flowing Ar atmosphere.



Figure 3.18: *Synthesis of CaZnOS:Mn by solid state reaction.*

3.1.2.3 Material Characterization

The synthesized materials were characterized using a spectrofluorometer, a scanning electron microscope (SEM), an optical microscope and an X-Ray diffractometer (XRD). The following results concern the $\text{CaZn}_{0.99}\text{Mn}_{0.01}\text{OS}$ in (a) and $\text{Ca}_{0.97}\text{Li}_{0.06}\text{Zn}_{0.99}\text{Mn}_{0.01}\text{OS}$ in (b) synthesized according to *Tu et al.*, [21] by solid state reaction and sintered 3 hours at 1100°C in argon atmosphere as previously detailed.

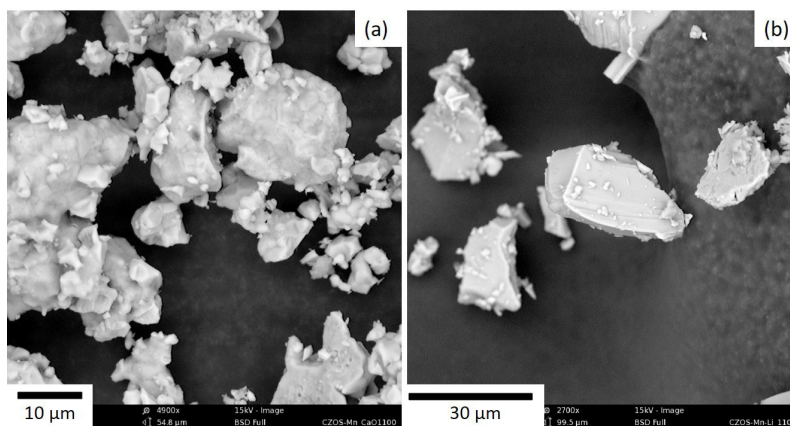


Figure 3.19: *SEM images of $\text{CaZn}_{0.99}\text{Mn}_{0.01}\text{OS}$ in (a) and $\text{Ca}_{0.97}\text{Li}_{0.06}\text{Zn}_{0.99}\text{Mn}_{0.01}\text{OS}$ in (b) synthesized by solid state reaction and sintered 3 hours at 1100°C in argon atmosphere.*

The SEM allows to see the size and morphology of our materials, as shown in figure 3.19. In (a) we find rather spherical particles which are smaller than the ones in

(b). Their size is about 20-30 μm . CaZnOS:Mn,Li particles are larger and well crystallized and display a plate-like shape. Their size spans from 50 to 100 μm . These results are consistent with the ones found by *Tu et al.* [21]. It is stated that the morphology of the co-doped CaZnOS could be attributed to the active role of LiCO_3 .

The powders were also observed under an optical microscope as shown figure 3.20 using the bright-field mode (a) and crossed polarization (b). The particles of $\text{Ca}_{0.97}\text{Li}_{0.06}\text{Zn}_{0.99}\text{Mn}_{0.01}\text{OS}$ show diameters up to 100 μm can be easily identified, the crossed polarization shows a homogeneous yellow color appearing on the plate-like particles for the mono-crystals. We see that tther particles are not birefringent in this direction.

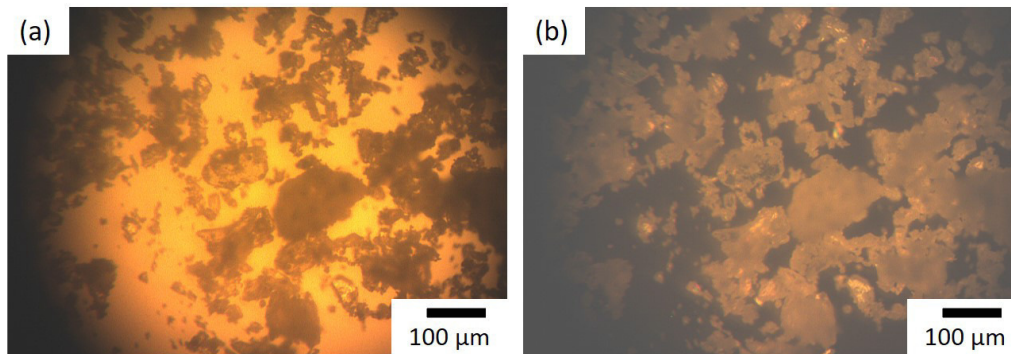


Figure 3.20: Optical microscope images of $\text{Ca}_{0.97}\text{Li}_{0.06}\text{Zn}_{0.99}\text{Mn}_{0.01}\text{OS}$ in bright-field mode (a) and crossed polarization (b).

Figure 3.21 illustrates the photoluminescence and excitation spectra of our two materials. The excitation spectra of both phosphors show similar curves. The main excitation band is between 276 and 280 nm and a smaller peak can be found around 337 nm. These two bands could be respectively attributed to the host lattice absorption and the absorption of Mn^{2+} ions [21] from d-d transition. The samples show an intense red luminescence centered at 610 nm when excited at 280 nm originating from the ${}^4T_1({}^4G) - {}^6A_1({}^6S)$ transition of Mn^{2+} ions.

We also notice that the PL intensity of Mn doped CaZnOS is stronger than that of Li co-doped CaZnOS. According to the same authors, it may result from the generation of some defects by the lithium doping in the phosphor lattice. Another smaller band is also visible around 530 nm. This band was also found by *Zhang et al.*, [23] in their investigation on the effect of the Mn concentration on CaZnOS. They attribute this emission to some defect centers formed by Mn^{2+} doping because no emission is recorded in undoped CaZnOS.

Figure 3.22 shows XRD patterns. Impurity phases are identified in CaZnOS:Mn. The peaks correspond to the CaZnOS reference diffractogram and to the ZnS and CaO patterns which means that the synthesized phosphor is not single-phased, while CaZnOS:Mn,Li diffractogram shows peaks belonging to CaZnOS and ZnS only. The main diffraction peak is located at 31.4° ascribed to the lattice plane [0004]. This peak is stronger in the Li co-doped material. *Tu et al.* [22] suggest that the co-doped oxysulfide exhibited the *c*-axis oriented direction. The intensities of the other peaks differ from one pattern to the other.

The mechanoluminescent nature of CaZnOS:Mn (and CaZnOS:Mn,Li) is visible after sintering as orange and red lights are emitted during grinding. The synthesized 1% Mn-doped material displays particles of 20-30 μm in diameter. The photoluminescence spectrum shows a large and intense emission band peaking at 608 nm and smaller one centered around 530 nm upon excitation at 280 nm. The XRD diffractogram highlights a hexagonal crystal structure but with the presence of impurities belonging to the CaO phase.

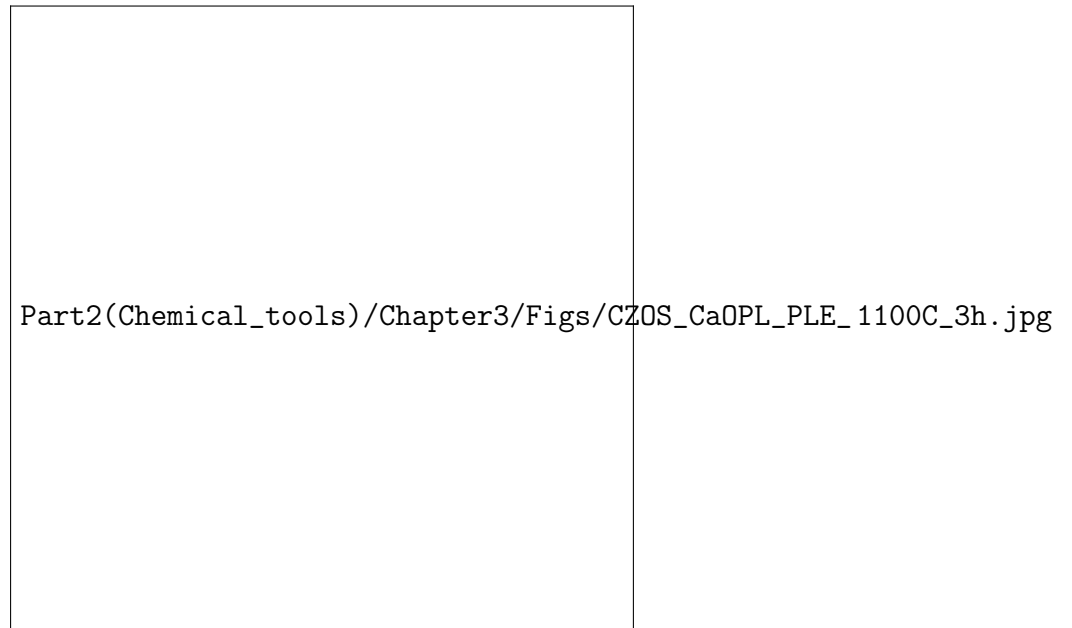


Figure 3.21: *Excitation and photoluminescence spectra of CaZnOS:Mn and CaZnOS:Mn,Li. Sintering conditions: 1100° C for 3h, argon atmosphere.*

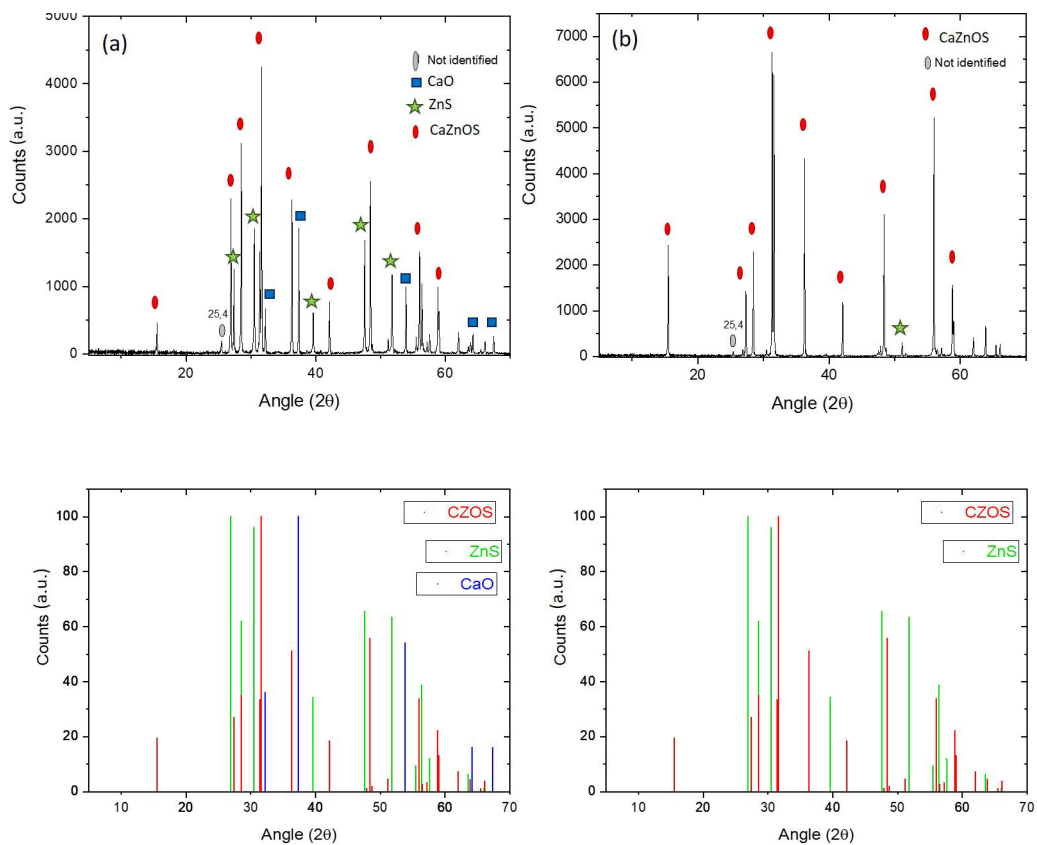


Figure 3.22: *Top: XRD diffractograms of CaZnOS:Mn ((a)) and CaZnOS:Mn,Li ((b)). Sintering conditions: 1100° C for 3h in argon atmosphere. Bottom: XRD references corresponding to the CaZnOS phosphors.*

CaZnOS:Mn,Li exhibits a hexagonal structure but no impurity peak is detected belonging to CaO. The particles are plate-like and their size ranges from 50 to 100 μm . Its photoluminescence spectra is not different from CaZnOS:Mn with the presence of two bands at 608 nm and \approx 530 nm. The addition of lithium changed the shape of the particles from spherical to plate-like particles with smoother surfaces and a significant increase in their size. This change is caused by low melting LiCO_3 .

3.1.2.4 Influence of synthesis parameters

Here, we investigate the influence of the Mn doping on CaZnOS:Mn. The following doping concentrations were considered: 0.1%, 0.2%, 0.6%, 2%, 6% and 10%. The particles were sintered 3 hours at 1100°C under the protection of argon. The actual doping concentrations were not measured. The spectral behaviour is examined and reported and XRD analysis was performed to verify any addition of impurities due to the increasing doping.

Doping concentration

The luminescence of CaZnOS:Mn²⁺ was investigated through changes in the concentration of Mn²⁺. The emission spans from yellow to red with the following concentrations: 0.1%, 0.2%, 0.6%, 2%, 6% and 10% when irradiated with a 256 nm UV light as illustrated figure 3.23. The samples were sintered at 1100°C for 3 hours in an argon atmosphere. The 0.2% and 0.6% samples exhibit a yellow shade whereas the 10% CaZnOS:Mn is more red. At 2%, the powder exhibits a bright orange photoluminescence.

Figure 3.24 shows the emission spectra of CaZnOS:Mn. We notice that depending on the doping concentration, the emission shifts from 610 nm to 618 nm upon an excitation at $\lambda_{ex} = 280$ nm. This main asymmetrical band is particularly intense for CaZnOS:Mn@0.6% and 2%. To explain the origin of this red shift *Zhang et al.* [23] calculated values of the band gap which gradually decrease with increasing Mn²⁺ concentration. The Mn²⁺ doping induced the introduction of trap levels. Moreover, this red shift can also result from the formation of Mn²⁺ pairs at higher concentrations. Mn²⁺ pairs can reduce the energy difference between ground and first excited states. The emission is then at lower energy than that of single ions [92, 93]. Interestingly, the band at 534 nm is present for samples 0.1%, 0.2% and 0.6%, with decreasing intensity as the concentration of Mn increases, and it disappears completely for the 2%, 6% and 10% samples. It suggests that this band results from defect centers induced by Mn²⁺ doping [23].

In order to highlight the appearance of the 530 nm emission band, the influence of the excitation wavelength on the emission is studied for two samples: the 0.6% and 2% Mn-doped CaZnOS. The samples are excited at wavelengths ranging from 250 nm to 350 nm, the results are presented figure 3.25.

The spectra of the 0.6%-Mn concentration sample show three bands peaking at 612 nm, 582 nm and another one around 532 nm. For λ_{ex} ranging from 250 nm to 280 nm, two bands are visible: the 612 nm, which is the main band, and the 532 nm, present as a wide weak band. The latter disappears completely at higher excitation wavelength while the 612 nm band decreases in intensity as the excitation wavelength increases as well, and is then replaced by a less intense 582 nm emission band at $\lambda_{ex} = 340$ nm and 350 nm. *Xu et al.*[94] also found a 580 nm emission band for an excitation at 336 nm attributed to the same ${}^4T_1({}^4G) - {}^6A_1({}^6S)$ transition of Mn²⁺ ions.

The CaZnOS:Mn 2% spectra display two emission bands, one at 614 nm and another at 582 nm. The first one appears for excitation wavelengths spanning from 250 nm to 320 nm. The intensity decreases as λ_{ex} increases. The 582 nm emission band arises for higher excitation wavelength, from 330 nm to 350 nm, with decreasing intensity.



Part2(Chemical_tools)/Chapter3/Figs/CZOS_different_pourcentage_1100C_3h.jpg

Figure 3.23: Photographs of CaZnOS:Mn powders at different doping percentages (0.1%, 0.2%, 0.6%, 2%, 6% and 10%) sintered 3h at 1100°C under a 256 nm UV light.

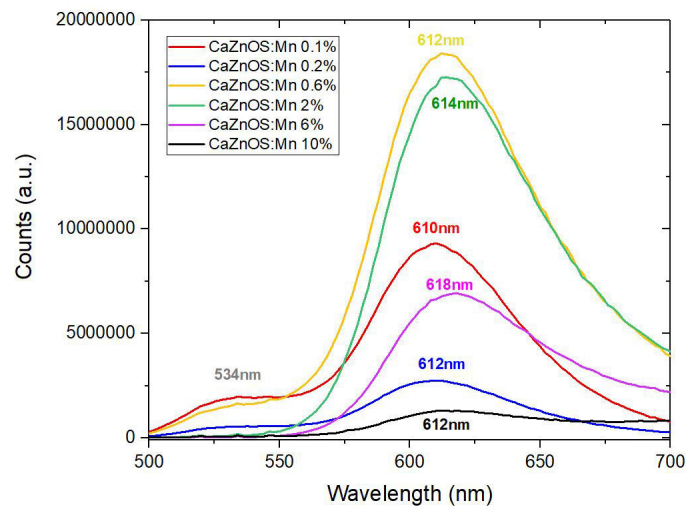


Figure 3.24: Emission spectra of CaZnOS:Mn at different doping concentrations (0.1%, 0.2%, 0.6%, 2%, 6% and 10%) sintered 3h at 1100°C upon an excitation of $\lambda_{ex} = 280\text{ nm}$.

The 0.6% Mn doped CaZnOS phosphor exhibits a large and intense 612 nm emission band for excitation wavelengths from 250 nm to 310 nm. This band shifts toward a lower wavelength (around 582 nm) at higher λ_{ex} . Moreover, for low Mn concentration materials, a shouldering around 532 nm is visible along with the main 612 nm emission,

which is not present for high Mn concentration compounds.

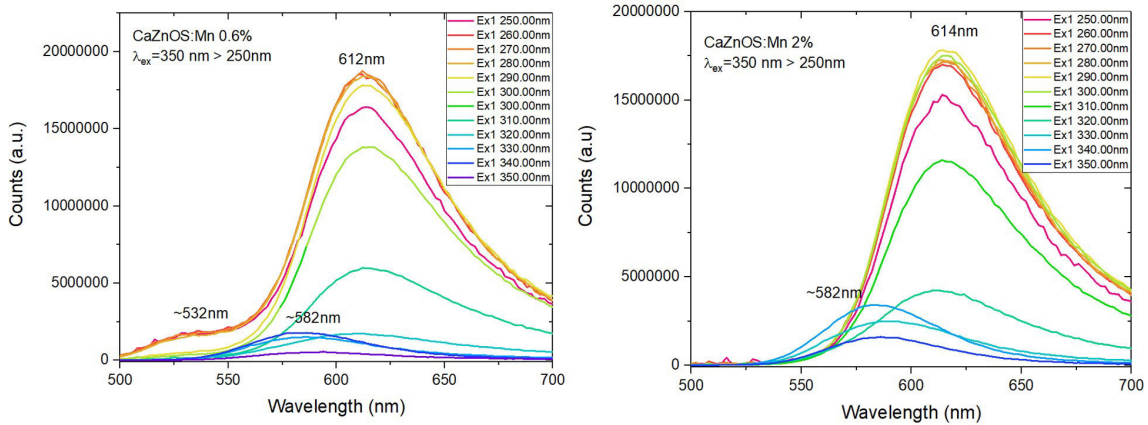


Figure 3.25: Emission spectra of CaZnOS:Mn 0.6% (right), 2% (left) sintered 3h at 1100°C (argon atmosphere) upon an excitation λ_{ex} spanning from 250 nm to 350 nm.

The diffractograms of CaZnOS:Mn powders are presented figure 3.26. As previously mentioned, these powders were sintered 3 hours at 1100°C in an argon atmosphere. For all four samples (the 1%, 2%, 6% and 10% Mn concentrations), peaks belonging to the CaZnOS phase, i.e. hexagonal, are present. An unidentified peak at 25.4° is seen only in the 1% sample in (a) (earlier observed in figure 3.22). The 2%, 6% and 10% are all three similar to one another with equivalent peak intensities.

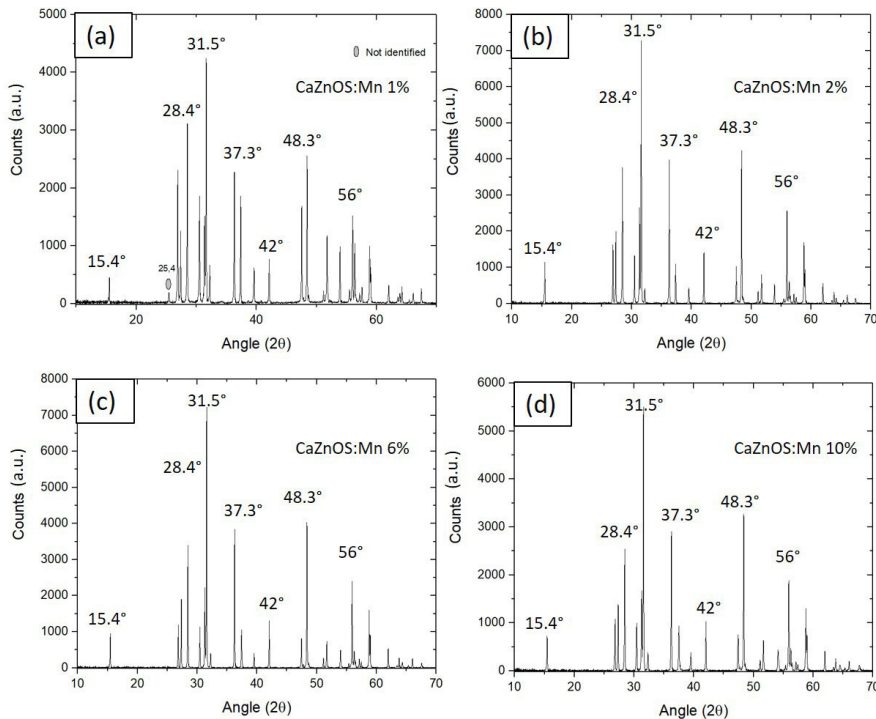


Figure 3.26: XRD diffractograms of CaZnOS:Mn powders at different doping percentages (1%, 2%, 6% and 10%) sintered 3h at 1100°C , argon atmosphere.

The spectral properties of CaZnOS:Mn change as a function of the dopant's concentration. The sample was doped at 0.1%, 0.2%, 0.6%, 2%, 6% and 10%. The photoluminescence spectra show two emission bands for the 0.1%, 0.2% and 0.6% samples:

a weak one around 530 nm and large and intense one around 612 nm at an excitation wavelength of 280 nm. The 612 nm emission is attributed to ${}^4T_1({}^4G) - {}^6A_1({}^6S)$ transition of Mn^{2+} ions, whereas the 530 nm emission results from defect centers formed by Mn^{2+} doping. These two emissions are highly dependent on the excitation wavelength as they are substituted for a 582 nm emission band for excitations exceeding 330 nm.

At high Mn concentrations (2%, 6% and 10%), only the 612 nm emission band stands at an excitation wavelength of 280 nm. At excitation superior to 320 nm, the 612 nm emission is also replaced by the 582 nm band.

All these materials are identified as hexagonal from their XRD diffractograms with unidentified phases for low Mn concentrations. The CaZnOS:Mn@2% exhibits the most intense luminescence with a unique emission band at 614 nm.

Sintering temperature

Pellets of CaZnOS with a doping Mn concentration of 1% were sintered at 3 different temperatures: 1100°C, 1200°C and 1300°C for 3 hours in an argon atmosphere. They were ground to powders before being characterized using SEM, XRD measurement devices and a spectrofluorometer.

The SEM images figure 3.27 show the morphology of said powders. Images (a) and (b) are very similar. We see mostly large CaZnOS:Mn particles, from 20 to 50 μm , and distinguish the junctions where smaller particles aggregated by sintering. The particle in figure (c) looks smoother than the others and the edges melted a little. In addition to that, the sample stuck to the crucible which indicates that the temperature was too high and caused the pellet to melt. We notice very little porosity for all three powders.

Figure 3.28 gathers information about the crystal structure and emission of Mn-doped CaZnOS powders sintered at different temperatures. (a), (b) and (c) represent the diffractograms of our materials at 1100°C, 1200°C and 1300°C, respectively. The peaks belong to either the ZnS, CaZnOS or CaO phases except the peak at 25.4° which remained unidentified.

Diffractograms (a) and (b) are similar and show that the ZnS is the main phase. In (c) most peaks belonging to that phase disappeared and the CaZnOS phase dominates but there are also traces of the CaO phase. Unlike 1100°C and 1200°C, we also see broader peaks at 17.9°, 25.3°, 28.6°, 34°, 46.9° and 50.8°. The peaks at 17.9° and 44.9° are new as they do not appear in (a) nor (b), they do not belong to any of the CaZnOS, ZnS or CaO phases, and thus remain undetermined.

The emission spectra of CaZnOS:Mn can be found in (d). For $\lambda_{ex} = 280$ nm, the emission changes according to the sintering temperature. At 1100°C, we see the two bands around 610 nm and 534 nm, whereas at 1200°C only the band at 612 nm is visible. The green curve, which represents the emission spectra for the 1300°C sintered powder, shows a large band at 587 nm.

The temperature did not impact the grain growth during sintering but caused melting of the powder at high temperature, namely 1300°C. The CaZnOS:Mn@1100°C had two emission bands: one around 610 nm and the other around 530 nm, whereas CaZnOS:Mn@1200°C only had the 610 nm band. However, the photoluminescence spectra showed a spectral shift with the presence of a unique emission band around 587 nm for CaZnOS:Mn@1300°C. The XRD diffractograms showed that the powders are not-single-phased but show CaZnOS, ZnS and CaO phases (hexagonal).

3.1.2.5 Conclusion

Doped CaZnOS is a piezoelectric material which exhibits mechanoluminescent property when ground. It was synthesized via solid state reaction. CaZnOS:Mn (and CaZnOS:Mn, Li) was obtained by mixing ZnS, CaO and $MnCO_3$ (and $LiCO_3$) and sintered



Figure 3.27: SEM images of CaZnOS:Mn powders at 1% doping synthesized via solid state reaction at different sintering temperatures, 1100° C, 1200° C and 1300° C for 3 hours in an argon atmosphere.

at 1100° C for 3h in an argon atmosphere. The two materials have different morphologies: CaZnOS:Mn is made of spherical microparticles whose size ranges from 20 to 30 μm , whereas CaZnOS:Mn,Li displays large plate-like particles (50-100 μm in size). However, they display a hexagonal crystal phase which is purer with the introduction of lithium. At 1% Mn doping, their photoluminescence spectra are similar at an excitation wavelength of 280 nm with two emission bands: an intense one around 610 nm and a weaker one around 530 nm. The first one results from the ${}^4T_1({}^4G) - {}^6A_1({}^6S)$ transition of Mn^{2+} ions, whereas the second emission originates probably from defect centers related to Mn^{2+} doping.

The concentration of the dopant influences the intensity of luminescence. To design the most intense material, we have doped CaZnOS at 0.1%, 0.2%, 0.6%, 2%, 6% and 10% of Mn. The 530 nm emission band disappears for high Mn concentrations (2%, 6% and 10%). Moreover, a 582 nm emission band appears for excitation wavelengths higher than 320 nm.

As for the sintering conditions, the temperature plays an important role in the homogeneity and morphology of the particles as well as in the emission spectra which shifts as the temperature increases. At 1300° C, the particles start to melt and the photoluminescence displays a large band centered at 587 nm for an excitation wavelength of 280 nm. The XRD analysis showed a loss in diffraction peaks for that same sample.

For our study, the selected protocol for the synthesis of Mn-doped CaZnOS is:

- Method: Solid state reaction,
- Mn-doping: 2%,

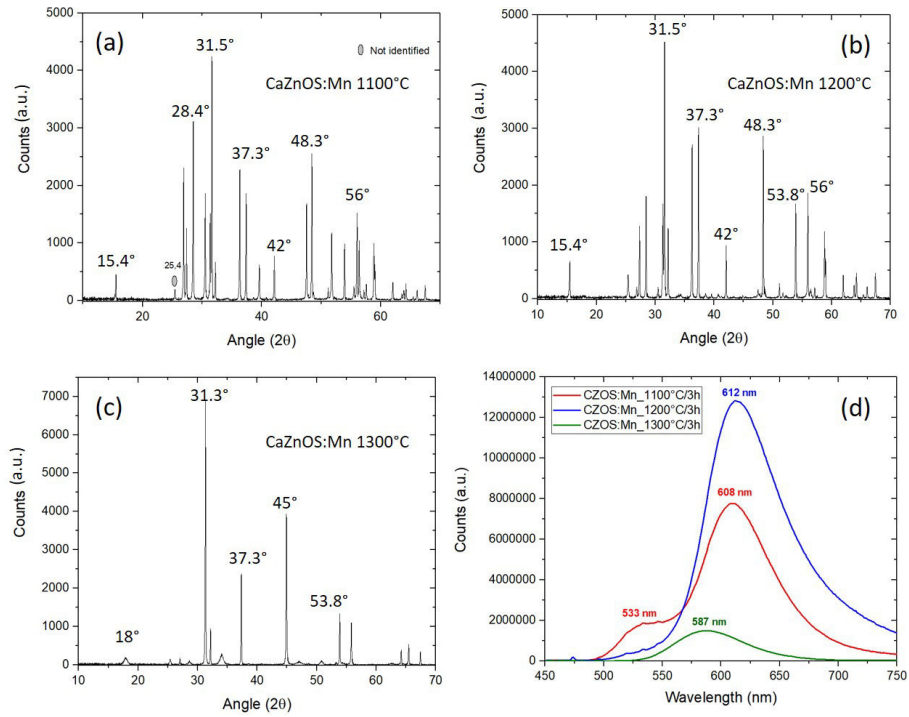


Figure 3.28: (a-c) XRD diffractograms and (d) Emission spectra at an excitation wavelength $\lambda_{ex} = 280$ nm of CaZnOS:Mn powders at 1% doping synthesized via solid state reaction at different sintering temperatures, 1100°C, 1200°C and 1300°C.

- Sintering conditions: 3h at 1100°C in argon atmosphere.

3.2 Other doped-ZnS phosphors

The study of elastico-mechanoluminescence requires a large variety of materials: EML phosphor, soft polymer and testing device. In the previous chapter, we have seen that ZnS:Cu from Gwent Group exhibits bright EML over repeated cycling of stretching and releasing actions. Despite its efficiency, and the precious information we gathered thanks to it, we were limited in the understanding of the phenomena. To help us widen our comprehension through the materials approach, we started synthesizing our own materials (cf. section 3.1) and searched for new suppliers with a well-furnished phosphor catalogue.

Shanghai Keyan Phosphor Technology Co. Ltd. (KPT) offers products meant for lighting display and energy-saving through electroluminescent (EL) wires and EL panels, infrared (IR) instruments using IR laser testing, phosphor materials for EL and scintillation purposes, electrochromic film and moisture proof film [95]. We have selected a number of phosphors: ZnS:Cu (Al₂O₃ coated and non-coated) and ZnS:Mn (Al₂O₃ coated). Their characterization is presented in this section. SEM-EDX, optical microscope, XRD and a spectrofluorometer were used for the optical and structural characterization of these phosphors.

3.2.1 Material Selection

We have purchased EML phosphors known to be suited for EML like ZnS:Mn and ZnS:Cu. These materials are known to be already coated with aluminium oxide but this company has also uncoated phosphor particles. Purchasing both of these materials, namely coated and uncoated, would facilitate the study of the influence and role of this coating on the EML process.

The following phosphors were purchased from Shanghai Keyan Phosphor Technology Co. Ltd. (KPT):

Reference	Type	Emitting color	Chemical composition
502	B	Blue-Green	ZnS:Cu
512	S, C	Green	ZnS:Cu
611	B, C	Orange	ZnS:Mn

Table 3.2: *Table of the phosphors purchased from Shanghai Keyan Phosphor Technology Co.,Ltd. (KPT) and their given properties.*

The type model corresponds to:

- TYPE B: Average particle size 29 μm , high brightness, heat resistance, suitable for application to plastic and enamel panel.
- TYPE S: Average particle size 9 μm , better brightness, homogeneous emitting effect, suitable for application to glass and plastic panel.
- TYPE C: Average particle size 29 μm , with characteristic of particle surface being coated, it has good humidity resistance, prolonged application lifetime, high brightness, no need of sealed package, suitable for application to plastic panel

The particles of S type (9 μm in diameter) were not selected for our EML study because of their small size. Also, the 611B powder displayed a brown colour and very weak photoluminescence under UV-light. Only the 502B, 512C and 611C were later used, the others will not further be detailed.

3.2.2 Phosphor characterization

Shanghai Keyan Phosphor Technology Co. Ltd. (KPT) provided the grain size, colour of emission and the presence, or not, of the Al_2O_3 coating. However, the 502B, 512C and 611C powders were further characterized using SEM-EDX, XRD, a spectrofluorometer and an optical microscope.

3.2.2.1 502B: ZnS:Cu phosphor

The 502B phosphor material is a Cu-doped ZnS with a particle size of $29 \mu\text{m}$ indicated by the supplier. The optical and structural properties were determined and are presented figures 3.29 and 3.30.

The SEM image, figure 3.29 (a), shows particles with smooth and others with rough surfaces. Their size swings between 10 to $40 \mu\text{m}$ and are rather homogeneous. Zn and S elements are detected by the EDX analysis. When excited at 360 nm, the particles exhibit a broad band centered at 484 nm which confirms the blue-green emission from the datasheet of the supplier, cf. (c). The green emission of ZnS:Cu originates from the recombination between the shallow donor level (sulfur vacancy) and the t_2 level of Cu^{2+} . The Zn^{2+} ions in ZnS are substituted by the Cu^{2+} which are embedded in the ZnS. Peng *et al.* [96] observed a shift in longer wavelength with the increase of the Cu^{2+} concentration.

The XRD diffractogram shows the hexagonal (hcp) crystal structure (or wurtzite) with the presence of peaks at 26.88° , 28.5° , 30.5° , 39.5° , 47.5° , 51.7° and 56.3° corresponding to the planes [2110], [2420], [1211], [2112], [1120], [2113] and [1122], respectively.

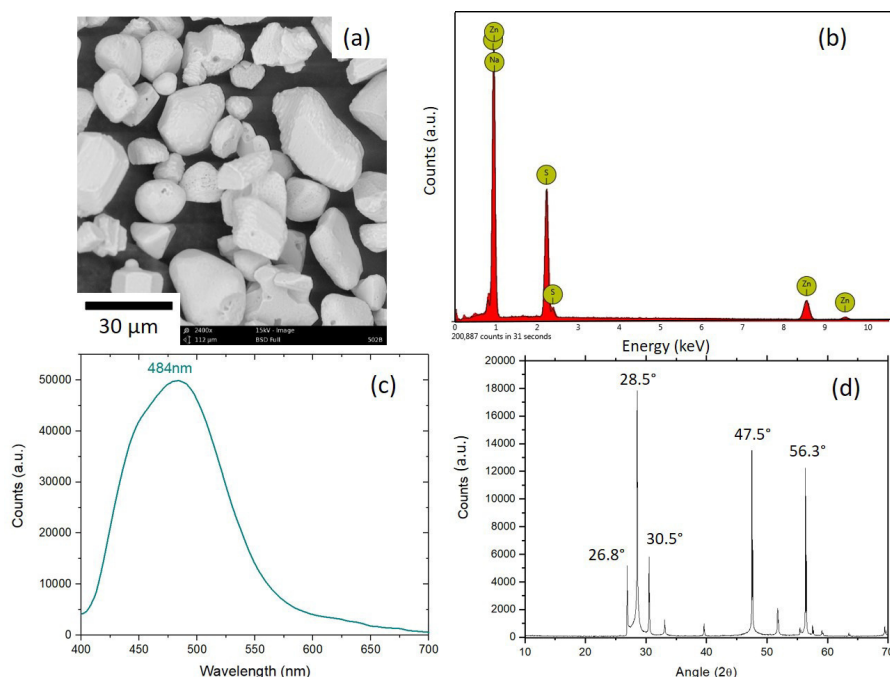


Figure 3.29: Characterization of 502B commercial ZnS:Cu particles. (a) SEM image. (b) EDX analysis. (c) Emission spectrum, band peaking at 484 nm, under excitation wavelength $\lambda_{ex} = 360$ nm. (d) XRD diffractogram.

The optical microscope images figure 3.30 were taken using the bright-field mode (a) and crossed polarization (b). The particles are translucent in (a) but exhibit various colors in (b) mainly yellow and orange for the observed direction which prove the birefringent nature of the material and that each grain of 502B is a mono-crystal.

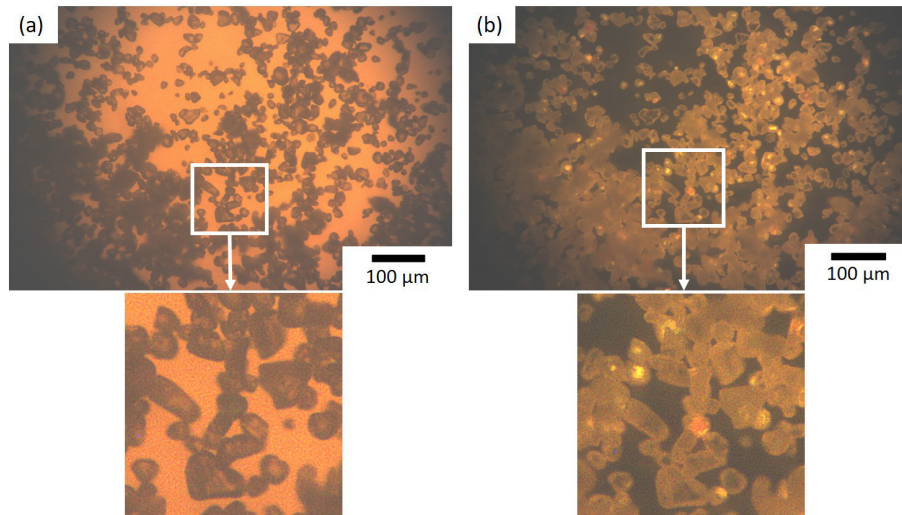


Figure 3.30: *Optical microscope images of ZnS:Cu 502B particles using bright-field mode (a) and crossed polarization (b).*

3.2.2.2 512C: Al₂O₃-coated ZnS:Cu phosphor

The 512C phosphor material is a Cu-doped ZnS with a particle size of 29 μm and an Al₂O₃ coating indicated by the supplier. The optical and structural properties were determined and are presented figures 3.31 and 3.32.

The SEM image, figure 3.31 (a), shows big particles with smooth surfaces. Their size swings between 20 to 50 μm . They are rather homogeneous and are accompanied by smaller grains about less than 1 μm in diameter. Zn, S, Al and O elements are detected by the EDX analysis. The presence of Al and O confirms that the particles are coated with aluminium oxide. When excited at 360 nm, the particles exhibit a broad band centered at 500 nm, it is consistent with the ZnS:Cu emission material. However, we notice an emission shift between 502B and 512C (484 nm and 500 nm, respectively). This can be due to a higher Cu concentration in the 512C material [96]. These concentrations were not communicated by the supplier. (c) is the XRD diffractogram of 512C. It highlights the hexagonal crystal structure of this material.

The optical microscope images figure 3.32 were taken using the bright-field mode (a) and crossed polarization (b). The particles are translucent in (a) but exhibit yellow and orange colors in (b). 512C is birefringent in this direction which makes it a mono-crystal.

3.2.2.3 611C: Al₂O₃-coated ZnS:Mn phosphor

The 611C phosphor material is a Mn-doped ZnS with a particle size of 29 μm and an Al₂O₃ coating indicated by the supplier. The optical and structural properties were

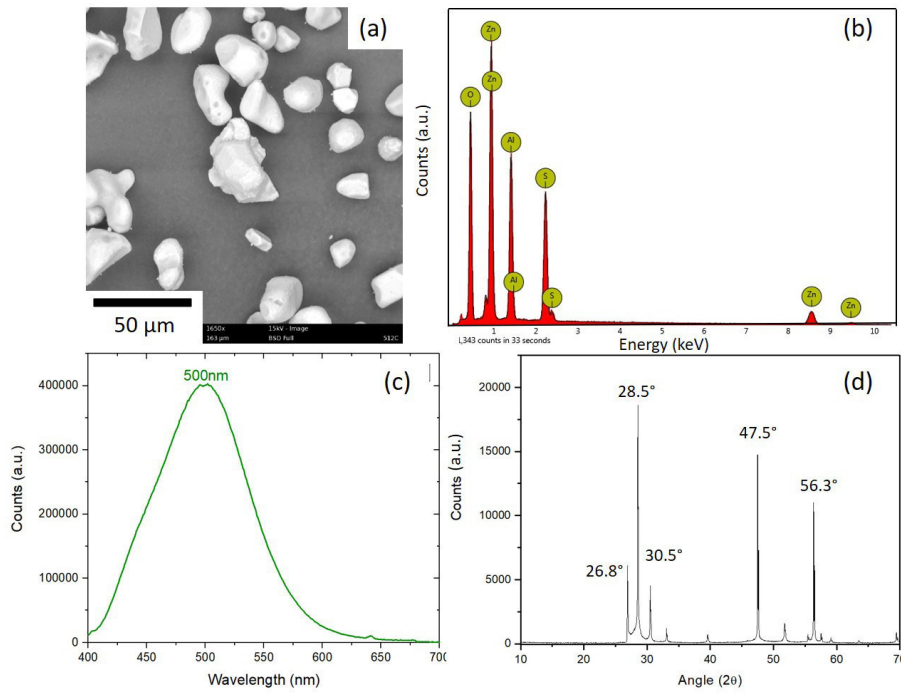


Figure 3.31: Characterization of commercial 512C particles: Al_2O_3 -coated ZnS:Cu. (a) SEM image. (b) EDX analysis. (c) Emission spectrum, band peaking at 500 nm, under excitation wavelength $\lambda_{ex} = 360$ nm. (d) XRD diffractogram.

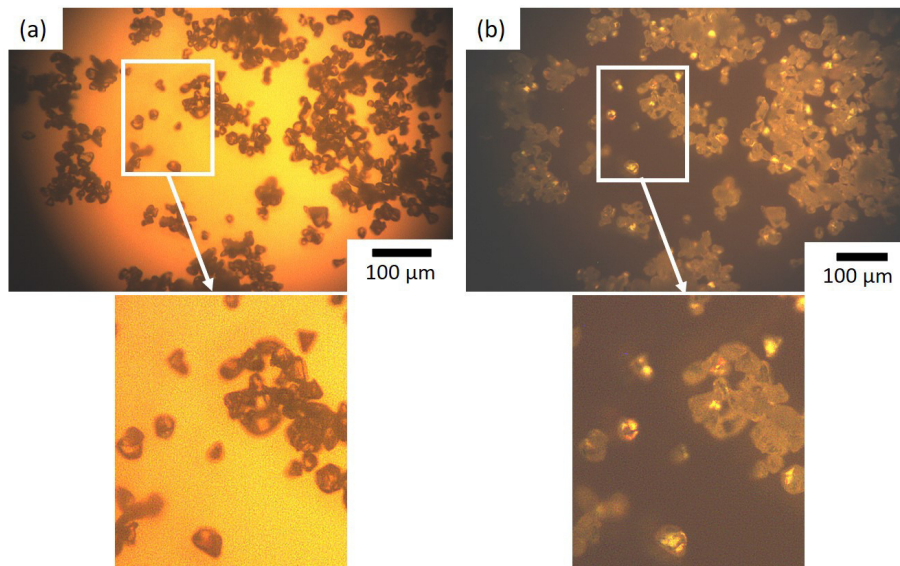


Figure 3.32: Optical microscope images of ZnS:Cu 512C particles using bright-field mode (a) and crossed polarization (b).

determined and are presented figures 3.33.

The SEM image, figure 3.33 (a), shows big particles with a size between 20 to 50 μm . Smaller particles are also found in this sample about 1 to 5 μm in size. Zn, S, Al and O elements are detected by the EDX analysis. The presence of Al and O confirms that the particles are coated with aluminium oxide. When excited at 360 nm, the particles exhibit a broad band centered at 585 nm which is consistent with the orange emission exhibited by Manganese doped zinc sulfide. The diffraction peaks in (d) show a cubic crystal structure

with the peaks at 28.5° , 47.5° and 56.3° . They correspond to the planes $[11\bar{2}1]$, $[22\bar{4}0]$ and $[51\bar{4}1]$ which are typical of this phase.

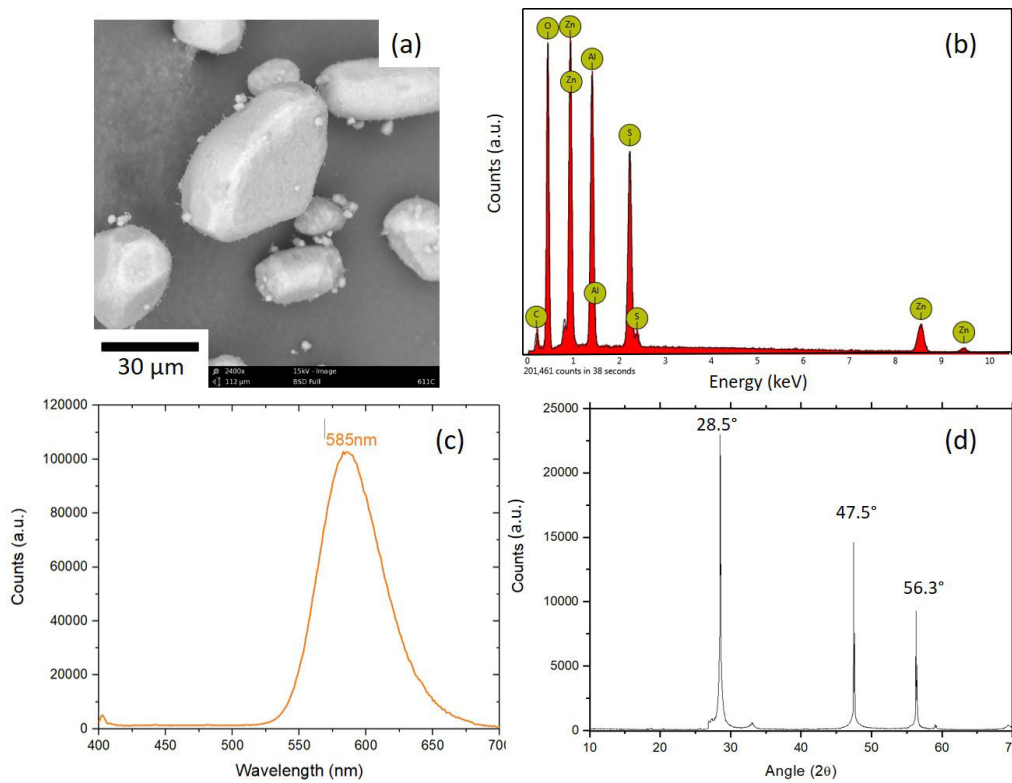


Figure 3.33: Characterization of commercial 611C Al_2O_3 -coated ZnS:Mn . (a) SEM image. (b) EDX analysis. (c) Emission spectrum, band at 585 nm, excitation wavelength $\lambda_{ex} = 360$ nm. (d) XRD diffractogram.

3.2.3 Conclusion

In addition to the Gwent ZnS:Cu phosphor, three more ZnS -based phosphors were purchased from KTP phosphors in a form of powders: 502B, 512C and 611C. The XRD analysis showed a hexagonal close-packed (hcp) crystal structure for 502B and 512C phosphors. Although being the same material (ZnS:Cu) their photoluminescence spectra differ from one another. 502B exhibited a large emission band at 485 nm whereas 512C showed an emission centered around 500 nm at an excitation wavelength of 360 nm. The green emission of ZnS:Cu originates from the recombination between the shallow donor level (sulfur vacancy) and the t_2 level of Cu^{2+} . Peng *et al.* [96] observed a shift in longer wavelengths with the increase of the Cu^{2+} concentration. The observed emission shift can be due to synthesis parameters themselves, which are unknown from us, like the concentration of the dopant. With the increase of the Cu^{2+} concentration a red shift is observed [96].

Moreover, the 512C is coated with aluminium oxide (Al_2O_3), which is not the case of 502B. From a structural point of view, 512C phosphor should be as efficient as the Gwent ZnS:Cu . They have the same morphology, crystal structure and coating. Also, comparing 502B and 512C materials will help understand the effect of the aluminium oxide coating that some authors believe to be necessary for EML.

611C material is a manganese-doped zinc sulphide (ZnS:Mn) also coated with Al_2O_3 . Unlike the two others, this phosphor displayed a cubic crystal structure and an

orange emission band around 585 nm at an excitation wavelength of 360 nm. This emission originates from the ${}^4T_1-{}^6A_1$ transition of the Mn^{2+} ions. The three materials share a similar feature: the particle size, ranging from 30 to 40 μm on average.

3.3 Particle coatings

We present in this section the coating procedure in order to study its effect on the EML process through the surface modification of the phosphor particles. By doing so, the interaction between the particles and their matrix (the PDMS) should change depending on the nature of the coating itself. These modifications should also have an impact on the elasto-mechanoluminescence (EML) and provide information on the mechanism responsible for the emission of light, either piezoelectricity or triboelectricity. Piezoelectricity requires a heavy load on the particle to trigger luminescence which means a strong bond between the particle and the polymer. Triboelectricity requires that these two materials interact weakly with each other. The matrix would stick poorly to the particle during deformation.

We have previously introduced the aluminium oxide coating (or Al_2O_3) usually found in commercially available phosphors meant for electroluminescence applications. It was developed for phosphor stability. It is suggested [55] that the presence of this coating is essential for achieving bright EML. Therefore, we propose here several chemical routes to cover and coat microparticles with different materials: Al_2O_3 , SiO_2 and teflon. Moreover, we present the morphological and structural properties of the coated particles through SEM and XRD analysis.

3.3.1 Aluminum oxide coating Al_2O_3

Aluminium oxide or alumina can be mainly found in nature as corundum which is its crystalline polymorphic α phase. It is mostly known as the precious gemstones ruby and sapphire. It is commonly used as a protective coating to prevent oxidation in metals.

The synthesis of Al_2O_3 can be performed via different techniques like atomic layer deposition (ALD) [97], chemical vapor deposition (CVD) [98], pulsed laser deposition (PLD) [99], sol-gel [100, 101] and magnetron sputtering [102]. Originally used for electroluminescent purposes, ZnS microparticles ($ZnS:Cu,Cl$, $ZnS:Cu,Al$, $ZnS:Cu,Mn,Al$ and $ZnS:Cu$) can be subject to deterioration due to electrical driving conditions, like high applied frequency, and to environmental phenomena like humidity. That is why hermetic encapsulation ensures the durability of the phosphors.

Aluminium oxide has a large range of applications in thin film form. It is used as a water repellent [103], a protective layer [104], a dielectric [105], to enhance the electrochemical performance and structural stability of cathode materials such as $Li(Ni_xCo_xMn_x)O_2$ with $x = 1/3$ [106] and $LiCoO_2$ [107, 108, 109]. It also improves high-voltage cycling stability [97]. It was reported that elasto-mechanoluminescence can only be triggered with the presence of this coating on ZnS:Cu microparticles embedded in a soft polymer matrix like polydimethylsiloxane (PDMS). This observation is in favour of the triboelectricity model where Al_2O_3 tends to easily create positive charges due to its ranking on the triboelectricity scale (figure 1.14) and PDMS tends to create negative charges.

Although well documented, it is difficult to coat properly our particles and many methods were tried before finding a suitable one. After several attempts, we propose here a new approach based on the thermal decomposition (chemical decomposition caused by heat) of aluminium isopropoxide [110, 111, 112]:

In a 100 mL three neck round bottom flask, 1 g (or 5 mmol) of $\text{Al}(\text{O-i-Pr})_3$, 1 g of $\text{ZnS}:\text{Cu}$ particles and 20 mL of ODE are mixed together. The right and left apertures of the flask are sealed with septa. The flask is then placed in a heating mantle, and under constant magnetic stirring. The temperature is set at 280°C . The container is degassed and placed under Ar flow through the middle aperture of the flask. When the temperature reaches around 200°C , the solution starts to boil. A needle is pricked onto one septum until the steam stops. At 280°C , the solution is left for 90 min. Next, the flask is cooled down at 50°C using compressed air, after which, 30 mL of hexane are added. Finally, the solution is washed twice with ethanol. The following chemical reaction takes place:



Thanks to the EDX mapping analysis, it is possible to verify if the coating succeeded. Figure 3.34 shows 502B particles coated with aluminium oxide. The mapping on the right shows Zn and S (in pink and green, respectively), as they are the two constituents of the material, and Al and O as well. The particle and its contours are well discernible using only the Al and O elements (in yellow and blue, respectively). This proves that the Al_2O_3 was successfully deposited on the surface of the particle. However, not all particles could be coated completely, and each sample requires multiple washings because of all the residual aluminium.

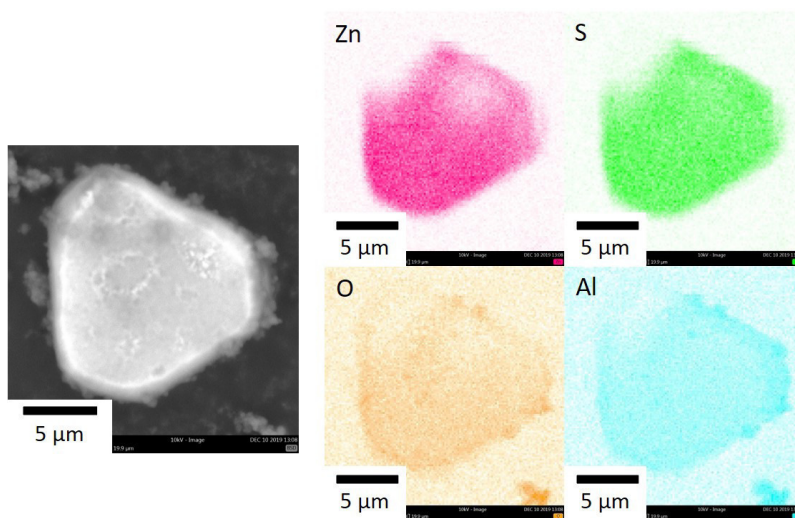


Figure 3.34: EDX mapping analysis of $\text{ZnS}:\text{Cu}$ particles coated with aluminium oxide Al_2O_3 . Detection of Zn, S, O and Al.

The fluorescence of the samples was directly examined using a 256 nm UV lamp and compared to that of a non-coated sample and no difference was detected by the naked eye.

A PXRD measurement of the coated particles showed that the alumina did not have an impact on the crystal structure as the deposited layer is not thick enough to be seen, as shown figure 3.36 (a). A diffractogram of the aluminium oxide obtained using the synthesis without ZnS microparticles is presented in (b). It shows a large and intense peak at 8° and other weak peaks around 16° , 27° , 49° and 65° . Except the first diffraction peak, the others could match that of boehmite, an aluminium oxide hydroxide for which the XRD pattern can be found figure 3.35. Our coating could be a nano-boehmite because of the width of the peaks.

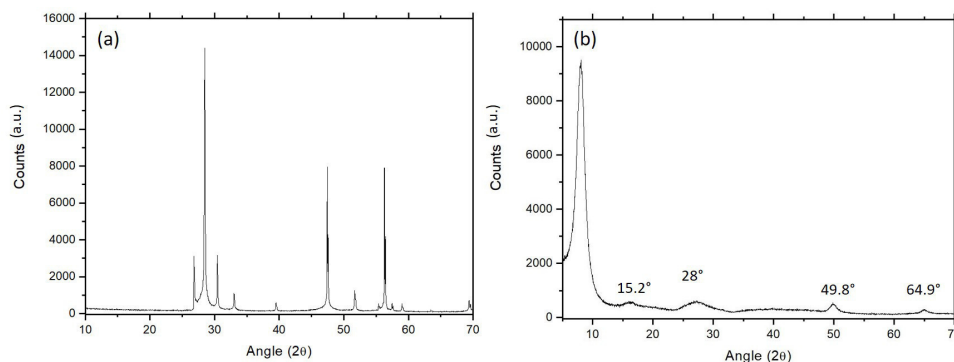


Figure 3.35: XRD diffractograms of Al_2O_3 -coated $\text{ZnS}:\text{Cu}$ 502B (a) and Al_2O_3 (b).

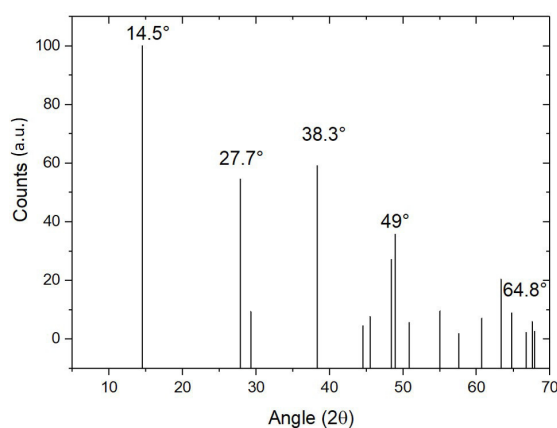


Figure 3.36: XRD diffractograms of boehmite. From the American Mineralogist Crystal structure Database.

3.3.2 Silicon dioxide (SiO_2) coating

Silica coatings are generally used to protect from degradation, enhance the chemical and thermal stability of nanoparticles as well as their dispersion. This coating was chosen because of its position on the triboelectricity scale (figure 1.14) which is next to Al_2O_3 . If we consider Al_2O_3 being a luminescence booster, SiO_2 might act the same way.

One of the most effective and direct routes to coat particles is using the Stöber process. Discovered by Werner Stöber in 1968 [113], this method allows the controlled growth of spherical silica particles of uniform size using tetraethylorthosilicate (or TEOS) as a precursor reacted with water in an alcoholic solution under basic conditions. The hydrolysis of TEOS molecules generates silica monomers that condense to create larger structures. Thanks to this process, it is possible to obtain particles ranging from 0.05 μm to 2 μm in diameter. As an example, the following table gives the size of the obtained particles depending on the quantities of the starting materials:

Particle size	TEOS	EtOH	NH_4OH 28%	H_2O
200 nm	30 mL	750 mL	50 mL	10 mL
450 nm	30 mL	750 mL	90 mL	-
730 nm	30 mL	750 mL	135 mL	-

Table 3.3: Table of the quantities of the materials used in a Stöber process.

It is possible to use this method to grow silica particles or to coat other nanopar-

ticles with SiO_2 . This last application is widely reported in the literature. By modifying the Stöber method, it is possible to coat various nanoparticles like silver [114, 115, 116] as it ensures a good colloidal stability in water and allows the control of the distance between metal nanoparticles through silica shell thickness. Other examples of core-shell spheres can be found in $\text{ZrO}_2@SiO_2$ [117] or gold nanoparticles with stable silica by ultrasound-assisted Stöber method [118].

The influence of SiO_2 on our microparticles is studied using the chemical method described below:

In a beaker, 25 mL of ethanol and 4.5 mL of NH_4OH in 28% H_2O are stirred together. 13 g of ZnS particles are added to the mixture. Finally, 1 mL of TEOS is injected at 1 mL/h rate. The beaker is covered with parafilm and kept 12 hours on a magnetic stirrer. It is later washed, first, with ethanol and, then, with water. To finish, it is dried in an oven at 60°C for 8 hours.

The simple EDX analysis shows the presence of Zn, S, Al, Si and O. The detection of Si hints toward the successful SiO_2 coating. To confirm this first analysis, an EDX mapping is performed (cf. figure 3.38). All the previously mentioned elements are visible along with the silicium which hugs the particle figure.

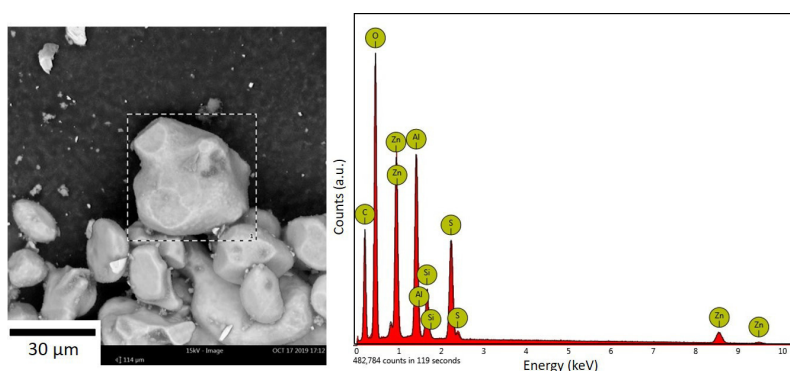


Figure 3.37: SEM image and EDX analysis of ZnS:Cu particles (512C) coated with silicon dioxide SiO_2 . Detection of Zn, S, O, Al and Si.

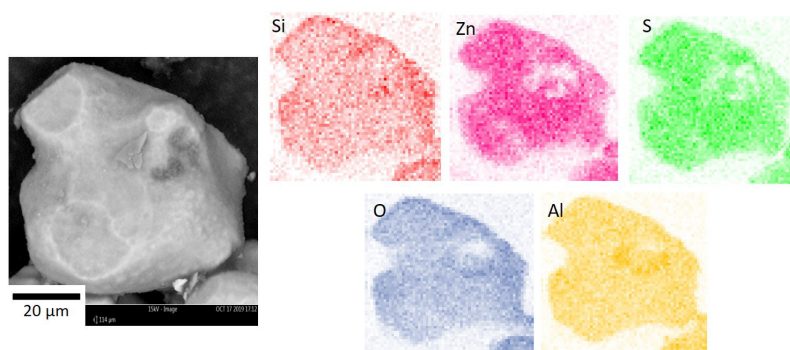


Figure 3.38: EDX mapping analysis of ZnS:Cu particles (512C) coated with silicon dioxide SiO_2 . Detection of Zn, S, O, Al and Si.

Also, the fluorescence of the samples was directly examined using a 256 nm UV lamp and compared to that of a non-coated sample and no difference was detected.

3.3.3 Tetrafluoroethylene TFE coating

Superhydrophobic surfaces are of great interest as they exhibit anti-sticking contamination prevention, water repellency and self-cleaning functions. This property opens the door to several applications as it can be used in windows and car windshield, in textile [119] or even paint additives. This coating can show omniphobic (a surface which repels -almost- everything) property which can be used in biomedical devices [120]. *Zhou et al.*[121] report using polydimethylsiloxane (PDMS), filled with fluorinated alkyl silane functionalised silica nanoparticles and fluorinated alkyl silane, as the material to produce a superhydrophobic coating on fabrics. This process proved to be effective as the material is resistant and durable against chemical and mechanical tests.

In the present work, we want **to tune the adhesion force between the particle and the PDMS matrix**. By coating our phosphor microparticles with a fluoroalkylsilane we ensure their hydrophobicity, and therefore, their weak interaction with the polymer, i.e. the polymer and the particles do not stick to one another. To do so, we applied the following protocol:

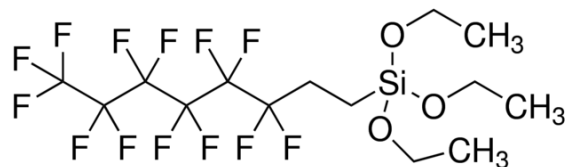


Figure 3.39: Chemical structure of the 1H, 1H, 2H, 2H - Perfluorooctyltriethoxysilane purchased from Sigma Aldrich [26].

A 1 mL of NH_4OH in 28% H_2O and 8 mL ethanol (EtOH) solution is prepared. We add 5g of the chosen phosphor powder (ZnS:Cu 502B) and finally 90 μL of perfluorooctyltriethoxysilane. The solution is stirred at room temperature for one hour. It is then washed 4 times with ethanol and dried in an 80°C oven for 4 hours. After complete drying, we drop water on the powder. If the powder does not wet, the particles are hydrophobic and, hence, were successfully coated.

The ZnS:Cu-502B and ZnS:Cu@ Al_2O_3 -512C, ZnS:Cu-Gwent, CaZnOS:Mn, ZnS:Mn and ZnS:Mn@ Al_2O_3 -611C were all successfully coated with perfluorooctyltriethoxysilane and were later incorporated in a PDMS matrix for mechanical testing. Their fluorescence using a 256 nm UV lamp did not exhibit any difference with that of a non-coated samples. The diffractogram shown figure 3.40 displays the same peaks belonging to a hexagonal (wurtzite) phase as seen figure 3.29 (d). The coating did not modify the crystal structure of the ZnS:Cu material as it is not present in a quantity large enough to induce change.

3.3.4 Conclusion

Aluminium oxide (Al_2O_3) coating is generally used as a water repellent on materials but scientific experiments have shown that ZnS:Cu material does not exhibit EML without the presence of this coating. Modifying the surface of the phosphor particles results in changes in the interaction between said particles and their matrix, namely PDMS. In the case of Al_2O_3 , it seems like it could be acting as a luminescence booster in the case of EML. This fact matches the triboelectricity theory where two materials become electrically charged after being in contact. Therefore, we have coated 502B ZnS:Cu particles with Al_2O_3 using $\text{Al}(\text{O}-i\text{-Pr})_3$. The surface modification did not alter the crystal structure

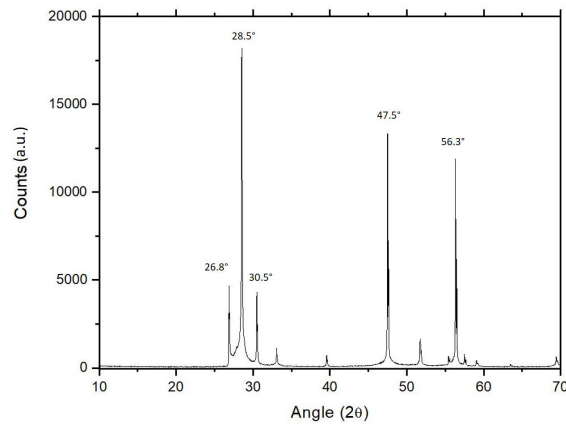


Figure 3.40: *Diffractogram of the ZnS:Cu 502B coated with tetrafluorosilane.*

of the material (hexagonal) but the crystal phase of the coating itself resembles that of boehmite. Unfortunately, this protocol is in need for optimization.

Similarly to Al_2O_3 , silicon oxide (SiO_2) acts as a protective layer on particles to prevent them from degradation and is next to Al_2O_3 on the triboelectric scale (figure 1.14). A modified Stöber process was successfully experimented to coat 502B and 512C ZnS:Cu microparticles.

The influence of a third coating was considered: teflon. Usually, teflon is used for superhydrophobicity. We have used perfluorooctyltriethoxysilane to realise this coating on several materials: 502B, 512C, Gwent, 611C and CaZnOS:Mn.

The chemical modifications of the microparticles' surfaces did not impact the photoluminescence properties and crystal structures of our materials.

The table below summarizes the phosphors presented in this chapter along side the surface modification applied to each:

Coating	Material
SiO_2	ZnS:Cu 502B ZnS:Cu 512C ZnS:Cu Gwent
Teflon	Synthesized ZnS:Mn Al_2O_3 -coated ZnS:Cu Gwent Al_2O_3 -coated ZnS:Mn 512C ZnS:Mn 502B Al_2O_3 -coated ZnS:Cu 611CC Synthesized CaZnOS:Mn/Mn,Li

Table 3.4: *Table of the studied phosphor materials and the implemented coatings.*

3.4 Conclusion

In this chapter we have presented several materials which can be used to study by a "material approach" the properties of elastico-mechanoluminescence and help us determine what makes an EML system efficient. The study with Gwent ZnS:Cu in the previous chapter led us to question the parameters that could influence the emission of light.

We have synthesized a 1% manganese-doped zinc sulphide (ZnS:Mn) using a microwave reactor followed by a sintering step. The microparticles showed a hexagonal crystal structure and a large emission band around 585 nm. This emission originates from the ${}^4T_1-{}^6A_1$ transition of the Mn^{2+} ions. The synthesis results in monocrystals of about 40 μm size on average but with high porosity levels. This porosity decreases with increasing Mn concentration in the ZnS crystal and increasing sintering temperature. The photoluminescence intensity is influenced by the sintering temperature: when the temperature increases, the emission band is more intense. We notice that the most intense photoluminescence was recorded for the ZnS:Mn doped at 2%.

CaZnOS is another synthesized material that we selected for its mechanoluminescent nature, its piezoelectric property and hexagonal crystal structure. All three elements are also found in the ZnS:Cu phosphor. The EML behaviour of this material and ZnS:Cu could be similar due to their shared characteristics. By solid state reaction, we were able to synthesize CaZnOS:Mn/Mn,Li microparticles. The spectral, structural and microscopic analysis helped determine the proper synthesis parameters for these two materials. CaZnOS:Mn is made of spherical particles of 30 μm in diameter whereas CaZnOS:Mn,Li exhibits large plate-like particles of 50-100 μm . Upon 280 nm excitation, the photoluminescence spectra of these two phosphors show two emission bands: an intense one around 610 nm and a weaker one around 530 nm. The first one results from the ${}^4T_1({}^4G) - {}^6A_1({}^6S)$ transition of Mn^{2+} ions, whereas the second emission originates from defect centers formed by Mn^{2+} doping.

Other commercially available EL phosphors were purchased: ZnS:Mn and ZnS:Cu. These phosphors are coated with aluminium oxide like Gwent ZnS:Cu but a non-coated ZnS:Cu could also be acquired. The two ZnS:Cu exhibit a similar hexagonal crystal structure but their photoluminescence spectra show a band at 485 nm for the non-coated phosphor and 500 nm for the Al_2O_3 -coated one. This difference could be due to a different Cu concentration: at higher concentration the spectrum shifts toward higher wavelengths. The coated ZnS:Cu should exhibit the same EML that of Gwent because they have the same morphology, crystal structure and coating. The commercial Al_2O_3 -coated ZnS:Mn material shows an orange emission centered around 585 nm caused by the Mn^{2+} ions and exhibits a cubic crystal structure.

Since the coating element seems to play an important role in the intensity of the light emitted by the samples during EML, we investigated this area by proposing different coating: Al_2O_3 , SiO_2 and teflon. The modified particles are then embedded in a PDMS matrix. The addition of a coating changes the interaction between the particle and the polymer which impacts the luminescence. This aspect will be presented in the next chapter.

Chapter 4

Mechanism of elastico-mechanoluminescence

The study of the elastico-mechanoluminescence (EML) requires specific tools: a composite material made of a phosphor like ZnS:Cu designed for EML, an elastomer like polydimethylsiloxane (PDMS), and an experimental device to induce an elastic deformation on the sample. Previously, we highlighted the importance of having a phosphor material that would exhibit intense and bright EML. Based on the literature, the ZnS:Cu (copper-doped zinc sulphide) appears to be the only (as far as we know) efficient referenced material without any clear explanations. *Chandra et al.* [36, 122] (cf. Chapter 1) presented a theory based on piezoelectricity. Many of the observations made on the subject do not comply with it, leading to the emergence of an alternative theory: Triboelectricity, proposed by *Sohn et al.* [10]. Our EML composite material is rather complex because parameters such as the polymer matrix, the nature of the excitation, the duration of the excitation and the nature of the phosphor itself including its surface state, influence the luminescence.

We want to present a more complete and coherent mechanism which would be consistent with the results that we obtained. To do so, we focus on the ZnS:Cu purchased from Gwent Group. This phosphor has an Al₂O₃ coating determined after an EDX analysis (cf. chapter 2). Thanks to our new understanding of the phenomenon, it was possible to implement a model.

The surface modifications presented in chapter 3, section 3.3 are also used for a better understanding of the phenomenon. The Gwent ZnS:Cu itself went through two chemical surface modifications: SiO₂ and teflon (TF). Furthermore, the influence of the PDMS matrix on the EML was also studied and is presented here.

In this chapter the following abbreviations are used:

- Gwent: ZnS:Cu phosphor from Gwent Group
- Gwent@SiO₂: SiO₂-coated Gwent phosphor
- Gwent@TF: Teflon-coated Gwent Phosphor
- S-R: Stretching-Releasing
- SC: Slow catalyst
- FC: Fast catalyst
- RTV: Room Temperature Vulcanization

4.1 Elastico-mechanoluminescence of Gwent ZnS:Cu

In order to propose an alternative model, we have questioned all the following elements: the phosphor, the matrix, the excitation and, of course, the previously proposed mechanisms. We have developed samples based on earlier publications using polydimethylsiloxane (PDMS) and implemented a stretching and releasing testing device. Although a significant amount of data was acquired, no interpretation was entirely satisfactory. That is why, in addition to the EML responses, we have compared the response to the displacement, observed the sample under an optical microscope and studied its behaviour upon stretching. Moreover, we added computer simulations using Python to mimic the shape of our signal during S-R cycles. All these information became pieces of evidence in favour of the triboelectricity model.

In chapter 1, we have introduced a well known material suited for elastico-mechanoluminescent (EML) measurements: copper-doped zinc sulphide or ZnS:Cu. This green emitting phosphor is well studied and used to fabricate various mechanoluminescent devices. We have used that same material for our own experiments. Mixed with polydimethylsiloxane (7:3, phosphor:PDMS weight ratio), the samples shaped as strips emitted light during elastic deformation and first observations on such a system could be made (cf. chapter 2).

The experience consists of stretching "S" the sample and releasing "R" it. This S-R cycle is repeated over a determined period of time. The PMT-based setup was used for the experiments and the following parameters were used:

- Acceleration: 4.000 cm.s^{-2}
- Velocity: 4 cm.s^{-1}
- Displacement: 62.5%
- Integration time PMT: 10 ms
- The experiment is conducted in a black box.

Figure 4.1 shows the elastico-mechanoluminescence response of the Gwent material. We find in (a) the whole EML response. We can observe the shape of the emission during 5 S-R cycles at the beginning (around 200 s) in (b) and at the end of the experiment (around 5000 s) in (c). The EML signal was recorded over almost 7500 cycles. The displacement curves in red, in (d) and (e), can be read as such, from left to right:

- When the curve reaches zero the sample is at a 0% deformation,
- The curve goes up which coincides with the sample being stretched,
- At the maximum of the emission intensity, the deformation is maximum corresponding to when the sample is 62.5% stretched,
- The red line goes back down, the sample is being released,
- At zero, the sample is back to its resting position.

This curve enables to pinpoint the exact deformation percentage for which the emission occurs.

Based on figure 4.1 we can highlight the following observations:

- The EML intensity increases. The number of stretching-releasing (S-R) cycles increases over time and so does the emitted light (cf. (a) whole response). Compared to $\text{SrAl}_2\text{O}_3:\text{Eu,Dy}$ material, which is a persistent luminescence phosphor, the sample does not need UV-irradiation to recover its EML.
- The EML response comprises 2 distinctive emissions: a large band and a sharp peak (cf. EML at 200 s (b) and 5000 s (c)). Thanks to the displacement curves (d) and (e) in red, it is possible to attribute the first emission to the stretching phase and the second to the releasing phase.

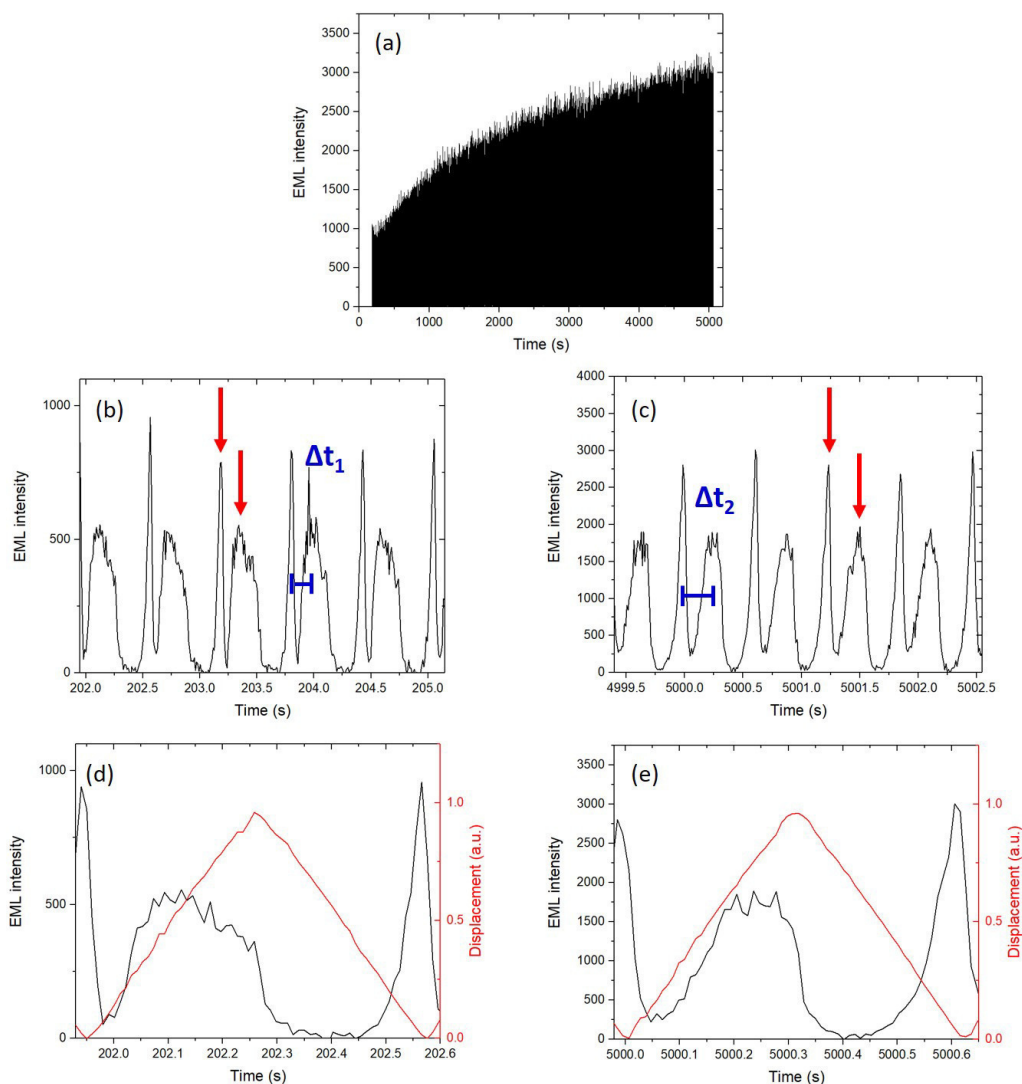


Figure 4.1: *Elastico-mechanoluminescent response of Gwent ZnS:Cu material. (a) Whole response. (b-c) Close-ups taken from the beginning (b), around 200 s, and the end (c), around 5000 s, of the signal. (d-e) EML intensity of one S-R cycle (in black) accompanied by the displacement curve (in red) at around 200 s (d) and 5000 s (e) of the experiment.*

- In (b) we notice that the "R" peak from a previous cycle is very close to the "S" peak of the next cycle (marked with red arrows). What we see is a R-S pattern. This behaviour changes over time as demonstrated in (c): $\Delta t_1 = 0.15s$ while $\Delta t_2 = 0.25s$. The "S" peak is moving away from "R"; its position is shifting from the one it previously held.

Alternatively, we can represent the light intensity as a function of the displacement, cf. figure 4.2. (a) and (b) were drawn from data taken at 200 s and 5000 s of the EML signal and displacement. The S-R movement exhibits an "infinite ∞ " shape. The arrows in blue represent the first step of the deformation (stretching) and the yellow ones show the second step (releasing). When stretching begins, the light decreases until $x = 0.2$ (or 0.3) and then increases. The light describes the same behaviour during the releasing phase. We see that the S emission is wide whereas the R one is short. The maximum value of the R emission is recorded at 0, when the sample is back to its starting length at 0% deformation.

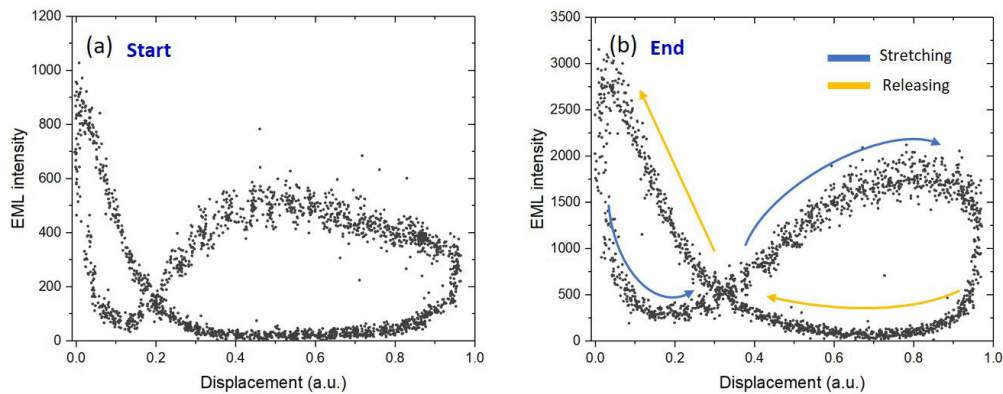


Figure 4.2: *Elastico-mechanoluminescence of Gwent ZnS:Cu as a function of the displacement drawn from data taken at 200 s (a) and 5000 s (b).*

One S-R cycle can be divided into three emission phases (cf. figure 4.3):

1. Emission during stretching,
2. Decrease and then absence of light during two thirds of the releasing,
3. Emission peak at the end of the releasing.

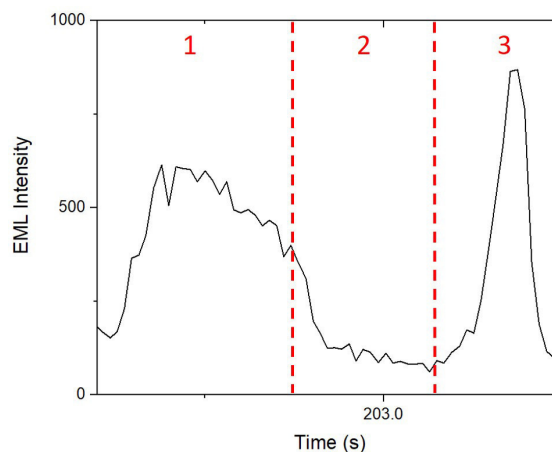


Figure 4.3: *Elastico-mechanoluminescence of Gwent ZnS:Cu over one S-R cycle. 1, 2, 3: emission phases.*

In this chapter we propose an EML model to describe these emission phases.

4.2 When the EML models are put to the test

Mainly two models were proposed to explain elasto-mechanoluminescence: the piezoelectrically-induced trap-depth reduction model proposed by *Chandra et al.*, and the triboelectricity-induced luminescence proposed by *Sohn et al.* We have detailed these models in the first chapter 1.3. Which one is consistent with our results? In this section, we further our investigation by first calculating the generated electric field during elastic deformations and compare it to required values of electric field to trigger luminescence. Then, we exhibit images taken by an optical microscope of the composite material during stretching. This work led toward triboelectricity being the most likely mechanism for EML.

4.2.1 Piezoelectrically-induced trap-depth reduction

Chandra et al. [36] proposed a model for elastically-mechanoluminescence for ZnS:Mn material based on piezoelectrically induced trap-depth reduction. The deformation of crystalline structures generates an internal electric field for which we need to give a few orders of magnitude. The trap-depth of charge carriers decreases with increasing piezoelectric field and after a threshold electric field, the trapped electrons get released. The recombination of these electrons with the hole centres results in the excitation of the luminescent centres.

The detrapping of charge carriers needs an external electric field of the order of 10^5 Vcm^{-1} [9, 51] and the impact ionization needs an internal electric field of the order of 10^6 Vcm^{-1} . Let us roughly estimate the piezoelectric fields (internal and external) generated by a composite material Gwent-PDMS when a 10 N force is applied; corresponding to the order of magnitude in our experiments. Force values were extracted from the experiments conducted using the camera-based setup where the applied force was measured continuously.

The piezoelectric constant d_{33} of ZnS:Mn crystals is $3.2 \times 10^{-12} \text{ CN}^{-1}$ [50], If $F = 10 \text{ N}$ and $A = 5 \text{ cm}^2$ (active area of the composite material = stretched section) then $P_{th} = 2 \times 10^4 \text{ Pa}$.

Therefore, the piezoelectric charge density ρ is:

$$\begin{aligned}\rho &= d_{33}P_{th} \\ \rho &= 3.2 \times 10^{-12} \times 2 \times 10^4 \text{ Cm}^{-2} \\ \rho &= 6.4 \times 10^{-8} \text{ Cm}^{-2}\end{aligned}$$

The external piezoelectric field E_{ext} is given by:

$$\begin{aligned}E_{ext} &= \frac{\rho}{\epsilon_0}, \\ E_{ext} &= \frac{6.4 \times 10^{-8}}{8.8 \times 10^{-12}} \\ E_{ext} &= 7.27 \times 10^3 \text{ Vm}^{-1} \\ E_{ext} &= 72.7 \text{ Vcm}^{-1}\end{aligned}$$

where ϵ_0 is the permittivity of free space equal to $8.85 \times 10^{-12} \text{ C}^2 \text{ N}^{-1} \text{ m}^{-2}$. The internal electric field E_{int} is:

$$\begin{aligned}E_{int} &= \frac{E_{ext}}{\epsilon_r} \\ E_{int} &= \frac{72.7}{8.8} \\ E_{int} &= 8.26 \text{ Vcm}^{-1}\end{aligned}$$

where ϵ_r is the relative permittivity of ZnS and is equal to 8.8

$E_{ext} = 72.7 \text{ Vcm}^{-1}$ and $E_{int} = 8.26 \text{ Vcm}^{-1}$ are five and six orders of magnitude, respectively, inferior to the required values to trigger detrapping and impact ionization. According to these results, the observed EML cannot be induced by piezoelectricity as the field generated is not high enough.

4.2.2 Triboelectricity-induced luminescence

This model was introduced by *Sohn et al.* [10]. It is based on the idea that triboelectricity causes EML. This phenomenon results from the soft friction at the interface between two different materials or the separation of these two materials after being in contact with one another. Each surface becomes electrically charged (positive or negative). It is compatible with the enhancement of EML with the presence of an aluminium oxide coating on ZnS:Cu particles because Al_2O_3 tends to create positive charges while PDMS tends to create negative charges (cf. figure 1.14).

The Gwent ZnS:Cu@PDMS composite material was observed under an optical microscope, the results are presented figure 4.4. In (a) we see microparticles embedded in the polymer, they are of various shapes and sizes. When the sample is stretched at 65% from its initial length, we notice that new shapes appear beside the particles and form what we have called "comets". Upon stretching, the matrix detaches itself from the particle and a vacuum pocket is formed. This phenomenon happens only when the sample is stretched as the PDMS is "glued" back to the particles when it is back to its original length. Each time the sample is extended the comets appear and then disappear when it is back to normal.

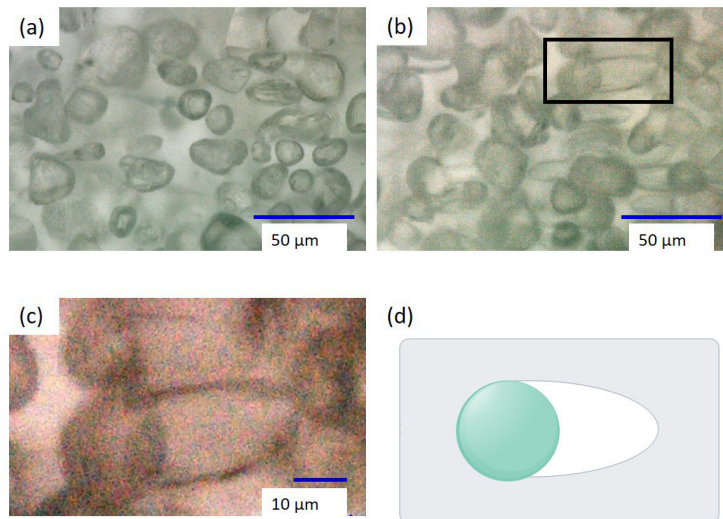


Figure 4.4: Images of the composite material under an optical microscope. (a) Sample at rest, (b) 65% stretching, (c) Close up on a single particle during a 65% deformation, (d) Schematic diagram of a single particle (in green) in a polymer matrix (in grey) at 65% stretching.

In 2019, *Park et al.* [123] published an article in which they offered a new self-powered luminescent textile system. The light emission is stimulated by random body motion and is due to triboelectrification. Woven fibers were fabricated with ZnS:Cu embedded in PDMS. They demonstrate that under deformation, the phosphor microparticle detaches itself from its matrix creating an internal and external triboelectric field during the contact and the separation, respectively.

This unstick-stick behaviour hints toward the triboelectricity theory as two different materials, namely the Al_2O_3 -coated ZnS:Cu microparticles and the PDMS, after contact with each other, become electrically charged in opposite signs. Consequently, visible light is generated.

In order to test experimentally the importance of the creation of comets, i.e. the unstick-stick behaviour, we performed an experiment which results can be found figure 4.5. It shows the average brightness recorded from the sample over 22 S-R cycles. The applied

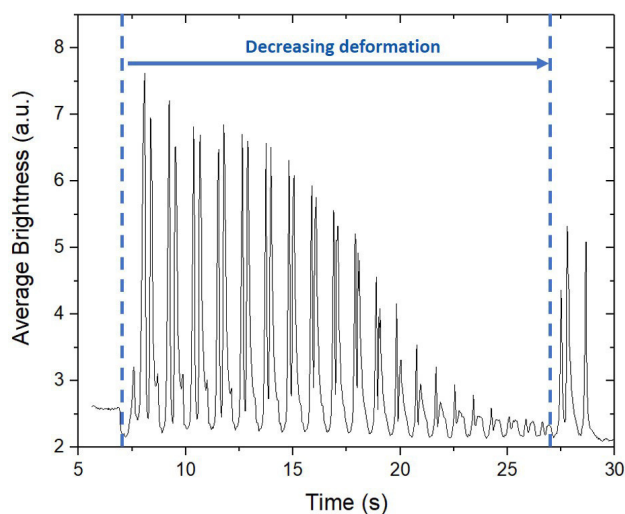


Figure 4.5: *Elastico-mechanoluminescent response of the Gwent ZnS:Cu material at variable applied deformation.*

deformation is not constant as, for each performed cycle, the deformation is reduced by 2.5%. The sample does not return to its starting point and is in a constant more or less stretched position. We observe a declining luminescence over time. Despite the presence of comets, the particles cannot stick back to the PDMS matrix and unstick at a new S-R cycle. Thus, it prevents the creation of charges in the composite material. The last peaks, visible around 27 s, are consequent to a full deformation with the sample returning to its "zero" position.

We can compile these data:

- Phase 1: Stretching
 1. The motorized arms start stretching the sample,
 2. At some point, "comets" start forming,
 3. The separation of the two materials (ZnS:Cu particles and PDMS) create electric charges on both surfaces (cf. figure 4.6),
 4. The sample starts emitting light,
 5. When the deformation is at 100% of its set value, the EML decreases and reaches its ground level,
- Phase 2: Releasing
 1. The sample relaxes gradually to reach its initial position,
 2. Meanwhile, no EML is recorded,
 3. When the sample is almost back to its starting point (deformation very close to 0%), a bright light is emitted as a consequence of the sudden disappearance of "comets",
 4. The EML intensity decreases rapidly and reaches its ground level,
- A new S-R cycle begins.

4.2.3 Proposed mechanism

Our observations and calculations tend to point at triboelectricity as responsible phenomenon of elasto-mechanoluminescence. We assumed that the separation of the PDMS from the particles generates electrical charges on both surfaces. We propose the following process for the trigger of EML using the schematic band diagram presented figure 1.10 during the two phase emissions (stretching, releasing):

- The polymer detaches itself from the particle forming a vacuum pocket. It generates electrical charges on both surfaces. Al_2O_3 tends to accumulate positive charges whereas the PDMS tends to accumulate negative charges (as represented on the triboelectricity scale figure 1.14 chapter 1) (1),
- Because of the energy barrier formed by the vacuum pocket, the electrons stay trapped in the PDMS,
- The hot charge carriers (holes) can create an electron-hole pair, or exciton (2), when relaxing through Auger processes,
- The energy is transferred to the Cu^{2+} ions and results in a green light emission characteristic of the Cu^{2+} ions (3),
- When the sample is released, the energy barrier disappears. Hot electrons can create excitons as well, or recombine with the holes still present in the microparticle (4),
- The energy is transferred to Cu^{2+} ions and results in the emission of a green light characteristic of the ions (5).

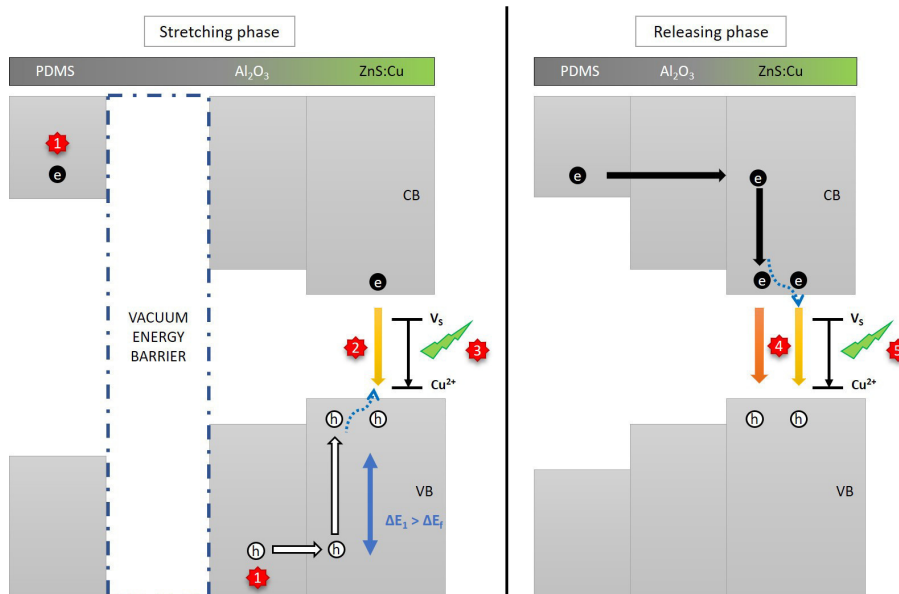


Figure 4.6: Band diagrams of the Gwent $\text{ZnS:Cu@Al}_2\text{O}_3$ - PDMS sample for the stretching (left) and releasing phases (right). VB: Valence Band. CB: Conduction Band.

4.2.4 Alternative explication

The previous mechanism is based on the fact that two processes (Auger and charges recombination) are responsible for the light emission: one during the stretching (Auger) and the other during the releasing. However, we can consider the semi-alternative possibility: When the sample is stretched it causes local restickings, i.e. if a surface S of the particle is freed from the polymer after a deformation d , then a restoring force could cause resticking of the said polymer on a smaller surface s of the particle. The emission during the stretching phase would result from the sum of many restickings. If this is the case, then only one process is responsible for the light emissions (stretching and releasing) which is electron-hole recombination only.

4.2.5 Conclusion

To explain EML, the piezoelectric model was discarded due the weak electric field generated during the deformation of the sample. We have established that the elasto-mechanoluminescence of a composite material made of ZnS:Cu phosphor and PDMS increases over time under constant mechanical deformation, here being stretching and releasing. The luminescence consists of two emission peaks: the first one is emitted during the stretching phase and the second one during the releasing phase. When a sample is elongated and observed under an optical microscope, "comet"-shaped forms are visible. These "comets" are in fact vacuum pockets formed between the particle and the polymer. When the sample is released these "comets" disappear but reappear when stretched again.

When the composite material is stretched, the PDMS detaches itself locally from the ZnS:Cu particles. Because ZnS:Cu and PDMS are two dissimilar materials, electric charges are created on the surfaces of both materials by triboelectric effect. Through the Auger process, a first emission of light is recorded. This emission corresponds to the peak of the stretching phase. When the sample is released, the polymer sticks back to the particle. The remaining charge carriers, through Auger and electron-hole recombination, cause the second light emission: the peak of the releasing phase. However, one can consider that only electron-hole recombination is responsible for both emissions. It would mean that the first emission (stretching) comprises multiple emissions resulting from local restickings of the polymer to the particles because of the presence of a restoring force.

4.3 Computer simulation of EML

We have suggested that the EML phenomenon is based on triboelectricity after highlighting the "comets" formed between the polymer and the ZnS:Cu particles during stretching. Thanks to that, we have been able to propose a mechanism explaining the two observed emission peaks. In order to simulate the shapes of these peaks with respect to the displacement, we introduce a threshold deformation which constitutes the minimum value required to trigger the luminescence and at which the polymer detaches itself from the particle. The rationalization of EML is possible thanks to this parameter and it is used for the computer simulation. It is then possible to model the EML behaviour of one particle and generalise it to fit the behaviour of several particles.

4.3.1 Threshold force

Figure 4.7 shows the EML intensity of the Gwent material during one S-R cycle with the according displacement curve (in red). During the first deformation phase (the stretching), we notice that the sample does not emit light immediately when the red curve

goes up. The same behaviour happens during the second deformation phase (the releasing) when the displacement curve goes down. Instead, the luminescence starts after a specific deformation value. We refer to this value as the *threshold deformation* D_{th} which can be regarded as the equivalent of a *threshold force* F_{th} . During the stretching, the light emission begun at a low deformation value (around 20% of the total stretching) and then stops when the deformation is maximum. As for the R emission it occurs after 75% of the total releasing.

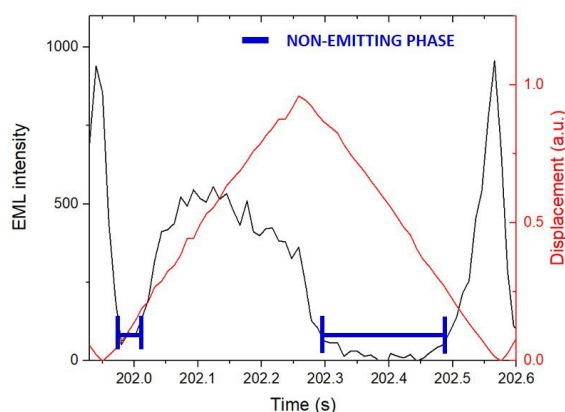


Figure 4.7: *EML intensity of Gwent ZnS:Cu of one S-R cycle (in black) accompanied by the displacement curve (in red) at around 200 s of the experiment.*

D_{th} depends on the interaction between the particle and the PDMS. If the polymer sticks heavily to the particle, a high deformation D_{th}^H (or F_{th}^H) is required to trigger luminescence. But, if the polymer unsticks easily from the particle, light will be emitted at a lower deformation D_{th}^L (or F_{th}^L). In the case of the Gwent material, the emission is triggered for a low deformation threshold.

4.3.2 Working principle of the computer simulation

When the sample is stretched, we need a deformation to induce EML. This deformation needs to be high enough to allow the PDMS to unstick from the particles. After which, it sticks back to them at a very low deformation close to zero. Our model is based on the asymmetry of this deformation.

Considering a spherical particle, the polymer unsticks from the particle at a threshold deformation D_{th} (or F_{th}^H) creating a vacuum pocket (or "comet") between the two materials forming an angle θ . This pocket widens as the deformation (or force) force keeps increasing and so does θ (figure 4.8). The amount of light emitted at an instant i depends on the free area of the particle at i and $i - 1$.

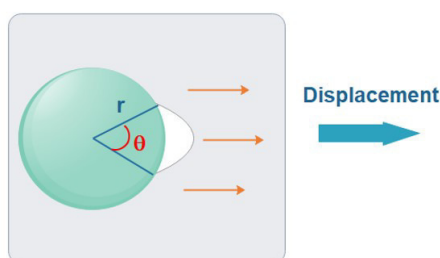


Figure 4.8: *Schematic of a creation of a vacuum pocket after a threshold force (or deformation).*

It means that:

$$\begin{aligned} emittedlight(i) &\propto Area(i) - Area(i - 1) \\ \text{with } Area(i) &= 2\pi r^2(1 - \cos\theta) \\ Area(i) &= 2\pi r^2\left(1 - \frac{D_{th}}{D(i)}\right) \end{aligned}$$

where,

$$\begin{aligned} D(i) &= strain(i) \cdot Section \cdot E_y, \\ \text{with } strain(i) &= i \cdot freq \cdot MaxElong \end{aligned}$$

and,

$$D_{th} = D(i) \cdot MaxElong \cdot Section \cdot E_y$$

We consider that the experiment is conducted at a 1 Hz frequency. $D(i)$ is the applied deformation at instant i . The maximum elongation is set at 60%. E_y represents Young's modulus in Pa and the calculations are applied for a section of about 1cm x 1mm.

It is possible to recreate the behaviour of the first peak (stretching) by changing D_{th} . D_{th} is a free parameter and its effect is illustrated figure 4.9 for three different values of D_{th} : (a)-low, (b)-medium and (c) high. The S emission occurs at different stretching values: for D_{th}^L (a) the emission is quick to happen, on the contrary, when D_{th}^H (c) the emission is delayed. These results match our experimental results and interpretation.

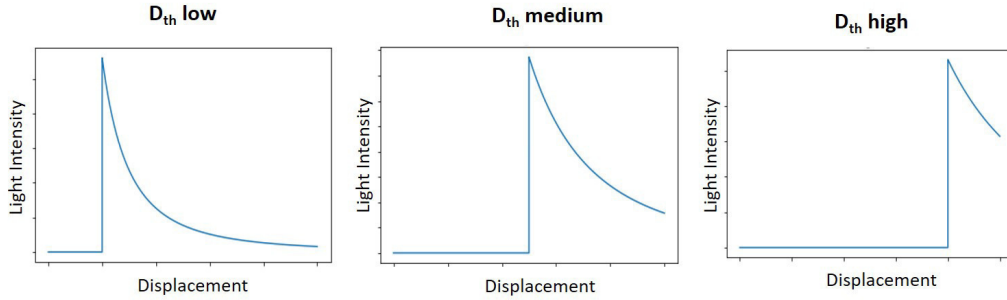


Figure 4.9: *Stretching emission for different values of D_{th} . Simulated data.*

Our composite material is made of millions on microparticles. There are ≈ 10.000 per mm^2 , and the PDMS detaches itself from each one at a different D_{th} . We also have a shape dispersion, thus, we consider a distribution of D_{th} represented by a Gaussian curve as shown figure 4.10. This distribution depends on the bond strength between the particles and the polymer. In the program, the values of the mean value of the threshold deformation $Mean_{D_{th}}$ and the standard deviation $\sigma_{D_{th}}$ can be set for the two phases of a cycle, namely the stretching and the releasing.

Finally, to complete the model, we need to introduce an additional parameter: When the stretching stops, the S emission decreases. As shown in figure 4.16, the decrease is the same for the two curves as they are perfectly superimposed on one another in this area. Several parameters could be responsible for this decay. One of them is the lifetime of ZnS:Cu which was measured and is presented figure 4.12. It shows decay curves of said phosphor at two excitation wavelengths (470 nm and 517 nm). The lifetime is one order of magnitude shorter than the duration of the decrease noticed in the S emission and cannot explain it.

Another parameter could be the **characteristic time of unsticking** τ corresponding to the time response of the polymer to a deformation. It induces a delay between

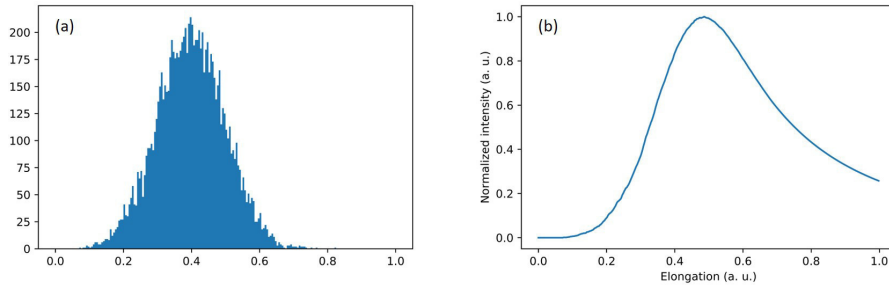


Figure 4.10: (a) Histogram of the distribution of the deformation threshold D_{th} for 10,000 particles. (b) EML signal during the unsticking. Simulated data.

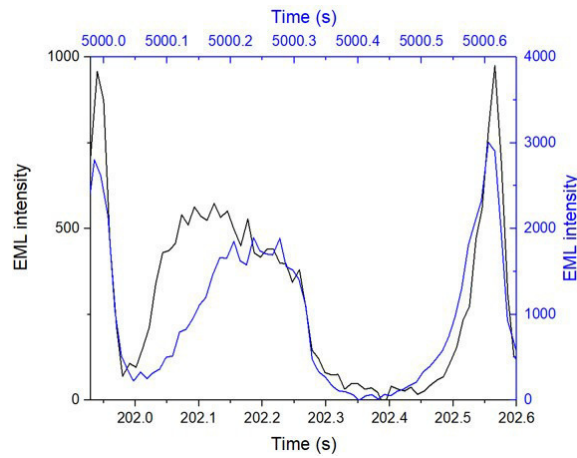


Figure 4.11: Comparison of the elasto-mechanoluminescent response of Gwent ZnS:Cu material through one stretching-releasing cycle taken from the beginning (in black) and the end (in blue) of the experiment.

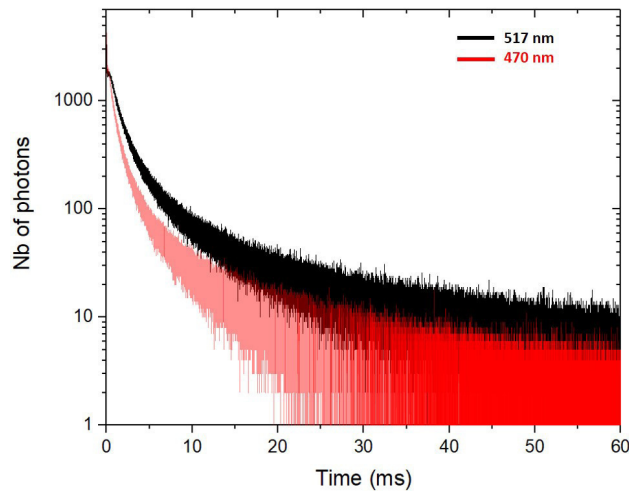


Figure 4.12: Decay curves of the Gwent ZnS:Cu@PDMS sample. Excitation at 470 nm (in red) and 517 nm (in black).

the moment a deformation $D > D_{th}$ (or a force $F > F_{th}$) is applied and the moment the polymer actually detaches itself from the microparticle. This means that if $D > D_{th}$ is applied at i_1 , the polymer detaches itself at i_2 with $i_2 - i_1 = \tau$. This time was estimated at

$\tau = 40$ ms and was necessary for the simulation as it allowed a significantly better fitting of the experimental data.

With this program we can mimic the EML intensity as a function of the displacement of Gwent, as seen in figure 4.13, and extract the values of $MeanD_{th}$ for this material:

- For the stretching: $MeanD_{th} = 0.6$ and $\sigma_{D_{th}} = 0.21$
- For the releasing: $MeanD_{th} = 0.03$ and $\sigma_{D_{th}} = 0.07$

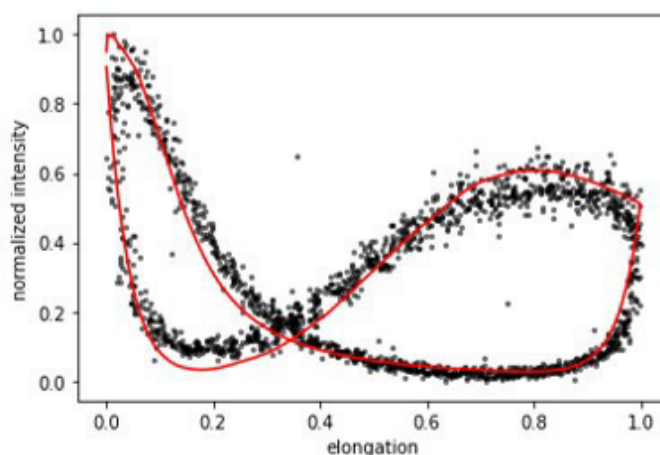


Figure 4.13: *EML intensity as a function of the displacement for Gwent ZnS:Cu: experimental results in black dots, computer simulation results in red.*

The Gwent ZnS:Cu exhibits luminescence at a low deformation threshold which means that the polymer can unstick easily from the particle when it is stretched. **These simulations tend to demonstrate that the strategy is to consider different effects that act on D_{th} : namely, the polymer and surface treatments.**

4.4 Evolution of the EML signal

The EML of Gwent ZnS:Cu changes over time. The emitted light increases over time and we have noticed that the S and R emissions shift as the number of cycles increases.

We have linked the emission of light to the presence of "comets" formed during stretching. The number of these "comets" play an important role in the intensity of EML. Moreover, the repeated deformation causes premature ageing and deterioration of the polymer. Consequently, the emission peaks' see their shapes change slightly over time. This phenomenon is known as the Mullins effect and is explained in this section.

4.4.1 Evolution of the EML intensity

Elastico-mechanoluminescence is triggered thanks to the formation of "comets", but how are they linked to the increase of the EML signal over time?

We have observed a Gwent ZnS:Cu-PDMS sample at different times during and S-R experiment: before starting the experiment, after 30 minutes and after 75 minutes. Each time, the sample is held at 65% deformation and placed under an optical microscope. The results are shown figure 4.14. Despite being extended, the sample does not show any "comet-like" forms before the experiment begins. This indicates that the PDMS matrix strongly adheres to the microparticles. As the experiment runs, they start appearing. After 30 min, (b) shows a 12% "comets" whereas (c) exhibits 45% after running the experiment

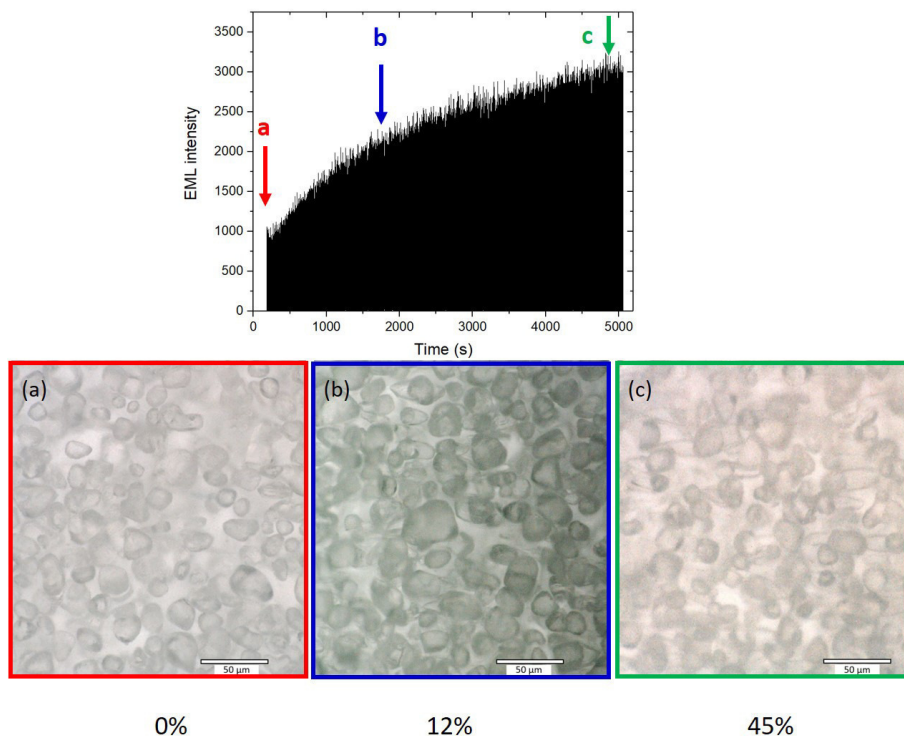


Figure 4.14: *Top: Elastico-mechanoluminescent response of the Gwent ZnS:Cu material. Bottom: (a-c) optical microscope images of the composite material taken at different times of the experiment: beginning (0s), middle (1500s) and end (4500s), respectively.*

for 75 min. The increase of the number of "comets" coincides with the increase of the EML intensity.

At the beginning, few "comets" are created, and the light intensity is weak. In addition to the self-recovery process, the number of "comets" increases and results in the increase of the EML intensity. The inhomogeneity of the particle sizes and shapes can be responsible for this. Although the applied deformation is constant, the particles do not respond the same way and luminescence is triggered for different D_{th} .

By considering that the number of particles is finite in a sample and that a comet is formed beside each particle, we can assume that the EML intensity should reach a plateau after a certain time. We have conducted the same experiment on this material for 17 hours. However, the light intensity kept on increasing. It seems that this system requires longer durations for the EML to stabilize.

4.4.2 Impact of polymer ageing

Elastic deformation modifies the mechanical properties of polymers. In the case of EML, it induces visible changes in the emission. The EML signal being composed of two distinctive peaks it is possible to monitor their shapes and positions over time.

4.4.2.1 Evolution of the S and R emissions

Figure 4.15 compares the EML response over time, (a-c) taken after 200 s of the experiment (beginning) and (b-d) after 5000 s (the end).

In (a) we notice that the S peak is close to the R emission of the previous deformation cycle. This behaviour changes over time as demonstrated in (b). The S peak

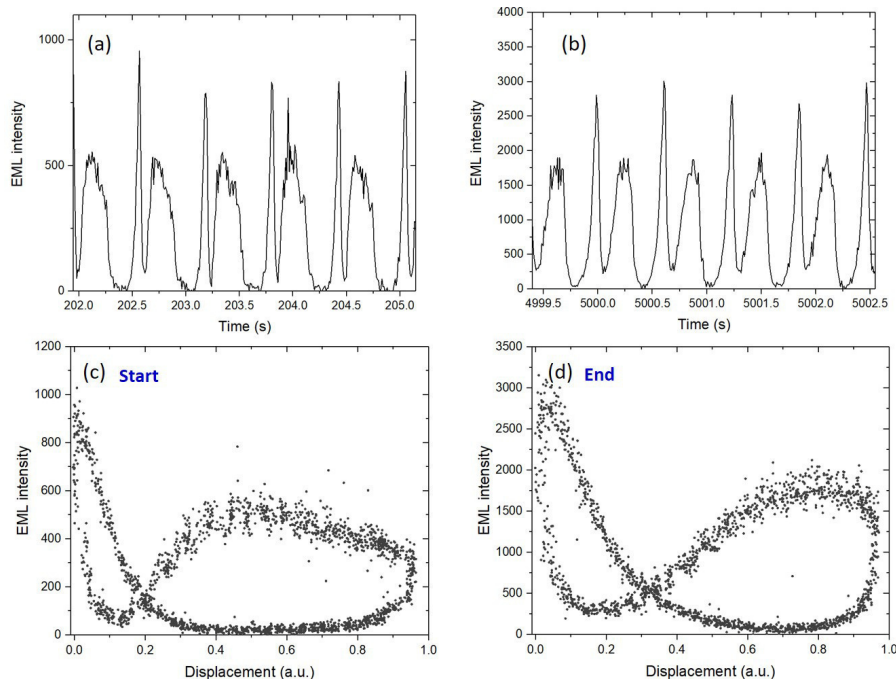


Figure 4.15: *Elastico-mechanoluminescence of Gwent ZnS:Cu at 200 s and 5000 s of the stretching-releasing experiment, (a) and (b) respectively. EML intensity as a function of the displacement at 200 s (c) and 5000 s (d) of the experiment.*

is moving away from R; its position is shifting from the one it previously held. This results from the softening of the polymer due to repeated S-R cycling.

Figure 4.16 shows one S-R cycle from the beginning (in black) and the end (in blue) of the EML response overlaid on one another. Although the emission during the S phase stops similarly, the band is larger at the beginning. The deterioration of the sample alters the elastic properties of the matrix. D_{th} shifts toward higher values over repeated elastic deformation and the emission is less extended in time. Also, the maximum of the releasing peak occurs when the sample is back to its starting point at 0% deformation. As the experiment proceeds, the deformation required to trigger luminescence becomes more important.

4.4.2.2 Mullins Effect

Mullins effect (named after *Leonard Mullins* in 1947), also known as **stress-softening**, is the decay of elastic stiffness. It describes the behaviour of filled and non-filled rubber-like materials upon loading, unloading and reloading. They exhibit a change in their mechanical properties resulting from the first extension. Although studied for a long time and physical interpretations abound on this phenomenon, none benefits from a full agreement. The models include several phenomena such as bond ruptures, molecules slipping, filler clusters rupture, chain disentanglement, chain retraction, network rearrangement, and composite microstructure formation [124].

Figure 4.17 shows the ideal Mullins effect of rubber under tension. It shows the mechanical changes suffered by the polymer during deformation. Upon the very first loading, path *A* is followed then path *B* toward the state 0 when the unloading occurs at 1. If the rubber is reloaded, the behaviour will follow path *B* and then path *D* if the tension goes beyond point 1. When unloading occurs at 2, the material retracts along path *C* and if the sample is reloaded again, the stress-strain behaviour follows path *C* [27]. Most of

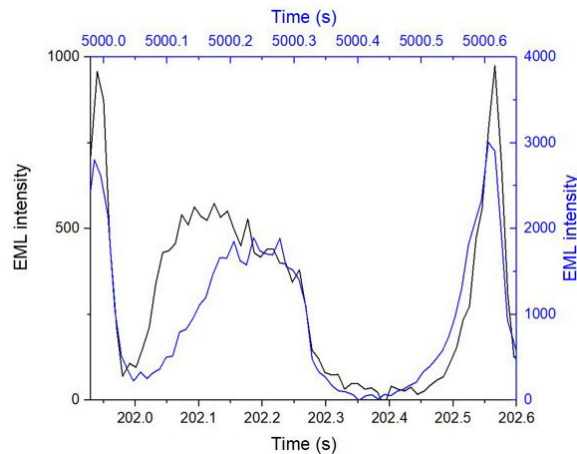


Figure 4.16: Comparison of the elasto-mechanoluminescent response of the Gwent ZnS:Cu material through one stretching-releasing cycle taken from the beginning (in black) and the end (in blue) of the same experiment.

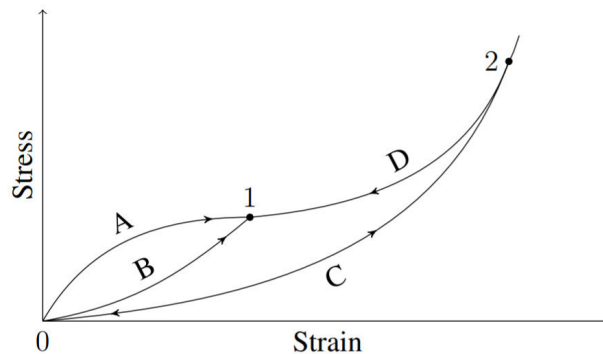


Figure 4.17: The idealised behaviour of stress-softening in rubber. From [27]

the softening, which is characterized by a lower resulting stress for the same applied strain, appears after the first load.

4.4.3 Conclusion

The EML signal comprises three emission areas: The first one intervenes during the stretching phase. The emission occurs after a threshold deformation which shifts toward higher values as the deformation continues. This shift is due to the Mullins effect where the mechanical properties of the polymer are modified because of the repeated S-R cycling.

The second one occurs as the releasing phase begins. The S emission decreases during 100 ms before the R emission starts. The lifetime of ZnS cannot be the only one responsible for this decrease as it is too small (10 ms). After deformation, a response time elapses, called a characteristic time of unsticking, for which the polymer unsticks from the particle after a deformation D . However, these two elements might not be sufficient to explain the light decrease in this area.

The third emission area comprises the R peak. This emission is shorter than the S one but widens over time. Its maximum value is recorded at 0% deformation. It coincides with the sample recovering its original length when the polymer sticks back to the particles.

The overall light intensity of the Gwent ZnS:Cu-PDMS material increases as the

number of S-R cycles increases as well. This increase is related to the growing number of "comets" formed during the S-R cycles.

4.5 Influence of surface modifications

The ZnS:Cu@PDMS is a complex system and the EML is influenced by the nature of two components, the phosphor and the polymer. The interaction between the particles and the polymer greatly affects the threshold deformation D_{th} for which the EML occurs. This interaction can be controlled as to have low or high D_{th} by modifying the surface of the particles themselves. The strategy is to demonstrate its impact on the EML.

We focused the demonstration on two coatings: silicon dioxide (SiO_2) and teflon TF on the elastico-mechanoluminescence of Gwent-PDMS composite material.

4.5.1 Silicon Dioxide coating SiO_2

We find silica coatings on nanoparticles used as protective layers or to enhance their stability. This coating should modify the EML signal because we change the bond between the polymer and the particles. Moreover, it was chosen for our study because, like Al_2O_3 , it tends to create positive charges as shown on the triboelectricity scale (cf. figure 1.14) and should, therefore, enhance the luminescence. However, it is not as we observed.

The Gwent ZnS:Cu particles are already coated with Al_2O_3 , but an additional layer of SiO_2 was deposited on them. Through repeated S-R cycling we obtain figure 4.18. The EML intensity of the Gwent@ SiO_2 sample is represented in (a) over 3 hours. The brightness increases slightly until 1000 s and then remains constant. We notice that the intensity is very low compared to Gwent figure (20 times lower after 1 hour). The SiO_2 extinguished the luminescence of Gwent phosphor. It is possible that the effect of SiO_2 was altered because the particles were already coated with aluminium oxide.

The S and R peaks are shown in (b) and (c) and are not packed with one another and become more symmetrical over time.

Figure 4.19 represent the EML intensity as a function of the displacement. They show the superposition of several S-R cycles taken around 80 s and 10500 s of the experiment, (a) and (b) respectively. The curve is flattened at the start of each phase in (a). However, it becomes "rounder" toward the end in (b), the emission is more uniform.

It is possible to mimic the behaviour of this material using computer simulation. Figure 4.20 shows a fit of the results obtained through simulation (in red) and those obtained experimentally (black dots). Therefore, we can extract the mean value of the threshold force for the light to be emitted using the program:

- For the stretching: $MeanD_{th} = 0.65$ and $\sigma_{D_{th}} = 0.25$
- For the releasing: $MeanD_{th} = 0.05$ and $\sigma_{D_{th}} = 0.125$

When compared to Gwent:

$$MeanD_{th}^{Gwent@SiO_2} > MeanD_{th}^{Gwent} \text{ for the stretching}$$

$$MeanD_{th}^{Gwent@SiO_2} > MeanD_{th}^{Gwent} \text{ for the releasing.}$$

$$D_{th}^{Gwent@SiO_2} > D_{th}^{Gwent}$$

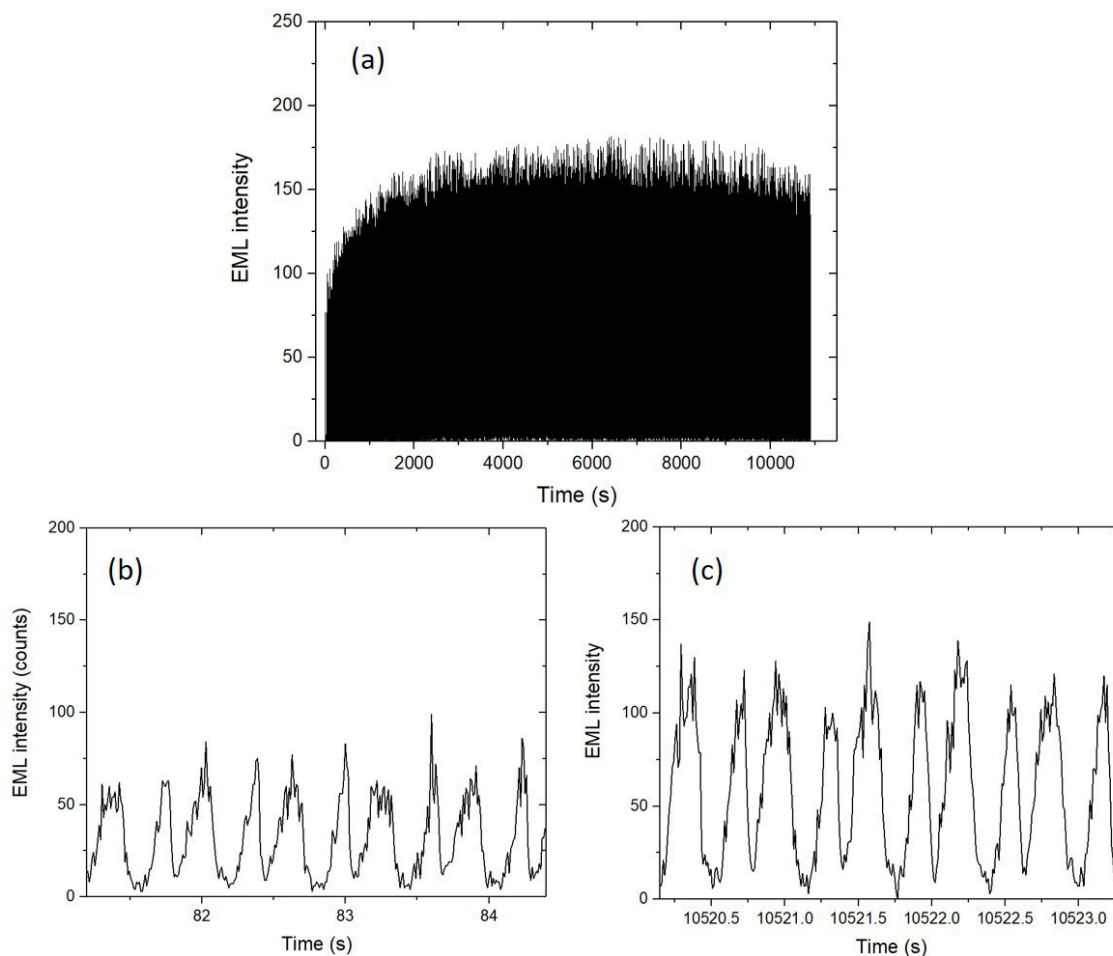


Figure 4.18: *Elastico-mechanoluminescence response of the Gwent@SiO₂ sample using the PMT-based setup. (a) whole response as a function of time. Close ups at the beginning (b) and at the end (c) of the signal, respectively.*

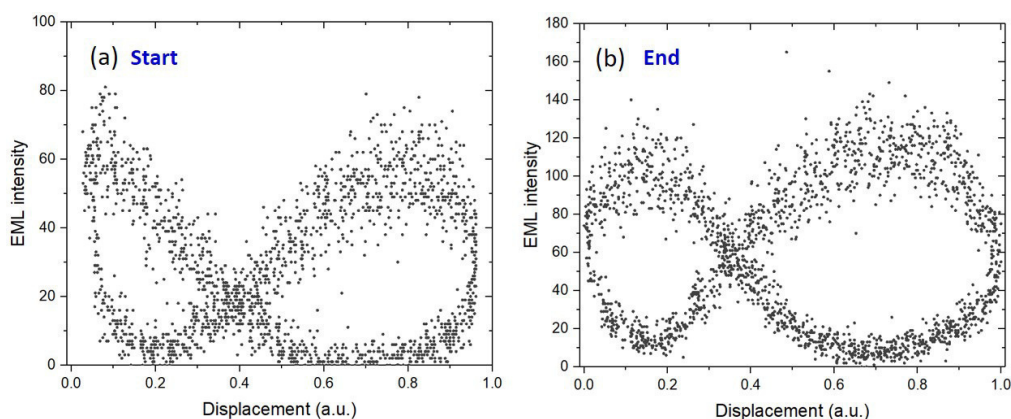


Figure 4.19: *Elastico-mechanoluminescence response of the Gwent@SiO₂ sample using the PMT-based setup as a function of the displacement. Plots of the beginning (a) and the end (b) of the signal.*

4.5.2 Teflon coating

Teflon (TF) coating is known for transforming surfaces into superhydrophobic ones. By coating with TF we intend to suppress the wetting ability of the particles.

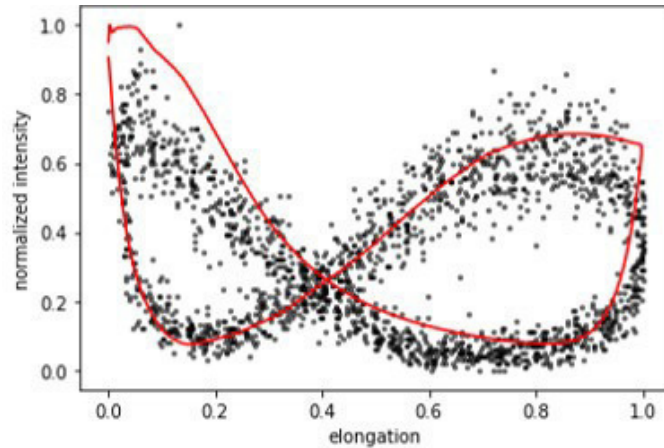


Figure 4.20: *Light intensity as a function of the displacement of Gwent@SiO₂: experimental result in black dots, computer simulation result in red.*

Therefore, the bond strength between the PDMS and ZnS:Cu should be weak. It should result in an enhanced EML.

A Gwent ZnS:Cu@TF was experimentally tested and the results are presented figure 4.21.

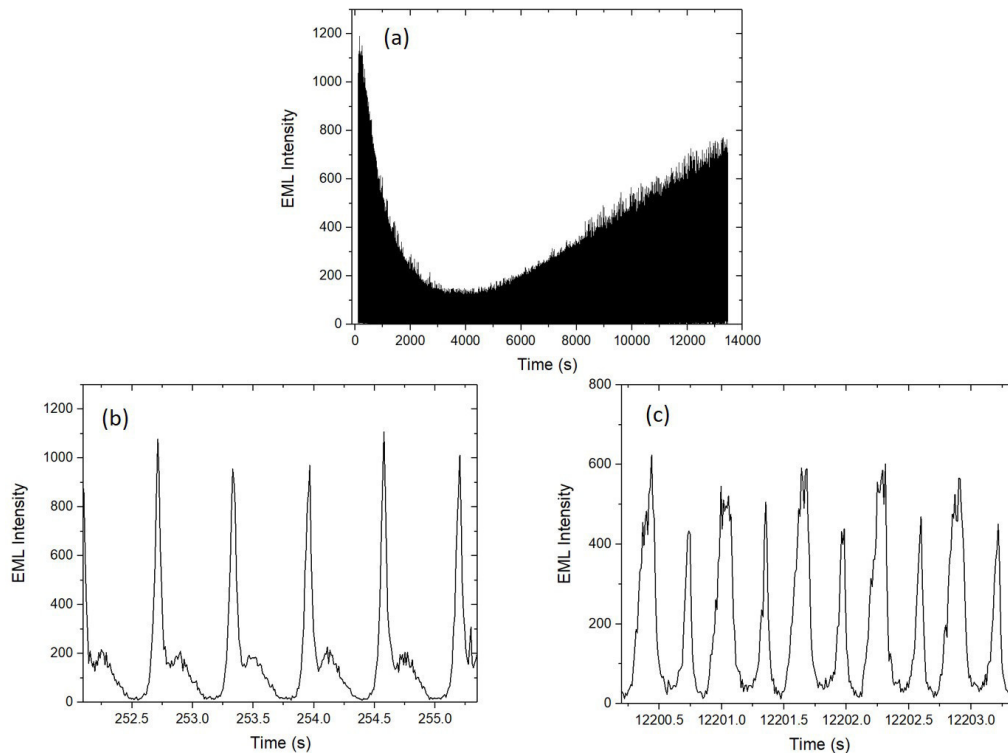


Figure 4.21: *Elastico-mechanoluminescence response of the Gwent@teflon sample using the PMT-based setup. (a) whole response as a function of time. Close ups from the beginning (b) and the end (c) of the signal.*

The teflon coated ZnS:Cu material exhibits bright and intense luminescence during the first cycles of the experiment. Yet, the EML diminishes quickly and reaches a minimum value from 3000 s to 5000 s before going up again linearly. By the end of the experiment, the luminescence has still not reached the value recorded at the beginning.

Surprisingly, that emission is primarily composed of the light emitted during the releasing phase. (b) shows that the emission during the stretching phase is really weak. That band is closely attached to the previous R peak. As the number of S-R cycles increases, the input of that band increases as well until it becomes as intense as the R peak, or even more intense (cf. (c)).

Figure 4.22 corroborates the aforementioned observations. It shows the EML intensity as a function of the displacement. (a) shows an intense R peaks compared to the S ones. The maximum of the S emission occurs shortly after the beginning of a new S-R cycle. Its light then decreases. However, (b) shows that the S emissions is as intense as the R ones. During the first deformation phase, the curve goes up linearly, attains a maximum value and drops as the second deformation phase begins. The shift in the position of the maximum of emission shows that the value of the deformation threshold increased due to the Mullins effect.

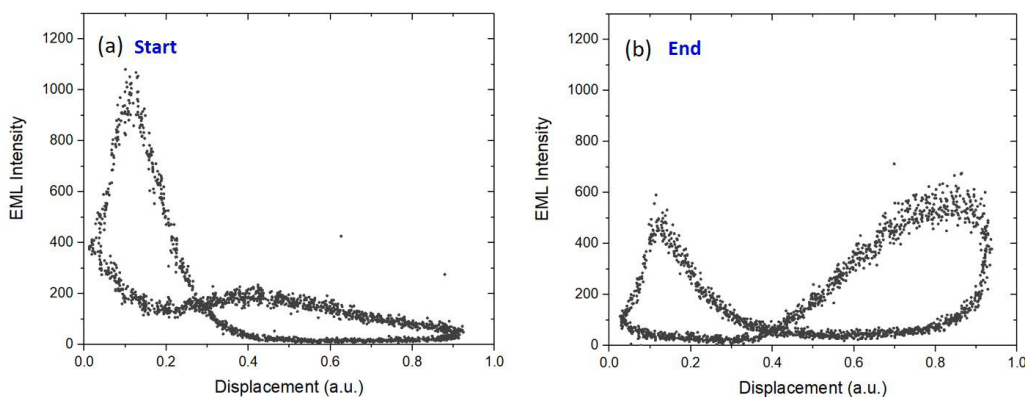


Figure 4.22: *Elastico-mechanoluminescence response of the Gwent ZnS:Cu@teflon (TF) sample using the PMT-based setup as a function of the displacement. Plots from the beginning (a) and the end (b) of the experiment.*

The TF should weaken the bond between the particles and their matrix and facilitate the outbreak of "comets", and therefore, result in a low D_{th} . Our model can be applied in the case of Gwent@TF and it results in figure 4.23. The experimental results (in black dots) and the simulated data (in red) are overlaid on one another. Therefore, we can extract the mean value of the threshold deformation for the light to be emitted using the program:

- For the stretching $MeanD_{th} = 0.2$ and $\sigma_{D_{th}} = 0.25$
- For the releasing $MeanD_{th} = 0.1$ and $\sigma_{D_{th}} = 0.04$

$MeanD_{th}$ of Gwent@TF during stretching is very low which is consistent with our experimental results and coherent with our approach for the use of teflon. It lowered the deformation threshold, but did not enhance the luminescence.

4.5.3 Conclusion

Gwent ZnS:Cu particles coated with SiO₂ embedded in PDMS showed weaker luminescence than uncoated Gwent particles during an S-R experiment. The S and R emissions remained almost the same throughout the entire experiment (intensity, shape). The teflon coating influenced also the elastico-mechanoluminescence. Instead of increasing the light intensity, as expected, the brightness started by decreasing (step 1) for one hour before rising again (step 2). During the first step, the S emission was almost extinguished and only the R emission remained. During the second step, the S emission increased and

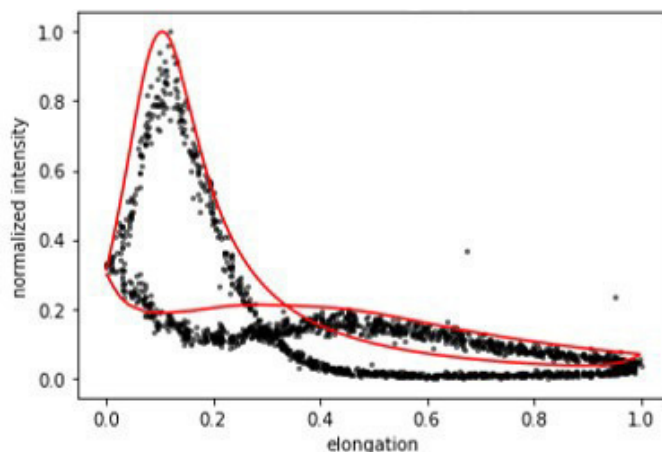


Figure 4.23: *Light intensity as a function of the displacement of Gwent@teflon: experimental result in black dots, computer simulation result in red.*

became as intense as the R one. The Gwent particles have already an Al_2O_3 coating which might inhibit the action of any additional coating.

Thanks to computer simulations, it was possible to mirror the experimental results obtained with Gwent@ SiO_2 and Gwent@TF. Moreover, values of $MeanD_{th}$ were extracted and are presented table 4.1

$$MeanD_{th}^{Gwent@SiO_2} > MeanD_{th}^{Gwent} > MeanD_{th}^{Gwent@TF}$$

Gwent@ SiO_2		Gwent		Gwent@TF	
S	R	S	R	S	R
0.65	0.05	0.6	0.03	0.28	0.1

Table 4.1: *Values of $MeanD_{th}$ obtained from computer simulations for Gwent ZnS:Cu, Gwent@ SiO_2 and Gwent@TF. S: stretching, R: releasing.*

The values of D_{th} given by our model were all obtained using the same $\tau = 40$ ms, the characteristic time of unsticking. This parameter could be linked to the polymer itself.

4.6 Influence of the Matrix on EML

We have shown the way to obtain an efficient and bright EML composite material and proposed a model based on our observations as well. In this section, we focus on the polymer and its influence on the EML. Over the course of this thesis, we have modified the surface of our phosphor particles by chemical treatments to change the bond strength between the polymer and the particles. Another way to accomplish that is to change the polymer matrix. Therefore, we have changed the PDMS in which the ZnS:Cu particles are incorporated.

The results that were presented so far were obtained using an RTV bi-component PDMS using a "fast catalyst" (FC). However, the same PDMS exists also with a "slow catalyst" (SC) that modifies the behavior of the whole luminescent composite. The FC allows the curing reaction to be done fast. The chemical composition of the catalysts was not found from the providers. However, the technical sheet of tin catalysts from SONG-WON provided useful information. For a moderate to rapid cure catalyst, dimethyltin

di-neodecanoate $C_{22}H_{44}O_4Sn$ is used. For a slow cure, we find the following catalysts:

- Dibutyltin dilaurate (rigid, flexible PVC) $C_{32}H_{64}O_4Sn$
- Dioctyltin dilaurate $C_{40}H_{80}O_4Sn$
- Dioctyltin di-neodecanoate $C_{36}H_{72}O_4Sn$

We see that the chemical formula changes whether we use a slow or a fast catalyst. Using different PDMSs can influence the light emission as the mechanical properties of the composite material change. To test this assessment, new samples were made:

- Wacker Elastosil RT A/B PDMS + Gwent particles,
- Esprit Composite RTV PDMS with a slow catalyst + Gwent particles.

The Wacker Elastosil is also a bi-component PDMS using a platinum catalyst. Its curing depends on the temperature as the higher the temperature is the faster the cure.

Changing the PDMS does not influence the photoluminescence properties of the composite material. These samples were mechanically tested using the stretching-releasing device which comprises a photomultiplier, an optical fibre and an optical density coupled to a laser to track the movement of the sample. The functioning of this setup was detailed in chapter 2. In addition to that, the samples with RTV-slow catalyst as matrix were also tested with the camera-based setup which is also detailed in chapter 2.

The experimental conditions and the EML results are presented in this section for each sample and setup.

4.6.1 RTV slow catalyst

The Gwent/RTV-SC sample was experimentally tested with two S-R devices: the camera-based one and the photomultiplier (PMT) one. The first setup applied a symmetric elongation on the sample on both sides and the detection is performed through a camera. Whereas with the second one, the deformation is applied only on one side of the sample and the detection is performed using an optical fiber connected to a PMT.

4.6.1.1 Camera-based setup

Figure 4.24 shows the results of the Gwent/RTV-SC with the camera-based setup. The experimental parameters used for this experiment are:

- Velocity: 4 cm.s^{-1}
- Displacement: 64%

In (a) we see that the average brightness decreases rapidly and almost drops to 0 after 2 minutes. As the displacement is set to be constant, the applied force also decreases over time. On average, at the end of an experiment, the samples are 1.1 cm longer.

(b) and (c) represent close-ups of (a) at two different times: at the beginning of the experiment (5 s) and at the end (111 s), respectively. In both graphs, we clearly distinguish a repeated pattern composed of two peaks. They represent the luminescent response of the sample during the stretching phase S (wide peak) and releasing phase R (sharp and intense peak).

The S emission is also characterized by two small peaks. It is noteworthy to add that the S emission shifts as it is no longer as close to the R peak as it was in (b), whereas the R peak remains the same. This finds an explanation in the Mullins effect. The D_{th}

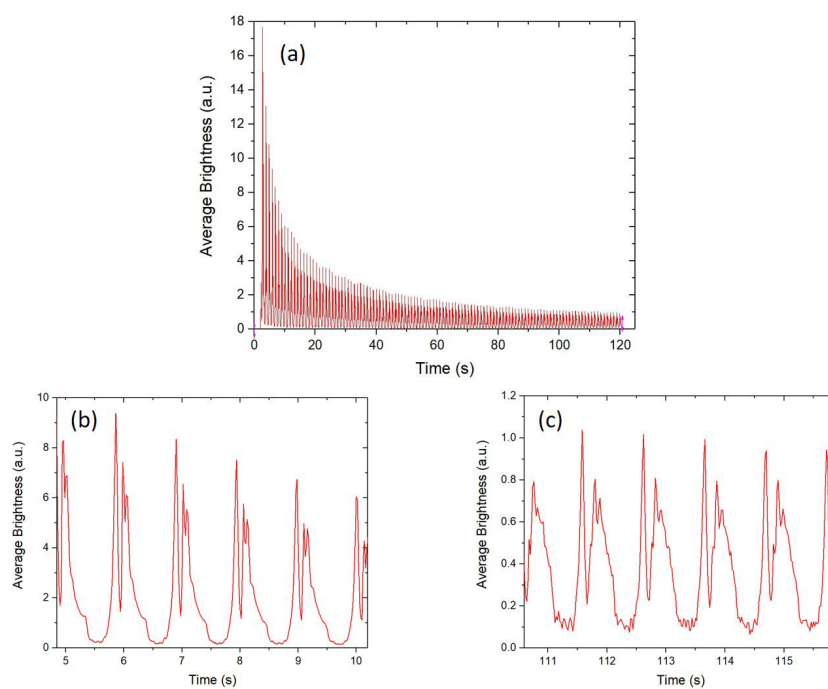


Figure 4.24: *Elastico-mechanoluminescence response of the Gwent/RTV-SC sample using the camera-based setup. (a) whole response. (b-c) close ups at the beginning (b) and at the end (c) of the signal.*

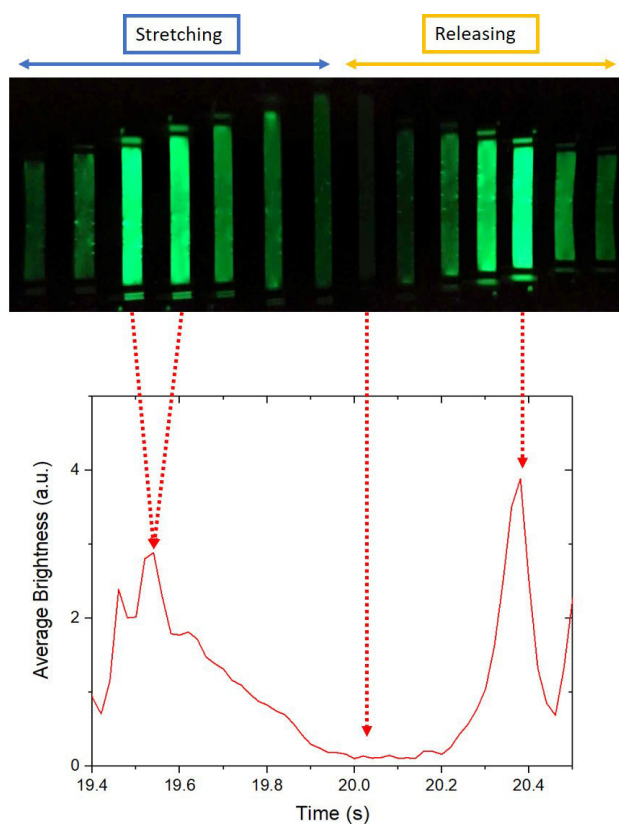


Figure 4.25: *Successive images of Gwent ZnS:Cu/PDMS-SC extracted from a film during an EML experiment (top). Average brightness as a function of time, one S-R cycle (bottom).*

changed toward higher values because the sample needs a higher deformation in order emit light.

The camera records a film from which the successive images of figure 4.25 were extracted. The S and R peaks can be identified on these images. The maximum intensity exhibited by the sample occurs for a low D_{th} during the S phase. The R emission takes place at the end of the S-R cycle.

4.6.1.2 Photomultiplier setup

Figure 4.26 shows the EML response of a Gwent/RTV-SC sample over one hour. Here, the emitted light is detected thanks to an optical fiber connected to a photomultiplier (PMT). The experiment was conducted using the following parameters:

- Acceleration: 4.000 cm.s^{-2}
- Velocity: 4 cm.s^{-1}
- Displacement: 62.5%
- Integration time PMT: 10 ms

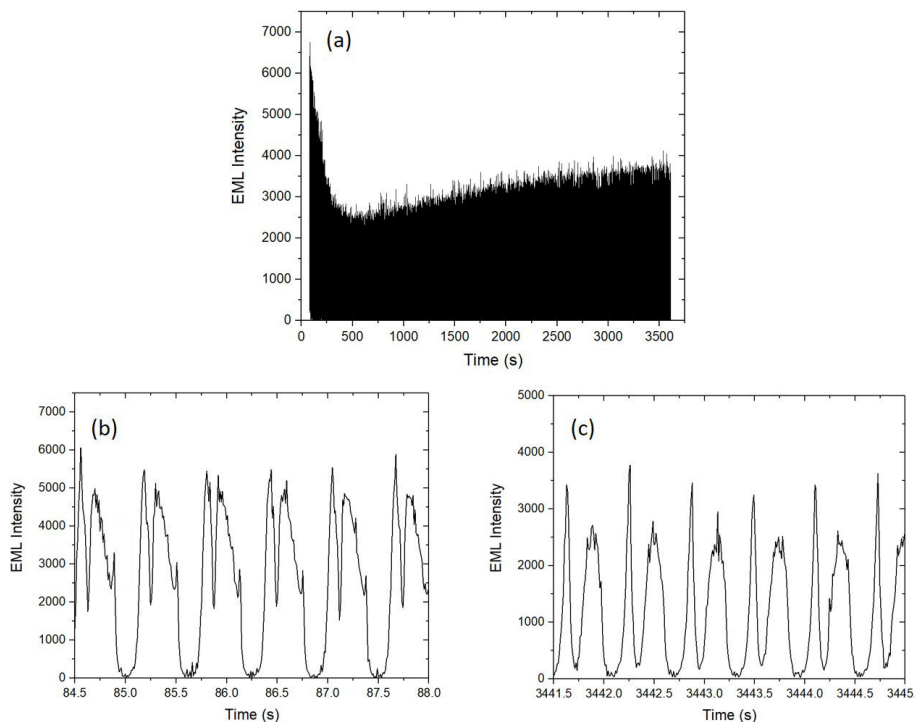


Figure 4.26: *Elastico-mechanoluminescence response of the Gwent/RTV-SC sample using the PMT-based setup. (a) whole response. Close ups at the beginning (b) and at the end (c) of the signal.*

The luminescence starts high and decreases quickly (a). It reaches a minimum at around 400 s before increasing slowly. In (b) the two peaks corresponding to the S and R phases are visible. However, as seen figure 4.24 (b), these peaks are close to one another. The R phase is sharp and the S one is larger and close to the former. They appear to be both of the same light intensity. Toward the end of the graph (cf. (c)), these two peaks changed. Over time, the S peak shifts and is less intense than the R peak.

In figure 4.27 two S-R signals are overlaid on one another: one is taken at 85 s (in black) and the second at 3442 s (in blue). We see clearly that the emission starts later

in the second case because the force required for the EML to occur is higher which also shifts the maximum emission value. However, the R emission starts at the same moment, with no shift in the maximum.

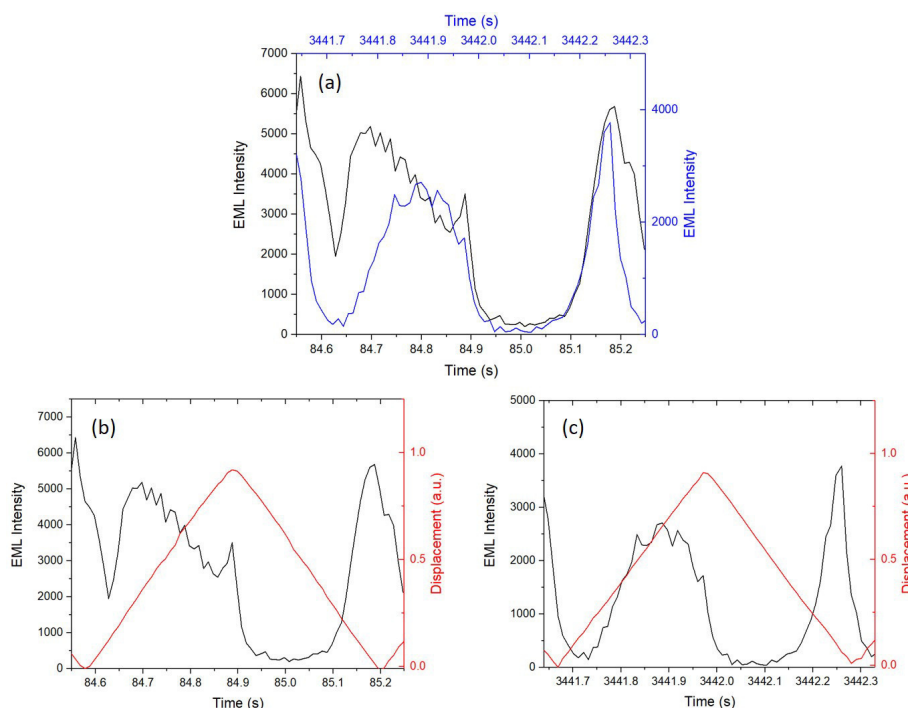


Figure 4.27: *Elastico-mechanoluminescence response of the Gwent/RTV-SC sample using the PMT-based setup. (a) Superimposition of two S-R responses (black and blue). (b) and (c) S-R response with a displacement curve (in red) taken from the beginning and the end of the signal, respectively.*

We find in (b) and (c) the EML response accompanied by the displacement curve in red. As the deformation is initiated, emission of light occurs almost at the same time, as seen in (b), D_{th} is low. When the deformation is at its maximum, a small peak is recorded and then the luminescence decreases. This decrease might be due to several parameters like the ZnS lifetime and a characteristic time of unsticking. When the sample is relaxing, EML occurs just before the end.

It is also possible to see differences in the EML signal thanks to figure 4.28. It represents the EML intensity as a function of the displacement corresponding to the end of the EML response seen in figure 4.26 (b) and (c). First, we see the difference in the light intensity which is stronger in (a). Then, we see that the junction shifted. The S emission is wide but it shifts over time reducing its duration.

4.6.1.3 Conclusion

The use of RTV-SC instead of RTV-FC influenced the EML behaviour of Gwent phosphor. We have been able to experiment with these samples using two experimental setups. In both cases, the EML intensity decreases during the first 5 minutes. The S and R emissions are similar with a large S emission triggered at low D_{th}^1 , and a shorter R peak. Thanks to the PMT setup, we could record for one hour and observe the evolution of the EML signal. After the rapid decrease, the intensity of the emitted light rises slowly. Due to the matrix softening, the S emission shifted and is now triggered for a higher D_{th}^2 ($D_{th}^2 > D_{th}^1$).

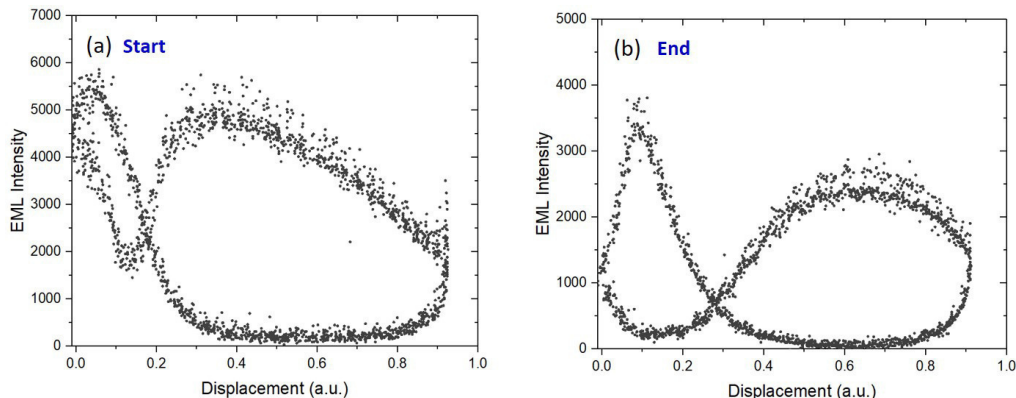


Figure 4.28: *EML response as a function of the displacement of Gwent/RTV-SC. Drawn from data in figure 4.26 (b-c).*

Compared to Gwent RTV-FC, this material exhibits a higher light intensity as the beginning of the experiment. However, with the RTV-FC the EML increases only and D_{th} is higher. The PDMS is more easily removed from the particles during stretching with RTV-SC than with RTV-FC which explains the high intensity at the start of the experiment.

4.6.2 Wacker Elastosil RT A/B

The Gwent/Elastosil sample was only tested using the photomultiplier setup, the results can be found figure 4.29 and 4.30.

The light intensity is very high at the beginning, equivalent to RTV-SC, but diminishes quickly. The experiment could not be conducted over periods of time longer than 500 s. The sample breaks very easily during the experiment. Although the decrease in the brightness was confirmed several times, we cannot dismiss the possibility of a later increase as observed in the case of the Gwent/RTV-SC figure 4.26. The details of the behaviour of that sample are shown figure 4.30.

The S peak is wider at the beginning of the experiment and lasts ≈ 0.27 s, in (b) this emission lasts 0.19 s. As seen in the previous subsection, this peak changes due to the constant mechanical stress applied to the polymer. Over time, the releasing peak is very weak and brief (≈ 0.15 ms instead of ≈ 0.23 s around 55 s of the experiment) and only the S peak stands out.

4.6.3 Conclusion

The RTV PDMS has a high value of elongation at break (900%) but the introduction of particles reduces this elongation. The Gwent/RTV-SC sample exhibits intense luminescence during the first cycles of stretching-releasing. This luminescence decreases but increases again after about 400 s. The rapid decrease can be explained by the Mullins effect because of the degradation of the sample. After that, one could assume that the sample reaches a "Mullins effect plateau" which prevents the luminescence from keep on declining.

The Wacker Elastosil PDMS had a low value of elongation at break of 100%. The embedded ZnS:Cu microparticles in the polymer weakened its resistance to deformation. The sample would break upon stretching faster than the sample made of RTV PDMS.

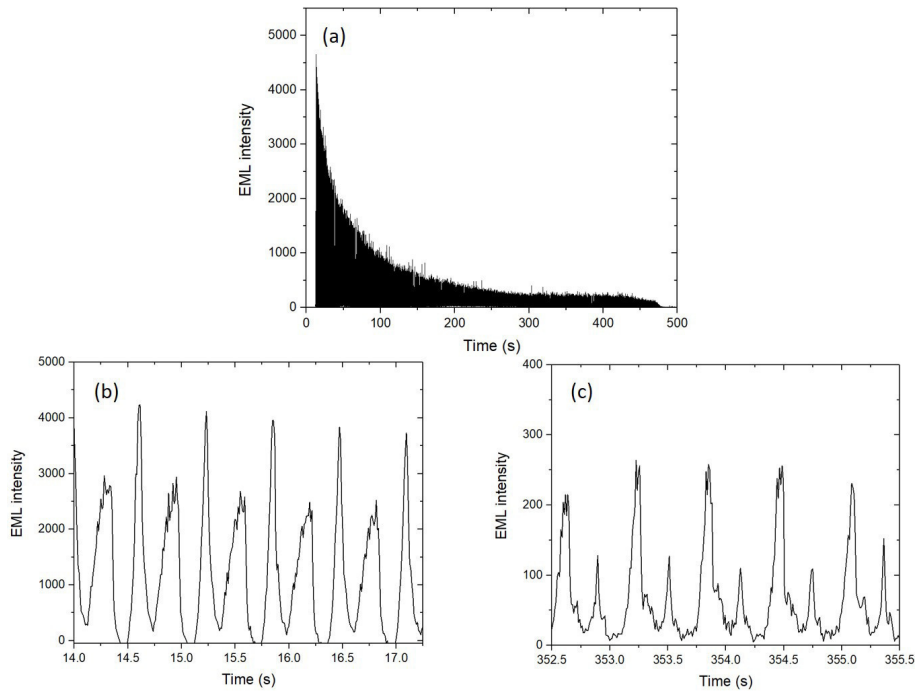


Figure 4.29: *Elastico-mechanoluminescence response of the Gwent/Elastosil sample using the PMT-based setup. (a) whole response. Close ups at the beginning (b) and at the end (c) of the signal.*

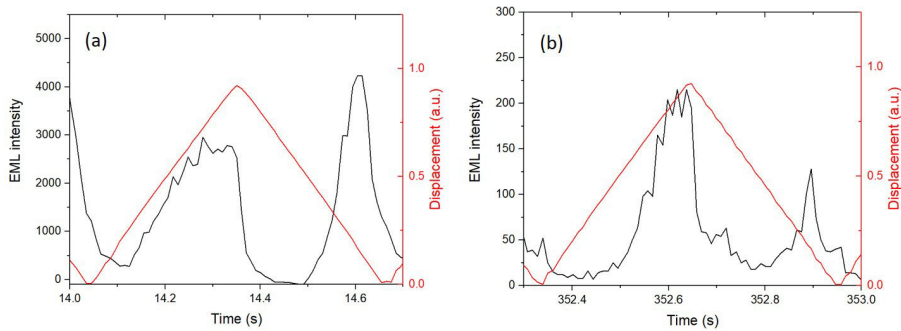


Figure 4.30: *(a) and (b) Elastico-mechanoluminescence response of the Gwent/Wacker-Elastosil sample using the PMT-based setup with the displacement curve in red, at 54 s and 392 s of the experiment, respectively.*

However, the Gwent/Elastosil does exhibit EML which also decreases during the first minutes of the S-R experiment.

These two PDMSs (RTV-SC and Wacker Elastosil) changed the EML because of their mechanical properties. Unlike RTV-FC, they induce a decrease in the luminescence during the first minutes of the elastic deformation. Moreover, their respective D_{th} also increases over time quickly.

4.7 Conclusion & Discussion

The elasto-mechanoluminescence (EML) study on the Gwent ZnS:Cu@Al₂O₃ particles embedded in a polydimethylsiloxane (PDMS) matrix brought much information. Thanks to the results from the stretching and releasing experiments, the observations could be interpreted and well understood. Hopefully, an EML model could be suggested in this chapter.

The Gwent ZnS:Cu@Al₂O₃ showed an increase in the EML intensity as the deformation spreads over time. The presence of two peaks was detected. Each of these peaks can be assigned to either the stretching or the releasing phase of the mechanical deformation. This is possible due to their dissimilarity. Moreover, their shapes and duration change over time and these aspects could be explained by the Mullins effect which affects the elasticity of the sample because of the deterioration of the polymer. **In addition, we have introduced the notion of a threshold deformation D_{th} also regarded as the equivalent of a threshold force F_{th} .** This element is very important as it has an impact on the intensity of the luminescence. As observed under an optical microscope, the PDMS comes off from the ZnS:Cu microparticles forming upon stretching what we have named "comets". These "comets" are made of a vacuum pocket created while the particle is separated from the matrix. We have shown that the number of "comets" is directly linked to the EML intensity: the more "comets" are present, the more intense the luminescence. This is only possible after a threshold force determined by the system itself as it depends on the strength bond between the phosphor and the polymer. On the one hand, if the particle sticks heavily to its matrix, D_{th} will be high. On the other hand, if the particle and the PDMS interact weakly with each other, then, D_{th} will be low. Thanks to this understanding, it was possible to change the surface of the particles and, therefore, change D_{th} . We have also demonstrated that the matrix itself plays a role in the intensity of the EML: the more rigid the polymer is, the less EML is recorded due to the absence of "comets".

Our work lead us to favour the triboelectricity explanation for this phenomenon, although we identified that the mechanism behind the light emission was different for each phase. When the polymer detaches itself from the particle, and due to the dissimilarity of the two compounds, electrical charges are created in both materials. Consequently, we suggest that only an Auger process takes place during stretching, and Auger + electron-hole recombination during the releasing. This is what causes the emission of light.

On those grounds, it is now possible to tune and control the intensity of other materials like bare ZnS:Cu, ZnS:Mn and CaZnOS:Mn/Mn,Li through surface modifications using SiO₂ and teflon (TF).

Chapter 5

Beyond Gwent Group material

Can our model be applied to other materials rather than only Gwent ZnS:Cu coated with Al₂O₃? In the first part of this chapter, we focus on the materials introduced in chapter 3. Their elasto-mechanoluminescence is explored through stretching-releasing deformation using the photomultiplier-based setup.

The input model via computer simulations allows us to extract values of threshold deformations and establish comparisons which help us determine the reliability of this model. To do so, we present EML results of 502B, a non-coated ZnS:Cu, and 512C, a phosphor similar to Gwent as it is an aluminium oxide-coated material. Moreover, We have implemented 2 additional coatings for 502B and 512C: SiO₂ and teflon. In addition to Cu-doped material, we present luminescence responses of ZnS:Mn and CaZnOS:Mn,Li.

5.1 Cu-doped materials

In the previous chapter, we have presented an EML model for Gwent ZnS:Cu. Thanks to it, it is possible to extract coherent threshold deformation values depending on the surface modification applied to the microparticles. Thus, we have proved that D_{th} is lower in the case of teflon-coated particles, and higher for SiO₂-coated particles in the case of Gwent. This model could allow us to understand other materials as well.

This section gathers the EML results of the ZnS:Cu 512C and 502B phosphors. The surface of the phosphor particles for these two materials was modified by adding a layer of SiO₂ or teflon. The results obtained by computer simulation are presented and compared to previous results.

The following parameters were used for the experiments:

- Acceleration: 4.000 cm.s⁻²
- Velocity: 4 cm.s⁻¹
- Displacement: 62.5%
- Integration time PMT: 10 ms
- Experiment conducted in a black box

5.1.1 502B: uncoated ZnS:Cu phosphor

Most elasto-mechanoluminescent experiments use zinc sulphide coated with aluminium oxide. This coating is said to be essential to trigger EML [55]. We have seen on a triboelectricity scale figure 1.14 that Al₂O₃ tends to easily create positive charges which

favours the triboelectricity model. But can a non-coated ZnS:Cu still exhibit EML? The 502B phosphor in a non-coated ZnS:Cu and we propose to verify the importance of this coating in this section. Furthermore, 502B was also coated with SiO₂ and teflon and the EML results for each are presented below. This way, it is possible to see the influence of each coating on the luminescence of bare ZnS:Cu.

5.1.1.1 EML behaviour of 502B

The 502B is a ZnS:Cu purchased from KTP phosphors. The morphological and chemical characterizations of this material are presented in chapter 3.

Figure 5.1 shows the EML response of 502B. In (a) the whole response is showed over the course of 6500s. During the first S-R cycles this material emits a low signal as shown in (b) compared to 512C. We distinguish the S and R emissions: the first one is wide, starts at 30% of the stretching and lasts about 0.25 s, whereas the R one is thin and more intense and lasts ≈ 0.1 s (cf. (d)). 502B also shows a very weak luminescence and the S and R peaks visible in (b) eventually disappear, as seen in (c). The first light emissions can be caused by electron detrapping although the sample was not exposed to light prior to testing.

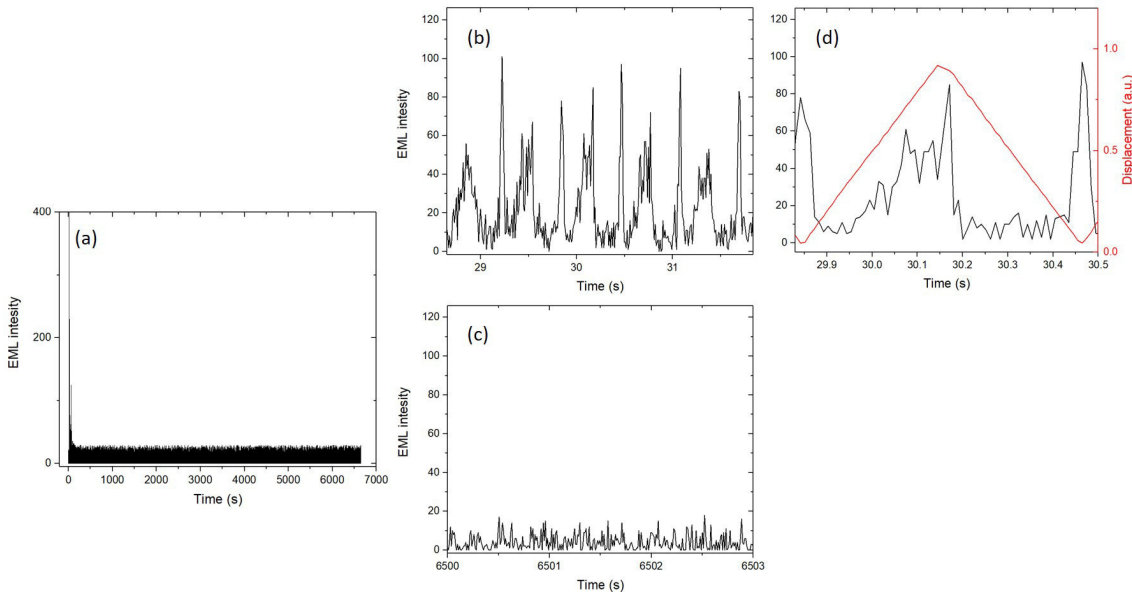


Figure 5.1: *Elastico-luminescent response of 502B ZnS:Cu. (a) whole response. (b) and (c) close-ups taken from the beginning and the end of the experiment, respectively. (d) one S-R cycle (in black) and the displacement curve (in red) taken from (b).*

Contrary to Gwent, these phosphors are not Al₂O₃ coated. It suggests that the absence of Al₂O₃ does disable EML. We suggest that the polymer sticks too much to the particles to cause triboelectricity. Modifying the surface of the microparticles changes the interaction between the polymer and the particles, and plays a major role on EML. Aluminium oxide acts as an EML booster. Can we expect the same from SiO₂ and teflon?

5.1.1.2 EML behaviour of SiO₂-coated 502B-ZnS:Cu

SiO₂ and Al₂O₃ are close to each other on the triboelectricity scale, they both have the ability to become positively charged during separation from a different material.

The EML results of 502B ZnS:Cu particles coated with SiO₂ are presented figure 5.2. SiO₂ enhanced the luminescent response of this material as shown in (a). The

light intensity decreases slightly until 2000 s of the experiment and then remains rather constant until the end. (b) shows a close up of the EML signal taken from the end of the experiment after 6500 s of S-R cycling. The shapes of the S and R emissions remain the same throughout the entire experiment, however, their intensities vary. The S emission describes a wide band starting at low D_{th} and lasts 0.30 s. The R emission is sharp and lasts about 0.15 s (cf.(c)).

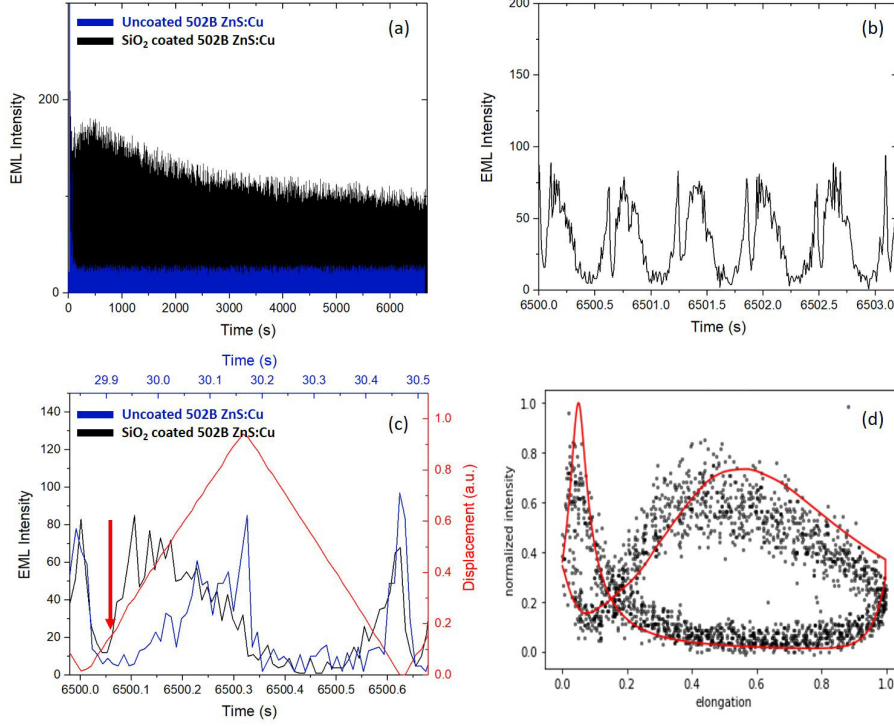


Figure 5.2: *Elastico-luminescent response of SiO₂-coated 502B ZnS:Cu. (a) whole response (in black) compared to un-coated 502B (in blue). (b) close-up. (c) one S-R cycle of 502B@Si₂ (in black), un-coated 502B (in blue) and the displacement curve (in red). (d) EML intensity as a function of the displacement, experimental (black dots) and computer simulation results (red). (b), (c) and (d) data taken at 6500 s of the experiment.*

The recorded light proves that SiO₂ acted as EML enhancer and lowered the threshold for which the luminescence is triggered. This is seen by the early appearance of the S emission (red arrow in (c)). Although not represented here, the S and R emission did not change over time. The graph in (d) shows the experimental (in black dots) and the computer simulation (in red) results. They represent the EML intensity as a function of the displacement. As the sample starts stretching, a large emission occurs represented by the large band on the right. When the releasing begins, the emission stops and the line goes in the opposite direction to the displacement axis. Finally, the peak visible on the left represents the R emission, and, then, a new S-R cycle begins. To obtain this graph, it is necessary to select a large number of S-R cycles for a representative EML behaviour in the selected range. We notice that the experimental and the simulation results are overlaid on one another which shows that our model is also fitted for this material. Moreover, we can extract threshold deformation values (deformation for which the emission occurs):

- $D_{th}^{502B@SiO_2} = 0.4$ and $\sigma_{D_{th}^{502B@SiO_2}} = 0.18$ for the stretching,
- $D_{th}^{502B@SiO_2} = 0.05$ and $\sigma_{D_{th}^{502B@SiO_2}} = 0.01$ for the releasing.

5.1.1.3 EML behaviour of teflon-coated 502B

The experimental results for the 502B@TF material are presented figure 5.3. The material exhibits intense and bright luminescence as it is 10 times brighter than the one recorded for 502B@SiO₂ (image (a)). It remains constant, around 130,000 photons/s, during the whole experiment (8000 s). Teflon is a much better EML booster than SiO₂ for 502B. The S and R peaks can be seen in (b) at 6500 s of the experiment, their shapes do not change over time.

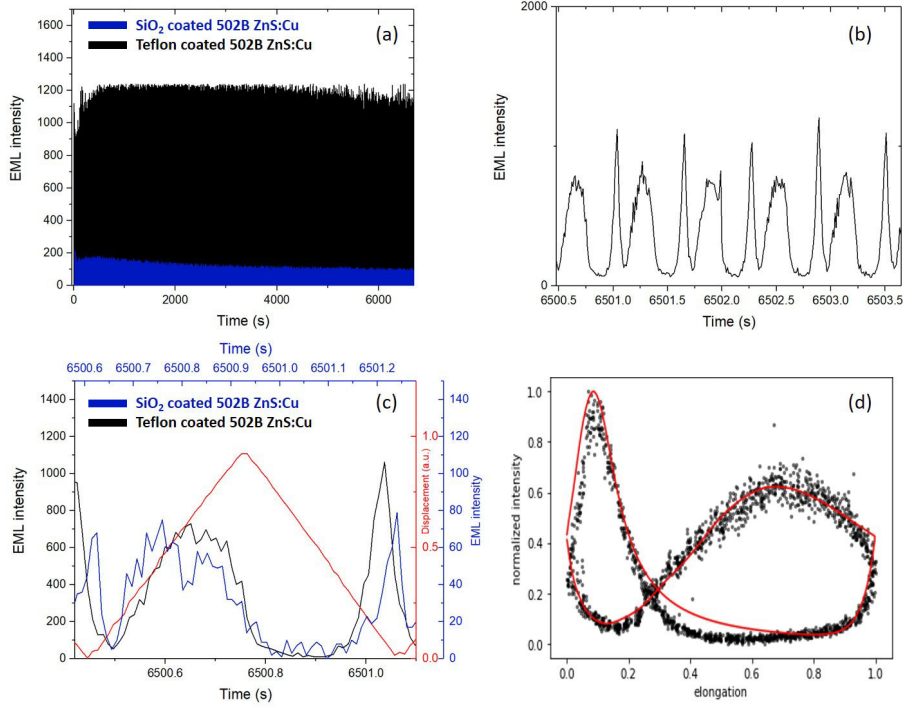


Figure 5.3: *Elastico-luminescent response of teflon-coated 502B ZnS:Cu. (a) whole response (in black) compared to un-coated 502B (in blue). (b) close-up. (c) one S-R cycle of 502B@TF (in black), un-coated 502B (in blue) and the displacement curve (in red). (d) EML intensity as a function of the displacement, experimental (black dots) and computer simulation results (red). (b), (c) and (d) data taken at 6500 s of the experiment.*

The S and R emissions resemble those observed for 502B@SiO₂ but the threshold deformation is higher for the teflon-coated particles, confirmed by graph (d). The computer simulation gave us the following threshold deformation values:

- $D_{th}^{502B@TF} = 0.5$ and $\sigma_{D_{th}^{502B@TF}} = 0.19$ for the stretching,
- $D_{th}^{502B@TF} = 0.085$ and $\sigma_{D_{th}^{502B@TF}} = 0.04$ for the releasing.

5.1.1.4 Conclusion

502B is a non-coated ZnS:Cu. During the stretching and releasing experiments, it did not show EML except during the first S-R cycles. This behaviour can be explained by the surface conditions of the particles. On non-coated microparticles, the PDMS sticks heavily and can hardly be detached and form what we referred to as "comets" probably due to the surface roughness of the particles. It is the formation of these comets that triggers luminescence through triboelectricity (as explained in the previous chapter). However, we have been able to make this non-coated ZnS:Cu a light emitting phosphor. To make the

polymer stick more or less to the particles, one needs to change the surface treatment of the particles by coating them. The coating modifies the roughness and the strength bond between the polymer and the phosphor. SiO₂ and teflon coatings both acted as EML boosters but teflon was more efficient with an increase of the EML intensity of one order of magnitude. Teflon is a molecular coating which preserves the roughness of the particles whereas SiO₂ smooths these surfaces. Interestingly, the changes in the mechanical properties of the PDMS induced by the Mullins effect were not observed. The S and R emissions do not significantly shift as the number of S-R cycles increases.

The previously proposed model via computer simulation could effectively be used to determine the threshold deformation values of this material. It showed that

$D_{th}^{ZnS:Cu@SiO_2} < D_{th}^{ZnS:Cu@TF}$ which might be due to porosity decrease resulting from the SiO₂ coating.

Because of the very few S-R cycles recorded for the un-coated ZnS:Cu, it was not possible to extract D_{th} .

5.1.2 512C ZnS:Cu coated with Al₂O₃ phosphor

The EML results of the 512C ZnS:Cu phosphor are presented in this section. 512C is a ZnS:Cu phosphor already coated with aluminium oxide also purchased from KTP phosphors. Its characterizations are presented in chapter 3. The EML response of this material was studied alongside the impact of the addition of SiO₂ and teflon on the phosphor microparticles. The chemical protocols of these coatings were presented chapter 3, section 3.3. This material is, in principle, analogous to Gwent ZnS:Cu. It is composed of 30 μm particles, on average, which are coated with Al₂O₃ and exhibit a hexagonal (wurtzite) crystal structure.

5.1.2.1 EML behaviour of 512C-ZnS:Cu coated with Al₂O₃

The EML after stretching-releasing (S-R) cycling of the sample is presented figure 5.4. The light emission increases linearly over time as does the number of S-R cycles. This behaviour was also observed in the case of the Gwent ZnS:Cu, cf. (d). (b) shows the emission peaks belonging to the stretching and releasing phases taken at 8600 s of the experiment. At this stage, the emissions are almost symmetrical.

Although not presented here, the S and R peak change over time. Each emission lasts longer at the beginning of the experiment. This difference is due to the constant deformation of the polymer. This behaviour is analogous to Gwent (ZnS:Cu@Al₃O₃).

The experimental data shown in (c) in black dots represent the EML intensity as a function of the displacement. We expected this material to give the same D_{th} values as Gwent but the red line overlaying our experimental result gives the following values:

- $D_{th}^{512C} = 0.8$ and $\sigma_{D_{th}^{512C}} = 0.25$ for the stretching (as compared to the Gwent, $D_{th}^{Gwent} = 0.6$ and $\sigma_{D_{th}^{Gwent}} = 0.21$).
- $D_{th}^{512C} = 0.13$ and $\sigma_{D_{th}^{512C}} = 0.05$ for the releasing.

Although being the same EML system, these results indicate that a new parameter is responsible for this difference which might be the roughness of the particles.

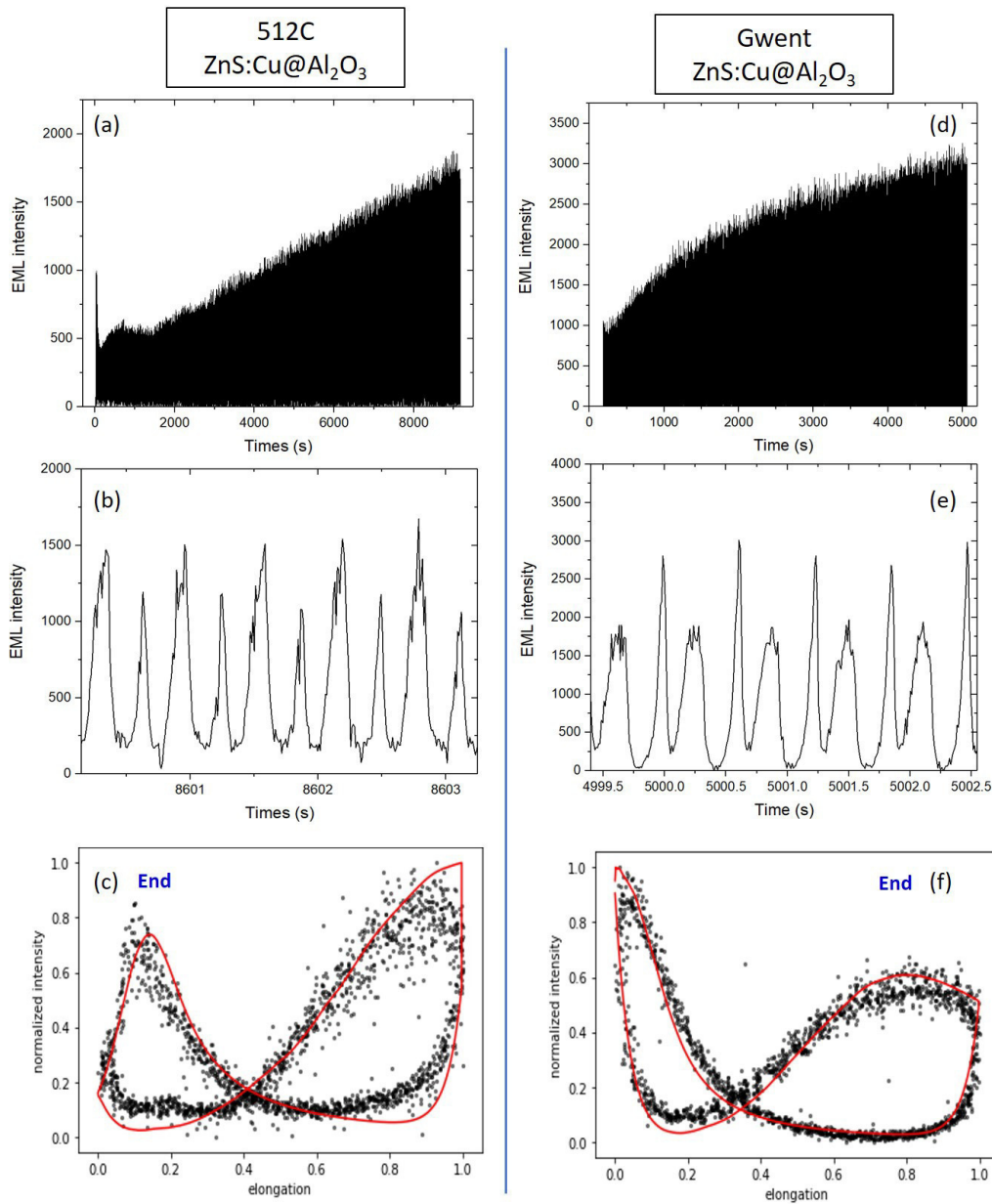


Figure 5.4: *Elastico-luminescent response of 512C (ZnS:Cu@Al₂O₃) (a-c), compared to Gwent (ZnS:Cu@Al₂O₃) (d-f). (a),(d) whole response. (b),(e) close-ups taken from the end of each the experiment. (c),(f) EML intensity as a function of the displacement, experimental (black dots) and computer simulation results (red).*

5.1.2.2 EML behaviour of SiO₂-coated 512C-ZnS:Cu coated with Al₂O₃

We have previously seen that a silicon dioxide coating on Gwent ZnS:Cu particles extinguishes the luminescence but increases it for 502B, an un-coated ZnS:Cu. In the case of SiO₂-coated 512C particles, the EML results are shown figure 5.5. The intensity of the emitted light is almost constant during the 7000 s of the experiment (corresponding to ≈ 11200 S-R cycles). Compared to the blue signal which represents the EML of 512C, the EML is 10 times less intense at the beginning and 30 times at the end of the experiment (a). This coating extinguished the luminescence almost completely but the S and R emissions are still visible. (c) shows the superimposition of experimental (black dots) and computer simulated (red line) data. The experimental results are very noisy caused by the low EML

intensity but the shape can still be reproduced by the computer and gives the following results:

- $D_{th}^{512C@SiO_2} = 0.45$ and $\sigma_{D_{th}^{512C@SiO_2}} = 0.15$ for the stretching,
- $D_{th}^{512C@SiO_2} = 0.1$ and $\sigma_{D_{th}^{512C@SiO_2}} = 0.04$ for the releasing.

This value is lower than D_{th}^{512C} but the light intensity shows that the bond between the phosphor particles and the polymer is stronger than for non- SiO_2 coated ZnS:Cu particles. This result is consistent with $Gwent@SiO_2$, but $D_{th}^{512C@SiO_2} < D_{th}^{Gwent@SiO_2}$.

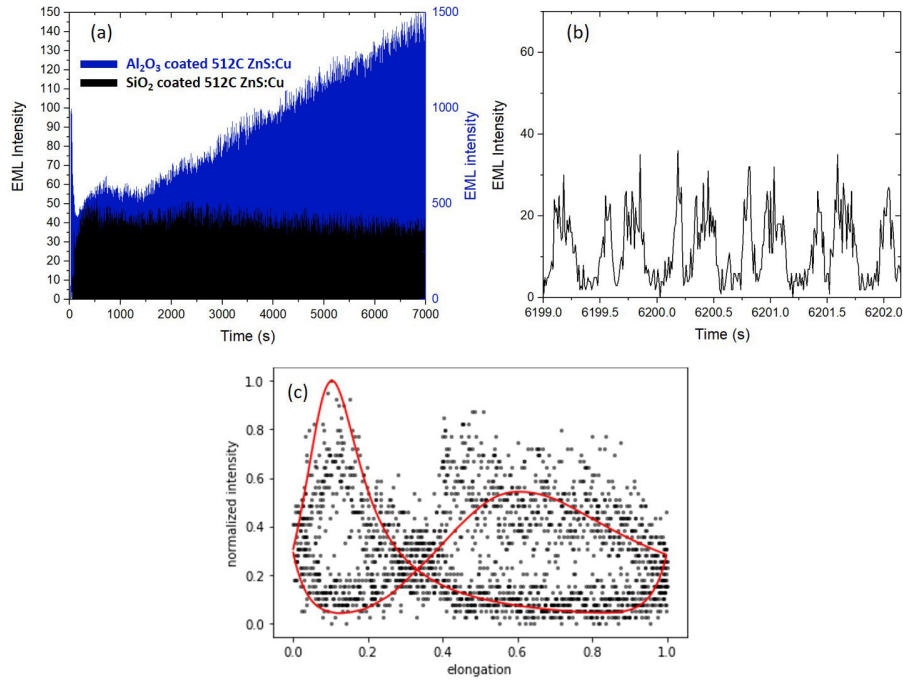


Figure 5.5: *Elastico-luminescent response of SiO_2 -coated 512C ($ZnS:Cu@Al_2O_3$). (a) whole response (in black) compared to un-coated 512C (in blue). (b) close-up. (c) EML intensity as a function of the displacement, experimental (black dots) and computer simulation results (red). (b) and (c) data taken from the end of the experiment.*

5.1.2.3 EML behaviour of teflon-coated 512C-ZnS:Cu coated with Al_2O_3

The EML results of the teflon (TF)-coated 512C particles are presented figure 5.6. The light emission intensity begins high (4000 s photons/10 ms) and then decreases but remains more or less constant from 2000 s. Compared to figure 5.4, we see a clear enhancement of the light emission as it is 8 times stronger at the beginning of the experiment (until ≈ 1000 s) and 1.5 times stronger at the end (around 8000 s). This behaviour is very different from the $Gwent@TF$ EML result as the teflon diminished the emitted light.

The S and R peaks are spaced out almost evenly in the 512C@TF material and are of the same intensity as shown in figure 5.6 (b). However, the emission of light was expected to start sooner because of the hydrophobic property of teflon and confirmed by $Gwent@TF$. This property would facilitate the detachment of the polymer from the particle. It means that light is emitted for a low deformation (low D_{th}). Thanks to the simulated data, we obtain the following values:

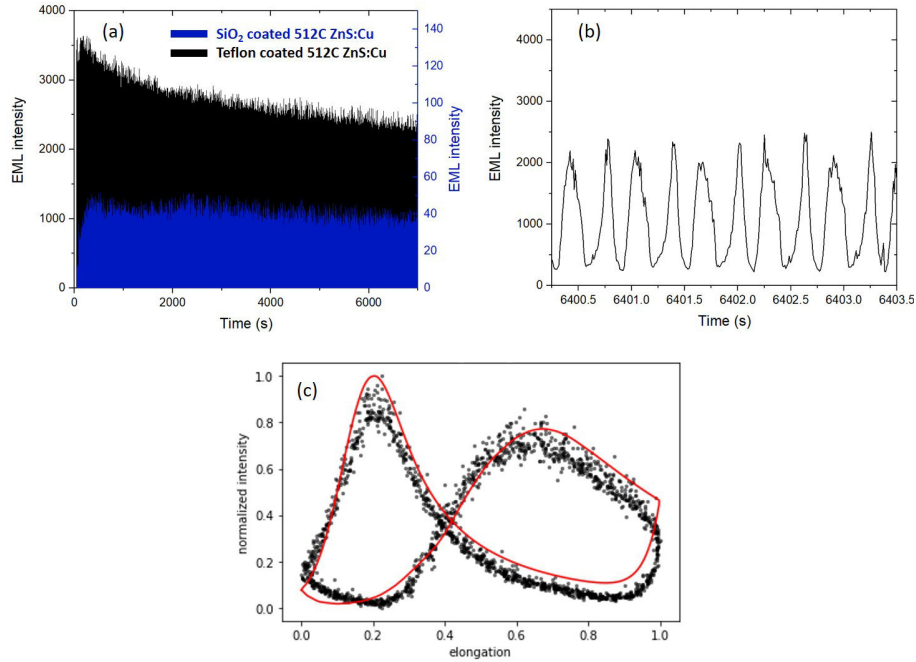


Figure 5.6: *Elastico-luminescent response of teflon-coated 512C (ZnS:Cu@Al₂O₃). (a) whole response (in black) compared to 512C@SiO₂ (in blue). (b) close-up. (c) EML intensity as a function of the displacement, experimental (black dots) and computer simulation results (red). (b) and (c) data taken from the end of the experiment.*

- $D_{th}^{512C@TF} = 0.5$ and $\sigma_{D_{th}^{512C@TF}} = 0.15$ for the stretching,
- $D_{th}^{512C@TF} = 0.18$ and $\sigma_{D_{th}^{512C@TF}} = 0.055$ for the releasing.

5.1.2.4 Conclusion

The 512C ZnS:Cu material is similar to Gwent ZnS:Cu from a morphological and crystallographic points of view. The elastico-mechanoluminescent response of 512C is similar to Gwent with a bright light emission which increases over time but Gwent shows a more efficient luminescence than 512C. This difference could be caused by the fabrication parameters and the coating which result in differences in the roughness and porosity of the material. The emission of 512C was influenced by the repeated S-R cycling. The deformation needed to trigger luminescence increased over time (and so did D_{th}) because of the Mullins effect.

SiO₂ diminishes the luminescence of 512C while teflon enhances it. Our model is able to simulate our experimental data and gives values of D_{th} . However, when compared to Gwent, we do not obtain the same results:

$$D_{th}^{Gwent@SiO_2} > D_{th}^{Gwent} > D_{th}^{Gwent@TF}$$

$$D_{th}^{512C} > D_{th}^{512C@TF} > D_{th}^{512C@SiO_2}$$

5.1.3 Conclusion on Cu-doped materials

512C and 502B are both ZnS:Cu and display different behaviours during S-R experiments: 512C exhibits bright and intense luminescence while 502B does not exhibit any. However, coating 502B with SiO₂ or teflon triggers luminescence which appears more

intense in the case of the TF coating. In the case of 512C, SiO₂ operates as luminescence extinguisher and teflon as enhancer. The action of SiO₂ is inhibited or altered by the presence of Al₂O₃. This result was also seen in Gwent@SiO₂. Moreover, SiO₂ and TF influence the mechanical properties of PDMS. The deformation needed to trigger EML becomes higher over time for 512C which results in a shift of the S and R emissions ($D_{th}(t)$ increases). Yet, the two coatings somehow prevent this phenomenon.

By changing the surface of the particles, it is possible to control the luminescence itself. The Al₂O₃ coating is essential for EML but it can also be replaced by SiO₂, for a moderate brightness, or teflon, for an intense light.

Our computer simulation model could be applied to these materials but the extracted values of D_{th} for the teflon-coated were expected to be lower.

Material	$MeanD_{th}$	Initial EML intensity*	Final EML intensity*
502B	-	100	-
502B@SiO ₂	0.4	180	80
502B@TF	0.5	1200	1200
512C	0.8	500	1500
512C@SiO ₂	0.45	40	30
512C@TF	0.5	3500	2500

Table 5.1: Summary table of Values of $MeanD_{th}$ and EML intensities of the Cu-doped materials.
*: photons/10ms

To make our surface treatments, we have taken into account only the ability of the composite material to create "comets". Nevertheless, other parameters come into play which are: **the bond polymer-particle, the roughness, the charge generation by triboelectricity, and the charge injection within the luminescent centre.**

5.2 Mn-doped materials

We have experimentally studied the EML nature of Cu-doped materials and used our model to extract consistent values of deformations. We want to transpose this model onto other materials. We have previously synthesized new materials which happen to be Mn-doped. This section comprises EML results of commercial ZnS:Mn (611C), synthesized ZnS:Mn and synthesized CaZnOS. The phosphors exhibit an orange emission resulting from the Mn²⁺ ions but their EML is not well understood. Does the modification of dopant change the EML completely? If so, is the EML similar for ZnS and CaZnOS? According to our model, it should not change.

The same stretching-releasing setup was used for these materials. It is important to mention that the spectral sensitivity of the photomultiplier is quite poor in the orange-red range rendering the signal/noise ratio rather poor.

5.2.1 611C ZnS:Mn@Al₂O₃ phosphor

611C material is a manganese-doped zinc sulphide already coated with aluminium oxide. The parameters used for this synthesis are unknown as this phosphor was purchased from KTP, Ltd. The full characterization of this material is presented chapter 3, subsection 3.2.2.3. This material displays a cubic crystal structure with an emission band around 585nm.

The EML response of 611C is presented figure 5.7 and shows that this material can emit light under elastic deformation. (a) represents the whole response over 9500 s (\approx

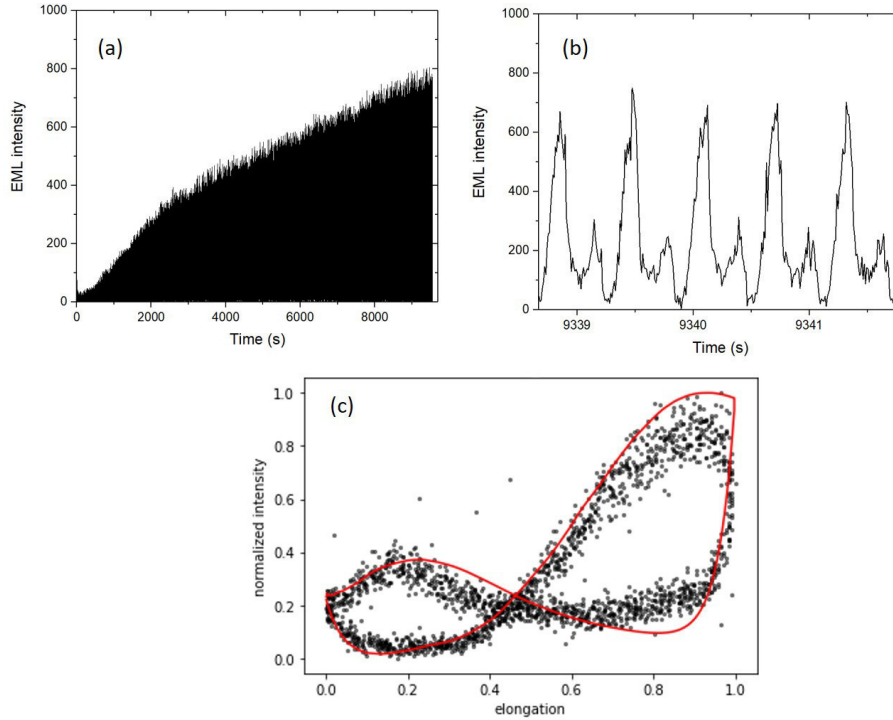


Figure 5.7: *Elastico-luminescent response of 611C (ZnS:Mn@Al₂O₃). (a) whole response. (b) close-up taken from the end of the experiment. (c) EML intensity as a function of the displacement, experimental (black dots) and computer simulation results (red).*

15000 cycles). Like Cu-doped materials, the light intensity increases linearly over time (a) with two emissions during the stretching and releasing (b). These features show that the dopant does not influence the EML. However, the signal's shape is unusual as it is dominated by the S emission. It is possible that the porosity of the phosphor particles makes our composite material less efficient. By running the simulation, we obtain the following values of D_{th} :

- $D_{th}^{611C} = 0.71$ and $\sigma_{D_{th}^{611C}} = 0.2$ for the stretching ($D_{th}^{611C} = 0.6$ for Gwent ZnS:Cu@Al₂O₃),
- $D_{th}^{611C} = 0.2$ and $\sigma_{D_{th}^{611C}} = 0.15$ for the releasing.

5.2.2 ZnS:Mn microwave synthesis

ZnS:Mn nanoparticles were synthesized using a microwave reactor which were then sintered in order to obtain microparticles of 30 μm in diameter. Their photoluminescence spectrum shows a large band centered at 585 nm, and, unlike 611C, it has a hexagonal crystal structure.

The EML response of ZnS:Mn during stretching-releasing experiment is presented figures 5.8. The breaks in the graph correspond to interruptions of the S-R cycling during the experiment. The SMAC linear actuator is voluntarily stopped for a few minutes and then put back on. 3 signals from the same experiment are shown.

ZnS:Mn shows a decreasing luminescence over time. This decrease is rapid and ends with no emission at all. This behaviour resembles an ML system like with the presence of SrAl₂O₄:Eu,Dy. Interestingly, when the deformation is stopped and started again after a few minutes, the sample exhibits once more the same luminescence intensity. The longer the break, the more intense is the emitted light as shown with the third signal (starting at $\approx 1300s$) after a 10 min pause. During those breaks the sample was not irradiated with any

light source and remained in the dark. However, there is a self-recovery phenomenon which does not occur at each cycle but rather after a stop in the deformation itself. It differs from the observations made with Gwent and 512C (ZnS:Cu) and even 611C (Al₂O₃-coated ZnS:Mn) where the luminescence increases over time.

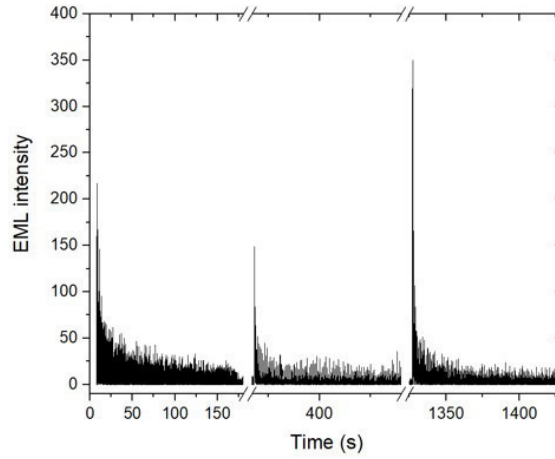


Figure 5.8: *Elastico-luminescent response of synthesized ZnS:Mn.*

Figure 5.9 (a) shows S-R cycling of ZnS:Mn over 300 s accompanied by close ups of the emission in (b) and (c). (b) shows the emission over 5 S-R cycles. The emitted light is dominated by the stretching peak. It reaches a maximum value at maximum deformation and drops immediately at the beginning of the releasing phase. The releasing peak is very weak and disappears after a few cycles. Its emission starts at the same time as the releasing phase and does not show any maximum value.

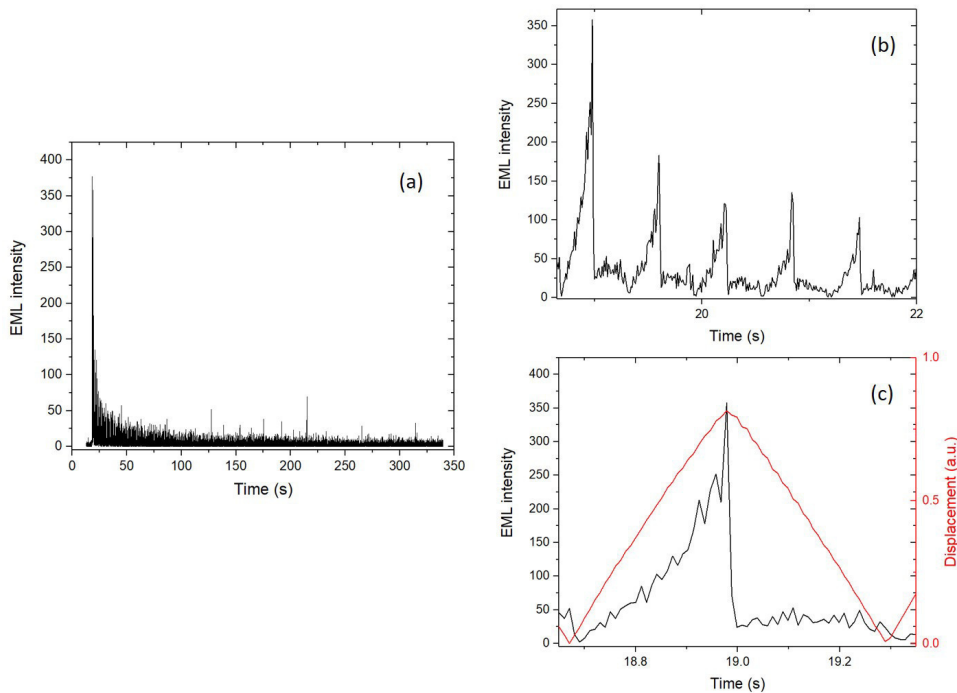


Figure 5.9: *Elastico-luminescent response of synthesized ZnS:Mn.* (a) whole response. (b) close-up taken from the beginning of the experiment. (c) one S-R cycle (in black) and the displacement curve (in red).

The morphology of our material could be responsible for this EML response. Upon stretching, the microparticles could crumble due to poor densification. This material is also fracto-ML which means that it exhibits light during fracture. The recorded light could result from multiple fractures of the particles. This hypothesis suggests that the emission should stop at some point. Yet, a new emission peak is recorded after an interruption. It is possible that the rough surfaces of these microparticles increases the bond between them and the polymer. During the releasing phase, the polymer cannot stick back completely to the particles because of this roughness. The R emission becomes impossible to trigger and results in a lower S emission. This process can only be restored if the system is given enough time to relax. If so, the polymer has time to stick back completely to the microparticles and it will give rise to a bright luminescence as observed when the experiment is paused and resumed.

611C, Gwent and 512C describe the same EML response: the emitted light increases over time and the sample is subject to mechanical changes because of the repeated S-R cycling; the S and R emissions shift. This shows that the use of a different dopant does not influence the EML.

ZnS:Mn shows a decrease in the EML during S-R experiments. The luminescence is almost solely composed of the light emitted during the stretching phase. Despite the loss of luminescence after a few S-R cycles, it is recovered after an interruption of the cycling of only few minutes. Although being the same material, the EML behaviour of this material and 611C contrasts with one another which could be due to the morphology of our material.

ZnS:Mn was also coated with teflon and the EML response was enhanced by one order of magnitude. A silica coating might have diminished the roughness of the particles which might help restore the EML like the one observed in the case of 611C (Al₂O₃-coated ZnS:Mn).

5.2.3 CaZnOS:Mn,Li

CaZnOS is a piezoelectric, mechanoluminescent material. The Mn doping gives a red emission originating from the ${}^4T_1(4G) - {}^6A_1(6S)$ transition of Mn²⁺ ions. The following results concern CaZnOS:Mn,Li. This phosphor was chosen over CaZnOS:Mn because of its crystal purity given by the lithium. We have studied CaZnOS:Mn,Li-PDMS composite material under stretching and releasing deformation. Unlike the other samples, it is very rigid which makes it hard to deform and perform several S-R cycles to compare its EML response with others. As a result, we have recorded only few stretching emissions. However, the addition of a teflon (TF) coating softened the sample and S-R cycles could be performed more easily.

The elasto-mechanoluminescence of CaZnOS:Mn,Li@TF is presented figure 5.10. The breaks visible in (a) correspond to interruptions in the experiment like previously described. (b) represents the emission during 5 S-R cycles. (c) shows one S-R cycle with the corresponding displacement curve in red. The EML results of CaZnOS:Mn,Li@TF is analogous to ZnS:Mn and ZnS:Mn@TF:

- Rapid decrease of the emitted light,
- Domination of the S emission and disappearance of the R emission,
- Self-recovery of luminescence after a few minutes' interruption.

However, the luminescence is not completely recovered after each interruption. The intensity of the first emission is never regained. Unfortunately, teflon did not enhance the luminescence of this material. The intensity is the same for coated and uncoated CaZnOS:Mn,Li. The EML results indicate that the interaction between the PDMS and the particles remained unchanged. This could be due to the morphology of the particles. The

synthesized CaZnOS:Mn,Li has plate-like particles. We can consider that the unsticking action could be more difficult with this geometry than with spherical particles. Moreover, as for ZnS:Mn , the surface roughness and irregularities can be responsible for the luminescence behaviour of this material.

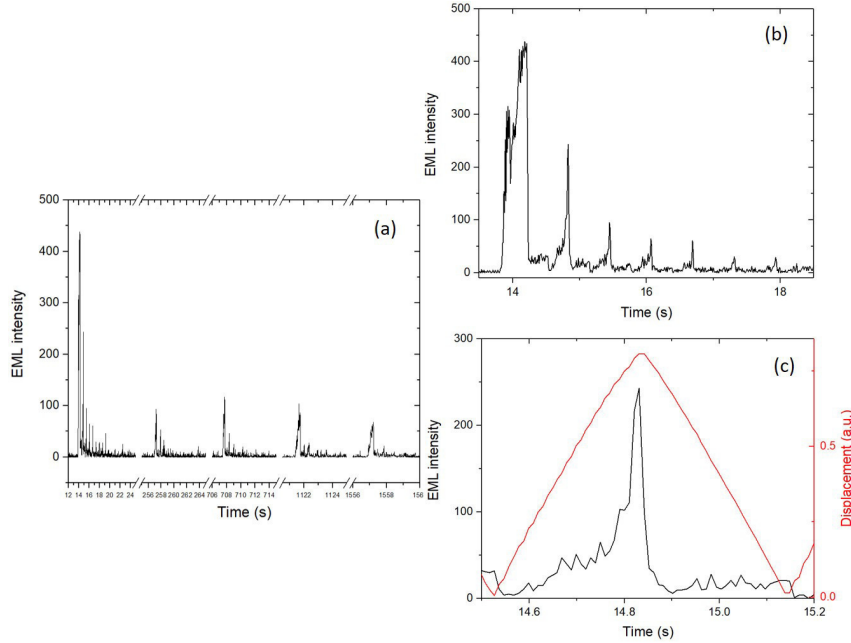


Figure 5.10: *Elastico-luminescent response of CaZnOS:Mn,Li@TF . (a) whole response. (b) close-up taken from the beginning of the experiment. (c) one S-R cycle (in black) with the displacement curve (in red).*

5.2.4 Conclusion on Mn-doped materials

We have presented in this section the EML results of Mn-doped materials: commercial 611C (ZnS:Mn), synthesized ZnS:Mn and CaZnOS:Mn,Li .

The S-R experiments revealed that 611C displays the same EML as 512C and Gwent (ZnS:Cu). The EML increases as the number of S-R cycles increases as well. This result is consistent with our proposed model confirming the triboelectric nature of the mechanism involved in elasto-mechanoluminescence.

Unlike 611C, the synthesized ZnS:Mn and CaZnOS:Mn,Li showed a decrease in luminescence during the experiments. It is only constituted of the light emitted during the first deformation phase. This emission lasts as long as the stretching phase (around 0.30 s) which is caused by a low deformation threshold. Interestingly, even with a fast luminescence decrease, the light can be partially recovered after a few minutes' interruption in the S-R cycling. The fracto-ML nature of our synthesized ZnS:Mn , but also the roughness of the particles, could be preventing the PDMS from sticking back correctly and be responsible for the decrease of light intensity. The light recovery mechanism requires the PDMS to stick back to the particles. This can only be achieved if enough time is given to the composite material to recover its original condition, i.e. without mechanical deformation. Given the quality of our synthesized materials, it is difficult to conclude on the EML behaviour of these phosphors.

5.3 Conclusion & Discussion

We have explored elastically-mechanoluminescence using samples based on the same principle: phosphor particles embedded in a PDMS matrix. 5 materials were tested: 512C and 502B, which are Cu-doped ZnS, 611C and synthesized ZnS:Mn, and CaZnOS:Mn,Li.

Our EML results showed that the presence of a coating is important to trigger luminescence. Al_2O_3 , SiO_2 and teflon act as luminescence boosters as long as no other coating is present on the phosphor particles. The additional Al_2O_3 results in a bright and increasing luminescence, and SiO_2 and teflon enhance the light intensity. The enhancement of luminescence originates from the strength bond between the microparticles and the PDMS. If this bond is weak, it is more likely for the composite material to create electric charges after stretching by triboelectricity. That is why D_{th} of teflon-coated materials is weaker than of non-coated.

Our synthesized materials (ZnS:Mn and CaZnOS:Mn,Li) showed equivalent results under elastic deformation. Light is mainly emitted during stretching with decreasing intensity. However, the luminescence is restored after pausing the deformation. This behaviour is an important feature that differentiates commercial materials to synthesized ones. It could be explained by the non-controlled morphology of the powders. The commercial phosphors exhibit spherical and smooth microparticles whereas our synthesized phosphors exhibit rough and inhomogeneous particles. This change in morphology impacts directly the EML response.

General Conclusion

Elastico-mechanoluminescence (EML) offers a lot of potential applications. Its self-recovery property and the ability to convert a mechanical energy into light piqued the interest of scientists over the past decade and it became a suitable candidate for stress sensors, wearable devices, displays and light sources, and could also be designed for security purposes thanks to its reliability. EML is a sub-category of mechanoluminescence. Light is triggered by an elastic deformation which calls for samples capable of enduring such deformations. Composite materials composed of phosphor microparticles embedded in a soft polymer matrix were introduced. The typical EML material comprises copper-doped zinc sulphide (ZnS:Cu) microparticles and polydimethylsiloxane (PDMS). The EML is assessed by using an experimental setup which induces an elastic deformation like a stretching-releasing (S-R) device. Being able to observe such a phenomenon raised the question of its origin. Therefore, we have found two theories that explain EML: one was proposed by *Chandra et al.* suggesting that the elastic deformation generates a piezoelectric field strong enough to trigger EML. The other one states that electric charges can be created within the composite material *via* triboelectricity, it was proposed by *Sohn et al.* Confronting these two theories is what motivated this work, but what makes that EML system efficient?

We started by investigating the optical, morphological, chemical and structural properties of our composite material. ZnS:Cu is a piezoelectric compound. It exhibits a hexagonal crystal structure (hcp) and displays an emission band around 510 nm. The spherical particles are about 40 μm in diameter and are easily incorporated into the polymer matrix. The sample requires a matrix with appropriate mechanical properties like a high value of elongation at break. This parameter ensures a good elasticity to the polymer even after being mixed with the phosphor. We have implemented an S-R device to record the EML intensity over time using an optical fiber connected to a photomultiplier. Heretofore, published scientific reports did not display long experiments. Our setup allows long EML recordings that could last several hours. It is possible to monitor any variation and changes in the EML behaviour of any EML sample. The experimental results highlighted the self-recovery ability of the composite material without any form of irradiation. During S-R experiments, ZnS:Cu-PDMS exhibits bright luminescence whose intensity increases over time. The EML signal is composed of two emissions: the first emission occurs when the sample is stretched and the second when it is released. How can these observations help us understand the mechanism in question?

The second part of this work focused on finding out the effect responsible for EML. For *Chandra et al.* a high piezoelectric field can be generated. However, the applied force during S-R devices is inferior to 10N and is insufficient to trigger electric fields of the order of 10^5Vcm^{-1} . Consequently, it is not possible to accept that piezoelectricity is responsible for EML. *Sohn et al.* have raised this issue as well and proposed that triboelectricity was possible because of the separation of two surfaces. The composite samples were observed under an optical microscope. The microscope revealed the presence of a new element upon stretching. The elastic deformation forces the polymer to stretch and,

eventually, to detach itself from the particle it surrounds. This leads to the formation of vacuum pockets that we have named "comets", because of their shape, and then disappear when the sample is back to its original length. This observation confirms that triboelectricity is a consistent explanation for EML. We made assumptions that the first emission of light corresponding to the stretching phase could be caused by Auger process. When the sample is released, the polymer sticks back to the particle. The separated charge carriers, through Auger and electron-hole recombination, cause the second light emission. The formation of "comets" can only be achieved if the deformation is high enough to cause the detachment of the polymer from the microparticles. This value was referred to as threshold deformation D_{th} . On the one hand, if D_{th} is low, the emission coincides with the beginning of each deformation phase or it starts shortly after. If D_{th} is high, then the emission will occur after. Moreover, the number of "comets" is directly correlated to the intensity of EML: the more "comets" there are, the more intense the luminescence would be.

The S and R emissions do not remain unchanged throughout the entire experiment. We have noticed that their positions shift over time and their duration shrinks. On average, the S emission lasts 0.30 s during the first minutes of the experiment and only 0.25 s after at least one hour of constant S-R deformation. This is caused by an increase in the value of D_{th} . This change results from the constant S-R deformation applied on the polymer. Elastic deformation causes polymer softening and premature ageing, thus, changing their mechanical properties. The required deformation to trigger luminescence increases over time because the applied movement is unchanged. In 1947 a researcher confronted the issue of the change in the mechanical properties of filled rubbers, and it is now known as the Mullins effect. Thanks to this new understanding, we have established a model able to simulate the experimental results and extracted consistent threshold deformation values.

In light of these new elements, it should be possible to control the light emission by changing the bond strength between the polymer and the matrix by modifying the matrix and/or the surface of the phosphor microparticles through chemical treatments.

The addition of a coating like SiO_2 and teflon has proved to be effective in the enhancement of EML on ZnS:Cu particles like it was for those already purchased and coated with Al_2O_3 . However, an additional coating diminishes the luminescence of Al_2O_3 -coated particles which are usually available on the market.

A harder matrix will inhibit the formation of "comets" and therefore result in a lower luminescence intensity. Moreover, elastic deformations, being harder to perform, might break the sample and make it impossible to test. That is why a soft matrix is recommended for this kind of experiment. What about other materials?

We carried out our investigation even further by synthesizing our own materials: ZnS:Mn and CaZnOS:Mn,Li which are both mechanoluminescent materials and display a hexagonal crystal structure. The Mn doping causes orange and red light emissions for ZnS:Mn and CaZnOS:Mn,Li, respectively. Their luminescence behaviour is very different from commercial materials. The luminescence responds to stretching by an emission peak which decreases rapidly over repeated S-R cycles. This light can be restored after interrupting the mechanical deformation and resuming it a few moments later. It is most likely due to the poor quality of our materials and their shapes: the microparticles display irregular and inhomogeneous surfaces. The changes in the particles' morphology has a direct effect on the EML. This is supported by the fact that commercial ZnS:Mn powder showed similar EML response to Cu-doped materials for which the particles are controlled.

Through this work, we tried to bring additional elements to better understand EML. Although being mainly an exploratory study, we proposed the most inclusive explanation we could and, hopefully, offered new aspects to ponder. We could rationalise some observations but many new questions arose about the role of the shape, surface, size and roughness of the particles. Future exploration could further investigate the morphology of

the particles as to assess whether our synthesized materials could exhibit an EML similar to commercial phosphors with a better control of the shape and roughness of the particles. It would constitute an additional parameter for the selection of new materials which, thanks to an appropriate surface treatment like teflon, would also exhibit EML. We have shown that this EML is triggered by triboelectricity thanks to the outbreak of "comets". These "comets" were observed with an optical microscope in a static mode. A setup could be implemented as to observe the sample during deformation. A camera could be added to record a film of the outbreak of the "comets" after a threshold deformation. Moreover, this setup could bring a supplementary confirmation of the existing link between the number of "comets" and the EML intensity: an increasing number of "comets" results in a more intense EML, if all "comets" are formed then the EML intensity should describe a plateau.

Finally, if triboelectricity is indeed the only phenomenon in question, then it should be possible to achieve EML with other phosphors. Instead of only green or orange, the light emitted could spread all over the visible spectrum. Besides, by changing the strength bond between the polymer and the microparticles, we can either enhance the luminescence or diminish it through surface treatments. On those grounds, a lot more possibilities are at hand and the only limitation is our imagination.

French Summary

Résumé

L'Elastico-MécanoLuminescence (EML), qui est le phénomène où la luminescence est induite par la déformation élastique des solides, a connu un intérêt croissant ces dernières années. L'étude des matériaux composites de type phosphore-élastomère comme le ZnS:Cu/Mn incorporé dans une matrice de PDMS (polydiméthylsiloxane) émergea. De nombreux systèmes et appareils sont développés à partir de ce phénomène comme des fibres de tissus mécanoluminescentes, ou encore des panneaux d'affichage mécanoluminescents alimentés grâce à la force du vent. Cependant, l'origine de ce mécanisme n'est pas complètement établie. Un des modèles permettant d'expliquer l'EML invoque le processus d'auto-régénération de la mécanoluminescence par la réduction de la profondeur du piège induite par la piézoélectricité. Bien que ce modèle soit assez bien accepté, il est néanmoins contesté par d'autres auteurs qui proposent un mécanisme alternatif. Dans le cas d'un matériau composite ZnS: Cu-PDMS, il est démontré que la triboélectricité est également adaptée pour expliquer ce phénomène de luminescence. Cette théorie est soutenue par le fait qu'un matériau élaboré à base d'une matrice rigide, comme la résine, au lieu d'une matrice souple comme le PDMS rend l'EML impossible à produire.

Le travail présenté aborde les différents mécanismes de l'EML selon deux approches. L'une consiste à évaluer un matériau modèle en condition d'étirement et à en analyser la réponse optique. L'autre consiste à synthétiser différents matériaux et à tester leur efficacité en fonction de différents paramètres structuraux et morphologiques. Ainsi, différents phosphores (piézoélectriques ou non) et des hétérostructures, telles que ZnS:Cu, ZnS:Mn, CaZnOS: Mn/Mn, Li, sont dispersés dans des matrices à base de PDMS et caractérisés selon diverses conditions d'étirement. Les conclusions de ces résultats mènent à privilégier le modèle de la triboélectricité. Ce point important met en évidence l'importance de la surface des microparticules. Ainsi, des traitements chimiques de surface, comme des revêtements de silice SiO₂ ou de téflon, permettent d'étudier l'influence de la modification de surface des microparticules ainsi que de déterminer l'interaction entre ces dernières et le polymère. En effet, la force d'adhésion entre ces deux éléments joue un rôle central dans l'intensité de la lumière émise lors d'une déformation élastique. Cette approche fournit une meilleure compréhension du phénomène d'élastico-mécanoluminescence et nous a permis de proposer un mécanisme d'activation de l'EML et d'établir un modèle applicable aux différents matériaux que nous avons étudiés. Nous avons pu démontrer que plus l'interaction est faible et plus l'EML est intense via la mise en lumière d'éléments observés sous microscope optiques. Ces éléments placent la triboélectricité comme seul mécanisme responsable de l'EML. Cela a permis, entre autres, de rendre efficaces diverses microparticules commerciales, ce qui permet d'envisager d'étendre la gamme de luminophores pour cette application.

Contexte & Avant propos

L'industrie textile recherche l'innovation et est toujours à la recherche de nouveaux matériaux aux propriétés efficaces et inventives. Dans ce contexte, les textiles intelligents sont en plein essor et les vêtements lumineux suscitent de plus en plus d'intérêt. Le projet EFIGY (EFficient lumInous Glow Yarn), grâce auquel la recherche présentée a été initiée, suit cette voie. Il offre la possibilité d'explorer des propriétés optiques qui pourraient être intégrées directement dans le textile lui-même. Ce projet de recherche et développement porté par le centre d'innovation TECHTERA regroupe différents collaborateurs industriels et un laboratoire:

Collaborateur	Localisation	Rôle
Brochier Technologies (PME)	Villeurbanne (Rhône)	Porteur du projet/ Tissage
SATAB (Group)	Saint-Just-Malmont (Haute-Loire)	Tissage de rubans
Blanchard (PME)	Saint Julien Boutières (Ardèche)	Moulinier
JRC Reflex (PME)	Romans (Drôme)	Fournisseur d'additifs rétro réfléchissants
Massebeuf Textiles	Pont-de-Labeaume (Ardèche)	Gainage fils
IFTH	Flaviac (Ardèche)	Coordinateur/Filage/ Compoundage
iLM	Villeurbanne (Rhône)	Caractérisation/ Suivi scientifique

Les objectifs de ce projet sont les suivants:

- Développer des additifs lumineux pour les textiles,
- Développer des multifilaments phosphorescents pour la sécurité dans les transports et les bâtiments, les activités sportives et de loisirs (par exemple, équipement cycliste) et aussi pour les équipements de protection individuelle (par exemple, équipement de pompier),
- Développer des multi-filaments rétro réfléchissants pour le sport et les loisirs (haute visibilité),
- Développer des multi-filaments mécanoluminescents pour les textiles intelligents,
- Combinez les propriétés phosphorescentes et rétro réfléchissantes dans un tissu avec et sans fibres optiques.

Le rôle de l'ILM dans ce projet était, d'une part, d'établir les spécifications techniques et fonctionnelles en surveillant les additifs lumineux pour la rétro réflexion et la luminescence persistante; étudier les luminophores existants et vérifier leur qualité et comprendre l'impact de différentes sources lumineuses sur l'efficacité de certains luminophores. D'autre part, il était important de mettre en œuvre un protocole expérimental pour la caractérisation des matériaux phosphorescents et rétro réfléchissants (billes de verre), d'évaluer et de tester les fils rétro réfléchissants par des mesures de luminance. La première année de mon doctorat a été principalement consacrée au projet EFIGY. J'ai mis en place un dispositif optique qui excite différents phosphores à luminescence persistante avec différentes longueurs d'onde et mesuré leur rémanence selon des normes. Les matériaux rétro réfléchissants ont également été étudiés avec un second banc optique et comparés à des produits disponibles dans le commerce qui répondent aux normes. De plus, chaque matériau mesuré (luminescent persistant et rétro réfléchissant) a également été caractérisé en utilisant un microscope électronique à balayage (MEB) associée à la microanalyse par Energie Dispersive de rayons X (EDX). Cependant, cette étude n'est pas présentée dans

ce manuscrit.

Ce projet visait principalement à apporter une aide scientifique sur des produits pouvant être directement intégrés à l'industrie. Grâce à cela, il a également été possible d'explorer et d'approfondir un autre sujet: la mécanoluminescence ou ML. Ce type de luminescence est déclenché lorsqu'une action mécanique est appliquée à un solide comme l'écrasement, le pressage, la rupture ou le frottement. En dehors du spectre du projet EFIGY, l'étude de la ML présente un grand avantage du point de vue scientifique et aborde un réel problème physique: quel est le mécanisme de ce phénomène?

Le présent manuscrit se concentre uniquement sur les recherches et les travaux effectués sur la mécanoluminescence.

Introduction

L'homme a toujours cherché à échapper aux ténèbres. Il découvre le feu et vénère une étoile qui lui prodigue lumière et chaleur. Cette notion est si importante qu'elle se trouve dans le livre de Genèse 1:3 "*Et Dieu dit: "Que la lumière soit "et la lumière fut"*". Du silex à l'interrupteur, nous recherchons cette lueur, et bien que la comprendre aujourd'hui semble banale, certains phénomènes de lumière nous échappent encore.

Par exemple, un simple morceau de sucre est capable d'émettre de la lumière lors d'une fracture. Comment est-ce possible? En 1605, Francis Bacon a signalé ce phénomène pour la première fois dans son livre "The Advancement of Learning"; il a écrit: "*Ce n'est pas la propriété du feu seul de donner de la lumière ... un morceau de sucre en le grattant ou en le cassant*" [33]. Cette nouvelle découverte a ouvert la voie à ce qu'on appelle aujourd'hui la **mécanoluminescence**. Ce mot est composé de *mécano-*, qui signifie mécanique et de *-luminescence* qui provient du mot latin *lumen* signifiant "lumière". En d'autres termes, la mécanoluminescence décrit un phénomène dans lequel un solide émet de la lumière lorsqu'une action mécanique est appliquée sur lui. Par la suite, ce phénomène a été observé dans un grand nombre de matériaux ce qui a conduit à une classification plus large de ces composés. Étant donné que chaque matériau ML peut être déclenché différemment et dépend de différents paramètres, cette classification était nécessaire. Elle a été introduite pour la première fois par *Chandra et al.* En 1995 [34]. C'est ainsi que deux types principaux ont émergé: le premier est la Déformation-ML (DML), qui peut également être sous-catégorisée en fracto-ML, plastico-ML et élastico-ML. Le second est la Tribo-ML (TML) dans laquelle on retrouve la ML déclenchée par réaction chimique, électrification ou effet thermique. Dans le premier type (DML), la luminescence dépend du matériau lui-même alors que dans le second (TML), la luminescence dépend de la nature du matériau déformé ainsi que du matériau utilisé pour produire cette déformation. Bien que tous ces phénomènes nécessitent une compréhension plus approfondie, il en est un qui se démarque: **l'élastico-mécanoluminescence (EML)**. Contrairement aux autres catégories de ML, l'EML présente des propriétés d'auto-récupération. Une déformation élastique peut être appliquée sur un tel matériau et de la lumière est émise. Cette lumière peut être restaurée et libérée à nouveau lors d'une deuxième déformation, une troisième, et ainsi de suite. De plus, la nature non destructive des matériaux EML a permis aux chercheurs de concevoir de nouveaux appareils et technologies qui consomment moins d'énergie que les appareils électriques traditionnels.

Généralement, les dispositifs EML comprennent un luminophore émetteur, typiquement un sulfure de zinc dopé (ZnS), incorporé dans une matrice souple, telle que le polydiméthylsiloxane (PDMS). Une déformation élastique peut être effectuée de différentes manières. L'EML peut être généré par pression [15], flux d'air [5], mouvement humain [12], expressions faciales [14], et étirement et relâchement [4]. La luminescence est enregistrée par un spectroradiomètre capable de mesurer à la fois la longueur d'onde et l'amplitude de la lumière émise. Ces dispositifs flexibles peuvent être utilisés comme capteurs de pression, de fracture et d'impact.

La littérature est abondante concernant les dispositifs EML, cependant, l'origine de ce mécanisme n'est pas entièrement établie. Parallèlement à la classification ML, *Chandra et al.* ont proposé un modèle EML invoquant le processus d'auto-récupération de la mécanoluminescence par la réduction de la profondeur du piège induite par la piézoélectricité. Il est basé sur l'idée que la propriété de piézoélectricité est déclenchée par la déformation des structures cristallines, génère un champ électrique interne, qui aide à la libération des porteurs de charge piégés (électrons et trous). Cette explication est proposée dans le cas des phosphores SrAl₂O₄:Eu,Dy [35] et ZnS:Mn [?]. Ces deux matériaux sont

largement utilisés pour les applications EML, mais ils présentent des comportements très différents. $\text{SrAl}_2\text{O}_4:\text{Eu,Dy}$ est un phosphore à luminescence persistante qui nécessite une irradiation UV pour restaurer sa luminescence. ZnS:Mn , par contre, ne requiert pas cette irradiation UV. Malgré cette divergence, le modèle de Chandra semble s'appliquer aux deux. C'est l'un des éléments qui a conduit d'autres scientifiques à remettre en question ce modèle, et un mécanisme alternatif a été proposé. Dans le cas d'un matériau composite ZnS:Cu-PDMS , il a été montré que la triboélectricité [10] convient également pour expliquer ce phénomène. La triboélectricité résulte du frottement ou de la séparation de deux surfaces de deux matériaux différents, créant ainsi des charges électriques sur les deux matériaux. Mais lequel des deux modèles explique vraiment EML?

Ce travail de recherche a été réalisé avec ces éléments à l'esprit avec une question centrale étant: Quel est le mécanisme le plus inclusif que nous puissions proposer pour expliquer l'EML? Pour cette étude, le candidat choisi est une poudre de sulfure de zinc dopé au cuivre (ZnS:Cu) incorporée dans un polymère PDMS. Ce matériau est bien documenté et présente la lumière la plus brillante lors d'une déformation élastique. Le premier objectif est de comprendre le comportement de ce matériau composite. Cela se fait par la fabrication d'échantillons, la caractérisation, la mise en œuvre d'un banc de mesure et des simulations informatiques. Le second est d'optimiser le luminophore pour augmenter l'intensité lumineuse par des modifications chimiques des particules elles-mêmes, et contrôler leur efficacité. Comme troisième objectif, nous voulons synthétiser et développer d'autres luminophores.

1. Le premier chapitre est consacré à l'état de l'art et aux aspects théoriques de la mécanoluminescence. L'élastico-mécanoluminescence est détaillée avec les différentes applications et dispositifs conçus jusqu'à présent, accompagnés des modèles EML proposés. Notre matériau principal, à savoir le sulfure de zinc dopé, est également présenté.
2. Le second traite de l'étude expérimentale du ZnS:Cu , en le caractérisant puis en produisant les premiers échantillons et en les testant avec un dispositif d'étirement et de relâchement afin d'étudier le comportement optique. Notre système étant composé de deux matériaux principaux (phosphore et polymère), des aspects plus fondamentaux du PDMS sont présentés.
3. Le troisième chapitre est consacré aux outils chimiques à notre disposition pour la synthèse et l'optimisation des matériaux. Les protocoles chimiques de synthèse de ZnS:Mn , CaZnOS:Mn/Mn,Li et trois revêtements de particules sont présentés: dioxyde de silicium SiO_2 , oxyde d'aluminium Al_2O_3 et téflon. De plus, d'autres matériaux de sulfure de zinc achetés (ZnS:Mn et ZnS:Cu) sont introduits parallèlement à leurs caractérisations chimiques, spectrales, morphologiques et optiques.
4. Le quatrième chapitre propose une interprétation du comportement élastomécanoluminescent de ZnS:Cu lors de la déformation (étirement-relâchement). Les impacts de la matrice polymère et les conditions de surface des microparticules des phosphores sont également étudiés. Des simulations informatiques et des observations au microscope optique ont façonné notre compréhension du phénomène et, heureusement, ces éléments nous ont permis de modifier la luminescence, de l'augmenter ou de la diminuer.
5. Enfin, dans le cinquième chapitre, les résultats expérimentaux d'autres matériaux sont présentés, à savoir, ZnS:Mn et CaZnOS:Mn,Li .

Chapitre 1: Convertir l'énergie mécanique en lumière

Au cours de la dernière décennie, un nombre important d'articles ont été publiés. Dans le cadre des dispositifs respectueux de l'environnement, l'élastico-mécanoluminescence est devenue un sujet à la mode car elle correspond à un convertisseur direct d'énergie mécanique en lumière. Il permet aux chercheurs d'imaginer et de concevoir de nouveaux dispositifs et d'adapter les matériaux afin d'augmenter l'intensité de la luminescence, sa durée et sa longueur d'onde d'émission. De tels systèmes sont conçus pour des applications dans la détection de stress [58], la cartographie dynamique de la pression [15], les affichages et sources de lumière [5] et la détection de champs électriques et magnétiques [59].

Il s'agit d'une alternative prometteuse aux moyens énergivores. L'objectif principal est de pouvoir valoriser la lumière émise et de développer d'autres luminophores, mais un gros obstacle se dresse sur le chemin. Les mécanismes de la ML ne sont pas complètement compris et une explication complète est nécessaire. Jusqu'à présent, le modèle de piézoélectricité, sur lequel la plupart des scientifiques s'accordent, répond à quelques questions concernant deux matériaux principaux ZnS:Mn et SrAl₂O₄:Eu, Dy. En appliquant ce modèle aux particules de ZnS:Cu dans une matrice molle, nous remarquons qu'il ne parvient pas à expliquer la luminescence de ce système car le champ piézoélectrique requis pour induire la luminescence n'est pas créé en raison d'une charge insuffisante appliquée sur les particules. Cela a conduit à l'émergence d'une nouvelle théorie "la luminescence induite par triboélectricité" [10]. Ce modèle ne prend pas en compte la création d'un champ piézoélectrique mais tient plutôt pour responsable le frottement entre les particules et la matrice comme source de la génération de porteurs de charge dans le cristal [10].

De plus, même si ZnS et SrAl₂O₄ appartiennent à la catégorie EML, leur luminescence se comporte différemment. Dans le cas de l'aluminate de strontium, la luminescence apparaît lors du chargement de typiquement 1000 N sur une résine époxy contenant les particules de luminophore et disparaît après des sollicitations répétées. Cette EML ne peut être entièrement récupérée qu'après irradiation UV de l'échantillon [60]. Pourtant, pour un échantillon constitué de particules de ZnS:Cu noyées dans une matrice comme le PDMS, il n'a pas besoin d'irradiation pour récupérer son EML [4]. Cela montre qu'une nouvelle classification des matériaux EML est peut-être nécessaire et que ce processus a encore besoin d'un mécanisme complet pouvant être appliqué à n'importe quel matériau EML. Grâce à cette compréhension, nous avons pu modifier ou développer des particules émettrices et atteindre les objectifs des scientifiques d'une luminescence plus intense et, ainsi, façonner des systèmes efficaces pour des applications pratiques.

Chapitre 2: Un système modèle

De nombreux articles scientifiques sur l'élastico - mécanoluminescence (EML) décrivent un système efficace. Cependant, les échantillons EML ne sont pas faciles à concevoir et nécessitent des matériaux spécifiques afin d'observer une luminescence brillante et intense lors de l'étirement. Les deux matériaux de départ étant le ZnS dopé au Cu et le polymère PDMS doivent être bien choisis. Tout d'abord, la poudre de phosphore doit présenter des particules de taille spécifique entre 20 et 40 μm , et être recouvertes d'oxyde d'aluminium Al_2O_3 . Deuxièmement, le polymère doit présenter une élasticité élevée. De plus, l'échantillon lui-même doit être suffisamment robuste pour supporter des déformations élastiques répétées.

La réponse EML a montré des résultats intéressants. Les expériences consistent en une déformation répétée d'un échantillon en forme de languette. L'échantillon passe d'une position initiale, où il est au repos, à une position d'étirement maximum, définie par l'utilisateur. Ce cycle est ensuite répété n fois. Grâce à l'utilisation de deux configurations expérimentales différentes, nous pouvons recueillir de nombreuses informations utiles. Nous avons observé la présence de deux pics d'émission: le premier correspond à la phase d'étirement, et le second à la phase de relâchement. Nous notons que ces pics sont différents les uns des autres et changent en fonction de la configuration utilisée.

Après avoir pu observer ce phénomène, de nombreuses questions se posent: quels sont les paramètres induits pour l'efficacité de la EML? Comment expliquer le comportement EML lors de la déformation? Pourquoi l'intensité lumineuse augmente-t-elle dans un cas, diminue-t-elle dans l'autre? Pouvons-nous concevoir un système plus efficace? Le sulfure de zinc est-il le seul matériau approprié pour l'EML? Telles sont les questions auxquelles nous tenterons de répondre dans les prochains chapitres.

Chapitre 3: Synthèses de Matériaux et Traitements de surface

Dans ce chapitre, nous avons présenté plusieurs matériaux qui peuvent être utilisés pour étudier, par une «approche matérielle», les propriétés d'élastico - mécanoluminescence et nous aider à déterminer ce qui rend un système EML efficace. L'étude avec le ZnS:Cu dans le chapitre précédent nous a conduit à nous interroger sur les paramètres pouvant influencer l'émission de lumière.

Nous avons synthétisé un sulfure de zinc dopé au manganèse 1% (ZnS:Mn) à l'aide d'un réacteur micro-ondes suivi d'une étape de frittage. Les microparticules ont montré une structure cristalline hexagonale et une large bande d'émission autour de 585 nm. Cette émission provient de la transition ${}^4T_1 - {}^6A_1$ des ions Mn^{2+} . La synthèse conduit à des monocristaux d'environ 40 μm de taille moyenne mais avec des niveaux de porosité élevés. Cette porosité diminue avec l'augmentation de la concentration de Mn dans le cristal de ZnS et l'augmentation de la température de frittage. L'intensité de la photoluminescence est influencée par la température de frittage: lorsque la température augmente, la bande d'émission est plus intense. On remarque que la photoluminescence la plus intense a été enregistrée pour le ZnS:Mn dopé à 2%.

CaZnOS est un autre matériau synthétisé que nous avons sélectionné pour sa nature mécanoluminescente, sa propriété piézoélectrique et sa structure cristalline hexagonale. Ces trois éléments se retrouvent également dans le phosphore ZnS:Cu. Le comportement EML de ce matériau et du ZnS:Cu pourrait être similaire en raison de leurs caractéristiques communes. Par réaction à l'état solide, nous avons pu synthétiser des microparticules de CaZnOS:Mn/Mn,Li. L'analyse spectrale, structurale et microscopique a permis de déterminer les paramètres de synthèse appropriés pour ces deux matériaux. CaZnOS:Mn est constitué de particules sphériques de 30 μm de diamètre alors que CaZnOS:Mn,Li présente de larges particules en forme de plaques de 50-100 μm . Lors d'une excitation à 280 nm, les spectres de photoluminescence de ces deux luminophores montrent deux bandes d'émission: une intense autour de 610 nm et une plus faible vers 530 nm. La première résulte de la transition ${}^4T_1({}^4G) - {}^6A_1({}^6S)$ des ions Mn^{2+} , tandis que la seconde émission provient des centres de défauts formés par le dopage Mn.

D'autres phosphores électroluminescents sont disponibles dans le commerce et ont été achetés: ZnS:Mn et ZnS:Cu. Ces matériaux sont revêtus d'oxyde d'aluminium (comme le ZnS:Cu étudié dans le chapitre 1) mais un ZnS:Cu non revêtu a pu également être acquis. Les deux ZnS:Cu présentent une structure cristalline hexagonale similaire mais leurs spectres de photoluminescence montrent une bande à 485 nm pour les particules non revêtues et à 500 nm pour celles revêtues d' Al_2O_3 . Cette différence pourrait être due à une concentration de Cu différente: à une concentration plus élevée, le spectre se déplace vers des longueurs d'onde plus élevées. Le ZnS:Cu revêtu doit présenter la même EML que le ZnS:Cu du chapitre 1 car ils ont la même morphologie, la même structure cristalline et le même revêtement. Quant au matériau commercial ZnS: Mn revêtu d' Al_2O_3 , il montre une émission orange centrée autour de 585 nm causée par les ions Mn^{2+} et présente une structure cristalline cubique.

Puisque l'élément de revêtement semble jouer un rôle important dans l'intensité de la lumière émise par les échantillons lors de l'EML, nous avons étudié ce domaine en proposant différents revêtements: Al_2O_3 , SiO_2 et téflon. Les particules modifiées sont ensuite intégrées dans une matrice PDMS. L'ajout d'un revêtement modifie l'interaction entre la particule et le polymère ce qui a un impact sur la luminescence. Cet aspect sera présenté dans le chapitre suivant.

Chapitre 4: Mécanisme de l'élastico - mécanoluminescence

L'étude d'élastico-mécanoluminescence (EML) sur les particules de ZnS:Cu revêtues d'une couche de Al₂O₃ incorporées dans une matrice de polydiméthylsiloxane (PDMS) a apporté de nombreuses informations. Grâce aux résultats des expériences d'étirement et de relâchement, les observations ont pu être interprétées et bien comprises.

Le ZnS:Cu@Al₂O₃ a montré une augmentation de l'intensité EML à mesure que la déformation se poursuit. La présence de deux pics a été détectée. Chacun de ces pics peut être attribué soit à la phase d'étirement, soit à la phase de relâchement de la déformation mécanique. Cette distinction est possible en raison de leur dissemblance: le premier pic est large alors que le second est fin. De plus, leurs formes et leur durée changent dans le temps et ces aspects pourraient s'expliquer par l'effet Mullins qui affecte l'élasticité de l'échantillon en raison de la détérioration du polymère. **De plus, nous avons introduit la notion de déformation seuil D_{th} , également considérée comme l'équivalent d'une force seuil F_{th} .** Cet élément est très important car il a un impact sur l'intensité de la luminescence. Comme observé au microscope optique, le PDMS se détache des microparticules de ZnS:Cu, formant, lors de l'étirement, ce que nous avons appelé "comètes". Ces "comètes" sont constituées d'une poche de vide créée entre la particule et la matrice. Nous avons montré que le nombre de "comètes" est directement lié à l'intensité EML: plus il y a de "comètes", plus la luminescence est intense. Ceci n'est possible qu'après une déformation seuil déterminée par le système lui-même car elle dépend de la force d'adhésion entre le phosphore et le polymère. D'une part, si la particule colle fortement à sa matrice, D_{th} sera élevée. D'un autre côté, si la particule et le PDMS interagissent faiblement l'un avec l'autre, alors D_{th} sera faible. Grâce à cette compréhension, il a été possible de changer la surface des particules et, par conséquent, de changer D_{th} . Nous avons également démontré que la matrice elle-même joue un rôle dans l'intensité de l'EML: plus le polymère est rigide, moins l'EML est intense en raison de l'absence de «comètes».

Nos travaux nous amènent à privilégier la théorie de triboélectricité, bien que nous ayons identifié que le mécanisme derrière l'émission de lumière était différent pour chaque phase. Lorsque le polymère se détache de la particule, et en raison de la dissemblance des deux composés, des charges électriques sont créées dans les deux matériaux. Par conséquent, nous suggérons que seul un processus Auger a lieu pendant l'étirement, et Auger + recombinaison électron-trou pendant le relâchement. C'est ce qui provoque l'émission de lumière.

Grâce à cela, il est désormais possible d'ajuster et de contrôler l'intensité d'autres matériaux tels que le ZnS:Cu, le ZnS:Mn et le CaZnOS:Mn / Mn,Li grâce à des modifications de surface en utilisant la silice SiO₂ et le téflon (TF).

Chapitre 5: Influence des traitements de surface

Nous avons exploré l'élastico-mécanoluminescence à l'aide d'échantillons composés de particules de phosphore incorporées dans une matrice PDMS. 5 matériaux ont été testés: les 512C et 502B, qui sont des ZnS dopé au Cu; le 611C et les deux matériaux synthétisés ZnS:Mn et CaZnOS:Mn,Li.

Nos résultats EML ont montré que la présence d'un revêtement est importante pour déclencher la luminescence. Al_2O_3 mais aussi SiO_2 et le téflon agissent comme des boosters de luminescence tant qu'aucun autre revêtement n'est présent sur les particules de phosphore. L'ajout de l' Al_2O_3 se traduit par une luminescence brillante et croissante. La silice et le téflon augmentent également l'intensité lumineuse. L'amélioration de la luminescence provient de la force d'adhésion entre les microparticules et le PDMS. Si cette liaison est faible, il est plus probable que le matériau composite crée des charges électriques après étirement par triboélectricité. C'est pourquoi D_{th} de matériaux revêtus de téflon est plus faible que pour les autres.

Nos matériaux synthétisés (ZnS:Mn et CaZnOS:Mn,Li) ont montré des résultats équivalents sous déformation élastique. La lumière est principalement émise lors de l'étirement avec une intensité décroissante. Cependant, la luminescence est restaurée après la mise en pause de la déformation. Ce comportement est une caractéristique importante qui différencie les matériaux commerciaux des matériaux synthétisés. Cela pourrait s'expliquer par la morphologie non contrôlée des poudres. Les phosphores commerciaux présentent des microparticules sphériques et lisses tandis que nos poudres synthétisées présentent des particules rugueuses et inhomogènes. Ce changement de morphologie impacte directement le signal EML.

Conclusion & Perspectives

L'élastico-mécanoluminescence (EML) est un domaine de recherche intéressant rempli de nombreuses applications potentielles. Sa propriété d'auto-régénération a suscité l'intérêt des scientifiques au cours de la dernière décennie et il est devenu un candidat approprié pour des capteurs de pression, des écrans et les sources de lumière, et pourrait également être utilisé à des fins de sécurité grâce à sa fiabilité. L'EML est une sous-catégorie de la mécanoluminescence. La lumière est déclenchée par une déformation élastique qui nécessite des échantillons capables de supporter de telles déformations. Des matériaux composites composés de microparticules de phosphore incorporées dans une matrice polymère souple ont été introduits. Le matériau EML typique comprend des microparticules de sulfure de zinc dopé au cuivre (ZnS:Cu) et du polydiméthylsiloxane (PDMS). L'EML est évaluée en utilisant un banc de mesure qui induit une déformation élastique comme un dispositif d'étirement et de relâchement. Pouvoir observer un tel phénomène pose la question de son origine. Par conséquent, nous avons trouvé deux théories qui expliquent EML: l'une a été proposée par *Chandra et al.* suggérant que la déformation élastique génère un champ piézoélectrique suffisamment fort pour déclencher l'EML. L'autre stipule que des charges électriques peuvent être créées dans le matériau composite *via* la triboélectricité, cela a été proposé par *Sohn et al.* La confrontation de ces deux théories est ce qui a motivé ce travail. Qu'est-ce qui rend un système EML efficace?

Nous avons commencé par étudier les propriétés optiques, morphologiques, chimiques et structurelles de notre matériau composite. ZnS:Cu est un composé piézoélectrique. C'est un monocristal qui présente une structure cristalline hexagonale (hcp) et affiche et bande d'émission autour de 510 nm. Les particules sphériques ont un diamètre d'environ 40 μm et sont facilement incorporées dans la matrice polymère. L'échantillon nécessite une matrice avec des propriétés mécaniques appropriées comme une valeur élevée d'allongement à la rupture. Ce paramètre assure une bonne élasticité au polymère même après avoir été mélangé avec le phosphore. Nous avons implémenté un dispositif d'étirement et de relâchement pour enregistrer l'intensité EML en temps réel à l'aide d'une fibre optique connectée à un photomultiplicateur. Jusqu'à présent, les rapports scientifiques publiés ne présentaient pas de longues expériences. Notre configuration permet de longs enregistrements EML pouvant durer plusieurs heures. De ce fait, il est possible de surveiller toute variation et modification du comportement EML de tout échantillon EML. Les résultats expérimentaux ont mis en évidence la capacité d'auto-régénération du matériau composite sans aucune forme d'irradiation préalable. Au cours des expériences, le matériaux composite ZnS:Cu/PDMS présente une luminescence brillante dont l'intensité augmente avec le temps. Le signal EML est composé de deux émissions: la première émission se produit lorsque l'échantillon est étiré et la seconde lorsqu'il est libéré. Comment ces observations peuvent-elles nous aider à comprendre le mécanisme en question?

La deuxième partie de ce travail s'est concentrée sur la découverte de l'effet responsable de l'EML. Pour *Chandra et al.*, un champ piézoélectrique élevé peut être généré. Cependant, la force appliquée pendant les expériences est inférieure à 10 N et est insuffisante pour donner lieu à des champs électriques de l'ordre de 10^5Vcm^{-1} . Par conséquent, il n'est pas possible de conclure que la piézoélectricité est responsable de l'EML. *Sohn et al.* ont également soulevé cette question et proposé que la triboélectricité était possible en raison de la séparation de deux surfaces. D'où l'idée d'observer les matériaux composites sous microscope optique. Le microscope a révélé la présence d'un nouvel élément lors de l'étirement. La déformation élastique force le polymère à s'étirer et finalement à se détacher de la particule qu'il entoure. Cela conduit à la formation de poches de vide que nous avons nommées "comètes" en raison de leur forme, et qui disparaissent ensuite

lorsque l'échantillon retrouve sa longueur d'origine. Cette observation confirme que la triboélectricité est une explication cohérente pour l'EML. Nous avons émis l'hypothèse que la première émission de lumière correspondant à la phase d'étirement pourrait être provoquée par le processus Auger. Lorsque l'échantillon est libéré, le polymère adhère à la particule. Les porteurs de charge restants, par le processus Auger et la recombinaison électron-trou, provoquent la deuxième émission de lumière. La formation de "comètes" ne peut être obtenue que si la déformation est suffisamment élevée pour provoquer le détachement du polymère des microparticules. Cette valeur est appelée déformation seuil D_{th} . D'une part, si D_{th} est faible, l'émission coïncide avec le début de chaque phase de déformation ou elle commence peu de temps après. Si D_{th} est élevé, alors l'émission se produira après. De plus, le nombre de "comètes" est directement corrélé à l'intensité de l'EML: plus il y a de "comètes", plus la luminescence est intense.

Les émissions S (stretching = étirement) et R (releasing = relâchement) ne restent pas inchangées tout au long de l'expérience. Nous avons remarqué que leurs positions évoluent avec le temps et leurs durées diminuent. En moyenne, l'émission S dure 0,30 s pendant les premières minutes de l'expérience et seulement 0,25 s après au moins une heure de déformation S-R constante. Cela est dû à une augmentation de la valeur de D_{th} . Ce changement résulte de la déformation constante appliquée sur le polymère. La déformation élastique provoque un ramollissement du polymère et un vieillissement prématuré, modifiant ainsi leurs propriétés mécaniques. La force requise pour déclencher la luminescence augmente avec le temps car le mouvement appliqué reste inchangé. En 1947, un chercheur s'est confronté à la question du changement des propriétés mécaniques des caoutchoucs chargés, et il est maintenant connu sous le nom d'effet Mullins. Grâce à cette nouvelle compréhension, nous avons établi un modèle capable de simuler les résultats expérimentaux par des simulations informatiques et extrait des valeurs de déformation de seuil cohérentes.

À la lumière de ces nouveaux éléments, il est possible de modifier la force de liaison entre le polymère et la matrice en modifiant la surface des microparticules de luminophore par des traitements chimiques et/ou de modifier la matrice.

L'ajout d'un revêtement comme le SiO_2 et le téflon s'est avéré efficace dans l'amélioration de l'EML sur les particules de ZnS:Cu comme c'était le cas pour celles déjà achetées revêtues d' Al_2O_3 . Cependant, un revêtement supplémentaire diminue la luminescence des particules revêtues d' Al_2O_3 qui sont habituellement disponibles sur le marché.

Une matrice plus dure inhibera la formation de «comètes» et entraînera donc une intensité de luminescence plus faible. De plus, les déformations élastiques, plus difficiles à réaliser, peuvent casser l'échantillon et rendre impossible les tests de déformation. C'est pourquoi une matrice souple est recommandée pour ce genre d'expérience. Quant est-il des autres matériaux?

Nous avons poussé notre enquête encore plus loin en synthétisant nos propres matériaux: ZnS:Mn et CaZnOS:Mn,Li qui sont tous deux des matériaux mécanoluminescents et présentant une structure cristalline hexagonale. Le dopage Mn provoque une émission de lumière orange et rouge pour ZnS:Mn et CaZnOS:Mn, Li , respectivement. Leur comportement de luminescence est très différent des matériaux commerciaux. La luminescence répond à l'étirement par un pic d'émission qui diminue rapidement au cours de cycles d'étirement-relâchement répétés. Cette lumière peut être rétablie après avoir interrompu la déformation mécanique et redémarrée quelques instants plus tard. C'est probablement dû à la mauvaise qualité de nos matériaux et de leurs formes: les microparticules présentent des surfaces irrégulières et inhomogènes. Les changements de morphologie des particules ont un effet direct sur l'EML. Ceci est étayé par le fait que la poudre commerciale de ZnS:Mn a montré une réponse EML similaire aux matériaux dopés au Cu pour lesquels les particules sont contrôlées.

Une exploration future pourrait approfondir la question concernant la morpholo-

gie des particules afin d'évaluer si nos matériaux synthétisés pourraient ou non présenter une EML similaire aux matériaux commerciaux avec un meilleur contrôle de la forme et de la rugosité des particules. Il constituerait un paramètre supplémentaire pour la sélection de nouveaux matériaux qui, grâce à un traitement de surface approprié comme le téflon, présenteraient également une EML intense.

Nous avons montré que cette EML est déclenchée par la triboélectricité grâce à la formation de "comètes". Ces "comètes" ont été observées au microscope optique en mode statique. Un système pourrait être mis en œuvre pour observer l'échantillon pendant la déformation. Une caméra pourrait être ajoutée pour enregistrer un film de l'apparition des «comètes» après une déformation seuil. De plus, ce montage pourrait apporter une confirmation supplémentaire du lien existant entre le nombre de "comètes" et l'intensité EML: un nombre croissant de "comètes" se traduit par une EML plus intense, si toutes les "comètes" se forment alors l'intensité EML devrait décrire un plateau.

A travers ce travail, nous avons essayé d'apporter des éléments supplémentaires pour mieux comprendre l'EML. Nous avons proposé l'explication la plus inclusive possible et avons proposé de nouveaux angles de réflexion. Si la triboélectricité est bien le seul phénomène en question, alors il est possible de réaliser une EML avec n'importe quel phosphore. Au lieu d'être uniquement verte ou orange, la lumière émise pourrait se propager sur tout le spectre du visible. De plus, en modifiant la force d'adhésion entre le polymère et les microparticules, nous pouvons soit augmenter l'efficacité de la luminescence, soit la diminuer grâce à des traitements de surface. Pour ces raisons, beaucoup plus de possibilités sont à portée de main et la seule limite est notre imagination.

Bibliography

- [1] D. R. Vij, *Luminescence of Solids*. Springer US : Imprint : Springer, 1998. OCLC: 840285826.
- [2] X. Wang, C.-N. Xu, H. Yamada, K. Nishikubo, and X.-G. Zheng, “Electro-mechano-optical conversions in pr³⁺-doped BaTiO₃–CaTiO₃ ceramics,” vol. 17, no. 10, pp. 1254–1258, 2005. [_eprint: https://onlinelibrary.wiley.com/doi/pdf/10.1002/adma.200401406](https://onlinelibrary.wiley.com/doi/pdf/10.1002/adma.200401406).
- [3] J.-C. Zhang, X. Wang, X. Yao, C.-N. Xu, and H. Yamada, “Strong elastico-mechanoluminescence in diphase (ba,ca)TiO₃:pr³⁺ with self-assembled sandwich architectures,” vol. 157, no. 12, p. G269, 2010.
- [4] S. Moon Jeong, S. Song, S.-K. Lee, and B. Choi, “Mechanically driven light-generator with high durability,” vol. 102, no. 5, p. 051110.
- [5] S. M. Jeong, S. Song, K.-I. Joo, J. Kim, S.-H. Hwang, J. Jeong, and H. Kim, “Bright, wind-driven white mechanoluminescence from zinc sulphide microparticles embedded in a polydimethylsiloxane elastomer,” vol. 7, no. 10, pp. 3338–3346, 2014-07-22.
- [6] B. Chandra, V. Chandra, and P. Jha, “Elastico-mechanoluminescence and crystal-structure relationships in persistent luminescent materials and II–VI semiconductor phosphors,” vol. 463, pp. 62–67, 2015-04.
- [7] C. N. Xu, T. Watanabe, M. Akiyama, and X. G. Zheng, “Artificial skin to sense mechanical stress by visible light emission,” vol. 74, no. 9, pp. 1236–1238, 1999-03.
- [8] B. P. CHANDRA, R. N. BAGHEL, and V. K. CHANDRA, “MECHANOLUMINESCENCE GLOW CURVE OF ZnS:mn,” p. 10.
- [9] V. K. Chandra, B. P. Chandra, and P. Jha, “Strong luminescence induced by elastic deformation of piezoelectric crystals,” vol. 102, no. 24, p. 241105, 2013-06-17.
- [10] K.-S. Sohn, S. Timilsina, S. P. Singh, T. Choi, and J. S. Kim, “Mechanically driven luminescence in a ZnS:cu-PDMS composite,” vol. 4, no. 10, p. 106102, 2016-10.
- [11] Y. J. Kim, J. Lee, S. Park, C. Park, C. Park, and H.-J. Choi, “Effect of the relative permittivity of oxides on the performance of triboelectric nanogenerators,” vol. 7, no. 78, pp. 49368–49373, 2017.
- [12] S. M. Jeong, S. Song, H.-J. Seo, W. M. Choi, S.-H. Hwang, S. G. Lee, and S. K. Lim, “Battery-free, human-motion-powered light-emitting fabric: Mechanoluminescent textile,” vol. 1, no. 12, p. 1700126, 2017-12.
- [13] “Flexible and stretchable mechanoluminescent fiber and fabric - journal of materials chemistry c (RSC publishing).”

- [14] X. Qian, Z. Cai, M. Su, F. Li, W. Fang, Y. Li, X. Zhou, Q. Li, X. Feng, W. Li, X. Hu, X. Wang, C. Pan, and Y. Song, "Printable skin-driven mechanoluminescence devices via nanodoped matrix modification," vol. 30, no. 25, p. 1800291, 2018-06.
- [15] X. Wang, H. Zhang, R. Yu, L. Dong, D. Peng, A. Zhang, Y. Zhang, H. Liu, C. Pan, and Z. L. Wang, "Dynamic pressure mapping of personalized handwriting by a flexible sensor matrix based on the mechanoluminescence process," vol. 27, no. 14, pp. 2324–2331, 2015-04.
- [16] Smokefoot, "PDMS." <https://en.wikipedia.org/wiki/Polydimethylsiloxane#/media/File:PmdsStructure.png>, 2012.
- [17] E. J. Wong, "Modeling and control of rapid cure in pdms for microfluidic device applications," 2010.
- [18] "A new approach to fabricate pdms structures using femtosecond laser," 2013.
- [19] W. Brooke-Devlin, "Novel shear-thinning of aged PDMS/fumed silica admixtures and properties of related silicone elastomers," p. 160, 2012.
- [20] W. Silicones, "Addition Curig." <https://www.wacker.com/>.
- [21] D. Tu, D. Peng, C.-N. Xu, and A. Yoshida, "Mechanoluminescence properties of red-emitting piezoelectric semiconductor MZnOS:mn²⁺ (m = ca, ba) with layered structure," vol. 124, no. 6, pp. 702–705, 2016.
- [22] D. Tu, C.-N. Xu, and Y. Fujio, "Intense red emitting mechanoluminescence from CaZnOS : Mn , li with c-axis preferred orientation," vol. 04, no. 3, p. 1450017.
- [23] J.-C. Zhang, L.-Z. Zhao, Y.-Z. Long, H.-D. Zhang, B. Sun, W.-P. Han, X. Yan, and X. Wang, "Color manipulation of intense multiluminescence from CaZnOS:mn²⁺ by mn²⁺ concentration effect," vol. 27, no. 21, pp. 7481–7489, 2015-11-10.
- [24] Y. Du, Y. Jiang, T. Sun, J. Zhao, B. Huang, D. Peng, and F. Wang, "Mechanically excited multicolor luminescence in lanthanide ions," vol. 31, no. 7, p. 1807062.
- [25] M. Su, P. Li, S. Zheng, X. Wang, J. Shi, X. Sun, and H. Zhang, "Largely enhanced elastico-mechanoluminescence of CaZnOS: Mn²⁺ by co-doping with nd³⁺ ions," vol. 217, p. 116777.
- [26] S. Aldrich, "1H,1H,2H,2H-Perfluorooctyltriethoxysilane." <https://www.sigmaaldrich.com/>.
- [27] "Constitutive models for rubber VII."
- [28] A. Feng and P. F. Smet, "A review of mechanoluminescence in inorganic solids: Compounds, mechanisms, models and applications," vol. 11, no. 4, p. 484, 2018-03-23.
- [29] D. CORNING and SYLGARD, "Data Sheet: Sylgard 184, Silicone Elastome." <http://web.mit.edu/sriram/Public/Graphics/Sylgard184Datashheet.pdf>, 1998.
- [30] W. C. AG, "Data Sheet: ELASTOSIL RT601 A/B." <https://www.wacker.com/h/en-us/medias/ELASTOSIL-RT-601-AB-en-2020.02.10.pdf>, 2020.
- [31] E. Composite, "Data Sheet: Silicone RTV 67." <http://www.espritcomposite.fr/IMG/pdf/rtv67.pdf>, 2004.

-
- [32] L. Li, L. Wondraczek, L. Li, Y. Zhang, Y. Zhu, M. Peng, and C. Mao, "CaZnOS:nd³⁺ emits tissue-penetrating near-infrared light upon force loading," vol. 10, no. 17, pp. 14509–14516, 2018-05-02.
- [33] F. Bacon, *Advancement of Learning (1605)*, vol. 719. G. W. KITCHIN, M. A, EVERYMAN's LIBRARY ed., 1950.
- [34] B. P. Chandra and A. S. Rathore, "Classification of mechanoluminescence," vol. 30, no. 7, pp. 885–896, 1995. _eprint: <https://onlinelibrary.wiley.com/doi/pdf/10.1002/crat.2170300702>.
- [35] B. Chandra, R. Baghel, A. Luka, T. Sanodiya, R. Kuraria, and S. R. Kuraria, "Strong mechanoluminescence induced by elastic deformation of rare-earth-doped strontium aluminate phosphors," vol. 129, no. 7, pp. 760–766, 2009-07.
- [36] B. Chandra, V. Chandra, and P. Jha, "Piezoelectrically-induced trap-depth reduction model of elastico-mechanoluminescent materials," vol. 461, pp. 38–48, 2015-03.
- [37] V. Chandra, B. Chandra, and P. Jha, "Models for intrinsic and extrinsic elastico and plastico-mechanoluminescence of solids," vol. 138, pp. 267–280, 2013-06.
- [38] J.-C. G. Bünzli and K.-L. Wong, "Lanthanide mechanoluminescence," vol. 36, no. 1, pp. 1–41, 2018-01.
- [39] L. Wang, L. Xiao, H. Gu, and H. Sun, "Advances in alternating current electroluminescent devices," vol. 7, no. 7, p. 1801154. _eprint: <https://onlinelibrary.wiley.com/doi/pdf/10.1002/adom.201801154>.
- [40] M. Bredol and H. Schulze Dieckhoff, "Materials for powder-based AC-electroluminescence," vol. 3, no. 2, pp. 1353–1374, 2010-02-23.
- [41] L. Zhang, C.-N. Xu, H. Yamada, and N. Bu, "Enhancement of mechanoluminescence in CaAl₂Si₂O₈ : Eu²⁺ + by partial sr²⁺ + substitution for ca²⁺," vol. 157, no. 3, p. J50, 2010-01-04. Publisher: IOP Publishing.
- [42] S. M. Jeong, S. Song, S.-K. Lee, and N. Y. Ha, "Color manipulation of mechanoluminescence from stress-activated composite films," vol. 25, no. 43, pp. 6194–6200, 2013. _eprint: <https://onlinelibrary.wiley.com/doi/pdf/10.1002/adma.201301679>.
- [43] H. Zhang, Y. Wei, X. Huang, and W. Huang, "Recent development of elastico-mechanoluminescent phosphors," vol. 207, pp. 137–148, 2019-03.
- [44] H. Kumar, "Studies on optical properties of ZnS thin film by thermal evaporation technique," p. 5.
- [45] L. Wang, X.-T. Tao, J.-X. Yang, Y. Ren, Z. Liu, and M.-H. Jiang, "Preparation and characterization of the zns nanospheres with narrow size distribution," *Optical Materials - OPT MATER*, vol. 28, pp. 1080–1083, 06 2006.
- [46] K. Manzoor, S. R. Vadera, N. Kumar, and T. R. N. Kutty, "Multicolor electroluminescent devices using doped zns nanocrystals," *Applied Physics Letters*, vol. 84, no. 2, pp. 284–286, 2004.
- [47] K. A. Franz, W. G. Kehr, A. Siggel, J. Wiczoreck, and W. Adam, "Luminescent materials," in *Ullmann's Encyclopedia of Industrial Chemistry* (Wiley-VCH Verlag GmbH & Co. KGaA, ed.), p. a15_519, Wiley-VCH Verlag GmbH & Co. KGaA, 2000-06-15.
-

- [48] F. A. Kröger, “Inorganic crystal phosphors,” in *Ergebnisse der Exakten Naturwissenschaften*, pp. 61–144, Springer Berlin Heidelberg, 1956.
- [49] B. Chandra, C. Xu, H. Yamada, and X. Zheng, “Luminescence induced by elastic deformation of ZnS:mn nanoparticles,” vol. 130, no. 3, pp. 442–450, 2010-03.
- [50] M. Catti, Y. Noel, and R. Dovesi, “Full piezoelectric tensors of wurtzite and zinc blende ZnO and ZnS by first-principles calculations,” vol. 64, no. 11, pp. 2183–2190, 2003-11.
- [51] B. P. Chandra, V. K. Chandra, and P. Jha, “Microscopic theory of elastico-mechanoluminescent smart materials,” vol. 104, no. 3, p. 031102, 2014-01-20.
- [52] B. P. Chandra, “Luminescence induced by moving dislocations in crystals,” vol. 138, no. 1, pp. 119–137.
- [53] C.-N. Xu, T. Watanabe, M. Akiyama, and X.-G. Zheng, “Direct view of stress distribution in solid by mechanoluminescence,” vol. 74, no. 17, pp. 2414–2416, 1999-04-26.
- [54] H. Matsui, C.-N. Xu, Y. Liu, and H. Tateyama, “Origin of mechanoluminescence from mn-activated ZnAl₂O₄ : Triboelectricity-induced electroluminescence,” vol. 69, no. 23, 2004-06-24.
- [55] S. Krishnan, H. Van der Walt, V. Venkatesh, and V. B. Sundaresan, “Dynamic characterization of elastico-mechanoluminescence towards structural health monitoring,” vol. 28, no. 17, pp. 2458–2464, 2017-10.
- [56] S. W. Shin, J. P. Oh, C. W. Hong, E. M. Kim, J. J. Woo, G.-S. Heo, and J. H. Kim, “Origin of mechanoluminescence from cu-doped ZnS particles embedded in an elastomer film and its application in flexible electro-mechanoluminescent lighting devices,” vol. 8, no. 2, pp. 1098–1103, 2016-01-20.
- [57] D. Hu, X. Xu, J. Miao, O. Gidron, and H. Meng, “A stretchable alternating current electroluminescent fiber,” vol. 11, no. 2, p. 184.
- [58] S. Timilsina, K. H. Lee, I. Y. Jang, and J. S. Kim, “Mechanoluminescent determination of the mode i stress intensity factor in SrAl₂O₄:eu²⁺,dy³⁺,” vol. 61, no. 19, pp. 7197–7206, 2013-11.
- [59] M.-C. Wong, L. Chen, G. Bai, L.-B. Huang, and J. Hao, “Temporal and remote tuning of piezophotonic-effect-induced luminescence and color gamut via modulating magnetic field,” vol. 29, no. 43, p. 1701945, 2017. [_eprint: https://onlinelibrary.wiley.com/doi/pdf/10.1002/adma.201701945](https://onlinelibrary.wiley.com/doi/pdf/10.1002/adma.201701945).
- [60] M. Akiyama, C.-N. Xu, Y. Liu, K. Nonaka, and T. Watanabe, “Influence of eu, dy co-doped strontium aluminate composition on mechanoluminescence intensity,” vol. 97, no. 1, pp. 13–18, 2002-04.
- [61] S. M. Jeong, S. Song, H. Kim, K.-I. Joo, and H. Takezoe, “Mechanoluminescence color conversion by spontaneous fluorescent-dye-diffusion in elastomeric zinc sulfide composite,” vol. 26, no. 27, pp. 4848–4858, 2016-07.
- [62] S. Song, B. Song, C.-H. Cho, S. K. Lim, and S. M. Jeong, “Textile-fiber-embedded multiluminescent devices: A new approach to soft display systems,” p. S1369702119307424, 2019-09.

-
- [63] J. Zhang, L. Bao, H. Lou, J. Deng, A. Chen, Y. Hu, Z. Zhang, X. Sun, and H. Peng, "Flexible and stretchable mechanoluminescent fiber and fabric," vol. 5, no. 32, pp. 8027–8032.
- [64] "About gwent: <http://www.gwent.org/about.htm>."
- [65] S. et al., "United States Patent US6660184." <http://www.freepatentsonline.com/6660184.pdf>, 2003.
- [66] N. Carmichael, "European centre for ecotoxicology and toxicology of chemicals," in *Encyclopedia of Toxicology*, pp. 547–548, Elsevier, 2014.
- [67] J. C. Lötters, W. Olthuis, P. H. Veltink, and P. Bergveld, "The mechanical properties of the rubber elastic polymer polydimethylsiloxane for sensor applications," *Journal of Micromechanics and Microengineering*, vol. 7, pp. 145–147, sep 1997.
- [68] C. E. Brunchi, A. Filimon, M. Cazacu, and S. Ioan, "Properties of some poly(siloxane)s for optical applications," *High Performance Polymers*, vol. 21, no. 1, pp. 31–47, 2009.
- [69] SMAC, "SMAC-MCA. Actuators User Manual." <https://www.smac-mca.com/documents/PDFs/SMAC%20Actuators%20User%20Manual.pdf>.
- [70] SMAC, "LAC-1. Technical Reference Manual." <https://www.smac-mca.com/documents/PDFs/LAC-1%20Manual%20rev1.pdf>, 1997.
- [71] N. Instruments, "User Guide. NI USB-6001/6002/6003 Low-Cost DAQ USB Device." <http://www.ni.com/pdf/manuals/374259a.pdf>, 2014.
- [72] T. T. Q. Hoa, L. V. Vu, T. D. Canh, and N. N. Long, "Preparation of ZnS nanoparticles by hydrothermal method," vol. 187, p. 012081.
- [73] CEM, "Discover SP." <https://cem.com/en/discover-sp>.
- [74] X. Qian, Z. Cai, M. Su, F. Li, W. Fang, Y. Li, X. Zhou, Q. Li, X. Feng, W. Li, X. Hu, X. Wang, C. Pan, and Y. Song, "Printable skin-driven mechanoluminescence devices via nanodoped matrix modification," vol. 30, no. 25, p. 1800291, 2018-06.
- [75] J.-C. Zhang, C.-N. Xu, X. Wang, and Y.-Z. Long, "Novel elástico-mechanoluminescence materials $\text{CaZnOS} : \text{Mn}^{2+}$ and $\text{CaZr}(\text{PO}_4)_2 : \text{Eu}^{2+}$," vol. 04, no. 3, p. 1430003.
- [76] J.-C. Zhang, Y.-Z. Long, X. Yan, X. Wang, and F. Wang, "Creating recoverable mechanoluminescence in piezoelectric calcium niobates through pr^{3+} doping," vol. 28, no. 11, pp. 4052–4057, 2016-06-14.
- [77] D. Tu, C.-N. Xu, Y. Fujio, and A. Yoshida, "Tuning the mechano-optical conversion in CaZnOS with cu ion concentration," vol. 48, no. 47, p. 475105.
- [78] B. Huang, M. Sun, and D. Peng, "Intrinsic energy conversions for photon-generation in piezo-phototronic materials: A case study on alkaline niobates," vol. 47, pp. 150–171.
- [79] Z.-J. Zhang, A. Feng, X.-Y. Chen, and J.-T. Zhao, "Photoluminescence properties and energy levels of RE (RE = pr, sm, er, tm) in layered- CaZnOS oxysulfide," vol. 114, no. 21, p. 213518.
-

- [80] C. J. Duan, A. C. A. Delsing, and H. T. Hintzen, "Photoluminescence properties of novel red-emitting Mn^{2+} -activated MZnOS ($m = \text{Ca}, \text{Ba}$) phosphors," vol. 21, no. 6, pp. 1010–1016.
- [81] S. A. Petrova, V. P. Mar'evich, R. G. Zakharov, E. N. Selivanov, V. M. Chumarev, and L. Y. Udoeva, "Crystal structure of zinc calcium oxysulfide," vol. 393, no. 1, pp. 255–258.
- [82] T. Sambrook, C. F. Smura, S. J. Clarke, K. M. Ok, and P. S. Halasyamani, "Structure and physical properties of the polar oxysulfide CaZnOS ," vol. 46, no. 7, pp. 2571–2574.
- [83] S. R. D. S. Cheng-Jun Duan, Theresia Hubertus Hintzen, "ABOS:M-based phosphors and light sources containing these phosphors." <https://patents.google.com/patent/US8319417B2/en>, 2008.
- [84] T.-W. Kuo, W.-R. Liu, and T.-M. Chen, "High color rendering white light-emitting-diode illuminator using the red-emitting Eu^{2+} -activated CaZnOS phosphors excited by blue LED," vol. 18, no. 8, p. 8187.
- [85] R. Gulyaeva, E. Selivanov, A. Vershinin, and V. Chumarev, "Thermal expansion of CaZnOS ," *Inorganic Materials - INORG MATER-ENGL TR*, vol. 42, pp. 897–900, 08 2006.
- [86] Z. Qiu, C. Rong, W. Zhou, J. Zhang, C. Li, L. Yu, S. Liu, and S. Lian, "A strategy for synthesizing CaZnOS:Eu^{2+} phosphor and comparison of optical properties with CaS:Eu^{2+} ," vol. 583, pp. 335–339, 2014-01.
- [87] J.-C. Zhang, C.-N. Xu, S. Kamimura, Y. Terasawa, H. Yamada, and X. Wang, "An intense elasto-mechanoluminescence material CaZnOS:Mn^{2+} for sensing and imaging multiple mechanical stresses," vol. 21, no. 11, p. 12976, 2013-06-03.
- [88] W. Wang, D. Peng, H. Zhang, X. Yang, and C. Pan, "Mechanically induced strong red emission in samarium ions doped piezoelectric semiconductor CaZnOS for dynamic pressure sensing and imaging," vol. 395, pp. 24–28.
- [89] J.-C. Zhang, X. Wang, G. Marriott, and C.-N. Xu, "Trap-controlled mechanoluminescent materials," vol. 103, pp. 678–742, 2019-06.
- [90] J.-C. Zhang, Y.-Z. Long, X. Wang, and C.-N. Xu, "Controlling elasto-mechanoluminescence in diphasic $(\text{Ba,Ca})\text{TiO}_3:\text{Pr}^{3+}$ by co-doping different rare earth ions," vol. 4, no. 77, pp. 40665–40675.
- [91] C. Pan, J.-C. Zhang, M. Zhang, X. Yan, Y.-Z. Long, and X. Wang, "Intrinsic oxygen vacancies mediated multi-mechano-responsive piezoluminescence in undoped zinc calcium oxysulfide," vol. 110, no. 23, p. 233904.
- [92] C. Barthou, J. Benoit, P. Benalloul, and A. Morell, " Mn^{2+} concentration effect on the optical properties of $\text{Zn}_2\text{SiO}_4:\text{Mn}$ phosphors," *Journal of the Electrochemical Society*, vol. 141, no. 2, p. 524, 1994.
- [93] C. Ronda and T. Amrein, "Evidence for exchange-induced luminescence in $\text{Zn}_2\text{SiO}_4:\text{Mn}$," *Journal of Luminescence*, vol. 69, no. 5-6, pp. 245–248, 1996.
- [94] Z. Xu, Z. Xia, and Q. Liu, "Two-step synthesis and surface modification of $\text{CaZnOS}:\text{Mn}^{2+}$ phosphors and the fabrication of a luminescent poly (dimethylsiloxane) film," *Inorganic chemistry*, vol. 57, no. 3, pp. 1670–1675, 2018.

-
- [95] KTP, “Shanghai Keyan Phosphor Technology Co.,Ltd .” http://kpt.net.cn/en/home_en/, 2008-2020.
- [96] W. Peng, G. Cong, S. Qu, and Z. Wang, “Synthesis and photoluminescence of ZnS:cu nanoparticles,” vol. 29, no. 2, pp. 313–317, 2006-11.
- [97] A. M. Wise, C. Ban, J. N. Weker, S. Misra, A. S. Cavanagh, Z. Wu, Z. Li, M. S. Whittingham, K. Xu, S. M. George, and M. F. Toney, “Effect of Al_2O_3 coating on stabilizing $\text{LiNi}_{0.4}\text{Mn}_{0.4}\text{Co}_{0.2}\text{O}_2$ cathodes,” vol. 27, no. 17, pp. 6146–6154.
- [98] X. Duan, N. H. Tran, N. K. Roberts, and R. N. Lamb, “Single-source chemical vapor deposition of clean oriented Al_2O_3 thin films,” vol. 517, no. 24, pp. 6726 – 6730.
- [99] F. Di Fonzo, D. Tonini, A. Li Bassi, C. S. Casari, M. G. Beghi, C. E. Bottani, D. Gastaldi, P. Vena, and R. Contro, “Growth regimes in pulsed laser deposition of aluminum oxide films,” vol. 93, no. 3, pp. 765–769.
- [100] N. Avci, P. F. Smet, J. Lauwaert, H. Vrielinck, and D. Poelman, “Optical and structural properties of aluminium oxide thin films prepared by a non-aqueous sol–gel technique,” vol. 59, no. 2, pp. 327–333.
- [101] N. Avci, I. Cimieri, P. F. Smet, and D. Poelman, “Stability improvement of moisture sensitive CaS:eu²⁺ micro-particles by coating with sol–gel alumina,” vol. 33, no. 7, pp. 1032–1035.
- [102] B. M. Henry, A. G. Erlat, A. McGuigan, C. R. M. Grovenor, G. A. D. Briggs, Y. Tsukahara, T. Miyamoto, N. Noguchi, and T. Nijima, “Characterization of transparent aluminium oxide and indium tin oxide layers on polymer substrates,” vol. 382, no. 1, pp. 194 – 201.
- [103] K. Tadanaga, N. Katata, and T. Minami, “Super-water-repellent Al_2O_3 coating films with high transparency,” *Journal of the American Ceramic Society*, vol. 80, no. 4, pp. 1040–1042, 1997.
- [104] N. Avci, J. Musschoot, P. F. Smet, K. Korthout, A. Avci, C. Detavernier, and D. Poelman, “Microencapsulation of moisture-sensitive CaS:eu²⁺ particles with aluminum oxide,” *Journal of The Electrochemical Society*, vol. 156, no. 11, p. J333, 2009.
- [105] K. Vanbesien, P. D. Visschere, P. F. Smet, and D. Poelman, “Electrical properties of Al_2O_3 films for TFEL-devices made with sol–gel technology,” vol. 514, no. 1, pp. 323 – 328.
- [106] Y. Huang, J. Chen, F. Cheng, W. Wan, W. Liu, H. Zhou, and X. Zhang, “A modified Al_2O_3 coating process to enhance the electrochemical performance of $\text{Li}(\text{Ni}_{1/3}\text{Co}_{1/3}\text{Mn}_{1/3})\text{O}_2$ and its comparison with traditional Al_2O_3 coating process,” vol. 195, no. 24, pp. 8267–8274.
- [107] College of Material Science and Engineering, China Jiliang University, Hangzhou, 310018, Zhejiang, China and D. Zuo, “Comparative study of the electrochemical behaviors for LiCoO_2 electrode coated with two different Al_2O_3 coating layer,” pp. 5044–5057, 2017-06.
- [108] S. Oh, J. K. Lee, D. Byun, W. I. Cho, and B. Won Cho, “Effect of Al_2O_3 coating on electrochemical performance of LiCoO_2 as cathode materials for secondary lithium batteries,” vol. 132, no. 1, pp. 249–255.
-

- [109] J. Cho, Y. J. Kim, and B. Park, "Novel LiCoO₂ cathode material with Al₂O₃ coating for a Li ion cell," vol. 12, no. 12, pp. 3788–3791.
- [110] G. P. Shulman, M. Trusty, and J. H. Vickers, "Thermal decomposition of aluminum alkoxides¹," vol. 28, p. 4.
- [111] O. Mekasuwandumrong, H. Kominami, P. Praserttham, and M. Inoue, "Synthesis of thermally stable [U+2439]-alumina by thermal decomposition of aluminum isopropoxide in toluene," vol. 87, no. 8, p. 7.
- [112] K. Pansanga, O. Mekasuwandumrong, J. Panpranot, and P. Praserttham, "Synthesis of nanocrystalline alumina by thermal decomposition of aluminum isopropoxide in 1-butanol and their applications as cobalt catalyst support," vol. 24, no. 3, pp. 397–402.
- [113] W. Stöber, A. Fink, and E. Bohn, "Controlled growth of monodisperse silica spheres in the micron size range," vol. 26, no. 1, pp. 62–69.
- [114] Y. Kobayashi, K. Misawa, M. Takeda, M. Kobayashi, M. Satake, Y. Kawazoe, N. Ohuchi, A. Kasuya, and M. Konno, "Silica-coating of AgI semiconductor nanoparticles," vol. 251, no. 1, pp. 197–201.
- [115] Y. Kobayashi, H. Katakami, E. Mine, D. Nagao, M. Konno, and L. M. Liz-Marzán, "Silica coating of silver nanoparticles using a modified stöber method," vol. 283, no. 2, pp. 392–396.
- [116] Y. Kobayashi, K. Misawa, M. Takeda, N. Ohuchi, A. Kasuya, and M. Konno, "Preparation and properties of silica-coated AgI nanoparticles with a modified stober method," vol. 1074, pp. 1074–110–07.
- [117] A. Bai, H. Song, G. He, Q. Li, C. Yang, L. Tang, and Y. Yu, "Facile synthesis of core-shell structured ZrO₂@SiO₂ via a modified stöber method," vol. 42, no. 6, pp. 7583–7592.
- [118] J. L. Montaña-Priede, J. P. Coelho, A. Guerrero-Martínez, O. Peña-Rodríguez, and U. Pal, "Fabrication of monodispersed Au@SiO₂ nanoparticles with highly stable silica layers by ultrasound-assisted stöber method," vol. 121, no. 17, pp. 9543–9551.
- [119] H. Wang, J. Fang, T. Cheng, J. Ding, L. Qu, L. Dai, X. Wang, and T. Lin, "One-step coating of fluoro-containing silicananoparticles for universal generation of surface superhydrophobicity," no. 7, pp. 877–879.
- [120] M. Badv, I. H. Jaffer, J. I. Weitz, and T. F. Didar, "An omniphobic lubricant-infused coating produced by chemical vapor deposition of hydrophobic organosilanes attenuates clotting on catheter surfaces," vol. 7, no. 1, p. 11639.
- [121] H. Zhou, H. Wang, H. Niu, A. Gestos, X. Wang, and T. Lin, "Fluoroalkyl silane modified silicone rubber/nanoparticle composite: A super durable, robust superhydrophobic fabric coating," vol. 24, no. 18, pp. 2409–2412.
- [122] V. K. Chandra, B. P. Chandra, and P. Jha, "Self-recovery of mechanoluminescence in ZnS:Cu and ZnS:Mn phosphors by trapping of drifting charge carriers," vol. 103, no. 16, p. 161113, 2013-10-14.
- [123] H.-J. Park, S. Kim, J. H. Lee, H. T. Kim, W. Seung, Y. Son, T. Y. Kim, U. Khan, N.-M. Park, and S.-W. Kim, "Self-powered motion-driven triboelectric electroluminescence textile system," vol. 11, no. 5, pp. 5200–5207.

- [124] J. Diani, B. Fayolle, and P. Gilormini, "A review on the mullins effect," pp. 601-612.
Publisher: Elsevier.